Metabolic engineering studies with *Corynebacterium glutamicum* –

Exploring new ways to produce L-histidine & L-valine

Von der Fakultät 4: Energie-, Verfahrens- und Biotechnik der Universität Stuttgart
zur Erlangung der Würde eines Doktors der Naturwissenschaften
(Dr. rer. nat.) genehmigte Abhandlung

Vorgelegt von

Andreas Schwentner

aus Ellwangen (Jagst)

Hauptberichter:	Prof. Dr.-Ing. Ralf Takors
Mitberichter:	Prof. Dr. Bernhard Eikmanns

Tag der mündlichen Prüfung: 26.04.2019

Institut für Bioverfahrenstechnik der Universität Stuttgart

University of Stuttgart
Germany

2019

Voller Bewunderung für meine Schwester Julia.

SCIENTIFIC PUBLICITY

The experimental work (with exception of the whole genome DNA sequencing) presented in this manuscript was conducted under guidance and supervision of Prof. Dr.-Ing. Ralf Takors and Dr. Bastian Blombach at the Institute of Biochemical Engineering (University of Stuttgart, Germany) within the time span of 2014-2018.

The project was supported by the Fachagentur Nachwachsende Rohstoffe e.V. (FNR; Gülzow-Prüzen, Germany) and Evonik Creavis GmbH (Marl, Germany), Förderkennzeichen **22008014**.

Parts of this work have been published in peer-reviewed journals, which are listed in the following.

Schwentner, A., Feith, A., Münch, E., Busche, T., Rückert, C., Kalinowski, J., Takors, R., Blombach, B., 2018. Metabolic engineering to guide evolution – Creating a novel mode for L-valine production with *Corynebacterium glutamicum*. Metab. Eng. 47, 31–41. https://doi.org/10.1016/j.ymben.2018.02.015.

Schwentner, A., Feith, A., Münch, E., Stiefelmaier, J., Lauer, I., Favilli, L., Massner, C., Öhrlein, J., Grund, B., Hüser, A., Takors, R., Blombach, B., 2019. Modular systems metabolic engineering enables balancing of relevant pathways for L-histidine production with *Corynebacterium glutamicum*. Biotechnol. Biofuels 12, 65. https://doi.org/10.1186/s13068-019-1410-2.

Parts of this research have been presented at national and international conferences and excursions as posters[*] or oral presentations[#], which are listed in the following in chronological order from present to past.

[#] **Schwentner, A.**, Feith, A., Takors, R., Blombach, B., (08/2018) Modular metabolic engineering enables balancing of relevant pools for L-histidine production with *Corynebacterium glutamicum*. *First German Coryne Meeting 2018. Stuttgart, Germany.*

[*] **Schwentner, A.**, Feith, A., Münch, E., Busche, T., Rückert, C., Kalinowski, J., Takors, R., Blombach, B., (05/2018) Metabolic engineering to guide evolution – Creating a novel mode for L-valine production with *Corynebacterium glutamicum*. *DECHEMA Himmelfahrtstagung 2018. Magdeburg, Germany.*

[*] **Schwentner, A.**, Feith, A., Münch, E., Busche, T., Rückert, C., Kalinowski, J., Takors, R., Blombach, B., (04/2018) Metabolic engineering to guide evolution – Creating a novel mode for L-valine production with *Corynebacterium glutamicum*. *VAAM Annual Conference 2018, Wolfsburg, Germany.*

[#] **Schwentner, A.**, Feith, A., Münch, E., Busche, T., Rückert, C., Kalinowski, J., Takors, R., Blombach, B., (11/2017) Metabolic engineering to guide evolution – Creating a novel mode for L-valine production with *Corynebacterium glutamicum*. *Excursion to BRAIN AG, Darmstadt, Germany.*

[*] **Schwentner, A.**, Feith, A., Hoffart, E., Busche, T., Rückert, C., Kalinowski, J., Takors, R., Blombach, B., (09/2017) Metabolic engineering to guide evolution – Creating a novel mode for L-valine production with *Corynebacterium glutamicum*. *ProkaGENOMICS 2017: 7th European Conference on Prokaryotic and Fungal Genomics, Göttingen, Germany.*

[#] **Schwentner, A.**, Feith, A., Hoffart, E., Busche, T., Rückert, C., Kalinowski, J., Takors, R., Blombach, B., (09/2016) Metabolic engineering to guide evolution in *Corynebacterium glutamicum*. *VAAM 31. Symposium – Mechanisms of Gene Regulation 2016, Bad Bergzabern, Germany.*

[*] **Schwentner, A.**, Hoffart, E., Busche, T., Rückert, C., Kalinowski, J., Takors, R., Blombach, B., (05/2016) Metabolic engineering for directed evolution – Enhancing allocation of oxaloacetate as crucial precursor for L-lysine production in *Corynebacterium glutamicum*. *DECHEMA Himmelfahrtstagung 2016. Koblenz, Germany.*

[*] **Schwentner, A.**, Hoffart, E., Busche, T., Rückert, C., Kalinowski, J., Takors, R., Blombach, B., (03/2016) Metabolic engineering for directed evolution – Enhancing allocation of oxaloacetate as crucial precursor for L-lysine production in *Corynebacterium glutamicum*. *VAAM Annual Conference 2016, Jena, Germany.*

ACKNOWLEDGEMENTS

The preparation of this work would not have been possible without the help of numerous people in my social environment, within and without the scientific community. I want to use the following lines to thank these people.

Firstly, I want to thank Prof. Dr.-Ing. Ralf Takors who is my doctoral advisor and who provided all the necessities for creating this thesis, such as the excellent scientific equipment and valuable discussions.

I then want to thank my supervisor Dr. Bastian Blombach, who enlightened me with his deep and profound knowledge about *Corynebacterium glutamicum*. Thank you from the bottom of my heart for all the discussions about science and life. I wish you all the best as Professor.

I also want to thank Prof. Dr. Bernhard Eikmanns who willingly took on the task of being my second assessor and for staying in contact throughout all the years since I left Ulm.

I want to thank our project partners from Evonik Creavis GmbH, namely Dr. Johannes Öhrlein, Bastian Grund, and Dr. Steffen Schaffer and from Evonik Industries AG Dr. Kay Marin for their ongoing support and for the inspiring meetings and discussions that definitely broadened my horizons. I also want to express my gratefulness to Andrea Hüser from Evonik Nutrition & Care GmbH who kindly provided the overproduction construct for the GCV system from *Corynebacterium jeikeium*.

I further want to acknowledge our collaborators from Microbial Genomics and Biotechnology at the Center for Biotechnology of Bielefeld University, especially Prof. Dr. Jörn Kalinowski, Dr. Tobias Busche, and Dr. Christian Rückert, who provided the whole genome sequencing data.

It would be inconceivable to create a thesis without reliable and credible colleagues. Therefore, I want to thank all my co-workers at the Institute of Biochemical Engineering of the University of Stuttgart.
Especially and foremostly I want to thank André Feith who did a fantastic job in providing FBAs and SMP studies. André, thank you very much for this wonderful cooperation, for a multitude of intense discussions and for three years of joyful science.
Also, and no less important, I want to thank Eugenia Münch (formerly Hoffart) who supported work in the lab with her scientific passion and positive attitude. Eugenia, I really enjoyed working with you every single day, I really appreciated your work and I wish you all the best for your personal future.
I further want to express my thankfulness to my three students Judith Stiefelmaier, Daniela Romeo, and Ira Lauer who were helping my work significantly with their theses.

A specific reference goes to the working group of Molecular Biotechnology at the IBVT, namely Robert Nitschel, Felix Müller, Sebastian Grenz, and Julian Lange, and the extended working group including Michaela Graf and Joana Simen for all the subject-specific and non-subject-specific discussions throughout our years at IBVT.
Important contributors for this work were also Mira Lenfers-Lücker who supported me in the analytics laboratory with assistance during HPLC measurements.
I want to thank Andreas Freund, Salaheddine Laghrami, and Alexander Dietrich for their contributions to the bioprocess development, and especially Andreas for the joyful discussions about adventuring, cycling, and travelling.
A special citation is directed to Dr. Attila Teleki for enlightening me with his vast knowledge on how the world works, for plenty of illuminating conversations about Marx, Nietzsche, and Rilke.
Also, I want to thank Dr. Martin Siemann-Herzberg for being a critical questioner during all the seminars.
Thank you, Branca, for helping me get my life goals set up, Martina for keeping an eye on my chemical leftovers, Andrea for controlling the orders, and of course my favourite secretary, Ms. Reu for enduring all my issues with contracts, travelling, and especially holidays.
There are several colleagues unmentioned and I want to thank all of them for making my time at the IBVT such a pleasant one. Thanks, all of you, I will miss you for sure.

Also, I want to thank Tobias Hahn (University of Ulm) for providing the scanning electron microscopy pictures of *C. glutamicum*, and Dr. Heiko Gregorius for the motivating sports schedule.

My most profound thank you goes to Dr. Linda Höll for always standing by my side, never doubting me, instead all the time supporting me.

Another deeply important factor is my family, my mother Birgit who is always there, always trusting my decisions, my father Hans-Dieter who supports me with his best possible, and my loveable and joyful sister Julia, supporting me with her drive for adventure.

AUTHORS' CONTRIBUTIONS AND CO-WORKERS

The experimental work was conducted by myself, I interpreted the results, created figures and tables, and wrote the manuscripts, unless indicated otherwise. I was assisted by Eugenia Münch, Judith Stiefelmaier, Daniela Romeo, and Ira Lauer at the practical realization (all IBVT, University of Stuttgart). Prof. Dr.-Ing. Ralf Takors and Dr. Bastian Blombach conceptualized the projects (both IBVT, University of Stuttgart). The experimental design, interpretation of the experimental results, and writing of the manuscript was supported by Dr. Bastian Blombach and Prof. Dr.-Ing. Ralf Takors.

André Feith conducted the practical work, data analysis, and figures for Flux Balance Analyses (FBAs) and Systems Metabolic Profiling (SMP) and was assisted by Lorenzo Favilli and myself (all IBVT, University of Stuttgart). Interpretation of the results from FBAs and SMP was done by Prof. Dr.-Ing. Ralf Takors, Dr. Bastian Blombach, André Feith, and myself.

Prof. Dr. Jörn Kalinowski, Dr. Tobias Busche, and Dr. Christian Rückert (all CeBiTec, Bielefeld University) performed the whole genome sequencing and provided data of the genomic background of the evolved strains. Evaluation and interpretation were done by Dr. Bastian Blombach and myself.

Plasmids obtained from other people in the scientific / industrial community include pEKEx3-*aspA* and pEKEx3-*aspB* (obtained from Volker Wendisch, Bielefeld University), pK19*mobsacB zwf*^{A243T} and pK19*mobsacB gnd*^{S361F} (obtained from Evonik Industries AG), pJC4 *ilvBNCE* and pK19*mobsacB* Δ*pup* (obtained from Lothar Eggeling and Michael Bott, Forschungszentrum Jülich), pK19*mobsacB* Δ*ppc* (obtained from Bastian Blombach, University of Stuttgart), pK19*mobsacB* Δ*pyc* and pK19*mobsacB* Δ*pck* (obtained from Bernhard Eikmanns, University of Ulm), and pEC-XT99A_gcv_ OP1-Cjk (obtained from Andrea Hüser, Evonik Industries AG)

Prof. Dr.-Ing. Ralf Takors enabled access to the required infrastructure, such as laboratories and scientific equipment.

CONTENT

LIST OF FIGURES

LIST OF TABLES

NOMENCLATURE

Table 1. This table lists the used abbreviations of this work and gives their respective descriptions. For genes from the *C. glutamicum* ATCC 13032 genome, the cg numbers are derived from the https://coryneregnet.compbio.sdu.dk/v6/index.html database (last access: 28-06-2018).

Abbreviation	Description
% (v v^{-1})	Volume per volume percent
% (w v^{-1})	Weight per volume percent
ε	Extinction coefficient
μ	Growth rate or micro (in combination with SI units)
2×YT	2x yeast tryptone
2-PG	2-phosphoglycerate
3-PG	3-phosphoglycerate
5'-ProFAR	1-(5-phosphoribosyl)-5-[(5-phosphoribosylamino) methylideneamino] imidazole-4 carboxamide
6PG DH	Phosphogluconate dehydrogenase
A	Specific enzyme activity
a.o.	Among others
AA	Amino acid
ABC	ATP-binding cassette
aceA	Isocitrate lyase (encoding gene, cg2560)
aceB	Malate synthase (encoding gene; cg2559)
Acetyl CoA	Acetyl coenzyme A
ack	Acetate kinase (encoding gene, cg3047)
ADP	Adenosine diphosphate
AdSucc	Adenylosuccinate
AHAS	Acetohydroxy acid synthase
AICAR	5-aminoimidazole-4-carboxamide ribonucleotide
AIR	5-Aminoimidazole ribotide
ALE	Adaptive laboratory evolution
AMP	Adenosine monophosphate
asp	L-Aspartate
AspA	Aspartate ammonia-lyase
aspA	Aspartate ammonia-lyase (encoding gene; cg1697)
AspB	Aspartate aminotransferase
aspB	Aspartate aminotransferase (encoding gene; cg0294)
ATP	Adenosine triphosphate
B. subtilis	*Bacillus subtilis*
BenR	Bacterial regulatory protein
benR	Bacterial regulatory protein (encoding gene, cg2641)
BHI	Brain heart infusion
BHIS	BHI medium supplemented with sorbitol
BLAST	Basic local alignment search tool
bp	Base pair
BSA	Bovine serum albumin
c	Concentration
C. glutamicum	*Corynebacterium glutamicum*
C. jeikeium	*Corynebacterium jeikeium*

Abbreviation	Description
C_1	One carbon, in combination with unit or metabolism
CDW	Cell dry weight
CeBiTec	Center for Biotechnology, Bielefeld University
cg0617	Potential formate dehydrogenase (encoding gene)
$CGXII^{N/E/R}$	Minimal media
cis-	Referring to *cis-trans* isomerism, meaning "this side of"
COG	Clusters of orthologous categories
DAD	Diode array detector
DECHEMA	Deutsche Gesellschaft für chemisches Apparatewesen, Chemische Technik und Biotechnologie e.V.
dH_2O	Deionized water
DHAP	Dihydroxyacetone phosphate
DMSO	Dimethyl sulfoxide
DNA	Deoxyribonucleic acid
DNAP	DNA-polymerase
DO	Dissolved oxygen concentration
DTT	Dithiotreitol
E. coli	*Escherichia coli*
e.g.	Exempli gratia (for example)
EC	Energy charge
EDTA	Ethylenediamine tetraacetic acid
EF-TU	Elongation factor TU
EMS	Ethyl methanesulfonate
et al.	Et aliae (and others)
F 6-P	Fructose 6-phosphate
F-1,6-Bis-P	Fructose-1,6-bisphosphate
FACS	Fluorescence activated cell sorting
FAICAR	5-formamidoimidazole-4-carboxamide ribotide
FC	Fold change
FBA	Flux balance analysis
FDH	Formate dehydrogenase
fdhD	Putative formate dehydrogenase (encoding gene, cg0616)
fdhF	Formate dehydrogenase (encoding gene, cg0618)
fGAM	5'phosphoribosylformylglycine amidine
fGAR	phosphoribosyl-N-formylglcineamide

Abbreviation	Description
FID	Flame ionization detector
FLD	Fluorescence detector
Fmoc	9-Fluorenylmethoxy-carbonyl chloride
FNR	Fachagentur Nachwachsende Rohstoffe e.V.
fTHF	10-Formyltetrahydrofolate
fum	Fumarate
g	Gram
G6P	Glucose 6-phosphate
G6P DH	Glucose 6-phosphate dehydrogenase
GA3P	Glyceraldehyde 3-phosphate
GA3P-DH	Glyceraldehyde 3-phosphate dehydrogenase
gapA	Glyceraldehyde 3-phosphate dehydrogenase (encoding gene, cg1791)
GAR	Glycineamide ribonucleotide
GCV	Glycine cleavage system
gcvPTH	GCV (encoding genes) from *C. jeikeium*
Gdh	L-Glutamate dehydrogenase
gdh	L-Glutamate dehydrogenase (encoding gene, cg2280)
GDP	Guanosine diphosphate
GTP	Guanosine triphosphate
GlgE	Potential maltosyltransferase
glgE	Potential maltosyltransferase (encoding gene, cg1382)
Gln	L-glutamine
gltA	citrate synthase (encoding gene, cg0949)
glu	L-Glutamate
Gly / Gly	Glycine
glyA	Serine hydroxymethyltransferase (encoding gene, cg1133)
GMP	guanosine monophosphate
gnd	6-Phosphogluconate dehydrogenase (encoding gene, cg1643)
h	Hours
his / His	L-Histidine
HisA	5'ProFAR isomerase
hisA	5'ProFAR isomerase (encoding gene, cg2299)
HisB	Imidazoleglycerol phosphate dehydratase

Abbreviation	Description
hisB	imidazoleglycerol phosphate dehydratase (encoding gene, cg2303)
HisC	Histidinol phosphate aminotransferase
hisC	Histidinol phosphate aminotransferase (encoding gene, cg2304)
HisD	Histidinol dehydrogenase
hisD	Histidinol dehydrogenase (encoding gene, cg2305)
HisE	Phosphoribosyl-ATP pyrophosphatase
hisE	Phosphoribosyl-ATP pyrophosphatase (encoding gene, cg1699)
HisF	Synthase SU of IGP synthase
hisF	Synthase SU of IGP synthase (encoding gene, cg2297)
HisG	ATP phosphoribosyltransferase
hisG	ATP phosphoribosyltransferase (encoding gene, cg1698)
HisH	Glutaminase SU of IGP synthase
hisH	Glutaminase SU of IGP synthase (encoding gene, cg2300)
HisI	Phosphoribosyl-AMP cyclohydrolase
hisI	phosphoribosyl-AMP cyclohydrolase (encoding gene, 2296)
HisN	Histidinol-phosphate phosphatase
hisN	Histidinol-phosphate phosphatase (encoding gene, cg0910)
Hisol	L-histidinol
Hol-P	L-histidinol phosphate
HPLC	High performance liquid chromatography
HTH	Helix-turn-helix
i.e.	Id est (that is)
IAP	Imidazole-acetole phosphate
IBVT	Institute of Biochemical Engineering, University of Stuttgart
ICD	Isocitrate dehydrogenase
icd	Isocitrate dehydrogenase (encoding gene; cg0766)
ICL	Isocitrate lyase
IGP	Imidazole-glycerol phosphate
ilvC	Acetohydroxyacid isomeroreductase (encoding gene, cg1437)
ilvE	Transaminase B (encoding gene, cg2418)

Abbreviation	Description
IMP	Inosine monophosphate
ivlB	Acetolactate synthase large SU (encoding gene, cg1435)
ivlN	Acetolactate synthase small SU (encoding gene, cg1436)
Kan	Kanamycin
K_M	Michaelis Menten constant
L	Liter
LC	Liquid chromatography
lipA	Lipoyl synthase (encoding gene) from *C. jeikeium*
lipB	Lipoyl transferase (encoding gene) from *C. jeikeium*
LuxR	LuxR-type DNA-binding HTH domain
m	Meter or milli (in combination with SI units)
M	Molar (mol L^{-1})
MerR	MerR-type DNA-binding HTH domain
MGE	Metabolic engineering to guide evolution
min	Minutes
MOPS	3-(N-morpholino) propane sulphonic acid
mRNA	Messenger RNA
MS	Mass spectrometry *or* malate synthase
mTHF	5,10-Methylenetetrahydrofolate
n	Amount of substance
n	Nano (in combination with SI units)
N	Rotational speed
N_5-CAIR	5'-Phosphoribosyl-4-carboxy-5-aminoimidazole
NAD^+	Nicotinamide adenine dinucleotide (oxidized)
NADH	Nicotinamide adenine dinucleotide (reduced)
$NADP^+$	Nicotinamide adenine dinucleotide phosphate (oxidized)
NADPH	Nicotinamide adenine dinucleotide phosphate (reduced)
nt	Nucleotide
NTG	N-methyl-N'-nitro-N-nitrosoguanidine
o-	*Ortho*-
o/n	Overnight
ORF	Open reading frame

Abbreviation	Description
oriV	Origin of vegetative replication
P	Promoter (with subscript giving the respective gene)
$_P$	Product (superscript)
PCA	Protocatechuate or perchloric acid
PCk	Phosphoenolpyruvate carboxykinase
pck	Phosphoenolpyruvate carboxykinase (encoding gene, cg3169)
PCR	Polymerase chain reaction
PCx	Pyruvate carboxylase
PDHC	Pyruvate dehydrogenase complex
PEP	Phosphoenolpyruvate
PEPCk	PEP carboxykinase
PEPCx	PEP carboxylase
PFK	6-Phosphofructokinase
pfk	6-Phosphofructokinase (encoding gene, cg1409)
PGI	Phosphoglucoisomerase
pgi	Phosphoglucoisomerase (encoding gene, cg0973)
pgl	6-Phosphogluconolactonase (encoding gene, cg1780)
Pgm	Phosphoglucomutase
pgm	Phosphoglucomutase (encoding gene, cg2800)
P_i	inorganic phosphate
pK_a	Logarithmic acid dissociation constant
pos.	Position
pp.	Pages
ppc	Phosphoenolpyruvate carboxylase (encoding gene, cg1787)
PP_i	inorganic diphosphate
PPP	Pentose phosphate pathway
PRA	phosphoribosylamine
PR-AMP	phosphoribosyl-AMP
PR-ATP	phosphoribosyl-ATP
PRFAR	5-[(5-Phospho-1-deoxyribulos-1-ylamino)methylideneamino]-1-(5-phosphoribosyl) imidazole-4-carboxamid
PRPP	Phosphoribosyl pyrophosphate
prsA	PRPP synthetase (encoding gene, cg1075)
PrsA	PRPP synthetase, also ribose-phosphate diphosphokinase

Abbreviation	Description
pta	Phosphate transacetylase (encoding gene, cg3048)
PTS	Phosphotransferase system
ptsF	Fructose/mannitol-specific transport protein of PTS (encoding gene, cg2120)
PtsF	Phosphotransferase system for fructose
ptsG	Glucose-specific enzyme II BC component of PTS (encoding gene, cg1537)
PtsG	Phosphotransferase system for glucose
PurA	Adenylosuccinate synthase
purA	Adenylosuccinate synthase (encoding gene, cg3063)
PurB	Adenylosuccinate lyase
purB	Adenylosuccinate lyase (encoding gene, cg2876)
PurC	Phosphoribosylaminoimidazole-succinocarboxamide synthase
purC	Phosphoribosylaminoimidazole-succinocarboxamide synthase (encoding gene, cg2874)
PurD	PRA-glycine ligase
purD	PRA-glycine ligase (encoding gene, cg2878)
PurE	Phosphoribosylaminoimidazole mutase
purE	Phosphoribosylaminoimidazole mutase (encoding gene, cg0820)
PurF	Amidophosphoribosyltransferase
purF	Amidophosphoribosyltransferase (encoding gene, cg2857)
PurH	Bifunctional AICAR formyltransferase / IMP cyclohydrolase
purH	Bifunctional AICAR formyltransferase / IMP cyclohydrolase (encoding gene, cg0984)
PurK	Phosphoribosylaminoimidazole carboxylase
purK	Phosphoribosylaminoimidazole carboxylase (encoding gene, cg0816)
PurL	Phosphoribosylformylglycinamide synthase
purL	Phosphoribosylformylglycinamide synthase (encoding gene, cg2862)
PurM	Phosphoribosyl-formylglycinamidine cycloligase
purM	Phosphoribosyl-formylglycinamidine cycloligase (encoding gene, cg2856)

Abbreviation	Description
PurN	Phosphoribosylglycinamide formyltransferase, fTHF-dependent
purN	Phosphoribosylglycinamide formyltransferase (encoding gene, cg0983)
PurT	Putative phosphoribosylglycinamide formyltransferase, formate-dependent
purT	Putative phosphoribosylglycinamide formyltransferase, formate-dependent (encoding gene, cg3054)
PurU	Potential fTHF deformylase
purU	Potential fTHF deformylase (encoding gene, cg0457)
pyc	Pyruvate carboxylase (encoding gene, cg0791)
PyrE	Orotate phosphoribosyltransferase
pyre	Orotate phosphoribosyltransferase gene (encoding cg3071)
q_P	Biomass specific product formation rate
q_S	Biomass specific substrate uptake rate
Q-TOF	Quadrupole time-of-flight
^{R}	Resistant (superscript)
R5P	Ribose 5-phosphate
R^2	Coefficient of determination
ramA	Regulator of acetate metabolism A LuxR-type (encoding gene, cg2831)
ramB	Regulator of acetate metabolism B MerR-type (encoding gene, cg0444)
rcf	Relative centrifugal force
RNA	Ribonucleic acid
Rpi	Phosphopentose isomerase
rpi	Phosphopentose isomerase (encoding gene, cg2658)
rpm	Revolutions per minute
RT	Room temperature
s	Seconds (SI-unit)
$_S$	Substrate (subscript)
S. cerevisiae	*Saccharomyces cerevisiae*
S. typhimurium	*Salmonella enterica* serovar Typhimurium
sacB	Levansucrase (gene)
SAICAR	Phosphoribosyl-aminoimidazole-succinocarboxamide
SD	Standard deviation
sdaA	L-Serine dehydratase (encoding gene cg1852)

Abbreviation	Description
L-SerDH	L-Serine dehydratase
SHMT	L-serine hydroxymethyltransferase
SNP	Single nucleotide polymorphism
sp.	Species
SU	Subunit
T	Temperature or terminator (with subscript giving the respective gene)
t	Time
TAE	Tris-acetate and EDTA
TBAS	Tetrabutylammonium hydrogen sulfate
TCA	Tricarboxylic acid cycle
TES	Trace element solution
Tet	Tetracycline
THF	Tetrahydrofolate
Tkt	Transketolase
tkt	Transketolase (encoding gene, cg1774)
trpD	Anthranilate phosphoribosyltransferase (encoding gene, cg3361)
TrpD	Anthranilate phosphoribosyltransferase
T_{rrnB}	Terminator of the *E. coli rrnB* operon
tuf	Elongation factor EF-TU (encoding gene, cg0587)
UMP	Uridine monophosphate
UV	Ultraviolet
V	Volume
VAAM	Vereinigung für Allgemeine und Angewandte Mikrobiologie
Val	L-Valine
vs.	Versus
vvm	Volume per volume per minute
WGS	Whole genome sequencing
WT	Wild type
$_X$	Biomass (superscript)
XMP	Xanthosine monophosphate
y_{CO2}	Exhaust gas CO_2 part
y_{O2}	Exhaust gas O_2 part
$Y_{P/S}^{gly}$	Product/substrate yield for glycine
$Y_{P/S}^{his}$	Product/substrate yield for L-histidine
$Y_{X/S}$	Biomass/substrate yield

Abbreviation	Description
ZMP	Other name for AICAR
ZTP	5-amino-4-imidazolecarboxamide riboside 5triphosphate
zwf	SU of the glucose 6-phosphate dehydrogenase (encoding gene, cg1778)
α	CDW/OD_{600} correlation coefficient
α-KG	α-ketoglutarate
Δ	Delta (indicating gene deletions)

SUMMARY

Corynebacterium glutamicum is an established industrial host for large scale fermentations of several different products, most famously the amino acids L-glutamate and L-lysine. Its in-depth investigated metabolism is a driving force that enables synthesis of a wide range of products and constitutes a basis for the substitution of established petroleum-based processes by microbial fermentation processes with *C. glutamicum* as host. This work expands and consolidates the spectrum of *C. glutamicum* products by focusing on the two amino acids L-histidine (PART I) and L-valine (PART II).

PART I. In the first part of this thesis, *C. glutamicum* was engineered in a modularized metabolic engineering approach with LC/MS-QToF based systems metabolic profiling (SMP) and Flux Balance Analysis (FBA) for production of the amino acid L-histidine. This constitutes the first holistic, systems-based approach to develop L-histidine producing strains with *C. glutamicum*. Initially, L-histidine biosynthesis was tailored by introduction of a mutated variant of ATP phosphoribosyltransferase, the first enzyme in the pathway, which was released from feedback inhibition by L-histidine. Replacement of native promoters in front of the four operons containing L-histidine genes and of one internal promoter by stronger ones enabled the resulting strain *C. glutamicum* HIS7 to achieve a product yield of 0.066 ± 0.003 mol L-histidine per mol glucose. The strain additionally secreted equimolar amounts of glycine. HPLC analysis revealed heavily decreased intracellular adenylate concentrations as low as 6.6 ± 0.3 µmol ATP g_{CDW}^{-1}, 1.8 ± 0.1 µmol ADP g_{CDW}^{-1}, and AMP concentrations being below the detection limit of the applied system, compared to the *C. glutamicum* wildtype strain where adenylate concentrations were 15.7 ± 0.4 µmol ATP g_{CDW}^{-1}, 6.0 ± 0.6 µmol ADP g_{CDW}^{-1}, and 2.1 ± 0.8 µmol AMP g_{CDW}^{-1}. Despite the adenylate energy charge was stable. FBA identified ATP regeneration, required as energy source and as L-histidine backbone donor, as a crucial step for L-histidine production. Moreover, SMP of the engineered strains identified strong

intracellular accumulations of inosine monophosphate (IMP; 43× increased peak intensities) and adenylosuccinate (2× increased peak intensities) compared to the WT, which were solved by plasmid-based overproduction of the purine biosynthesis enzymes PurA and PurB. The resulting strain *C. glutamicum* HIS8 did not improve the product yield but readjusted the intracellular IMP, adenylosuccinate, and ATP levels to WT level and reinforced the intrinsic low ATP regeneration capacity to maintain a balanced energy state of the cell. Furthermore, SMP in *C. glutamicum* HIS8 indicated limitations in the supply with C_1 units essentially required for purine biosynthesis. Additional plasmid based production of the glycine cleavage (GCV) system from *C. jeikeium* accounted for the increased need for C_1 units and increased the yield to 0.086 ± 0.001 mol L-histidine per mol glucose. Finally, to increase phosphoribosyl pyrophosphate availability, we rerouted the carbon flux towards the oxidative pentose phosphate pathway by replacing the native translational start codon ATG of the phosphoglucoisomerase to GTG. This final strain *C. glutamicum* HIS10 showed a further increased product yield of 0.093 ± 0.003 mol L-histidine per mol glucose. In addition to these strains, several further strains were generated, focussing on pentose phosphate pathway and purine biosynthesis genes/enzymes, and characterized that might help unravelling efficient L-histidine overproduction with *C. glutamicum*. Selected strains were then used to establish a seed train for preliminary bioprocess studies in different laboratory scales in glass and steel tank reactors. These studies comprised investigations of the influencing factors pH, oxygen supply, and medium composition and provide the basis for future investigations.

PART II. In the second part of this work, we developed an evolutionary approach and evolved *C. glutamicum* strains that were suitable for L-valine production. Evolutionary approaches are often undirected and mutagen-based and result in strains with hundreds of mutations. We here developed and applied Metabolic engineering to Guide Evolution (MGE), an evolutionary approach enabling the identification of new targets to improve microbial producer strains. MGE is based on the idea to impair the cell`s metabolism by metabolic engineering, thereby generating guided evolutionary pressure. It consists of three distinct phases: (i) metabolic engineering to create the evolutionary pressure on the applied strain followed by (ii) a cultivation phase with growth as straightforward screening indicator for the evolutionary event, and (iii) comparative whole genome sequencing (WGS), to identify mutations in the evolved strains, which are eventually re-engineered for verification. Applying MGE, we evolved the PEP and pyruvate carboxylase deficient strain *C. glutamicum* Δ*ppc* Δ*pyc* to grow on glucose as substrate with rates up to 0.31 ± 0.02 h^{-1} which corresponds to 80% of the growth rate of the

wildtype strain. The intersection of the mutations identified by WGS revealed isocitrate dehydrogenase (ICD) as consistent target in three independently evolved mutants. Upon re engineering in *C. glutamicum* Δ*ppc* Δ*pyc*, the identified mutations led to diminished ICD activities (10%, 29%, and 55% of the native enzyme) and activated the glyoxylate shunt replenishing oxaloacetate required for growth. This manifested in isocitrate lyase activities of 0.33 ± 0.06, 0.32 ± 0.05, and 0.53 ± 0.07 U (mg protein)$^{-1}$ and malate synthase activites of and 0.44 ± 0.07, 0.42 ± 0.08, and 0.39 ± 0.03 U (mg protein)$^{-1}$, both inactive in *C. glutamicum* WT under the tested conditions. SMP analysis showed that the pools of citrate (fold change[FC]+12.1), isocitrate (FC+6.4), *cis*-aconitate (FC+13.2), and L-valine (FC+1.9) were significantly higher compared to *C. glutamicum* WT. As an alternative to existing L-valine producer strains based on inactivated or attenuated pyruvate dehydrogenase complex, we finally engineered the PEP and pyruvate carboxylase deficient *C. glutamicum* strains with identified ICD mutations for L-valine production by overexpression of the L-valine biosynthesis genes. Among them, *C. glutamicum* Δ*ppc* Δ*pyc* ICD^{G407S} (pJC4*ilvBNCE*) produced up to 8.9 ± 0.4 g L-valine L^{-1}, with a product yield of 0.22 ± 0.01 g L-valine per g glucose. By applying MGE, we evolved a PEPCx- and PCx-deficient strain to grow on a glycolytic substrate and identified an alternative mode for L-valine production with C. glutamicum that represents a suitable alternative to already existing production strains.

ZUSAMMENFASSUNG

Corynebacterium glutamicum ist ein bewährter Wirtsorganismus der Industrie für großskalige Fermentationen zur Herstellung diverser Produkte, darunter die Aminosäuren L-Glutamat und L-Lysin. Der detailliert untersuchte Metabolismus stellt eine treibende Kraft dar, die die Synthese einer breiten Palette an Produkten, die von industriellem Interesse sind, ermöglicht. Auf dieser Basis ist es möglich Erdöl-basierte Verfahren durch mikrobielle Fermentationsprozesse mit *C. glutamicum* als Wirt zu ersetzen. Die in der vorliegenden Arbeit präsentierten Ergebnisse festigen und erweitern das Spektrum der Produkte, das mit *C. glutamicum* synthetisierbar ist. Der Fokus liegt hierbei auf den beiden Aminosäuren L-Histidin (PART I) und L-Valin (PART II).

PART I. Im ersten Teil der vorliegenden Arbeit wurde *C. glutamicum* in einem modularisierten Metabolic Engineering-Ansatz mit Unterstützung einer LC/MS-QToF Plattform (Systems metabolic profiling) und Flux Balance Analysis (FBA) für die Produktion von L-Histidin optimiert. Dies stellt den ersten holistischen und systembasierten Ansatz dar, L-Histidin-produzierende Stämme mit *C. glutamicum* als Basis zu erzeugen. In einem ersten Schritt wurde die L-Histidinbiosynthese durch die Implementierung einer mutierten Variante der ATP-Phosphoribosyl-Transferase, dem ersten Enzym in der L-Histidinbiosynthese, verbessert, indem dieses von der Enzymhemmung durch L-Histidin befreit wurde. Der Austausch der nativen Promotoren der vier Operons, die L-Histidingene enthalten, sowie der Austausch eines internen Promotors durch stärkere Promotoren, führte zu einem Produktertrag von 0.066 ± 0.003 mol L-Histidin pro mol Glucose im resultierenden Stamm *C. glutamicum* HIS7. Zusätzlich zum Produkt L-Histidin sekretierte dieser Stamm äquimolare Mengen an Glycin. Mittels HPLC-Analyse konnte gezeigt werden, dass die intrazellulären Konzentrationen der Adenylate in den erzeugten Stämmen deutlich niedriger waren, als im Ausgangsstamm. Dies spiegelte sich in den niedrigeren Werten von 6.6 ± 0.3 µmol ATP g_{CDW}^{-1} und 1.8 ± 0.1 µmol ADP g_{CDW}^{-1} wider. Darüber hinaus lagen die Konzentrationen von AMP in allen L-Histidin-produzierenden Stämmen unterhalb des Detektionslimits des eingesetzten Systems. Trotz der

veränderten absoluten Werte der Adenylate blieb der Wert für die Energieladung (Energy charge) stabil. Erstellte FBAs identifizierten die Regeneration von ATP, welches sowohl verantwortlich für die Bereitstellung von Energie, als auch des Kohlenstoffgerüsts in der ersten Reaktion der Histidinbiosynthese ist, als einen wichtigen Schritt der L-Histidinproduktion. Durchgeführtes SMP der Produktionsstämme identifizierte deutliche intrazelluläre Akkumulationen von Inosinmonophosphat (IMP; 43-fach erhöhte peak intensitites) und Addenylosuccinat (2-fach erhöhte peak intensitites), im Vergleich zum *C. glutamicum* WT. Diese Akkumulationen konnten durch die homologe plasmidbasierte Überproduktion der Enzyme PurA und PurB aus der Purinbiosynthese gelöst werden. Der daraus resultierende Stamm *C. glutamicum* HIS8 zeigte keinen höheren Produktertrag, er wies jedoch ähnliche Konzentrationen der Metabolite IMP und Adenylosuccinat wie der *C. glutamicum* WT auf, sowie eine erhöhte ATP-Konzentration, was auf eine Verstärkung der zuvor schwachen Kapazität zur ATP-Regeneration hindeutet, um so einen ausgeglichenen energetischen Zustand der Zelle unter den Produktionsbedingungen zu gewährleisten. SMP in *C. glutamicum* HIS8 deutete weitere Limitierungen in der Versorgung mit C_1-Körpern an, die zwingend für die Purinbiosynthese benötgt werden. Um dem entgegen zu wirken, wurde das heterologe glycine cleavage (GCV) System aus *C. jeikeium* mittels eines weiteren Plasmids produziert, was den Produktertrag auf 0.086 ± 0.001 mol L-Histidin pro mol Glucose steigerte. Um die Verfügbarkeit des Vorläufermoleküls Phosphoribosylpyrophosphat zu verbessern, wurde zusätzlich der Kohlenstofffluss in Richtung des oxidativen Zweigs des Pentosephosphatwegs verbessert, indem das native Startcodon der Glucose-6-Phosphat-Isomerase von ATG zu GTG getauscht wurde. Der resultierende Stamm *C. glutamicum* HIS10 zeigte einen gesteigerten Produktertrag von 0.093 ± 0.003 mol L-Histidin pro mol Glucose. Zusätzlich zu diesen Stämmen, wurden weitere Stämme erstellt und charakterisiert, die unter anderem Veränderungen im Pentosephosphatweg und der Purinbiosynthese aufweisen. Das dadurch erhaltene Wissen kann in künftigen Experimenten eine weitere Steigerung der L-Histidinproduktion mit *C. glutamicum* ermöglichen. Ausgewählte Stämme wurden dazu eingesetzt, eine Animpfschiene für vorläufige Bioprozesstudien in Glas- und Stahlreaktoren (0,2 – 10 L Arbeitsvolumen) zu etablieren. In diesen Studien, welche die Basis für künftige Bioprozessstudien bilden, wurden die Einflussfaktoren pH-Wert, Sauerstoffversorgung und Medienzusammensetzung näher untersucht.

PART II. Der zweite Teil der vorliegenden Arbeit beschäftigte sich mit der Entwicklung eines neuen Evolutionsansatzes, mit dessen Hilfe Stämme auf Basis von *C. glutamicum* erzeugt

werden konnten, die sich für die Produktion von L-Valin eignen. Herkömmliche Evolutionsansätze sind oft ungerichtet und basieren auf Mutagenen, weshalb sie häufig in einer Vielzahl von Mutationen im Erbgut des Ausgangsstamms resultieren. Der neu entwickelte Ansatz mit dem Namen Metabolic Engineering to Guide Evolution (MGE) wird hier ein Evolutionsansatz präsentiert, der die Identifikation von neuen Angriffspunkten und die Verbesserung mikrobieller Produktionssysteme ermöglicht. MGE basiert auf der Idee den Metabolismus der Zelle durch Deletionen mittels Metabolic Engineering zu beeinträchtigen, um so gezielt Evolutionsdruck zu erzeugen. MGE besteht aus den nachfolgenden drei Phasen: (i) die Anwendung von Metabolic Engineering um Evolutionsdruck zu erzeugen, gefolgt von (ii) einer Kultivierungsphase, in der das Wachstum als simpler Indikator für eine erfolgte Evolution fungiert, und (iii) vergleichendes Whole Genome Sequencing (WGS), um Mutationen im Genom der evolvierten Stämme im Vergleich zum Wildtyp-Stamm zu identifizieren. Dies ermöglicht den Transfer der auf diesem Weg identifizierten Mutationen in den Ausgangsstamm und eine anschließende Evaluierung der Mutationen. Durch die Anwendung von MGE konnte der Stamm *C. glutamicum* Δ*ppc* Δ*pyc*, welcher Deletionen der Gene, die für die Pyruvat- und Phosphoenolpyruvatcarboxylase kodieren, enthält, evolvieren, sodass dieser mit Glucose als einziger Kohlenstoffquelle wachsen konnte. Die Wachstumsrate des resultierenden Stamms betrug $0.31 \pm 0.02\ h^{-1}$, was 80% der Wachstumsrate des *C. glutamicum* WT entspricht. Die Schnittmenge der Mutationen, die durch WGS identifiziert werden konnten, zeigte die Isocitratdehydrogenase (ICD) als gemeinsames Ziel in den drei evolvierten Stämmen. Die ICD-Mutationen führten nach Einbringung in den Ausgangsstamm *C. glutamicum* Δ*ppc* Δ*pyc* zu geringeren Aktivitäten der ICD (10%, 29% und 55% des nativen Enzyms) und aktivierten den Glyoxylatzyklus, der Oxalessigsäure für das Wachstum bereitstellte. Die Aktivierung des Glyoxylatzyklus zeigte sich in detektierbaren Aktivitäten der Isocitratlyase von 0.33 ± 0.06, 0.32 ± 0.05 und 0.53 ± 0.07 U (mg Protein)$^{-1}$ und der Malatsynthase von 0.44 ± 0.07, 0.42 ± 0.08 und 0.39 ± 0.03 U (mg Protein)$^{-1}$. Für beide Enzyme ist bekannt, dass sie inaktiv in *C. glutamicum* WT bei den hier getesteten Bedingungen sind. Die Analyse mittels SMP zeigte, dass die intrazellulären Pools von Citrat (fold change[FC]+12.1), Isocitrat (FC+6.4), *cis*-Aconitat (FC+13.2) und L-Valin (FC+1.9) im Vergleich zu *C. glutamicum* WT deutlich erhöht waren. Schließlich wurden die erstellten Stämme für die Produktion der Aminosäure L-Valin eingesetzt, um als Alternative zu den verfügbaren Valinproduzenten, die auf einer Inaktivierung oder Abschwächung des Pyruvatdehydrogenasekomplexes basieren, zu fungieren. Um den Kohlenstofffluss in Richtung

L-Valinbiosynthese zu verstärken, wurde das Plasmid pJC4*ilvBNCE* eingesetzt, das die wichtigen Gene zur Valinproduktion enthält. Unter den Produzenten zeigte *C. glutamicum* Δ*ppc* Δ*pyc* ICD^{G407S} (pJC4*ilvBNCE*) die höchste Produkkonzentration mit 8.9 ± 0.4 g L-Valin L^{-1}, was einem Produktertrag von 0.22 ± 0.01 g L-Valin pro g Glucose entspricht. Durch die erfolgreiche Anwendung von MGE, konnte ein Stamm mit Deletionen der Gene, die für die Pyruvat- und Phosphoenolpyruvatcarboxylase kodieren, evolviert werden. Dieser Stamm konnte mit Glucose als einziger Kohlenstoffquelle wachsen. MGE ermöglichte darüber hinaus die Identifizierung eines neuartigen Modus für die Produktion von L-Valin mit *C. glutamicum*, welcher auf ICD Mutationen basiert und eine geeignete Alternative zu bereits bestehenden Produktionsweisen repräsentiert.

CHAPTER 1: INTRODUCTION

1.1. General introduction

1.1.1. *Industrial biotechnology*

Biotechnology in general is defined as a broad area of science that investigates living systems and the catalysts performing their intrinsic reactions, such as enzymes, to develop useful products. Biotechnology is an ancient realm and has been used and promoted by humans for generations, culminating in nowadays modern fields of biotechnology. These comprise major areas like health care (medical biotechnology), agriculture and crop production, environmental biotechnology, and industrial (i.e. non-food) biotechnology. Nowadays, the major areas can be divided in several subcategories, including blue biotechnology (marine applications), green biotechnology (agricultural processes), red biotechnology (medical processes), gold biotechnology (bioinformatics), yellow biotechnology (food production), gray biotechnology (environmental applications), violet biotechnology (law, ethics, and philosophy), brown biotechnology (Management of arid lands), dark biotechnology (warfare), and white biotechnology (industrial processes) (Kafarski, 2012).

The here presented work is anchored in the field of white biotechnology, also known as industrial biotechnology. The term industrial biotechnology thereby means the advanced application of biotechnology for the sustainable processing and production of (bio)chemical products of a wide range. Products that might be synthesized include chemicals and pharmaceuticals, human and animal nutrition products, textiles, energy-related products, polymers, and a steadily increasing number of products from other areas. An important and emphasized pillar of industrial biotechnology is the factor of sustainability, which is mediated by the aim to substitute established (petro)chemically-based processes by enzyme- and/or

microorganism-based processes, with renewable (re)sources as substrates, instead of relying on unlasting resources, such as petroleum. These substrates might not only include sustainable and renewable sources, such as plant material, but can also include waste streams, such as sugar containing agricultural byproducts (e.g. molasses). That implies that industrial biotechnology, compared to petro-based processes, can not only promote resource conservation, but also mediates pollution prevention and cost reduction.

The underlying principle of industrial biotechnology are processes (either via fermentation or an enzymatic conversion) in which substrates are used to supply microorganisms with the nutrients they need to grow and produce the products of desire. Major fields to establish such bioprocesses include metabolic engineering (to develop the producer strains), bioprocess engineering (to establish, maintain, and improve the bioprocess), systems biology (computational modelling of complex biological systems), and in an increasing manner synthetic biology (to create artificial biological systems with improved characteristics)

The concept of Metabolic engineering was coined by scientists like Jay Bailey, Jay D. Keasling, Jens Nielsen, and Gregory Stephanopoulos and is defined as "the science of rewiring the metabolism of cells to enhance production of native metabolites or to endow cells with the ability to produce new products" (Nielsen and Keasling, 2016).

1.1.2. *Corynebacterium glutamicum*

The here presented work relies on *Corynebacterium glutamicum*, a relevant industrial production hosts of the last decades and a model organism of industrial biotechnology. The organism was isolated in 1957 by Kinoshita and co-workers as *Micrococcus glutamicus* and became famous for its ability to produce larger quantities of the amino acid L-glutamate under biotin limited conditions (Kinoshita et al., 2004, 1958, 1957). Later, it was renamed and reclassified to its recent conventional name *C. glutamicum* and has been isolated from several different soil environments since then (Abe et al., 1967). It belongs to the phylum of Actinobacteria and to the order Actinomycetales, and thus is a close relative of other model organisms of microbiology/infectiology, such as *C. diphtheriae*, *C. jeikeium*, and a distant relative of *Mycobacterium tuberculosis* and *Streptomyces coelicolor* (Bentley et al., 2002; Cole et al., 1998; Hoskisson, 2018; Tauch et al., 2005). This gives rise to the opportunity to transfer the knowledge gained with *C. glutamicum* on its close and distant relatives, among them some with medical/clinical relevance, e.g. *M. tuberculosis* or *C. diphtheriae*. *C. glutamicum* is a

Gram-positive organism with GC-content of about 54% (Kalinowski et al., 2003). Its cell shape is described as coryneform (i.e. irregularly rod-shaped) and it has no flagellum, rendering it unable of chemotaxis. It further has been described as non-acid fast, biotin auxotrophic, catalase-positive, and facultatively anaerobic, meaning proliferation under anaerobic conditions is possible when nitrate as final electron acceptor is available (Nishimura et al., 2007) or when complex components are available (Michel et al., 2015). The cell wall of *C. glutamicum* as a Gram-positive organism is stable and is composed of lipophilic mycolic acids (Bayan et al., 2003; Burkovski, 2013; Lanéelle et al., 2013; Marienfeld et al., 1997). The optimal growth temperature has been established to be around 30 °C and the pH optimum has been reported to range between 7.0 and 9.0 (Barriuso-Iglesias et al., 2008). Growth of *C. glutamicum* has been described as moderate, growing with rates of μ_{max} of up to 0.58 h^{-1} and 0.46 h^{-1} in minimal medium with D-glucose as carbon source (Bäumchen et al., 2007; Grünberger et al., 2012). Besides glucose, *C. glutamicum* can take up and use several other carbon sources, including other sugars, e.g. fructose, sucrose, mannose, and ribose, acids, e.g. acetate, lactate, and pyruvate, and alcohols, e.g. ethanol (Eggeling and Bott, 2005). Interestingly, unlike other organisms such as *E. coli*, *C. glutamicum* shows only very few examples of catabolite repression (Arndt and Eikmanns, 2007; Brückner and Titgemeyer, 2002; Görke and Stülke, 2008).

The most commonly deployed *C. glutamicum* strains were termed ATCC 13032 and R and of both the genome sequence has been published (Ikeda and Nakagawa, 2003; Kalinowski et al., 2003; Yang and Yang, 2017; Yukawa et al., 2007). The status as *generally recognized as safe* (GRAS) organism has opened a door for *C. glutamicum* to become a frequently deployed production host and intense investigations over several decades have generated vast knowledge of this organism, enabling the development of a broad range of genetic and metabolic engineering tools (Baritugo et al., 2018; Kirchner and Tauch, 2003; Nešvera and Pátek, 2011).

1.1.3. *C. glutamicum – central metabolism*

Since the here presented work mainly utilizes processes with D-glucose as the sole carbon source, the central metabolism of *C. glutamicum* will be introduced in the following with a focus on glucose-based growth.

When growing on the sugars glucose, fructose, or sucrose, the sugar is taken up specifically by the cell via a phosphoenolpyruvate (PEP) -dependent phosphotransferase system (PTS) and is,

during this process, subsequently phosphorylated. The PTS thereby operates by transferring a phosphoryl group from PEP onto the respective sugar-specific EII permease, which is catalysed by the PTS components EI, encoded by *ptsI*, and HPr, encoded by *ptsH* (Parche et al., 2001). An EII permease then transports the respective sugar into the cell, concomitantly phosphorylating it (Lengeler et al., 1994). For the three introduced sugars, the *C. glutamicum* genome encodes the specific EII permeases EII^{Glc} (encoded by *ptsG*), EII^{Fru} (encoded by *ptsF*), and EII^{Suc} (encoded by *ptsS*) for the uptake of glucose, fructose, and sucrose, respectively (Dominguez and Lindley, 1996; Kiefer et al., 2004, 2002; Moon et al., 2007, 2005).

Glucose 6-phosphate is then either channelled into glycolysis or pentose phosphate pathway (PPP). Both of them have been intensively investigated in *C. glutamicum* with enzymatic studies, genetic analysis, carbon flux analysis, and genome-wide studies in the last decades and profound reviews are available (Blombach and Seibold, 2010; Eikmanns, 2005; Sauer and Eikmanns, 2005; Yokota and Lindley, 2005).

Glucose 6-phosphate that enters the glycolytic pathway is then converted in several enzymatic steps to pyruvate. The overall reaction of glycolysis is

D-glucose + $2\times NAD^+$ $+2\times ADP$ $+2\times P_i$ → $2\times$pyruvate $+2\times NADH$ $+2\times H^+$ $+2\times ATP$ $+2\times H_2O$,

showing glycolysis' main functions besides supplying precursors for anabolism: converting the free energy released by the oxidation steps from glucose to pyruvate to generate the high energy compounds ATP and reduced NADH (Yokota and Lindley, 2005).

The PPP is separated into two parts (for an overview see Eggeling and Bott, 2005 and Yokota and Lindley, 2005). The first one is the oxidative branch, where glucose-phosphate stepwise is converted towards ribulose 5-phosphate and reducing equivalents in the form of NADPH are generated. These serve as reducing power for reductive reactions for the synthesis of cellular building blocks. Glucose 6-phosphate is converted to 6-phosphogluconolactone via the NADPH-generating reaction of the glucose 6-phosphate dehydrogenase (G6P DH, encoded by *zwf* and *opcA*) in a first step, which is then further converted to 6-phosphogluconate via the reaction of the 6-phosphogluconolactonase (encoded by *pgl*). Another NADPH-generating reaction, namely the 6-phosphogluconate dehydrogenase (6PG DH, encoded by *gnd*), then converts 6-phosphogluconate to ribulose 5-phosphate (Moritz et al., 2000), which is then converted to ribose 5-phosphate via the phosphopentose isomerase (encoded by *rpi*). Following this, the reaction of the PRPP synthetase takes place, converting ribose 5-phosphate to the crucial L-histidine precursor PRPP (see 1.2.2 L-HISTIDINE biosynthesis – structure and regulation, p.11).

In the second part of the PPP, the non-oxidative (reductive) branch, interconversions of five carbon sugars is conducted, to generate ribose 5-phosphate (for e.g. nucleic acid synthesis) and erythrose 4-phosphate (for e.g. aromatic amino acids synthesis). Important enzymes that catalyse the underlying reactions comprise transaldolase (Tal, encoded by *tal*) and transketolase (Tkt, encoded by *tkt*). The latter reshuffles the excess of phosphorylated sugars that originates in the PPP into glycolysis. Tkt mediates two reactions: (i) xylulose 5-phosphate + ribose 5-phosphate ↔ sedoheptulose 7-phosphate + glyceraldehyde 3-phosphate and (ii) xylulose 5-phosphate + erythrose 4-phosphate ↔ fructose 6-phosphate + glyceraldehyde 3-phosphate.

The overall reaction considering both the oxidative and the non-oxidative part of the PPP thus is 3×glucose 6-phosphate + 6×$NADP^+$ + 3×H_2O → 2×fructose 6-phosphate + glyceraldehyde 3-phosphate + 6×NADPH + 6×H^+ + 3×CO_2.

The ratio in which glycolysis and PPP are supplied with carbon depends on different factors. It has been shown that under aerobic growth conditions about 69% of the carbon is channelled in the PPP (Bartek et al., 2011). However, when the growth conditions proceed anaerobically, the PPP is close to inactive with only about 5% of carbon being channelled into PPP (Radoš et al., 2014).

The pyruvate that is generated in glycolysis is further converted via the pyruvate dehydrogenase complex (PDHC), a multi-enzyme complex consisting of the subunits pyruvate decarboxylase (E1), dihydrolipoamide acyltransferase (E2), and lipoamide dehydrogenase (E3). This complex catalyses the oxidative decarboxylation of pyruvate to acetyl-coenzyme A (CoA), subsequently generating NADH from NAD^+ (Eikmanns and Blombach, 2014). The PDHC has been identified and deployed as an attractive target for metabolic engineering with focus on different products in *C. glutamicum*, among these L-valine

The acetyl-CoA that is generated via the PDHC is then further converted in the tricarboxylic acid (TCA) cycle and completely oxidised to CO_2 (Bott and Eikmanns, 2013). It is active regardless of the carbon source and supplies the cell with energy in the form of ATP and reducing equivalents in the form of NADH and NADPH. The TCA is a highly dynamic cycle of metabolite conversions, which adjusts its enzymatic activities according to the environmental situation, e.g. according to available carbon source(s). Its overall reaction in *C. glutamicum* is given by Acetyl-CoA + NAD^+ + $NADP^+$ + 2×MQ + ADP + P_i + 2×H_2O → 2×CO_2 + NADH + NADPH + 2×MQH_2 + ATP + CoA-SH. One of TCA cycle's tasks is the provision of metabolites for the several biosynthetic pathways. These intermediates are

regularly withdrawn from the cycle, requiring frequent replenishment. This task is taken over by the anaplerotic reactions around the PEP-pyruvate-oxaloacetate node (Sauer and Eikmanns, 2005) and will be discussed in detail below (1.3.3 Anaplerotic reactions in *C. glutamicum*, p.30).

1.1.4. *C. glutamicum as industrial host*

Owing to its ability to produce larger quantities of the amino acid L-glutamate combined with increasing interest in monosodium glutamate (MSG) in the food culture of Japan, *C. glutamicum* got special attention (Scanning electron microscopy pricture shown in Fig. **1**, p.7). Despite L-glutamate being a non-essential amino acid for humans, the rise of its industrial production is strongly connected with the fact that it binds to *umami* (one of the five basic tastes, besides sour, sweet, bitter, and salty) receptors and is able to intensify the flavour of foods (Löliger, 2000; Yamaguchi, 1991). The development of the MSG industry, especially in Japan, continues until today and L-glutamate is produced with *C. glutamicum* in quantities of up to 3 million tonnes per year in 2015 (Ajinomoto Co., 2016). Besides L-glutamate, *C. glutamicum* has been intensively exploited for production of L-lysine, with quantities of above 2 million tonnes per year (Ajinomoto Co., 2016). Global players like Ajinomoto Co. (https://www.ajinomoto.com/) and Evonik Industries AG (https://corporate.evonik.de/de/) are participating in this field.

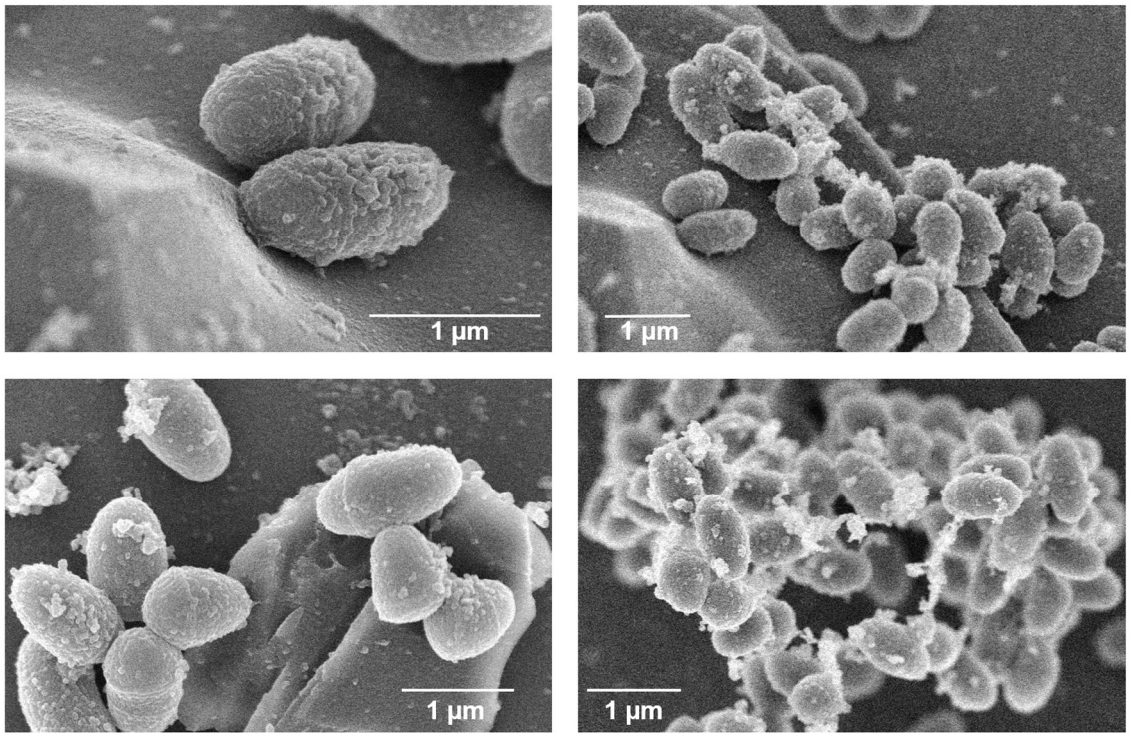

Fig. 1. Scanning electron microscopy pictures of *C. glutamicum* growing on different sorts of starch. Kindly provided by Tobias Hahn (University of Ulm), unpublished.

Meanwhile, despite still being especially famous for L-glutamate and L-lysine production, the portfolio of amino acids that *C. glutamicum* can produce has been expanded drastically, spanning almost all 20 proteinogenic amino acids. Besides the mentioned L-glutamate and L-lysine, studies (only a small selection of the available studies is given) for producing the following **L-amino acids** are available: L-alanine (Jojima et al., 2010), L-arginine (Jensen et al., 2015; Park et al., 2014), L-aspartate (Kalinowski et al., 2003), L-cysteine (Joo et al., 2017), L-glutamine (Liu et al., 2008), L-histidine (Kulis-Horn et al., 2015), L-isoleucine (Vogt et al., 2014b), L-leucine (Vogt et al., 2014a), L-methionine (Ying Li et al., 2016), L-phenylalanine (Zhang et al., 2015) , L-proline (Jensen et al., 2015), L-serine (Zhang et al., 2018), L-threonine (Wei et al., 2018), L-tryptophan (Ikeda and Katsumata, 1999), L-tyrosine (Ikeda and Katsumata, 1992), and L-valine (Oldiges et al., 2014).

Besides the proteinogenic amino acids, *C. glutamicum* has also been engineered to produce **non-proteinogenic amino acids**, such as L-ornithine and L-citrulline (Hwang et al., 2008; Jensen et al., 2015) and D-amino acids, such as D-serine and D-lysine (Stäbler et al., 2011).

Despite being particularly established as amino acids producer, *C. glutamicum* has been engineered to produce a wide range of products besides amino acids. Among these are

organic acids, such as pyruvate (Wieschalka et al., 2012), succinate (Litsanov et al., 2013), α-ketoglutarate (Li et al., 2016), 2-ketoisovalerate (Krause et al., 2010), and 2-ketoisocaproate (Bückle-Vallant et al., 2013), **alcohols**, such as ethanol (Jojima et al., 2014), isobutanol (Blombach et al., 2011), and 1,2-propanediol (Siebert and Wendisch, 2015), **vitamins**, such as pantothenate (Hüser et al., 2005),

The development of *C. glutamicum* to a production host being able to synthesize such a wide range of products is tightly connected with the steady increase of available metabolic engineering and systems biology tools (Nielsen and Keasling, 2016; Yadav et al., 2012) to targeted tailor *C. glutamicum* towards a certain product or group of products (a.k.a. platform organism). Further product groups comprise **carotenoids**, such as decaprenoxanthin and sarcinaxanthin (Heider et al., 2014), **diamines**, such as cadaverine (Mimitsuka et al., 2007) and putrescine (Nguyen et al., 2015), **fatty acids** (Takeno et al., 2013), and **polymers** and polymer-connected SUs, such as poly(3-hydroxybutyrate) (Jo et al., 2009) and 5-aminovaleric acid (Shin et al., 2016). Beyond these, the portfolio of *C. glutamicum* expands further in different product categories, including further natural and non-natural products (Becker and Wittmann, 2015, 2012; Heider and Wendisch, 2015)

The fact that *C. glutamicum* has been employed for the heterologous production of pharmaceutically relevant **proteins** (Freudl, 2017), finally emphasizes its relevance for industrial biotechnology.

As mentioned before, one of industrial biotechnology's advantages compared to competing petroleum-based processes, is the drawing on renewable resources as substrates for the microbial processes. However, these substrates often are rather heterologous than homologous substrates, making it in certain cases difficult to serve as fermentation substrates. Thus, production hosts are required to grow on a wide range of substrates, expanding from sugars over organic acids to alcohols. *C. glutamicum* has not only been engineered towards a wide product spectrum, but also towards a wide spectrum of substrates it can grow on, accounting the different available heterologous substrates originating from agricultural waste streams (Dahod et al., 2010; Mussatto et al., 2012). Besides the standardly used carbon source D-glucose (Pfeifer et al., 2017), *C. glutamicum* natively is able to grow on a variety of carbon sources, such as fructose (Kiefer et al., 2002), sucrose (Dominguez and Lindley, 1996), ribose (Wendisch, 2003), acetate (Gerstmeir et al., 2003), lactate (Bäumchen et al., 2007), mannose (Sasaki et al., 2011), ethanol (Arndt et al., 2008), and many more (for an overview see Eggeling and Bott, 2005).

Beyond natural substrates, the substrate spectrum of *C. glutamicum* has been expanded by metabolic engineering towards growth on non-native carbon sources, including arabinose (Kawaguchi et al., 2008), xylose (Buschke et al., 2013), starch (Seibold et al., 2006), galactose (Barrett et al., 2004), cellobiose (Adachi et al., 2013), and glycerol (Rittmann et al., 2008). In addition to the here listed substrates, pathways for many more have been implemented in *C. glutamicum* and the list is steadily increasing (Becker and Wittmann, 2015; Blombach and Seibold, 2010).

1.2. Introduction PART I

1.2.1. *L-Histidine*

Histidine exists as its two enantiomers L- and D-histidine, although the D-variant is physiologically irrelevant and is only accessible by chemical synthesis. Therefore, whenever the term histidine is used in this work, it relates to the L-enantiomer. Histidine was discovered in the late 19th century by Kossel and Hedin simultaneously (Vickery and Leavenworth, 1928) and the L-enantiomer is nowadays categorized as an essential amino acid for human infants and adults, belonging to the 20 standard proteinogenic amino acids (Kopple and Swendseid, 1975). Histidine contains an α-amino group, which is protonated under physiological conditions, a carboxylic acid group, which is deprotonated under physiological conditions, and an imidazole side chain, which is partially protonated under physiological conditions, classifying it as positively charged amino acid under these conditions (Nelson and Cox, 2009). Histidine as only representative of the 20 proteinogenic amino acids can switch between the protonated and unprotonated state due to the pK_a of about 6 of its imidazole group (Nelson and Cox, 2009).
These characteristics enable histidine to be a common ligand in metalloproteins and play an important role if the catalytic triad in several enzymes, underlining its physiologically prominent role (Liao et al., 2013; Polgár, 2005; Rebek, 1990). Histidine is connected to several diseases and exceeding physiological levels of histidine in humans was demonstrated to be connected to mutations in histidase. This disorder is formerly known as histidinemia, a benign inborn error of metabolism (Auerbach et al., 1962; Kawai et al., 2005).
Furthermore, histamine is produced from histidine by a single enzymatic step catalysed by histidine decarboxylase (Shahid et al., 2009). Histamine is a biogenic amine, which is known to play an important role in regulating human immune response and has been shown to be linked

to several allergic disorders, such as hay fever, allergic rhinitis, and urticaria (O'Mahony et al., 2011; Parsons and Ganellin, 2006).

Histidine has been reported to have several interesting effects, underlining its applicability in the medical and pharmaceutical sector: it has been shown to suppress inflammation and mediate insulin resistance (Feng et al., 2013), exhibit anti-inflammatory effect in monocytic leukemia and coronary arterial endothelial cells (Hasegawa et al., 2011; Hasegawa et al., 2012), to exhibit antioxidant properties by scavenging oxygen radicals (Wade and Tucker, 1998), to be effective against obesity in women (DiNicolantonio et al., 2018; Du et al., 2017), to potentially have beneficial effects against chronic cerebral hypoperfusion (Song et al., 2018), and to be connected with lowering blood pressure (Tuttle et al., 2012). Recently, it was reported that a diet rich in L-histidine is connected to increasing efficiency of the cancer treatment with the anti-cancer drug methotrexate, which was ascribed to histidine degradation (Frezza, 2018; Kanarek et al., 2018).

Beyond the medical sector, potential applications were suggested for the feed sector. Histidine supplementation was able to prevent cataract development in atlantic salmon (Waagbø et al., 2010). Further, histidine supplementation increased the formation of the histidine-containing dipeptides carnosine an anserine in the muscles of broilers, two metabolites that are connected to increased shelf-life, stability, and higher antioxidation capacity (Haug et al., 2008; Park et al., 2013).

In the food sector, L-histidine monochloride is already available as food supplementation product for health and muscle development, e.g. as used in body building (https://www.lambertshealthcare.co.uk/l-histidine-hcl-500mg-p8313/; last access 25-07.2018; https://www.bulkpowders.co.uk/histidine.html; last access 25-07.2018).

The physiological degradation of histidine is accomplished by an enzymatic system entitled histidine utilization (HUT) system, which is present in several prokaryotic and eukaryotic representatives and converts histidine to ammonia and L-glutamate (Bender, 2012). Interestingly, a HUT system is not encoded in the *C. glutamicum* genome, in contrast to the genomes of several other industrially relevant bacteria, such as *Pseudomonas putida* and *Bacillus subtilis* (Bender, 2012), which represents an advantage with respect to L-histidine production.

The Food and Nutrition Board (FNB) of the US Institute of Medicine has determined the recommended dietary allowance for L-histidine to be 14 mg per kg body weight per day for adults (https://www.nap.edu/read/10490/chapter/12, last access 25-07-2018). The World

Health Organisiation (WHO) suggested a daily requirement for adults to be 12 mg per kg (Wade and Tucker, 1998).

1.2.2. *L-Histidine biosynthesis – structure and regulation*

The biosynthetic pathway of the α-amino acid L-histidine has been investigated in prokaryotic representatives intensely during the past decades. These investigations mainly focused on the species *Salmonella enterica* serovar Typhimurium (*S. typhimurium*) and *E. coli* and several profound reviews are available on the molecular evolution of the pathway, structure and organisation of the participating genes and enzymes, and the underlying regulatory mechanisms (Alifano et al., 1996; Fani et al., 1995; Winkler and Ramos-Montañez, 2009). Besides bacteria, histidine biosynthesis has also been intensely studied in archaea (Fondi et al., 2009) and plants (Ingle, 2011).

Histidine biosynthesis has been a model pathway for studies of the relationship between the connections of carbon flux through a metabolic pathway and the regulatory component controlling the genes, gene products, and enzymes that are responsible for this flow. The role as a model pathway manifests for example in the contribution of the histidine pathway in understanding the mechanisms of basic regulation of biosynthetic pathways, such as feedback inhibition (of ATP phosphoribosyltransferase to L-histidine), the energy charge, and settings of enzyme levels. The histidine biosynthesis pathway contains several unusual and interesting metabolites and enzymatic steps and it is connected to several different other biosynthetic pathways, such as purine and thiamine biosynthesis (1.2.5 L-HISTIDINE related pathways, p.21).

Fundamental concepts of nowadays microbial physiology were investigated with the model pathway of histidine biosynthesis, such as the operon theory (e.g. Ames et al., 1961) or attenuation as a regulatory mechanism (Kasai, 1974) were first termed in relation to the histidine biosynthesis in *S. typhimurium* (Alifano et al., 1996). Description, investigation, and modification of the L-histidine biosynthesis in prokaryotic representatives has come a long way and since there is also valuable data published for the L-histidine biosynthesis in *C. glutamicum*, the following overview will mainly utilize these findings if not indicated otherwise (Kulis-Horn et al., 2014). Despite the basic L-histidine biosynthesis is the same in all living organisms, subtleties can vary strongly between different genera (Alifano et al., 1996).

In C. *glutamicum*, the biosynthetic L-histidine pathway consists of ten consecutive steps, starting with phosphoribosyl pyrophosphate (PRPP) and ATP as the two precursors for the first

reaction step (Fig. 2, p.13). Interestingly, PRPP is an important intermediate in several other pathways (reviewed in Hove-Jensen et al., 2016). The first step is catalysed by the ATP phosphoribosyltransferase HisG (encoded by *hisG*), which condensates ATP and PRPP to phosphoribosyl-ATP (PR-ATP), releasing pyrophosphate (PP_i). The ATP phosphoribosyltransferase has been shown to be the target of a potent allosteric feedback inhibition by L-histidine, which was investigated in detail in different organisms, among others in *Mycobacterium tuberculosis*, a close relative of *C. glutamicum* (Cho et al., 2003; Mizukami et al., 1994; Pacholarz et al., 2017; Pedreño et al., 2012). This feedback inhibition is of crucial importance, since it prevents the waste of the precursor molecules ATP and PRPP (Fig. 2, p.13). The enzyme in *C. glutamicum* has been characterized in detail and was shown to have a specific enzyme activity of 2.19 µmol min^{-1} mg^{-1} and Michaelis constants (K_m) of 0.08 mM for PRPP and 0.22 mM for ATP in glucose grown cells (Zhang et al., 2012), reflecting values obtained in *M. tuberculosis*, where K_m values are 0.26 mM for ATP and 0.05 mM for PRPP (Pedreño et al., 2012), and *E. coli*, where K_m values are 0.80 mM for ATP and 0.11 mM for PRPP (Tébar and Ballesteros, 1976). The second step is then performed by PR-ATP pyrophosphatase (HisE, encoded by *hisE*), an irreversible hydrolysis yielding phosphoribosyl-AMP (PR-AMP). Then, the purine ring of PR-AMP is opened by the action of the PR-AMP cyclohydrolase (HisI, encoded by *hisI*), releasing 1-(5-phosphoribosyl)-5-[(5-phosphoribosylamino) methylideneamino] imidazole-4 carboxamide (5'ProFAR). The fourth step is an internal redox reaction catalysed by 5'ProFAR isomerase (HisA, encoded by *hisA*), converting 5'ProFAR to 5-[(5-phospho-1-deoxyribulos-1-ylamino)methylideneamino]-1-(5-phosphoribosyl)imidazole-4-carboxamide (PRFAR).

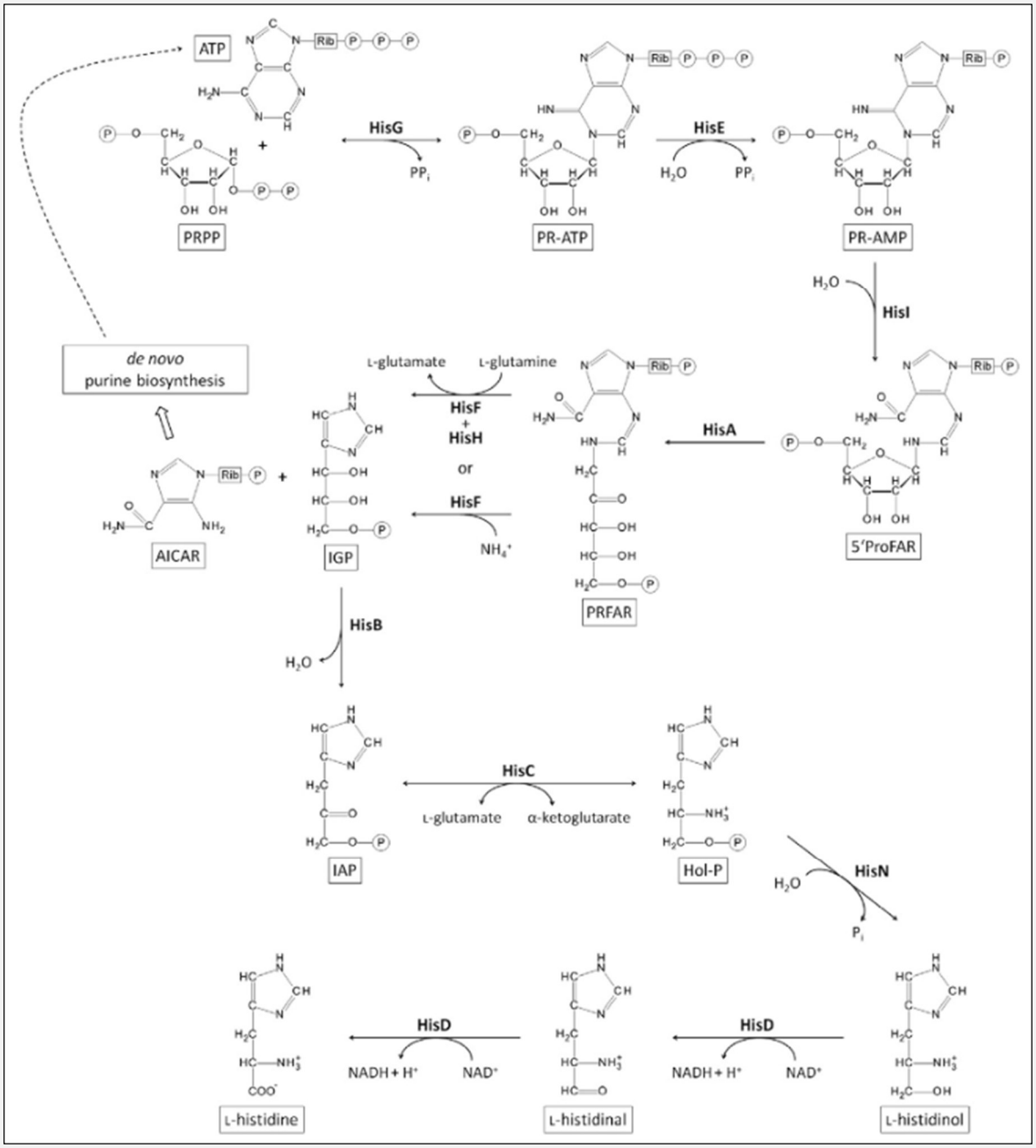

Fig. 2. Overview of the L-histidine biosynthetic pathway in *C. glutamicum*. Abbreviations: PRPP, phosphoribosyl pyrophosphate; ATP; adenosine triphosphate; PPi, pyrophosphate; PR-ATP, phosphoribosyl-ATP; PR-AMP, phosphoribosyl-AMP; 5′ProFAR, 1-(5-phosphoribosyl)-5-[(5-phosphoribosylamino)methylideneamino] imidazole-4 carboxamide; PRFAR, 5-[(5-phospho-1-deoxyribulos-1-ylamino)methylideneamino]-1-(5-phosphoribosyl)imidazole-4-carboxamide; IGP, imidazole-glycerol phosphate; AICAR, 1-(5′-phosphoribosyl)-5-amino-4-imidazolecarboxamide;IAP, imidazole-acetol phosphate; Hol-P, L-histidinol phosphate; Pi, phosphate; NAD+, oxidized nicotinamide adenine dinucleotide; NADH, reduced nicotinamide adenine dinucleotide; HisG, ATP phosphoribosyltransferase; HisE, phosphoribosyl-ATP pyrophosphatase; HisI, phosphoribosyl-AMP cyclohydrolase; HisA, 5′ProFAR isomerase; HisF, synthase SU of IGP synthase; HisH, glutaminase SU of IGP synthase; HisB, imidazoleglycerol-phosphate dehydratase; HisC, histidinol-phosphate aminotransferase; HisN, histidinol-phosphate phosphatase; HisD, histidinol dehydrogenase. **Taken from Kulis-Horn et al., 2014.**

The following step is performed by the imidazoleglycerol-phosphate synthase (IGP-synthase; HisFH, consisting of a synthase SU HisF and a glutaminase SU HisH; encoded by *hisF* and *hisH*, respectively). The roles of these two SUs in *C. glutamicum* has not yet been fully elucidated, however the gene product of *hisH* has been proven to be dispensable for histidine formation (in contrast to *hisA*,*B*,*C*,*D*,*E*,*F*,*G*,*I*) in *C. glutamicum* and plasmid based expression of *hisF* was shown to be able to complement both, a deletion of *hisF* and of *hisH*, respectively (Kulis-Horn et al., 2014). This reaction constitutes a link between the biosynthetic pathways of purines and histidine and results in two products, firstly IGP, which is channelled further towards L-histidine, and 1-(5′-phosphoribosyl)-5-amino-4-imidazolecarboxamide (AICAR), which is further converted in the *de novo* part of the purine biosynthesis. The sixth step in the histidine pathway is catalysed by the IGP dehydratase (HisB, encoded by *hisB*), which dehydrates IGP to the enol, which is then ketonized non-enzymatically to imidazole-acetol phosphate (IAP). IAP is then transaminated to L-histidinol phosphate (Hol-P) by histidinol-phosphate aminotransferase (HisC, encoded by *hisC*), using L-glutamine as amino donor and pyridoxal 5'-phosphate as cofactor (Marienhagen et al., 2008). The eighth step is catalysed by histidinol-phosphate phosphatase (HisN, encoded by *hisN*) that dephosphorylates Hol-P to L-histidinol (Mormann et al., 2006). Besides *hisH*, *hisN* is the only histidine gene in *C. glutamicum* that does not lead to a complete auxotrophy for histidine (Kulis-Horn et al., 2017, 2014). It has been shown that gene cg0911, encoding an enzyme with Hol-P phosphatase activity, can at least partially compensate a *hisN* deletion. Interestingly, cg0911 is part of one of the histidine operons in *C. glutamicum* (Fig. 3, p.15; Kulis-Horn et al., 2017). The final two steps of the L-histidine biosynthesis are then performed by the histidinol dehydrogenase (HisD, encoded by *hisD*), which first oxidizes L-histidinol to L-histidinal and further to L-histidine. HisD performs both reaction steps to prevent the instable L-histidinal intermediate from decomposing (Görisch and Hölke, 1985). During this reaction, two molecules of NAD^+ are reduced.

Based on a genome-scale model, one mol of L-histidine requires 9.4 mol ATP (Kulis-Horn et al., 2014). This value represents the third highest ATP demand of all 20 proteinogenic amno acids, only exceeded by those for L-arginine and L-tryptophan with 12.0 and 13.0 mol ATP per mol L-histidine, respectively (Kulis-Horn et al., 2014). One must keep in mind that the acquiration of the ATP backbone and its implementation into the first intermediate of the L-histidine biosynthesis is a unique feature of this reaction (see above) and does not occur in other amino acid biosynthesis pathways. In order to prevent energy loss, the histidine

biosynthesis requires stricr regulation. This regulation is not only mediated by a potent feedback inhibition of the ATP phosphoribosyltransferase by L-histidine, but also by transcriptional and translational mechanisms. On the transcriptional level, it has been demonstrated that operons *hisE*, *hisH*, and *hisD* are under positive control of the stringent response (Brockmann-Gretza and Kalinowski, 2006; Kulis-Horn et al., 2014). In *C. glutamicum* AS019, the 5' untranslated region (5'UTR) of the was demonstrated to be involved in transcriptional control of the respective operon (Jung et al., 2010). This regulation has not yet been confirmed for the shorter 5'UTR of the *hisD* operon in *C. glutamicum* ATCC 13032, however a translational control mechanism of this region was suggested (Kulis-Horn et al., 2014).

1.2.3. *Genomic organisation of the histidine genes*

The genomic organisation of the histidine genes in *C. glutamicum* ATCC 13032 has been investigated in detail and the following overview relies on published data if not indicated otherwise (Kulis-Horn et al., 2014). In *C. glutamicum* ATCC 13032 the histidine genes are organized in four operons, namely *hisE*-*hisG*, cg0911-*hisN*, *hisH*-*hisA*-*impA*-*hisF*-*hisI*-cg2294, and *hisD*-*hisC*-*hisB*-cg2302-cg2301 (Fig. 3, p.16) All histidine genes, except for *hisH*, have been shown to cause histidine auxotrophies upon deletion (*hisN* deletion leads to a strongly reduced growth). Apparently, these four transcriptional units not only contain histidine genes, but also protein-coding genes of other function (Fig. 3, p.16). Among these are cg2294, cg2301, and cg2302, whose functions have not yet been elucidated. Genes *impA* and cg0911 show high sequence similarities to *hisN* and might be connected to the strongly reduced growth phenotype of a Δ*hisN* strain. The operons containing cg0911 and *hisH* are transcribed as leaderless transcripts, meaning the transcription start is identical with the translation start, a rarely found phenomenon in Actinobacteria where about 20% of the genes are transcribed as leaderless transcripts (Zheng et al., 2011). The four operons are controlled by four primary promoters (P_{hisD}, P_{hisH}, P_{cg0911}, and P_{hisE}) and by four internal promoters (P_{hisB}, P_{hisA}, P_{hisF}, and P_{hisN}), the latter potentially reinforcing the expression of distal genes in larger operons to compensate for natural polarity or allowing temporary expression of certain genes of an operon (Alifano et al., 1996).

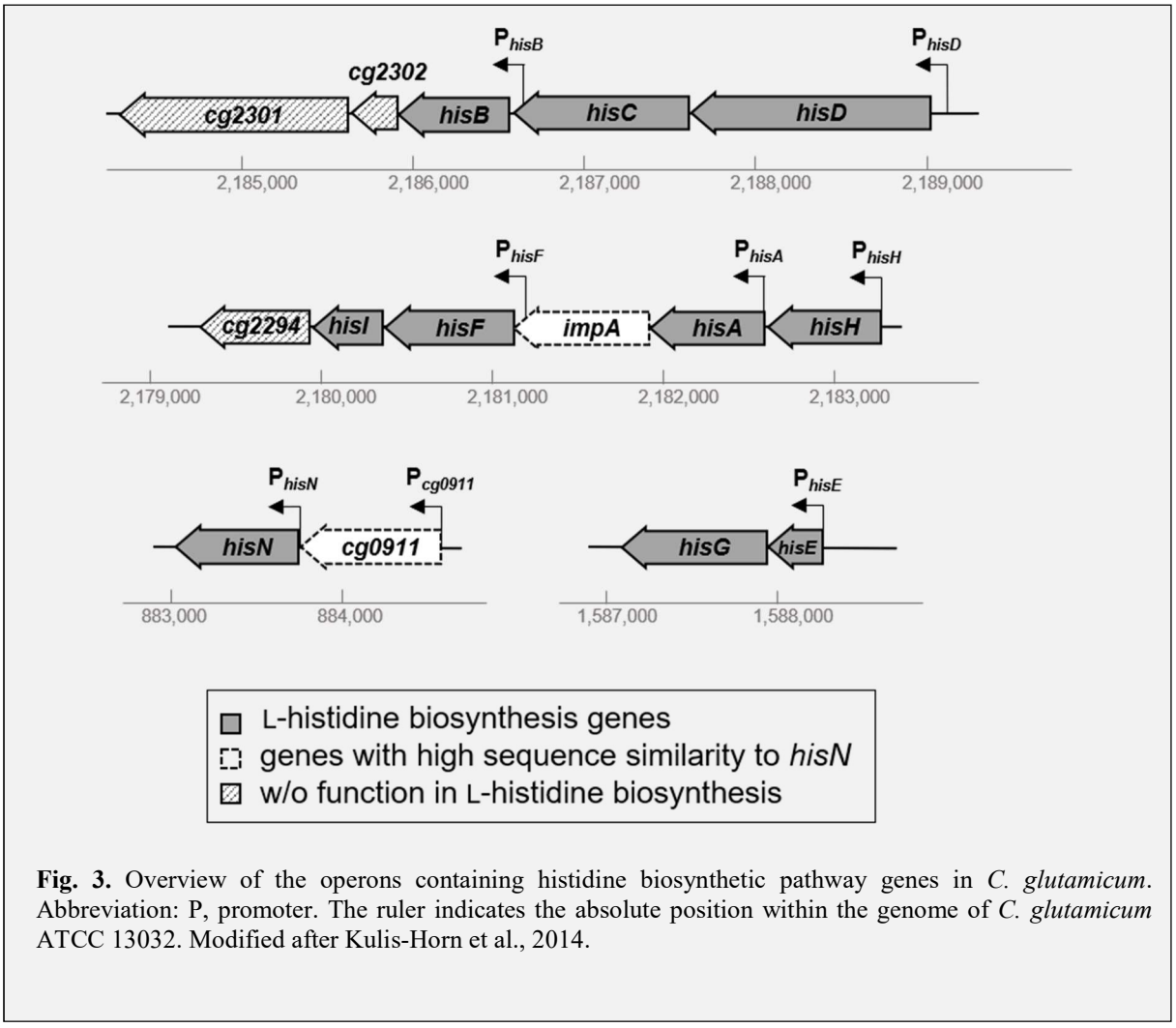

Fig. 3. Overview of the operons containing histidine biosynthetic pathway genes in *C. glutamicum*. Abbreviation: P, promoter. The ruler indicates the absolute position within the genome of *C. glutamicum* ATCC 13032. Modified after Kulis-Horn et al., 2014.

1.2.4. *Production of L-histidine*

Due to its properties, L-histidine is an attractive amino acid for the production in an industrial scale. Traditionally, L-histidine has been obtained via hydrolysis from proteins (Ikeda, 2003) or via the Strecker synthesis, a series of chemical reactions that synthesize an amino acid from an aldehyde or ketone (Harada, 1963; Shibasaki et al., 2008). With an increasing requirement for L-histidine due to its potential applications and the availability of techniques and methods to develop microbial producers, fermentation processes for the industrial scale production of L-histidine became interesting. In 2003, an estimated 400 t per year of L-histidine were produced annually via industrial fermentation processes, mainly applying *C. glutamicum* strains (in the past partially designated as *Brevibacterium flavum*) (Ikeda, 2003; Ivanov et al., 2013).

Examples for L-histidine producing strains in the literature are rare and solely focus on prokaryotic representatives. Despite investigations concerning elucidation of the L-histidine

biosynthetic pathways were mainly carried out in *S. typhimurium*, literature about L-histidine producer strains mainly focused on *C. glutamicum* (and related strains) and *E. coli*.

The classical L-histidine producing strains were obtained in the 1970s by mutagenizing *C. glutamicum* strains with NTG and focused on selecting mutants resistant to L-histidine analogues, such as 1,2,4-triazoelalanine and 2-thiazolealanine (Araki et al., 1974; Araki and Nakayama, 1971), investigations on the ATP phosphoribosyltransferase (Araki and Nakayama, 1974), and selecting for resistance markers for metabolites originating from histidine connected pathways, e.g. purines and pyrimidines (Araki et al., 1974). In further experiments, the production of L-histidinol from sugars by L-histidine auxotrophic strains of *C. glutamicum* (Araki and Nakayama, 1975) and related strains (Kubota et al., 1971) were investigated. Both produced quantities of L-histidinol, which were further converted to L-histidine by co-cultivating the L-histidinol producers either with *E. coli* or *C. glutamicum* strains, respectively (Araki and Nakayama, 1975; Kubota et al., 1971). In another approach, the ATP phosphoribosyltransferase from *C. glutamicum* was mutagenized with NTG and the plasmid-based overexpression of the resulting enzyme led to the accumulation of significant amounts of L-histidine upon fermentation with a mutagenized strain as host (Mizukami et al., 1994).

The invention and development of increasingly sophisticated techniques shifted the construction of microbial L-histidine producers from untargeted, mutagenesis approaches towards more targeted metabolic engineering approaches, with the ATP phosphoribosyltransferase and its feedback inhibition by L-histidine being in the focus. In an approach applying site directed mutagenesis, the enzyme was released from its feedback inhibition and the respective strain produced small amounts of L-histidine (Zhang et al., 2012). Another study of the ATP phosphoribosyltransferase comprising random mutagenesis and rational enzyme design underlined the potential of this target for L-histidine production (Kulis-Horn et al., 2015). Further metabolic engineering approaches in *C. glutamicum* comprised replacing the promoter of the gene *hisD* combined with the plasmid-based overexpression of genes *hisE* and *hisG*, which enabled production of L-histidine (Cheng et al., 2013).

Besides *C. glutamicum* strains, L-histidine production has also been investigated in *E. coli*, where the influence of the PRPP synthetase was studied. Mutant variants of the enzyme resistant to purine nucleotides were shown to be effective in L-histidine production (Klyachko et al., 2004b). Also, the overexpression of the *purH* gene, encoding the bifunctional

AICAR transformylase / IMP cyclohydrolase in *E. coli* has been reported to be beneficial for L-histidine production (Klyachko et al., 2004a). In a targeted metabolic engineering approach with *E. coli* the histidine feedback inhibition of ATP phosphoribosyltransferase was eliminated, an attenuator region was deleted, and the gene encoding the purine biosynthesis regulator protein PurR was deleted (Doroshenko et al., 2013). In a recent study with *E. coli*, the negative influence of AICAR on the ATP phosphoribosyltransferase was shown and construction of a strain overexpressing genes *purA* and *purH* led to improved AICAR to AMP recycling. Additional deletion of the *pitA* gene, encoding a transport system for inorganic phosphate, further proved beneficial for L-histidine production (Malykh et al., 2018). Other species that have been deployed for L-histidine production comprise *Serratia marcescens* and *Streptomyces coelicolor* via classical NTG treatment (Korajlija and Delíc, 1977). Beyond that, L-histidine production has been reported for regulatory mutants of *B. subtilits* (Jensen, 1969) and *S. typhimurium* (Sheppard, 1964), which were shown to excrete L-histidine into the medium.

Besides strain engineering, there are also studies on improving bioprocesses for L-histidine production available. Developed strategies with L-histidine producing *C. glutamicum* strains comprise establishment of a fed-batch process with optimized feed strategies, investigating boundary control of the growth rate, and proposing a separated growth and production phase for the process (Chim-Anage et al., 1991). The deployed carbon source for L-histidine production was investigated by using a metabolic flux pattern approach to evaluate glucose and acetate as substrates (Shimizu et al., 2002).

The manageable amount of available data for strains capable of L-histidine production indicates that the potential of this field has not yet been exploited. However, it also indicates the complexity of constructing microbial L-histidine producers.

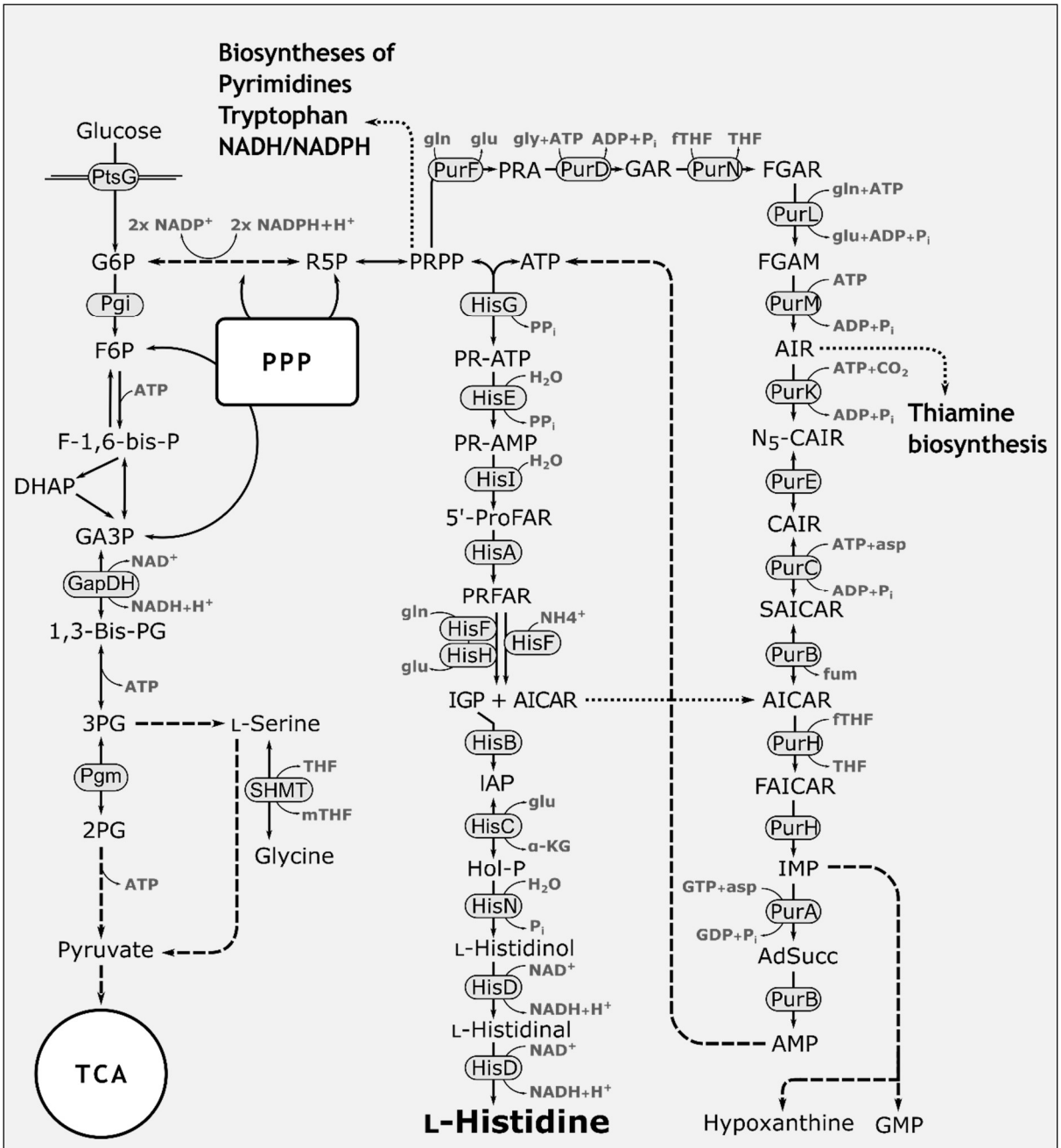

Fig. 4. Overview of the central carbon metabolism of *C. glutamicum* with focus on the histidine biosynthesis and the related pathways. Abbreviations: 2PG, 2-phosphoglycerate; 3PG, 3-phosphoglycerate; 5'-ProFAR, 1-(5-phosphoribosyl)-5-[(5-phosphoribosylamino) methylideneamino] imidazole-4 carboxamide; α KG, α-ketoglutarate; ADP, adenosine diphosphate; AdSucc, adenylosuccinate; AICAR, 1-(5′-phosphoribosyl)-5-amino-4-imidazolecarboxamide; AIR, 5-aminoimidazole ribotide; AMP, adenosine monophosphate; asp; L-aspartate; ATP, adenosine triphosphate; fTHF, 10-formyltetrahydrofolate; F-1,6-Bis-P, fructose-1,6-bisphosphate; F6P, fructose 6-phosphate; FAICAR, 5-formamidoimidazole-4-carboxamide ribotide; fGAM, 5'phosphoribosylformyl-glycineamidine; fGAR, phosphoribosyl-N-formylglcineamide; fum, fumarate; G6P, glucose 6-phosphate; GA3P, glyceraldehyde 3-phosphate; GAR, glycineamide ribonucleotide; GCV, glycine cleavage system; gln, L-glutamine; glu, L-glutamate; GMP, guanosine monophosphate; HisA, 5'ProFAR isomerase; HisB, imidazoleglycerol phosphate dehydratase; HisC, histidinol phosphate aminotransferase; HisD, histidinol dehydrogenase; HisE, phosphoribosyl-ATP pyrophosphatase; HisF, synthase subunit of IGP synthase; HisG, ATP phosphoribosyltransferase; HisH, glutaminase subunit of IGP synthase;

Legend Fig. 4. continued: HisI, phosphoribosyl-AMP cyclohydrolase; HisN, histidinol-phosphate phosphatase; Hol-P, L-histidinol phosphate; IAP, imidazole-acetole phosphate; IGP, imidazole-glycerol phosphate; IMP, inosine monophosphate; mTHF, 5,10-methylenetetrahydrofolate; N_5-CAIR, 5'-phosphoribosyl-4-carboxy-5-aminoimidazole; NAD^+/NADH, oxidized/reduced nicotine amide dinucleotide; $NADP^+$/NADPH, oxidized/reduced nicotine amide dinucleotide phosphate; Pgi, phosphoglucoisomerase; P_i/PP_i, inorganic phosphate/diphosphate; Pgm, phosphoglucomutase; PR-AMP, phosphoribosyl-AMP; PR-ATP, phosphoribosyl-ATP; PRA, phosphoribosylamine; PRFAR, 5-[(5-phospho-1-deoxyribulos-1-ylamino)methylideneamino]-1-(5-phosphoribosyl) imidazole-4-carboxamid; PRPP, phosphoribosyl pyrophosphate; PtsG, phospoenolpyruvate-dependent phosphotransferase system for glucose; PurA, adenylosuccinate synthase; PurB, adenylosuccinate lyase; PurC, phosphoribosylaminoimidazole-succinocarboxamide synthase; PurD, PRA-glycine ligase; PurE, phosphoribosylainoimidazole mutase; PurF, amidophosphoribosyltransferase; PurH, bifunctional AICAR formyltransferase / IMP cyclohydrolase; PurK, phosphoribosylainoimidazole carboxylase; PurL, phosphoribosylformylglycinamide synthase; PurM, phosphoribosylformylglycinamidine cycloligase; PurN, phosphoribosylglycinamide formyltransferase; R5P, ribose 5-phosphate; SAICAR, phosphoribosyl-aminoimidazolesuccinocarboxamide; SHMT, serine hydroxymethyltransferase; TCA, tricarboxylic acid cycle; THF, tetrahydrofolate. **Taken from Schwentner et al., 2019.**

1.2.5. *L-Histidine related pathways*

The histidine biosynthesis is only partly a linear pathway and bears several connections to other biosynthetic pathways that must be considered with respect to L-histidine overproduction (Fig. **4**, p.19). PRPP, one of the histidine precursor molecules is also an important intermediate and cofactor of other biosynthetic pathways in bacteria (reviewed in Hove-Jensen et al., 2016), such as *de novo* purine biosynthesis (Jensen et al., 2008; Zhang et al., 2008), pyrimidine biosynthesis (Turnbough and Switzer, 2008), L-tryptophan (Sprenger, 2007), nicotineamide adenine dinucleotides (Begley et al., 2001; Foster and Moat, 1980), and arabinogalactan, an important component of the cell wall of *Corynebacteria* (Alderwick et al., 2006). For an overview see Fig**. 5** on page 22. These pathways will be introduced in appropriate depth in the following with their greater or lesser connection(s) to the L-histidine pathway and their potential significance for L-histidine overproduction.

The most obvious connection of the L-histidine pathway is with the **purine biosynthesis**, due to a) the common precursor molecule PRPP, b) the common precursor molecule ATP, and c) AICAR as connecting molecule, being produced in one and further metabolized in the other pathway. The purine biosynthesis has been studied intensively in *E. coli*, where eleven enzymatic steps are needed to synthesize inosine monophosphate (IMP) from PRPP, while five molecules of ATP are consumed (Mueller et al., 1994; Zhang et al., 2008). The following overview uses the available reviews as basis (Brown et al., 2011; Jensen et al., 2008; Wyngaarden, 1976; Zhang et al., 2008). The complete pathway of purine biosynthesis can be separated in two coherent parts. In the first part, the ***de novo*** **purine biosynthesis**, the purine ring of inosine monophosphate (IMP), the endproduct of the *de novo* part, is generated by a stepwise addition of small molecules to the precursor PRPP. In the first step, amidophosphoribosyltransferase (PurF, encoded by *purF*) generates 5'phosphoribosylamine (PRA) by transferring an amino group from L-glutamine onto PRPP, simultaneously releasing pyrophosphate. PurF has been investigated in different organisms, mainly *E. coli* and *B. subtilis*, and was shown to be the target of a complex allosteric inhibition by the nucleotides AMP, ADP, GMP, and GDP in a synergistic manner (Chen et al., 1997; Zalkin, 1983; Zhou et al., 1994). PRA is further converted in the second step to glycineamide ribonucleotide (GAR), which is catalysed by the phosphoribosylamine-glycine ligase (PurD, encoded by *purD*) using glycine and ATP and releasing ADP and inorganic phosphate (P_i). The third enzymatic reaction is performed by phosphoribosylglycineamide formyltransferase (PurN, encoded by *purN*) and yields phosphoribosyl-*N*-formylglycineamide (FGAR). This reaction is one of the two (the

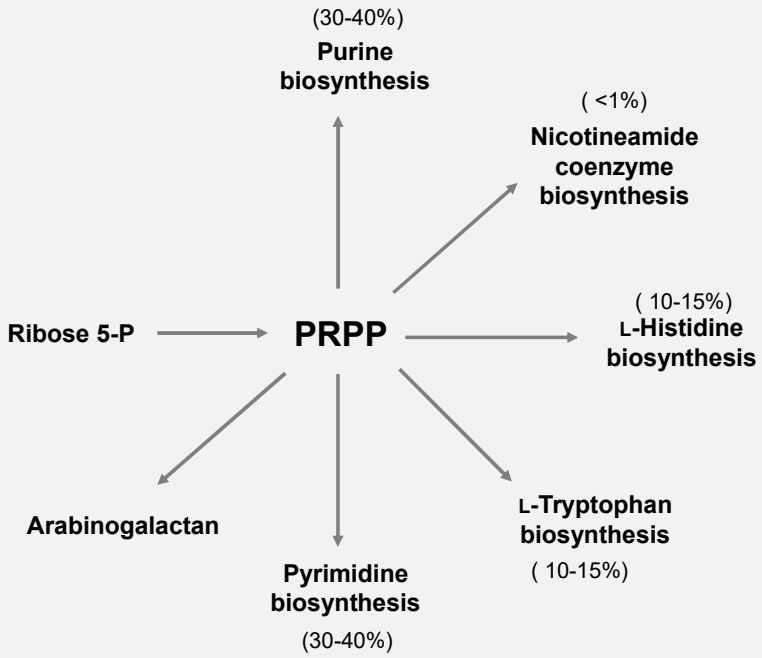

Fig. 5. Simplified overview of the utilization of phosphoribosyl pyrophosphate (PRPP) in *C. glutamicum*. Percentages in parentheses indicate the percentage of total used PRPP for *E. coli* and *S. enterica* in a minimal medium with glucose. Modified after Jensen et al., 2008

other being the tenth step by PurH) *N*10-formyltetrahydrofolate (fTHF) dependent reactions of the *de novo* purine biosynthesis, thus connecting purine biosynthesis with the one carbon (C_1) metabolism (Fig. **4**, p.19). In the fourth step, FGAR is converted to 5'-phosphoribosylformylglycineamide (FGAM) by phosphoribosylformylglycineamide synthase (PurL, encoded by *purL*), requiring ATP and L-glutamine as cofactors and releasing L-glutamate, ADP, and P_i. FGAM is converted to aminoimidazole ribotide (AIR) in the fifth step by the AIR synthetase (PurM, encoded by *purM*), utilizing ATP and releasing ADP, P_i, and H_2O. AIR is then converted in two steps to 5'phosphoribosyl-4-carboxy-5-aminoimidazole (CAIR) via N_5-carboxyaminoimidazole ribonucleotide (N_5-CAIR), catalysed by the N_5-carboxyaminoimidatole ribonucleotide synthetase (PurK, encoded by *purK*), requiring ATP and HCO_3^-, and by the N_5-carboxyaminoimidatole ribonucleotide mutase (PurE, encoded by *purE*). Despite the purine biosynthesis is conserved among all realms of life, this reaction cascade may differ between organisms and since data for *C. glutamicum* have not yet been conducted, the here presented sequence is given for *E. coli* (Brown et al., 2011; Zhang et al., 2008). Besides for PurK, AIR is also a substrate for the hydroxymethyl pyrimidine synthase, the first enzyme in the biosynthetic pathway of thiamine (Du et al., 2011; Leonardi and Roach, 2004). The eighth step of the purine biosynthesis is catalysed by phosphoribosylaminoimidazole

succinocarboxamide synthase (PurC, encoded by *purC*), which requires L-aspartate and ATP as cofactor and generates phosphoribosylaminoimidazolesuccinocarboxamide (SAICAR), ADP, and P_i. Then, adenylosuccinate lyase (PurB, encoded by *purB*) cleaves SAICAR to 5-aminoimidazole-4-carboxamide ribonucleotide (AICAR) and fumarate. The generated fumarate is further converted in the TCA cycle, whereas AICAR is used as substrate for the bifunctional phosphoribosylaminoimidazolecarboxamide formyltransferase / inosine monophosphate cyclohydrolase (PurH, encoded by *purH*) in the tenth step of the purine pathway and 5-formamidoimidazole-4-carboxamide ribotide (FAICAR) is generated. Just as the third step of the pathway, the tenth step requires fTHF as cofactor and connects purine biosynthesis with C_1 metabolism (Fig. 4, p.19). PurH then also catalyses the last step to produce inosine monophosphate (IMP) from FAICAR, releasing H_2O.

IMP marks the endpoint of the *de novo* part of the purine biosynthesis. It is a versatile precursor molecule for several different nucleobases, nucleosides, and nucleotides and the gateway for the ***salvage*** **purine biosynthesis** (Jensen et al., 2008; Murray, 1971; Peifer et al., 2012). In the salvage part, nucleobases and nucleosides are recovered from the degraded RNA and DNA. These salvage nucleobases and nucleosides might then be reconverted back to nucleotides (Jensen et al., 2008). With special importance for this work, one reaction IMP is undergoing is catalysed by adenylosuccinate synthetase (PurA, encoded by *purA*). This reaction requires guanosine triphosphate (GTP) as energy donor and L-aspartate, releasing guanosine diphosphate (GDP), P_i, and adenylosuccinate. Adenylosuccinate is then further converted to AMP via PurB, which also performs the ninth step of the *de novo* purine synthesis, again cleaving fumarate.

As described above, the *de novo* part of the purine biosynthesis comprises two reaction steps that require fTHF as donor of C_1 units in the form of a formyl group (Fig. 4, p.19). These molecules are part of the **one carbon metabolism** constituted by different tetrahydrofolate (THF) species that form a complex network of C_1 group donors (Arinze, 2005). Folate (vitamin B_9) serves as basis molecule and can bond with any of the C_1 fragments in its completely reduced form as THF. The C_1 fragments represent different oxidation states of the carbon atom and are metabolically interconvertible (Arinze, 2005). The C_1 metabolism, its complex network, and the underlying regulatory mechanisms have been investigated in several species, such as *E. coli* (Harvey and Dev, 1975; Meedel and Pizer, 1974) and *Saccharomyces cerevisiae* (Piper et al., 2000). In *C. glutamicum* the main source for the generation of THF molecules loaded with a C_1 unit that might be interconverted to other THF

species, appears to be the reaction of the serine hydroxymethyltransferase (SHMT, encoded by *glyA*) that converts L-serine to glycine and simultaneously loads a methylene group onto THF to yield *N*5,*N*10-methylene THF (mTHF), requiring pyridoxyl phosphate as cofactor (Lai et al., 2012; Schweitzer et al., 2009; Simic et al., 2002; Stolz et al., 2007). The mTHF originating from the SHMT reaction is then convertible to other THF species, such as *N*10-formyl THF (fTHF). This most likely happens via a two step reaction: mTHF is oxidized to *N*5,*N*10-methenyl THF and then via a cyclohydrolase reaction to fTHF (Arinze, 2005). The generated fTHF molecules serve as formyl group donors in the *de novo* purine biosynthesis.

In other organisms, among them also bacteria, such as *E. coli* (Okamura-Ikeda et al., 1993; Stauffer et al., 1986) or *Streptomyces griseus* (Tezuka and Ohnishi, 2014), the glycine cleavage (GCV) system is a further source for the generation of loaded THF species (Fig. 10, p.99). The GCV system is a multienzyme system that performs the reversible oxidation of glycine to CO_2 and ammonia, simultaneously generating mTHF from THF and NADH from NAD^+ (Kikuchi et al., 2008; Okamura-Ikeda et al., 1993). In *E. coli*, it consists of the four proteins P- (glycine dehydrogenase), H- (interacts with all other components), T- (aminomethyltransferase), and L-protein (dihydrolipoyl dehydrogenase) and has been characterized thoroughly (Okamura-Ikeda et al., 1993; Stauffer et al., 1986). However, a GCV system is not encoded in the genome of *C. glutamicum*.

Besides its role as starter molecule for the purine biosynthesis, PRPP is also required as cofactor in the **pyrimidine biosynthesis** pathway (Fig. 5, p.22). Beginning with L-glutamine, which is converted to carbamylphosphate, the pyrimidines uridine and cytidine nucleosides are generated (Turnbough and Switzer, 2008). Within this biosynthetic pathway, the reaction of orotate phosphoribosyltransferase (PyrE, encoded by *pyrE*) requires PRPP as cofactor to generate orotidine 5'-monophosphate from orotate.

PRPP is also required in the biosynthesis of the α-amino acid **L-tryptophan** (Fig. 5, p.22). Originating from chorismate, the second step of the biosynthesis is performed by the anthranilate phosphoribosyltransferase (TrpD, encoded by *trpD*), converting anthranilate to phosphoribosylanthranilate, consuming PRPP and releasing PP_i (Lambrecht and Downs, 2013; O'Gara and Dunican, 1995).

The *de novo* **biosynthesis of nicotineamide dinucleotides** comprises one enzymatic reaction that involves PRPP as cofactor (Foster and Moat, 1980). Namely, in *C. glutamicum* the quinolinate phosphoribosyltransferase (NadC, encoded by *nadC*) is converting quinolinate to nicotinate mononucleotide consuming PRPP and releasing PP_i and CO_2 (Teramoto et al., 2010).

Additionally, PRPP was shown to be consumed for the **synthesis of arabinogalactan**, a macromolecule that connects mycolic acids to peptidoglycan in the cell wall matrix of Corynebacterianeae, among them *C. glutamicum* (Alderwick et al., 2006).
In how far these PRPP consuming enzymatic steps interfere with the allocation of PRPP as precursor for the overproduction of L-histidine can only be speculated. Data are available for *E. coli* and *S. enterica* (Fig. 5, p.22), where the purine and pyrimidine biosynthesis each consume about 30-40% of the total intracellular PRPP amount, L-histidine and L-tryptophan biosynthesis consume each 10-15%, and the NAD *de novo* biosynthesis requires below 1% (Jensen et al., 2008). Since microbial arabinogalactan occurs only in species belonging to the order Actinomycetales suborder Corynebacterianeae (Alderwick et al., 2006), including well-known genera such as *Mycobacterium* and *Corynebacterium*, data is lacking to assess the amount of PRPP that is required for its synthesis. However, the proportions of pyrimidine and purine biosyntheses are far above the proportion of the L-histidine biosynthesis. This mediates insights in the amounts of carbon that are directed towards the respective PRPP consuming pathways.

1.2.6. *Energy metabolism*

The fundamental chemical requirements of a cell are primary biosynthetic intermediates, energy, and reducing power (Atkinson and Fall, 1967). Since *C. glutamicum* is a chemoorganotrophic organism, it relies on the energy potential of redox reactions as energy source and on organic compounds as electron donors and carbon sources. Its metabolism consists of a part in which energy is generated and of a biosynthetic part where cell components are synthesized and transported. The connection of the energy generating part and the biosynthetic part is accomplished, among others, by the nucleotides of the adenylate pool.
Nucleotides are essential components of all living organisms, constituting the building blocks for the nucleic acids, RNA and DNA, and serve as cofactors in sugar and lipid metabolism, polyamine biosynthesis, and others (Jensen et al., 2008). Nucleotides are either found as ribo- or as deoxyribonucleotides and occur as mono-, di-, or triphosphates. In many bacteria, the three adenylates ATP, ADP, and AMP are the prevalent nucleotide species and the role of ATP in the energy metabolism is established. It is the principal molecule of storing and transferring energy and as such required in biosynthetic pathways, for maintaining transmembrane gradients, and for such crucial procedures as cell division and movement. The biological

potential energy that is stored in ATP (30.5 kJ mol^{-1}) is utilized by all these reactions and the enzymatic hydrolysis of ATP generates ADP and P_i (Hara and Kondo, 2015). ADP and P_i are regenerated to ATP in bacteria in two ways: either by substrate level phosphorylation or by oxidative phosphorylation (Hara and Kondo, 2015; Zhou et al., 2009).

For human cells, it was shown that about 90% of the intracellular ATP is produced by phosphorylation of ADP by ATP synthase (De la Fuente et al., 2014).

Absolute concentrations of intracellular nucleotides in *S. enterica* were determined to be 3000 µM ATP, 250 µM ADP, and 100 µM AMP, whereas other triphosphate nucleotides are far below these numbers, with 900 µM GTP, 500 µM CTP, and 900 µM UTP (Bochner and Ames, 1982; Jensen et al., 2008). In *E. coli*, intracellular concentrations of the adenylate species have been determined to be 9.6×10^{-3} mol ATP L^{-1}, 5.6×10^{-4} mol ADP L^{-1}, and 2.8×10^{-4} mol AMP L^{-1} (Bennett et al., 2009). A common property of the nucleotides is the *N*-glycosyl bond that links the nucleobase to the pentose phosphate moiety, formed by a phosphoribosyltransferase from PRPP and a nitrogenous base (Jensen et al., 2008). The ribonucleotides are first produced as nucleoside monophosphates and then further converted to the respective di- and triphosphates by nucleoside mono- and diphosphate kinases (Jensen et al., 2008).

The energy charge (EC) was introduced in 1967 by Atkinson and co-workers as a measure of the cells energetic state and a fundamental metabolic control parameter (Atkinson and Walton, 1967). Its formula is defined as (ATP+0.5ADP)/(ATP+ADP+AMP) and uses the intracellular concentrations of the adenylates (Atkinson and Walton, 1967). The EC, by definition, varies between values of 0 and 1 and is numerically equal to half the average number of the anhydride-bound phosphate groups per adenosine moiety (Atkinson and Walton, 1967). Typical reported values for EC are between 0.8 – 0.9 in *E. coli* during exponential growth under aerobic conditions, which declines to around 0.5 when cells are starving carbon and in the stationary growth phase (Chapman et al., 1971; Franzen and Binkley, 1961). In *Bacillus megaterium*, metabolizing cells were shown to have ECs around 0.8, whereas in spores, the resting states of several bacteria, the EC declined to < 0.1 (Setlow and Kornberg, 1970). These findings can also be transferred to all sorts of cells, among these also eukaryotic species like *S. cerevisiae*, where the EC during exponential growth was reported to be 0.84 – 0.93 (Betz and Moore, 1967). An overview of ECs of species from all realms of life is given in Chapman et al., 1971. Generally spoken, an intact EC in metabolizing cells revolves around a value of 0.85 (Chapman et al., 1971).

Since ATP and the EC are such important factors for the performance of biotechnological producer strains and processes, they have been targeted with different strategies, which were reviewed in detail (Hara and Kondo, 2015; Zhou et al., 2009) and comprise metabolic engineering strategies, such as manipulating NADH availability, manipulation of the electron transfer chain, manipulating the regulation of oxygen supply and the proton gradient, or bioprocess strategies, such as enhancing the substrate utilization and the cells resistance against environmental stresses.

1.2.7. *Motivation*

Utilization and administration of L-histidine has been proven to be beneficial in several financially important sectors, such as the medical (DiNicolantonio et al., 2018; Du et al., 2017) and animal feed (Haug et al., 2008; Park et al., 2013) sectors. Due to its versatile applicability, increasing amounts of L-histidine can be expected to be required on the worldwide market. Despite global players like Ajinomoto Co. and DAESANG Corp. are running microbial bioprocesses to produce L-histidine, a glimpse in scientific literature about microbial L-histidine production reveals that this field is a relatively small area and has not been fully exploited. Most available works, especially the ones applying *C. glutamicum* as host, focus on mutagenesis approaches (see 1.2.4 Production of L-HISTIDINE, p.16) and a holistic, system-wide approach with this objective has not yet been tackled. The motivation for this work therefore was the construction of L-histidine producing mutants with *C. glutamicum* as host in a system-wide manner and establishing a bioprocess for the microbial production of L-histidine. Available data of published L-histidine producer strains based on different bacteria, such as *E. coli*, *C. glutamicum*, or *S. coelicolor* show very limited L-histidine yields, which at least partially can be attributed to the sophisticated and ATP intense L-histidine biosynthesis. The tightly regulated L-histidine biosynthesis is intertwined with several other pathways (see 1.2.5 L-HISTIDINE related pathways, p. 21) and efficient tackling of optimized overproduction requires the application of novel strategies to reach the demanding underlying economic standards. The experiments conducted in this work focused on gaining access to the complex L-histidine biosynthesis through the development of recombinant *C. glutamicum* producer strains. These demands were encountered with a combined approach of rational strain engineering (including modularized tackling of important metabolic pathways), with a sophisticated comparative metabolomics approach, entitled Systems Metabolic Profiling (conducted by André Feith,

IBVT, University of Stuttgart), with Flux Balance Analysis (conducted by André Feith, IBVT, University of Stuttgart), and with the subsequent development and implementation of preliminary bioprocess studies.

1.3. Introduction PART II

1.3.1. *Evolution approaches*

Nowadays, sophisticated metabolic engineering and synthetic biology approaches combined with new *omics* technologies and computational approaches are powerful tools to identify, modulate, and improve producer strains. However, these combined rational approaches sometimes are limited or impracticable. This holds especially true for organisms outside of the model organisms such as *E. coli* or *S. cerevisiae*, where knowledge of the metabolism and its regulation mechanisms is scarce. Thus, (directed) evolution approaches can be expedient where knowledge-based strain/protein engineering finds its limits.

The underlying principle of all evolutionary approaches is the acceleration of evolution, i.e. increasing mutation rates to generate genetic variety. In the classical way, this was achieved by mutagenizing cells with mutagenizing agents or radiation, such as N-methyl-N'-nitro-N-nitrosoguanidine (NTG) or ultraviolet (UV) light (Burns et al., 1986; Delić et al., 1970; Foster, 1991) evolution could be accelerated, thus creating genetic diversity in large libraries of mutants (Doudney and Young, 1962). The application of mutagenizing agents however is an undirected process where large numbers of mutations are introduced at random positions in the genome what brings several disadvantages with it, e.g. strain instability.

The introduction of directed evolution approaches in the early 1990s enabled more focused, user-defined evolution procedures, which are established nowadays in protein and metabolic engineering (Cobb et al., 2013a; Zhou and Alper, 2018). Generally, directed evolution imitates and accelerates the natural evolution process by increasing the mutation rate and screening rate of desired variants (Kumar and Singh, 2013; Zhu et al., 2018). These directed evolution approaches include sophisticated methods, such as error-prone PCR (Cadwell and Joyce, 1992), random insertion/deletion mutagenesis (Murakami et al., 2002), or saturation mutagenesis (Myers et al., 1985) and might be combined with the application of structural analogues to overcome feedback inhibition (Araki et al., 1974), but are also based on DNA recombination

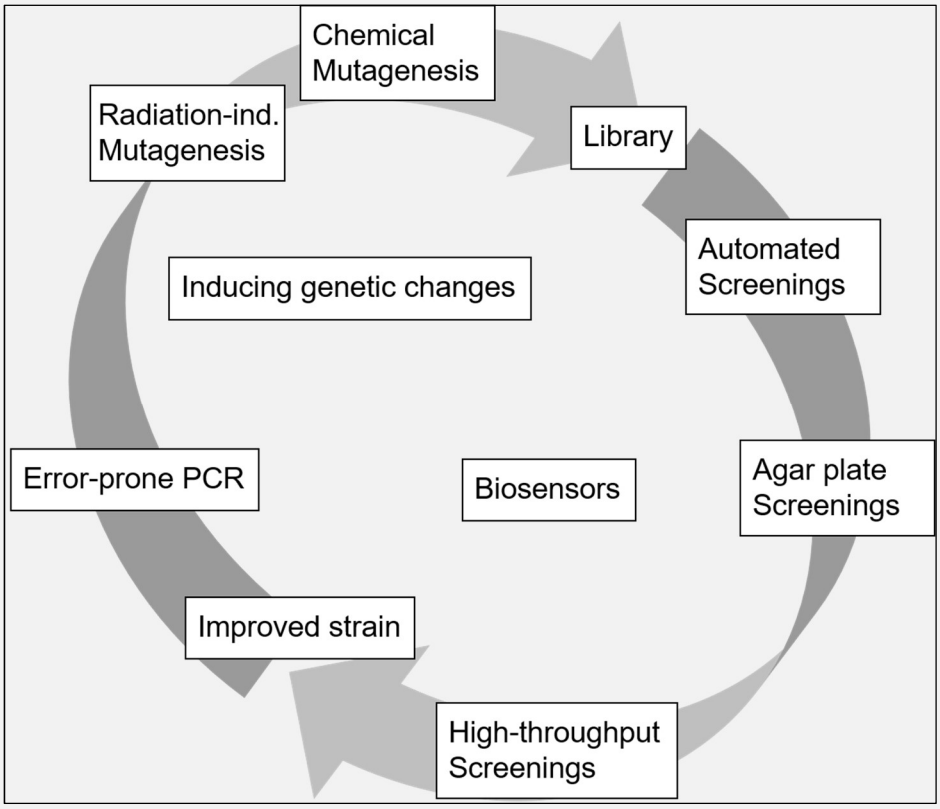

Fig. 6. Schematic overview of typical directed evolution approaches.

methods, such as DNA shuffling (Stemmer, 1994) or multiplex automated genome engineering (Wang et al., 2009). An example of a directed evolution approach is given in Fig. **6** on page 29. Like classical random mutagenesis, directed evolution approaches in metabolic engineering aim to identify new (non-rational) targets to improve a variety of traits resulting in improved producer strains and rely on the creation of large pools of genetic diversity, which require efficient screening approaches to identify clones with the desired phenotype (Cobb et al., 2013b). The decades of development of such methods led to increasingly larger mutant library sizes, recent approaches reaching numbers of up to 10^{10} clones (Zhou and Alper, 2018). However, screening (coupled with continuous evolution) of high throughput approaches remains a challenge (Zhou and Alper, 2018).

1.3.2. *Screening approaches*

The field of mutagenesis / directed evolution has come a long way and development of a steadily increasing number of evolution methods has increased library sizes from 10^3 clones up to 10^{10} clones (Zhou and Alper, 2018). Having induced the genomic variation, resulting in large libraries, the screening part becomes increasingly challenging, since it often is time- and money-consuming without available adequate screening methods (Bassalo et al., 2016; Chou and Keasling, 2013). This limitation was partially overcome by high-throughput screening techniques, such as *in vivo* fluorescence-based biosensors, which enable in combination with fluorescence-activated cell sorting (FACS) or droplet-based microfluidic sorting a pre-selection of the mutagenized strains by translating intracellular product formation into an optical readout, thereby narrowing down the entirety of mutagenized cells that needed to be screened (Agresti et al., 2010; Dietrich et al., 2010; Eggeling et al., 2015; Lin et al., 2017; Mahr et al., 2015). Although such methods allow the ultra-rapid screening of library sizes of up to 10^9 variants (Dietrich et al., 2010), the final identification of relevant mutations out of the mutational pool of the cell is still time-consuming since it requires laborious re-engineering for verification. This especially holds true in case of random mutagenesis, which yields large numbers of mutations per cell.

1.3.3. *Anaplerotic reactions in* C. glutamicum

A vital part of the central carbon metabolism of *C. glutamicum* is represented by the circular network of the anaplerotic reactions around the PEP-pyruvate-oxaloacetate-malate node (Sauer and Eikmanns, 2005). This circular network comprises specific carboxylation and decarboxylation reactions thus constituting a link between glycolysis and TCA cycle. This link is needed since intermediates of the TCA are constantly withdrawn for biosynthesis and thus anaplerotic reactions replenish this gap of TCA intermediates by using C3 units (PEP and pyruvate). On the other side, anaplerotic reactions are also the starting point of the gluconeogenesis, where C4 (oxaloacetate and malate) units are decarboxylated. Through this linkage, anaplerotic reactions have been shown to have great influences on TCA and glycolysis derived products in *C. glutamicum*, such as L-lysine and L-glutamate (Shirai et al., 2007; Yokota et al., 2017).

In *C. glutamicum*, the anaplerotic reactions comprise at least five reactions (Fig. 7, p.32), two of them fixating and incorporating CO_2/HCO_3^-, three of them producing CO_2:

a) Pyruvate carboxylase (PCx, encoded by *pyc*), converting pyruvate to oxaloacetate by an ATP-dependent carboxylation reaction. The enzyme requires biotin for the reaction (Peters-Wendisch et al., 1998).
b) PEP carboxylase (PEPCx, encoded by *ppc*), catalysing the irreversible formation of oxaloacetate from PEP, fixating CO_2 and releasing P_i (Peters-Wendisch et al., 1993).
c) PEP carboxykinase (PEPCk, encoded by *pck*), performing the GTP-dependent decarboxylation of oxaloacetate to PEP, releasing CO_2 (Jetten and Sinskey, 1993; Riedel et al., 2001).
d) Oxaloacetate decarboxylase (ODx, encoded by *odx*), performing the irreversible decarboxylation of oxaloacetate to pyruvate and CO_2 (Klaffl and Eikmanns, 2010).
e) Malic enzyme (MalE, encoded by *malE*), reversibly decarboxylating malate to pyruvate in an $NADP^+$-dependent manner, producing NADPH and CO_2 (Gourdon et al., 2000).

Compared with other organisms, the presence of both a PEPCx and a PCx is a special feature of *C. glutamicum*. The situation is different in other bacteria, e.g. in *B. subtilis* solely a PCx and in *E. coli* solely a PEPCx is present (Sauer and Eikmanns, 2005).

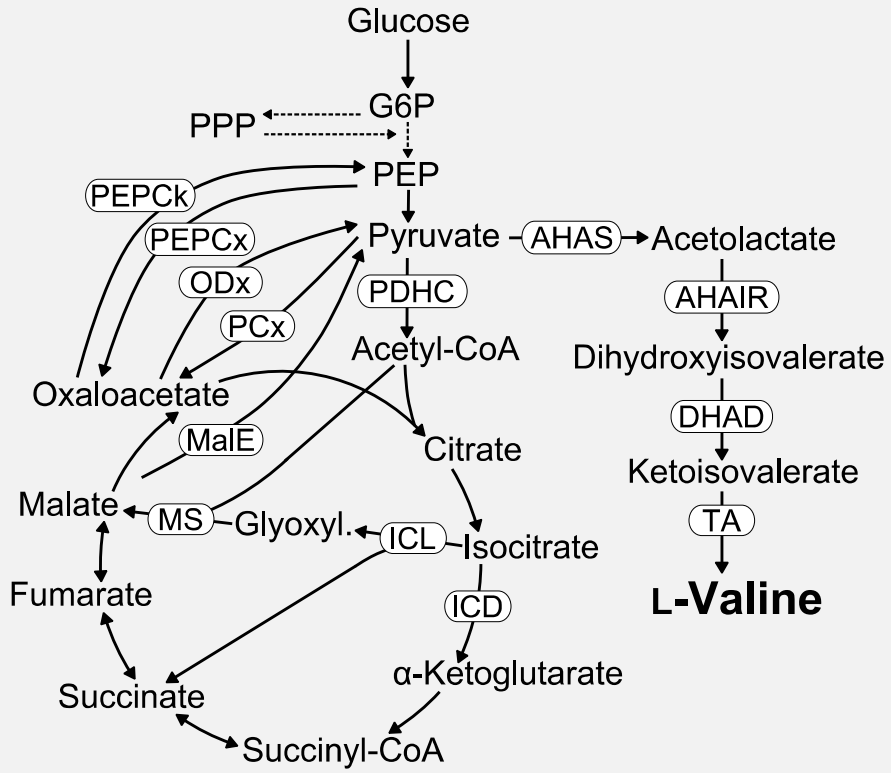

Fig. 7. Schematic overview of the anaplerotic reactions around the PEP-pyruvate-oxaloacetate node and the L-valine biosynthesis in *C. glutamicum*. Abbreviations: AHAIR, acetohydroxyacid isomeroreductase; AHAS, acetohydroxyacid synthase; CoA, coenzyme A; DHAD, dihydroxyacid dehydratase; G6P, glucose 6 phosphate; Glyoxyl., glyoxylate; ICD, isocitrate dehydrogenase; ICL, isocitrate lyase; MalE, malic enzyme; MS, malate synthase; ODx, oxaloacetate decarboxylase; PCx, pyruvate carboxylase; PEP, phosphoenolpyruvate; PEPCk, PEP carboxykinase; PEPCx, PEP carboxylase; PPP, pentose phosphate pathway; TA, transaminase B. **Taken from Schwentner et al., 2018.**

1.3.4. *Glyoxylate shunt in* C. glutamicum

When *C. glutamicum* is growing on substrates that enter the central carbon metabolism on the level of acetyl-CoA, such as acetate, fatty acids, or ethanol, the glyoxylate cycle (glyoxylate shunt) fulfils the task of replenishing the TCA cycle, i.e. providing oxaloacetate as acceptor molecule for acetyl-CoA to form citrate (Fig. 7, p.32). The glyoxylate cycle consists of five of the eight reactions of the TCA cycle and bypasses the two decarboxylating reactions of ICD and 2-oxoglutarate dehydrogenase complex, enabling net acquisition of carbon, which is impossible by serving the TCA under glycolytic conditions (Bott, 2007; Bott and Eikmanns, 2013). By this way, the glyoxylate cycle results in the net formation of one molecule of malate from two molecules of acetyl-CoA (Gerstmeir et al., 2003). With an active glyoxylate shunt, the carbon flux is diverted at the level of isocitrate, where it is either metabolised by the reaction

of isocitrate lyase (ICL, encoded by *aceA*) or by isocitrate dehydrogenase (ICD, encoded by *icd*) (Fig. 7, p.32).

ICD is participating in the TCA cycle and competes for isocitrate as substrate with ICL (Wendisch et al., 2000). ICD performs the decarboxylation reaction of isocitrate to 2-oxoglutarate (α-ketoglutarate), simultaneously generating NADPH and has been reported to have a specific enzyme activity of 1 U mg protein^{-1}, independent of the carbon source and the growth phase (Eikmanns et al., 1995). The affinity of ICD towards isocitrate was determined to be strong (K_m = 12 µM) (Eikmanns et al., 1995).

ICL on the other hand, is the first of the two glyoxylate shunt enzymes, malate synthase (MS, encoded by *aceB*) is the second one. Both enzymes have been characterized in detail in *C. glutamicum*. The ICL catalyses the cleavage of isocitrate to glyoxylate, the key intermediate of the glyoxylate shunt, and succinate (Reinscheid et al., 1994a). The specific activities of the ICL were determined to be about 0 U mg protein^{-1} when glucose was the sole carbon source and about 2.8 U mg protein^{-1} when acetate was the sole carbon source, showing a tight regulation of the glyoxylate shunt (Reinscheid et al., 1994a; Wendisch et al., 1997). The affinity of ICL towards isocitrate is moderate (K_m = 0.28 mM) and thus lying far below the one of ICD towards isocitrate (Gerstmeir et al., 2003).

The second glyoxylate shunt enzyme MS performs the irreversible condensation reaction of glyoxylate with acetyl-CoA to give malate (Reinscheid et al., 1994b). For MS, similar activity patterns were shown as for ICL. With glucose as sole carbon source, specific MS activities were about 0 U mg protein^{-1}, when acetate was the sole carbon source, specific MS activities increased to about 1.8 U mg protein^{-1} (Reinscheid et al., 1994b; Wendisch et al., 1997). However, when acetate is not available, the glyoxylate shunt is tightly regulated and inactive (Wendisch et al., 2000).

This regulation is mediated by the regulators of acetate metabolism RamA (Cramer et al., 2006) and RamB (Gerstmeir et al., 2004), two global transcriptional regulatory proteins that participate in expression control of genes involved in acetate and ethanol metabolism, glycolysis, gluconeogenesis, and lactate metabolism, amongst others (Auchter et al., 2011). With respect to the glyoxylate shunt, RamA has been demonstrated to act as positive regulator of the glyoxylate genes *aceA* and *aceB*, and of the acetate activating genes *ack* (encoding acetate kinase) and *pta* (encoding phosphotransacetylase) (Cramer et al., 2006; Shah et al., 2018). An overview of the RamA regulon is provided by Shah et al., 2018. RamA has further been demonstrated to negatively auto-regulate its own expression through binding to the identified

RamA binding motif, located in the promoter region of the *ramA* gene (Cramer and Eikmanns, 2007).

RamB, on the other side, was shown to be present in higher amounts when glucose was the sole carbon source, compared to acetate as sole source (Cramer et al., 2007). Both RamA and RamB bind to the *ramB* promoter region and *ramB* expression is negatively controlled by RamB and positively by RamA (carbon source dependent) (Cramer et al., 2007). This leaves the role of a RamB dependent repression of *aceA* and *aceB* in absence of acetate.

However, effector molecules of RamA and RamB are still unknown and have yet to be revealed (Shah et al., 2018).

The glyoxylate shunt with its participating genes/enzymes and their regulation machanisms represent interesting targets for metabolic engineering approaches, not only for TCA derived products and not only in *C. glutamicum*. Examples thereof are the production of succinate (Litsanov et al., 2012; Zhu et al., 2014), L-lysine (Kim et al., 1997), or α-ketoglutarate (Jo et al., 2012) with *C. glutamicum* and production of 5-aminolevulinic acid (Noh et al., 2017) or glycolate (Liu et al., 2018) with *E. coli*.

1.3.5. *L-Valine production*

The application of *C. glutamicum* for production of the α-amino acid L-valine has been pursued for years and several profound reviews on this topic are available, whereof the following overview makes use of (Lee et al., 2009; Oldiges et al., 2014; Wang et al., 2018). L-Valine is one of the three branched chain amino acids and has been described as an essential amino acid for humans (Oldiges et al., 2014). L-Valine is already applied in diverse sectors, such as food, feed, pharmaceutical, and cosmetics industries (Oldiges et al., 2014). As traditional methods for obtaining L-valine, extraction from natural protein sources or chemical synthesis were used (Oldiges et al., 2014).

The biosynthesis of L-valine, as well as of the two other branched chain amino acids L-leucine and L-isoleucine, in *C. glutamicum* originates from the central carbon metabolism intermediate pyruvate (Fig. 7, p.32). The first enzyme in the pathway, acetohydroxyacid synthase (AHAS, encoded by *ilvBC*) catalyses either the decarboxylation of pyruvate and either its condensation with another molecule of pyruvate to form acetolactate, the precursor of L-valine and L-leucine, or the condensation of pyruvate with 2-ketobutyrate to form acetohydroxybutyrate, the precursor of L-isoleucine (Elišáková et al., 2005). Control of the branched chain amino acid pathways is mediated by a feedback inhibition of AHAS by all of the three branched chain

amino acids and by expression control of the *ilvBNC* operon via an attenuation mechanism (Elišáková et al., 2005). The second step towards L-valine formation is performed by the acetohydroacid isomeroreductase (AHAIR, encoded by *ilvC*), which catalyses the isomerisation and reduction of acetolactate to dihydroxyisovalerate (Leyval et al., 2003). Then, dihydroxyacid dehydratase (DHAD, encoded by *ilvD*) dehydrates dihydroxyvalerate to α-ketoisovalerate. In the final step of L-valine biosynthesis, transaminase B (TA, encoded by *ilvE*) reversibly transfers an amino group from L-glutamate onto α-ketoisovalerate, yielding L-valine.

Concerning metabolic engineering in *C. glutamicum* with the objective to overproduce L-valine, several strategies have been conducted. Since L-valine derives from pyruvate, most metabolic engineering approaches targeted the PDHC (Fig. 7, p.32), either directly or indirectly to improve precursor availability in the form of accumulating pyruvate (Oldiges et al., 2014). This was achieved by a complete inactivation or by an attenuation of the PDHC via deletion of the *aceE* gene or reduction of its promoter activity by implementing weaker promoters (Blombach et al., 2009, 2008, 2007; Buchholz et al., 2013). Further, by applying anaerobic production conditions to reduce the activity of the TCA cycle (Hasegawa et al., 2013; Hasegawa et al., 2012) and by inactivation or attenuation of pantothenate biosynthesis to limit CoA availability, which is required for acetyl-CoA formation through the PDHC (Bartek et al., 2008; Elišáková et al., 2005; Holátko et al., 2009; Radmacher et al., 2002). Additionally, with the purpose to withdraw the surplus of pyruvate towards L-valine, commonly the respective L-valine biosynthesis genes or mutated variants thereof have been overexpressed (Oldiges et al., 2014; Radmacher et al., 2002).

1.3.6. *Motivation*

The rational design of producer strains is a relatively new field in the industrial biotechnology. Traditionally, producer strains have been designed and improved in an indirect manner, by applying mutagens that induce mutations in the genome of organisms, i.e. bacteria. Nowadays, available evolution approaches still apply mutagens to create genomic diversity in mutant libraries and by this speed up the natural process of evolution. The created mutants often bear hundreds of mutations in their genomes and must then be screened for the one desired mutation, mediating the desired phenotype. This includes laborious re-engineering and the screening process is often time-consuming and laborious, thus constituting a major bottleneck in the fast evolution of mutant strains. Additionally, evolution approaches are often applied when rational

strain engineering finds its limit in identifying new targets to improve producer strains. One prominent example for this is Adaptive Laboratory Evolution (ALE), which has also been applied for improving *C. glutamicum* strains (Mahr et al., 2015; Pfeifer et al., 2017).

The second part of this work therefore focused on the development of an evolutionary approach that deliberately omits the deployment of mutagens. This approach was entitled Metabolic engineering to Guide Evolution (MGE) and allows the evolution of producer strains, enables the easy identification of the phenotype generating mutations, and facilitates the identification and guided evolution of novel targets to improve producer strains. With the purpose to audit the developed method, we evolved a strain impaired in two anaplerotic reactions as an L-valine producing strain, subsequently identifying a novel mode for production of this amino acid besides the in literature established ones. Fig. **8** on page 36 shows a comparison of MGE with selected other available evolutionary approaches.

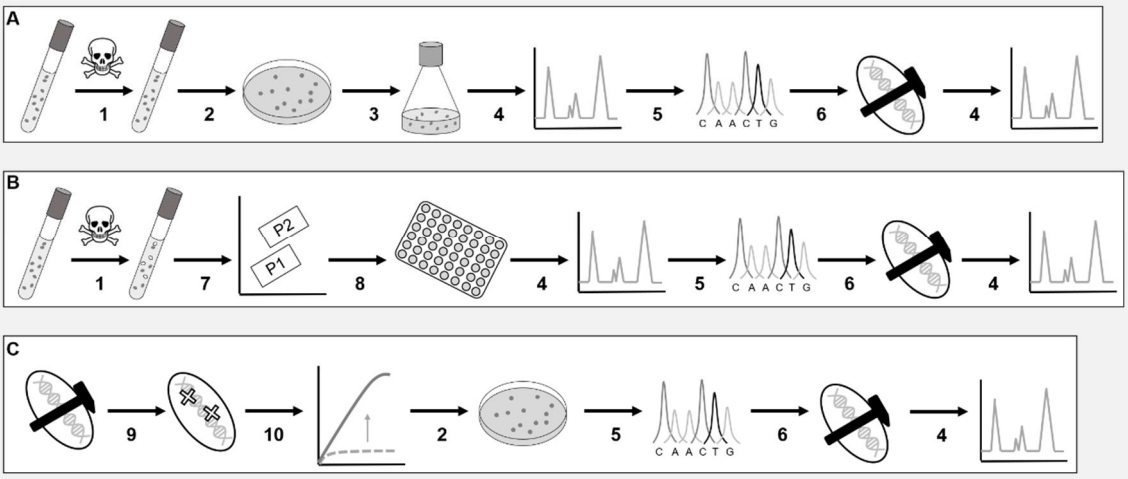

Fig. 8. Simplified schematic comparison of the principles of different evolutionary approaches, comprising classical mutagenesis (A), classical mutagenesis with a biosensor strain (B), and Metabolic engineering to Guide Evolution MGE (C). Numbers of the different steps mean: 1, inducing genomic mutations via mutagen; 2, isolating by plating; 3, cultivation; 4, quantification of the desired product; 5, genome sequencing; 6, metabolic (re-)engineering, targeted introduction of the identified mutations in a host strain; 7, biosensor strain enabled cell sorting according to production, e.g. via FACS; 8, small scale cultivation and high throughput screening for increased product formation; 9, metabolic engineering to generate selection pressure; 10, evolutionary cultivation with growth as indicator for evolved cells.

CHAPTER 2: MATERIALS AND METHODS

2.1. Bacterial strains, plasmids, and oligonucleotides

Table 2. A complete list of the strains constructed and/or used in this work with their names, relevant characteristic(s), and the source.

Strains	Relevant characteristic(s)	Source
Strains		
E. coli		
DH5α	F-ϕ80*lacZ*ΔM15 Δ(*lacZYA-argF*)U169 *endA1 recA1 hsdR17* (r_K^- m_K^+) *supE44 thi-1 gyrA96 relA1 phoA*	(Hanahan, 1983)
K-12 MG1655	Wildtype strain DSM 18039; F-, λ-, *ilvG-*, *rfb*-50, *rph*-1	German Collection of Microorganisms and Cell Cultures
C. glutamicum		
WT	Wildtype (WT) strain ATCC 13032	American Type Culture Collection
HIS1	*C. glutamicum* WT with the feedback inhibition released variant $HisG^{G233H-T235Q}$ (corresponding nucleotide exchanges: ggc742cat, acg748cag)	This work
HIS2	*C. glutamicum* HIS1 with implementation of P_{tuf} in front of the operon *hisD-hisC-hisB*-cg2302-cg2301	This work
HIS3	*C. glutamicum* HIS2 with implementation of P_{tuf} in front of the operon *hisH-hisA-impA-hisF-hisI*-cg2294	This work
HIS4	*C. glutamicum* HIS3 with implementation of P_{tuf} in front of the operon cg0911-*hisN*	This work
HIS5	*C. glutamicum* HIS1 with implementation of $P_{dapA\text{-}A16}$ in front of the operon *hisE-hisG*, additional exchange of the translational start codon from the native GTG to ATG for *hisE*	This work
HIS6	*C. glutamicum* HIS4 with implementation of $P_{dapA\text{-}A16}$ in front of the operon *hisE-hisG*, additional exchange of the translational start codon from the native GTG to ATG for *hisE*	This work
HIS7	*C. glutamicum* HIS6 with implementation of P_{sodA} in front of gene *hisF*	This work
HIS8	*C. glutamicum* HIS7 containing pJC4 *purApurB*	This work
HIS9	*C. glutamicum* HIS8 containing pEC-XT99A_gcv_ OP1-Cjk	This work
HIS10	*C. glutamicum* HIS9 with exchange of the translational start codon of gene *pgi* from ATG to GTG	This work
CM1	*C. glutamicum* HIS6 with exchange of the translational start codon of gene *pgi* from ATG to GTG	This work
CM2	*C. glutamicum* CM1 with the feedback inhibition released variant zwf^{A243T}	This work
CM2.1	*C. glutamicum* CM2.1 with the feedback inhibition released variant gnd^{S361F}	This work
CM3	*C. glutamicum* CM1 with the feedback inhibition released variant $prsA^{D122S}$	This work
HIS_{int}	*C. glutamicum* CM1 with an additional chromosomal integration of a cassette consisting of $P_{dapA\text{-}A16}$ *hisE-hisG*^{FB} T_{rrnB}	This work
PUR1	Strain CM1 with an in-frame deletion of gene *purF*	This work

Strains	Relevant characteristic(s)	Source
PUR2	Strain CM1 with an exchange of the translational start codon from GTG to TTG for gene *purF*	This work
PUR3	*C. glutamicum* CM1 with the feedback inhibition released variant $purF^{K348Q}$	This work
PUR4	*C. glutamicum* CM1 containing pJC4 *purH*	This work
HIS7.1	*C. glutamicum* HIS7 with exchange of the translational start codon of gene *pgi* from ATG to GTG	This work
HIS7.2	*C. glutamicum* HIS7 with exchange of the translational start codon of gene *gapA* from ATG to TTG	This work
HIS7.3	*C. glutamicum* HIS7 with exchange of the translational start codon of gene *pgm* from ATG to TTG	This work
HIS9.1	*C. glutamicum* HIS9 with exchange of the translational start codon of gene *gapA* from ATG to TTG	This work
HIS9.2	*C. glutamicum* HIS9 with exchange of the translational start codon of gene *pgm* from ATG to TTG	This work
Δ*purN*	*C. glutamicum* with deletion of gene *purN*	This work
Δ*purN* Δ*fdhF*	*C. glutamicum* Δp*urN* with in-frame deletion of gene *fdhF*	This work
Δ*purU*	*C. glutamicum* with in-frame deletion of gene *purU*	This work
HIS7 Δ*purU*	*C. glutamicum* HIS7 with in-frame deletion of gene *purU*	This work
CM1 P_{tuf}::*rpi*	*C. glutamicum* CM1 with P_{tuf} promoter in front of *rpi* gene	This work
HIS7 P_{gapA}:*hisEG*	*C. glutamicum* HIS7 with P_{gapA} in front of hisEG instead of $P_{dapA\text{-}A16}$	This work
HIS3 Δ*tkt*	*C. glutamicum* HIS3 with truncated version of the *tkt* gene	This work
HIS4 Δ*tkt*	*C. glutamicum* HIS4 with truncated version of the *tkt* gene	This work
HIS6 Δ*tkt*	*C. glutamicum* HIS6 with truncated version of the *tkt* gene	This work
HIS6 Δtkt^{S}	*C. glutamicum* HIS6 with a 4 bp deletion of the spacer of gene *tkt*	This work
HIS6 Δtkt^{SRbs}	*C. glutamicum* HIS6 with a 8 bp deletion of the spacer plus RBS region of gene *tkt*	This work
CM1 Δcg2314	*C. glutamicum* CM1 with an in-frame deletion of cg2314, encoding a potential purine regulator	This work
CM1 zwf^{ATG}	*C. glutamicum* CM1 with exchange of the translational start codon of gene *zwf* from GTG to ATG	This work
CM1 $prsA^{R}$	*C. glutamicum* CM1 with exchange of the native RBS of gene *prsA* against a modified variant	This work
HIS7 (pJC4 *hisD*)	*C. glutamicum* HIS7 with overexpression plasmid for gene *hisD*	This work
HIS7 (pJC4 *purApurB hisD*)	*C. glutamicum* HIS7 with overexpression plasmid for genes *purA*, *purB*, and *hisD*	This work
CM1 (pJC4 *purA*)	*C. glutamicum* CM1 with overexoression plasmid for gene *purA*	This work
CM1 Δ*pup*	*C. glutamicum* CM1 with deletion of gene *pup*	This work
PUR1 Δ*purD*	*C. glutamicum* PUR1 with deletion of gene *purD*	This work
Δ*ppc*	*C. glutamicum* WT with deletion of the *ppc* gene, encoding posphoenolpyruvate carboxylase	(Blombach et al., 2013)
Δ*ppc* Δ*pyc*	*C. glutamicum* Δ*ppc* with additional deletion of the *pyc* gene, encoding pyruvate carboxylase	(Schwentner et al., 2018)
Δ*ppc* Δ*pyc* Δ*pck*	*C. glutamicum* Δ*ppc* Δ*pyc* with deletion of the *pck* gene, encoding phosphoenolpyruvate carboxykinase	(Schwentner et al., 2018)
Δ*ppc* Δ*pyc* ICD^{A94D}	*C. glutamicum* Δ*ppc* Δ*pyc* with point mutation A94D in isocitrate dehydrogenase (ICD)	This work
Δ*ppc* Δ*pyc* ICD^{G407S}	*C. glutamicum* Δ*ppc* Δ*pyc* with point mutation G407S in isocitrate dehydrogenase	This work
Δ*ppc* Δ*pyc* ICD^{R453C}	*C. glutamicum* Δ*ppc* Δ*pyc* with point mutation R453C in isocitrate dehydrogenase	This work
Δ*ppc* Δ*pyc* ICD^{A94D} (pJC4*ilvBNCE*)	*C. glutamicum* Δ*ppc* Δ*pyc* ICD^{A94D} with overexpression plasmid for L-valine genes *ilvBNCE*	This work
Δ*ppc* Δ*pyc* ICD^{G407S} (pJC4*ilvBNCE*)	*C. glutamicum* Δ*ppc* Δ*pyc* ICD^{G407S} with overexpression plasmid for L-valine genes *ilvBNCE*	This work
Δ*ppc* Δ*pyc* ICD^{R453C} (pJC4*ilvBNCE*)	*C. glutamicum* Δ*ppc* Δ*pyc* ICD^{R453C} with overexpression plasmid for L-valine genes *ilvBNCE*	This work

Table 3. A complete list of the plasmids constructed and/or used in this work with their names, relevant characteristic(s), and the source.

Plasmid	Relevant characteristic(s)	Source
pK19*mobsacB*	Km^r, mobilizable (*oriT*), *oriV*	(Schäfer et al., 1994)
pK18*mobsacB* P*aceE dapA*-A16	pK18*mobsacB* carrying the *dapA*-A16 promoter	(Buchholz et al., 2013)
pK19*mobsacB* *hisG*^{FB}	pK19*mobsacB* carrying the nucleotide sequence of a modified *hisG* variant that encodes HisG with amino acid exchanges G233H and T235Q (corresponding nucleotide exchanges: ggc742cat, acg748cag)	This work
pK19*mobsacB* *hisD*-P_{tuf}	pK19*mobsacB* carrying promoter exchange to P_{tuf} for operon *hisD-hisC-hisB-cg2302-cg2301*	This work
pK19*mobsacB* *hisH*-P_{tuf}	pK19*mobsacB* carrying promoter exchange to P_{tuf} for operon *hisH-hisA-impA-hisF-hisI-*	This work
pK19*mobsacB* *hisN*-P_{tuf}	pK19*mobsacB* carrying promoter exchange to P_{tuf} for operon *cg0911-hisN*	This work
pK19*mobsacB* *hisE*^{ATG}-$P_{dapA\text{-}A16}$	pK19*mobsacB* carrying promoter exchange to $P_{dapA\text{-}A16}$ for operon *hisE-hisG* and an exchange of the translational start codon from the native GTG to ATG for *hisE*	This work
pK18*mobsacB* *zwf*^{A243T}	pK19*mobsacB* carrying the nucleotide sequence of a modified *zwf* variant that encodes a G6P DH with amino acid exchange A243T	Evonik Industries AG
pK19*mobsacB* *gnd*^{S361F}	pK19*mobsacB* carrying the nucleotide sequence of a modified *gnd* variant that encodes a 6PG DH with amino acid exchange G361F	Evonik Industries AG
pK19*mobsacB* *prsA*^{D122S}	pK19*mobsacB* carrying the nucleotide sequence of a modified *prsA* variant that encodes a PRPP synthetase with amino acid exchange D122S	This work
pK19*mobsacB* int::P_{dapA}*hisE*^{ATG} *hisG*^{FB}	pK19*mobsacB* carrying the nucleotide sequence of a cassette consisting of $P_{dapA\text{-}A16}$ *hisE*^{ATG}-*hisG*^{FB} T_{rrnB} for chromosomal integration between genes cg0901 and cg0902	This work
pK19*mobsacB* Δ*purF*	pK19*mobsacB* carrying an in-frame deletion of gene *purF*	This work
pK19*mobsacB* *purF*^{TTG}	pK19*mobsacB* carrying the nucleotide sequence for the exchange of the translational start codon of gene *purF* from GTG to TTG	This work
pK19*mobsacB* *purF*^{K348Q}	pK19*mobsacB* carrying the nucleotide sequence of a modified *purF* variant that encodes a amidophosphoribosyltransferase with amino acid exchange K348Q	This work
pK19*mobsacB* Δ*tkt*	pK19*mobsacB* carrying a in-frame deletion of the gene encoding transketolase	This work
pK19*mobsacB* Δ*tkt*^{S}	pK19*mobsacB* carrying a 4 bp deletion of the spacer region of the gene encoding transketolase	This work
pK19*mobsacB* Δ*tkt*^{SRbs}	pK19*mobsacB* carrying an 8 bp deletion of the spacer and RBS regions of the gene encoding transketolase	This work
pK19*mobsacB* *zwf*^{ATG}	pK19*mobsacB* carrying the nucleotide sequence for the exchange of the translational start codon of gene *zwf* from GTG to ATG	This work
pK19*mobsacB* *prsA*^{R}	pK19*mobsacB* carrying the nucleotide sequence of a modified RBS of gene *prsA*	This work
pK19*mobsacB* *prsA*^{D136A}	pK19*mobsacB* carrying the nucleotide sequence of a modified *prsA* variant that encodes a PRPP synthetase with amino acid exchange D136A	This work
pK19*mobsacB* *prsA*^{R87C}	pK19*mobsacB* carrying the nucleotide sequence of a modified *prsA* variant that encodes a PRPP synthetase with amino acid exchange R87C	This work
pK19*mobsacB* P_{tuf}:*rpi*	pK19*mobsacB* carrying promoter exchange to P_{tuf} for gene *rpi*	This work
pK19*mobsacB* Δ*pup*	pK19*mobsacB* carrying an in-frame deletion of gene *pup* encoding a prokaryotic ubiquitin-like system	(Küberl et al., 2014)
pK19*mobsacB* P_{gapA}:*hisE*^{ATG}*hisG*^{FB}	pK19*mobsacB* carrying promoter exchange to P_{gapA} for the modified operon *hisE-hisG*	This work
pK19*mobsacB* Δcg1305	pK19*mobsacB* carrying an in-frame deletion of gene cg1305 encoding a potential L-histidine transporter	This work
pK19*mobsacB* Δ*aroP*	pK19*mobsacB* carrying an in-frame deletion of gene *aroP* encoding a potential L-histidine transporter	This work

Plasmid	Relevant characteristic(s)	Source
pK19*mobsacB* Δcg2314	pK19*mobsacB* carrying an in-frame deletion of gene cg2314 encoding a potential purine regulator	This work
pK19*mobsacB* Δ*apt*	pK19*mobsacB* carrying an in-frame deletion of gene *apt* encoding a adenine pjosphoribosyltransferase	This work
pK19*mobsacB* *apt*^{TTG}	pK19*mobsacB* carrying the nucleotide sequence for the exchange of the translational start codon of gene *apt* from GTG to TTG	This work
pK19*mobsacB* *gapA*^{TTG}	pK19*mobsacB* carrying the nucleotide sequence for the exchange of the translational start codon of gene *gapA* from ATG to TTG	This work
pK19*mobsacB* *pgm*^{TTG}	pK19*mobsacB* carrying the nucleotide sequence for the exchange of the translational start codon of gene *pgm* from ATG to TTG	This work
pK19*mobsacB* Δ*purN*	pK19*mobsacB* carrying an in-frame deletion of gene *purN*	This work
pK19*mobsacB* Δ*fdhF*	pK19*mobsacB* carrying an in-frame deletion of gene *fdhF*	This work
pK19*mobsacB* Δ*purU*	pK19*mobsacB* carrying an in-frame deletion of gene *purU*	This work
pK19*mobsacB* Δ*purD*	pK19*mobsacB* carrying an in-frame deletion of gene *purD*	This work
pK19*mobsacB* Δ*ppc*	pK19*mobsacB* carrying a truncated version of the *ppc* gene	(Buchholz et al., 2013)
pK19*mobsacB* Δ*pyc*	pK19*mobsacB* carrying a truncated version of the *pyc* gene	(Peters-Wendisch et al., 1998)
pK19*mobsacB* Δ*pck*	pK19*mobsacB* carrying a truncated version of the *pck* gene	(Riedel et al., 2001)
pK19*mobsacB* ICD^{A94D}	pK19*mobsacB* carrying the nucleotide sequence for ICD amino acid exchange A94D	This work
pK19*mobsacB* ICD^{G407S}	pK19*mobsacB* carrying the nucleotide sequence for ICD amino acid exchange G407S	This work
pK19*mobsacB* ICD^{R453C}	pK19*mobsacB* carrying the nucleotide sequence for ICD amino acid exchange R453C	This work
pJC4	Km^r	(Cordes et al., 1992)
pJC4 *purA*	pJC4 overexpressing gene *purA* under control of P_{tuf} and T_{rrnB}	This work
pJC4 *purApurB*	pJC4 overexpressing genes *purA* and *purB* under control of P_{tuf} and T_{rrnB}	This work
pJC4 *hisD*	pJC4 overexpressing gene *hisD* under control of P_{sodA} and T_{lldD}	This work
pJC4 *purApurB* *hisD*	pJC4 overexpressing genes *purA* and *purB* under control of P_{tuf} and T_{rrnB} and *hisD* under control of P_{sodA} and T_{lldD}	This work
pJC4 *purH*	pJC4 overexpressing gene *purH* under control of P_{sodA} and T_{rrnB}	This work
pJC4 *sthA*	pJC4 overexpressing gene *sthA* from *E. coli* K-12 MG1655 under control of P_{tuf}	This work
pJC4*ilvBNCE*	Km^r, plasmid carrying the *ilvBNCE* genes from *C. glutamicum* encoding the L-valine biosynthetic enzymes acetohydroxyacid synthase, isomeroreductase, and transaminase B	(Radmacher et al., 2002)
pEC-XT99A_gcv_OP1-Cjk	IPTG-inducible overexpression plasmid for genes *gcvP*, *gcvT*, *gcvH*, *lipA*, and *lipB* from *C. jeikeium*, Tet^r	Evonik Industries AG
pEKEx3 *aspA*	pEKEx3 overexpressing gene *aspA*, Spec^r	Volker Wendisch
pEKEx3 *aspB*	pEKEx3 overexpressing gene *aspB*, Spec^r	Volker Wendisch

Abbreviations: Km^r, kanamycin resistance gene; Spec^r, spectinomycin resistance gene; Tet^r, tetracycline resistance gene.

Table 4. A complete list of the oligonucleotides used in this work including their short names, working names, sequences (5' to 3'), and their purpose/characteristic(s) sorted by short name in alphabetical order. The necessary homologous region for isothermal assembly and classical DNA ligation has been considered. Restriction sites are underlined and refer to the given restriction enzymes. Respective nucleotide exchanges are indicated in bold.

Short Name	Working name	Sequence 5' to 3'	Purpose, characteristic(s)
A94D1	icd_A94D_for	5'-CCGGAATTCGAACAGATCACAGAATCCAA C -3'	Primer #1 for flank1 for amino acid exchange A94D in ICD, *Eco*RI site underlined
A94D2	icd_A94D_2	5'- GTCCTGCAGTTCCTTAATA**T**CAGCCTTGAG CTGTGGAAC -3'	Primer #2 for flank1 for amino acid exchange A94D in ICD, nucleotide leading to amino acid exchange bold
A94D3	icd_A94D_3	5'- GTTCCACAGCTCAAGGCTG**A**TATTAAGGA ACTGCAGGAC -3'	Primer #1 for flank2 for amino acid exchange A94D in ICD, nucleotide leading to amino acid exchange bold
A94D4	icd_A94D_rev	5'- CGCGGATCCGATTGGGTCGGAGACCTTCA TC -3'	Primer #2 for flank2 for amino acid exchange A94D in ICD, *BamH*I site underlined
A94Dseq1	A94D_seq_1	5'- GTAGAACACTGTATTCTAG -3'	Sequencing primer to verify nucleotide exchange leading to A94D in *icd* by sequencing
A94Dseq2	A94D_seq_2	5'- GAACTTCATCAGCAGCGTC-3'	Sequencing primer to verify nucleotide exchange leading to A94D in *icd* by sequencing
A94Dseq3	A94D_seq_3	5'- CTCGCTGGACGCATCCTC -3'	Sequencing primer to verify nucleotide exchange leading to A94D in *icd* by sequencing
ABseq1		5'- GCGATTGAAGACCGTC -3'	Sequencing primer for pJC4 *purA purB*
ABseq2		5'- GCAATCGGCACCACCGGC -3'	Sequencing primer for pJC4 *purA purB*
ABseq3		5'- GCCTGCATGGGACGAAG -3'	Sequencing primer for pJC4 *purA purB*
ABseq4		5'- GTCACCGAACTGCTCAAC -3'	Sequencing primer for pJC4 *purA purB*
ABseq5		5'- GATGGAAGCAGGATCGCG -3'	Sequencing primer for pJC4 *purA purB*
aroP1	aroP_del1	5'- AGGTCGACTCTAGAGGATCCCCGGGAGAG TTCACAGGTTTAAGC -3'	Primer #1 for flank1 for deletion of *aroP*
aroP2	aroP_del2	5'- TATCGGCCTAGTATCAACCGTAAACCCAC -3'	Primer #2 for flank1 for deletion of *aroP*
aroP3	aroP_del3	5'- CGGTTGATACTAGGCCGATAGAAATTATT CTGGACGTCATG -3'	Primer #1 for flank2 for deletion of *aroP*
aroP4	aroP_del4	5'- TTGTAAAACGACGGCCAGTGAATTCTGAG CGGATCCGCGTCCG -3'	Primer #2 for flank2 for deletion of *aroP*
cg0901_for	cg0901_for	5'- CTTGCATGCCTGCAGGTCGACTTCTAGACC GTTCGGCTGACTCCTTC -3'	Primer #1 for amplification of flank1 for integrating *hisEG* cassette, *Xba*I site underlined
cg0901_rev	cg0901_rev	5'- GTGATAACTGCAGAACCAATGCATCATCA AAAAATCCGCCGTTCCTTG -3'	Primer #2 for amplification of flank1 for integrating *hisEG* cassette
cg0902_for	cg0902_for	5'- GTCGGTGAACGCTCTCCTACTAAGTGAGT TTGGATGCGGAAG -3'	Primer #1 for amplification of flank2 for integrating *hisEG* cassette
cg0902_rev	cg0902_rev	5'- GTGAATTCGAGCTCGGTACCCGGCCCGGG CTCACTAGTACGCGGATAAATG -3'	Primer #2 for amplification of flank2 for integrating *hisEG* cassette, *Xma*I site underlined
cg1305-1	1305_del1	5'- CTATGACCATGATTACGCCAAGCTTCAGA AGTATCCGCAACCC -3'	Primer #1 for flank1 for deletion of cg1305
cg1305-2	1305_del2	5'- CGAGTCTAGACGAGATGCTGACCTCGTTT C -3'	Primer #2 for flank1 for deletion of cg1305
cg1305-3	1305_del3	5'- CAGCATCTCGTCTAGACTCGCACGAAAAA GGC -3'	Primer #1 for flank2 for deletion of cg1305
cg1305-4	1305_del4	5'- TTGTAAAACGACGGCCAGTGAATTCAGTG GCGCCGTTGTAGCG -3'	Primer #2 for flank2 for deletion of cg1305

Short Name	Working name	Sequence 5' to 3'	Purpose, characteristic(s)
cg2314-1	cg2314_del1	5'- CTTGCATGCCTGCAGGTCGACtctagaGTGTTGGTACGGATGGAGTCG -3'	Primer #1 for flank1 for deletion of cg2314
cg2314-1	cg2314_del2	5'- GTGTGCACCTTCGGTATTTTCGACCTCATCTACCTCTTTTTCTTAATCTCTTACATC -3'	Primer #2 for flank1 for deletion of cg2314
cg2314-1	cg2314_del3	5'- GATGTAAGAGATTAAGAAAAAGAGGTAGATGAGGTCGAAAATACCGAAGGTGCACAC -3'	Primer #1 for flank2 for deletion of cg2314
cg2314-1	cg2314_del4	5'- CTTGCGGCAGCGTGAAGCTAGCGTGGGTGTGGTGACAGCTGCACTC -3'	Primer #2 for flank2 for deletion of cg2314
cg2314-5	cg2314_seq1	5'- GCGTCCAGCACCGATGAG -3'	Verification of cg2314 deletion
dapA1		5'- AACTGCAGAACCAATGCATTGGTTCTGCAGTTATCACACCC -3'	Primer #1 for amplification of $P_{dapA\text{-}A16}$, *Nsi*I site underlined
dapA2		5'- GGGAATTCCATATGAGGCTCCTTTTAAATCGAGCGGCTCCGGTCTTAGCTGTTAAACC -3'	Primer #2 for amplification of $P_{dapA\text{-}A16}$, *Nde*I site underlined
fdhF1	fdhF_del1	5'- GCTAGCTAGGACCCAGACGTTGTCTGCATCG -3'	Primer #1 for flank1 for deletion of *fdhF*, *Nhe*I site underlined
fdhF2	fdhF_del2	5'- CGGGCGCGGAAAATTCCCTGGTGTTTTTAGGTCACAGTCTAGACCCGGCAATTGAAC -3'	Primer #2 for flank1 for deletion of *fdhF*
fdhF3	fdhF_del3	5'- GTTCAATTGCCGGGTCTAGACTGTGACCTAAAAACACCAGGGAATTTTCCGCGCCCG -3'	Primer #1 for flank2 for deletion of *fdhF*
fdhF4	fdhF_del4	5'- CGCGGATCCCCGAATTTCTAGAGGCTCCTC -3'	Primer #2 for flank2 for deletion of *fdhF*, *BamH*I site underlined
fdhFdel1	fdhF_fw	5'- GTGCGATTCGGTACTTTGCAG -3'	Verification of *fdhF* deletion
fdhFdel2	fdhF_rev	5'- CTCGTTTCTGATGATGGCTGC -3'	Verification of *fdhF* deletion
G407S2	icd_G407S_2	5'- CTTCAGCCTTCTGAGCCATCAGAC**T**AACGTTAGGGACGGTACCCATGGTG -3'	Inner primer #1 for amino acid exchange G407S in ICD, nucleotide leading to amino acid exchange bold
G407S3	icd_G407S_3	5'- CACCATGGGTACCGTCCCTAACGTT**A**GTCTGATGGCTCAGAAGGCTGAAG -3'	Inner primer #2 for amino acid exchange G407S in ICD, nucleotide leading to amino acid exchange bold
gapA_seq1	gapA_fw	5'- GATCCTCAAATGACCAAG -3'	Sequencing primer for $gapA^{TTG}$
gapA_seq2	gapA_seq2	5'- GCAGCGTTGATGGACTC -3'	Sequencing primer for $gapA^{TTG}$
gapA_seq3	gapA_rev	5'- CAGATCGTAGTGCGAACG -3'	Sequencing primer for $gapA^{TTG}$
gapA1	gapA_1	5'- CAGGAAACAGCTATGACCATGATTACGCCAAGCTTGAAGCCTAAAAACGACCGAG -3'	Primer #1 for amplification of flank1 for integrating $gapA^{TTG}$
gapA2	gapA_TTG_2	5'- AACACGAATGGTCAAGTTG**T**GTCTCCTCTAAAGATTGTAG -3'	Primer #2 for amplification of flank1 for integrating $gapA^{TTG}$, nucleotide exchange bold
gapA3	gapA_TTG_3	5'- TAGAGGAGACACAAC**T**TGACCATTCGTGTTGGTATTAACG -3'	Primer #1 for amplification of flank2 for integrating $gapA^{TTG}$, nucleotide exchange bold
gapA4	gapA_4	5'- CGGCCAGTGAATTCGAGCTCGGTACCCGGGGATCCCATTGGTGCGAGGCAGTTGG -3'	Primer #2 for amplification of flank2 for integrating $gapA^{TTG}$
gcv_Cjk_MluI_XbaI		5'- CAGTCTAGAACGCGTGGAACCGACCATAGGGTCTTG-3'	Primer #2 for amplification of gene cluster *gcvPTH* from *C. jeikeium* genome
gcv_Cjk_start_EcoRV		5'- ATCGATATCCGAGAGGAGACACAACATGTCTTCTGCAGCTACTCGC-3'	Primer #1 for amplification of gene cluster *gcvPTH* from *C. jeikeium* genome
gnd_seq	gnd_check	5'- GTATTGCTACCACCGGCATCG -3'	Sequencing primer for introduction of nucleotide exchange in gene *gnd* leading to amino acid exchange S361F
gnd1	gnd_fw	5'- GGATGCTGAAACCGGCAAGC -3'	Primer #1 for introduction of nucleotide exchange in gene *gnd* leading to amino acid exchange S361F
gnd2	gnd_rev	5'- CCGAAGAAGTCGCGCTGTCC -3'	Primer #2 for introduction of nucleotide exchange in gene *gnd* leading to amino acid exchange S361F
hisD1		5'- CCCAAGCTTCGGTGTCGCTGAAGTTAAGTTCTG -3'	Outer primer #1 for exchange of native promoter with P_{tuf} in operon

Short Name	Working name	Sequence 5' to 3'	Purpose, characteristic(s)
			hisD-hisC-hisB-cg2302-cg2301, *Hind*III site underlined
hisD2		5'- CGCAGGTCAGTGACATTCAACATATGTAT TATGCATCTCGACCACCCCAGATTTACCTG -3'	Inner primer #1 for exchange of native promoter with P_{tuf} in operon *hisD-hisC-hisB-cg2302-cg2301*, *Nde*I and *Nsi*I sites underlined
hisD3		5'- CAGGTAAATCTGGGGTGGTCGAGATGCAT AATACATATGTTGAATGTCACTGACCTGCG -3'	Inner primer #2 for exchange of native promoter with P_{tuf} in operon *hisD-hisC-hisB-cg2302-cg2301*, *Nde*I and *Nsi*I sites underlined
hisD4		5'- CGCGGATCCCTCATCAACACCCAAGATGG AAC -3'	Outer primer #2 for exchange of native promoter with P_{tuf} in operon *hisD-hisC-hisB-cg2302-cg2301*, *BamH*I site underlined
hisD5	hisD_fw	5'- CCTACGAAAGGATTTTTTACCCATGTTGAA TGTCACTGACCTGCGAG -3'	Amplifying *hisD* for pJC4 *purApurB hisD* and pJC4 *hisD*
hisD6	hisD_rev	5'- CTTCTCTCATCCGCCAAAACAGTTAGGCCT CGTCGGTGGTGGGGAGG -3'	Amplifying *hisD* for pJC4 *purApurB hisD* and pJC4 *hisD*
hisE1		5'- CCCAAGCTTCTGACAGAGTTGAAGGCCCT CGAG -3'	Outer primer #1 for exchange of native promoter with $P_{dapA\text{-}A16}$ and change of the translational start codon from GTG to ATG in operon *hisE-hisG*, *Hind*III site underlined
hisE2		5'- CGTACAGCGAGTCAAATGTCTTCA**T**ATGT ATTATGCATCTCGGAGGATATTAGTCGAATA ATTTC -3'	Inner primer #1 for exchange of native promoter with $P_{dapA\text{-}A16}$ and change of the translational start codon from GTG to ATG in operon *hisE-hisG*, *Nde*I and *Nsi*I sites underlined, base exchange bold
hisE3		5'- GAAATTATTCGACTAATATCCTCCGAGAT GCATAATACATATGAAGACATTTGACTCGCT GTACG -3'	Inner primer #2 for exchange of native promoter with $P_{dapA\text{-}A16}$ and change of the translational start codon from GTG to ATG in operon *hisE-hisG*, *Nde*I and *Nsi*I sites underlined, base exchange bold
hisE4		5'- CGCGGATCCGCAACGTAGATGGCGATATC TTTAGG -3'	Outer primer #1 for exchange of native promoter with $P_{dapA\text{-}A16}$ and change of the translational start codon from GTG to ATG in operon *hisE-hisG*, *BamH*I site underlined
hisEG1	hisEG_1	5'- CGCAAGCTTGCGCTACCGGGCTGGCATGT TCG -3'	Primer #1 for flank1 for exchanging $P_{dapA\text{-}A16}$ promoter against P_{gapA} in modified *hisEG* operon, *Hind*III site underlined
hisEG2	hisEG_2b	5'- CAAAGATTTCGCAGCAGATGCAAAATCGG AGGATATTAGTCGAATAATTTC -3'	Primer #2 for flank1 for exchanging $P_{dapA\text{-}A16}$ promoter against P_{gapA} in modified *hisEG* operon
hisEG3	hisEG_5b	5'- GCATTTCCTACAATCTTTAGAGGAGACAC AACATGAAGACATTTGACTCGCTGTACG -3'	Primer #1 for flank2 for exchanging $P_{dapA\text{-}A16}$ promoter against P_{gapA} in modified *hisEG* operon
hisEG4	hisEG_6	5'- CGCGGATCCCTTCGTGGACATCAGCCTGG -3'	Primer #2 for flank2 for exchanging $P_{dapA\text{-}A16}$ promoter against P_{gapA} in modified *hisEG* operon, *BamH*I site underlined
hisEGseq1	hisEG_seq1	5'- CCTGCAGTACAGCGATATTG -3'	Sequencing primer for P_{gapA} in front of modified *hisEG* operon
hisEGseq2	hisEG_seq2	5'- CCTGCAGTACAGCGATATTG -3'	Sequencing primer for P_{gapA} in front of modified *hisEG* operon
hisEGseq3	hisEG_seq3	5'- CCTGCAGTACAGCGATATTG -3'	Sequencing primer for P_{gapA} in front of modified *hisEG* operon
hisF1		5'- CGCAAGCTTCTCCATGCCCATGCTGGGTA AACGC -3'	Primer #1 for integration of stop codon and P_{sodA} in front of *hisF*, *Hind*III site underlined

Short Name	Working name	Sequence 5' to 3'	Purpose, characteristic(s)
hisF2		5'- GTCACAAGCCCGGAATAATTGGCAG**TTAT** TTACTTGTACTCCTCATTTAACG -3'	Primer #2 for integration of stop codon and P_{sodA} in front of *hisF*, stop codon bold
hisF3		5'- GAAACCTACGAAAGGATTTTTTACCCATG GGCGTGGCAATTCGAGTTATTC -3'	Primer #5 for integration of stop codon and P_{sodA} in front of *hisF*
hisF4		5'- CGCGGATCCCGCCGCGCTTTGCCCACTCG ATTGC -3'	Primer #6 for integration of stop codon and P_{sodA} in front of *hisF*, *BamH*I site underlined
hisFseq		5'- CTGACACCGAAGGCCATC -3'	
hisG1		5'- CGCGGATCCCAGCTCGATTTGGGTATCAC CG -3'	Outer primer #1 for introduction of $hisG^{G233H\text{-}T235Q}$, *BamH*I site underlined
hisG2		5'- CCAGTTGTCGCGTGCCAGTGGGGATACCT GTGGATGGGATAAGCCTGGGGTTACTGC -3'	Inner primer #1 for introduction of $hisG^{G233H\text{-}T235Q}$, affected triplets underlined
hisG3		5'- GCAGTAACCCCAGGCTTATCCCATCCACA GGTATCCCCACTGGCACGCGACAACTGG -3'	Inner primer #2 for introduction of $hisG^{G233H\text{-}T235Q}$, affected triplets underlined
hisG4		5'- CGCGGATCCGTTGATGGTGGTTCGTGAGA TTTGG -3'	Outer primer #2 for introduction of $hisG^{G233H\text{-}T235Q}$, *BamH*I site underlined
hisGseq		5'- GGTATCCATCAAGCTTGG -3'	Sequencing primer for $hisG^{G233H\text{-}T235Q}$
hisH1		5'- CCCAAGCTTCGGAGTGAAATGAGGTCCTT GGTC -3'	Outer primer #1 for exchange of native promoter with P_{tuf} in operon *hisH-hisA-impA-hisF-hisI-cg2294*, *Hind*III site underlined
hisH2		5'- GAGAAGGGCGACAGTTTTGGTCATATGTA TTATGCATCTCCCTTCCTGAGAATGACGGCTA GTCG -3'	Inner primer #1 for exchange of native promoter with P_{tuf} in operon *hisH-hisA-impA-hisF-hisI-cg2294*, *Nde*I and *Nsi*I sites underlined
hisH3		5'- CGACTAGCCGTCATTCTCAGGAAGGGAGATG CATAATACATATGACCAAAACTGTCGCCCTTC TC -3'	Inner primer #1 for exchange of native promoter with P_{tuf} in operon *hisH-hisA-impA-hisF-hisI-cg2294*, *Nde*I and *Nsi*I sites underlined
hisH4		5'- CGCGGATCCGCACGAAGTAGAAACGCTCA TCAGG -3'	Inner primer #2 for exchange of native promoter with P_{tuf} in operon *hisH-hisA-impA-hisF-hisI-cg2294*, *BamH*I site underlined
hisN1		5'- CCCAAGCTTCGCATGAGCATTTCAGCCCA GTCC -3'	Outer primer #1 for exchange of native promoter with P_{tuf} in operon *cg0911-hisN*, *Hind*III site underlined
hisN2		5'- GCTCTGGATTAGTCATGCCTTCCATATGTA TTATGCATCTCGGTGGCGTTCTAAGAATCACA ATCG -3'	Inner primer #1 for exchange of native promoter with P_{tuf} in operon *cg0911-hisN*, *Nde*I and *Nsi*I sites underlined
hisN3		5'- CGATTGTGATTCTTAGAACGCCACCGAGA TGCATAATACATATGGAAGGCATGACTAATC CAGAGC -3'	Inner primer #2 for exchange of native promoter with P_{tuf} in operon *cg0911-hisN*, *Nde*I and *Nsi*I sites underlined
hisN4		5'- CGCGGATCCCACCGAACCACGTATAACCCAT GG -3'	Outer primer #2 for exchange of native promoter with P_{tuf} in operon *cg0911-hisN*, *BamH*I site underlined
int_seq1	int_seq_1	5'- CTGGCATGCGCCACTCCG -3'	Sequencing primer for genomic integration of *hisEG* cassette
int_seq2	int_seq_2	5'- CGGAGAGGTCTGGATTGC -3'	Sequencing primer for genomic integration of *hisEG* cassette
int_seq3	int_seq_3	5'- GTAGAGGTATCCATCAAGC -3'	Sequencing primer for genomic integration of *hisEG* cassette
int_seq4	int_seq_4	5'- CGTAGCGCCGATGGTAGTG -3'	Sequencing primer for genomic integration of *hisEG* cassette
int1	PdapAhisEG_for	5'- CAAGGAACGGCGGATTTTTTGATGATGCA TTGGTTCTGCAGTTATCAC -3'	Primer #1 for amplification of modified *hisEG* operon
int2	PdapAhisEG_rev	5'- CTTCTCTCATCCGCCAAAACAGCTAGATG CGGGCGATGCGG -3'	Primer #2 for amplification of modified *hisEG* operon

Short Name	Working name	Sequence 5' to 3'	Purpose, characteristic(s)
K348Qseq1	K348Q_seq	5'- CGAAGCCCGACTTGAAATCG -3'	Sequencing primer for *purF*^{K348Q}
K348Qseq2	K348Q_seq2	5'- CTCCCAAGTTTTCGACGAAC -3'	Sequencing primer for *purF*^{K348Q}
lipB-Cjk_start-EcoRV		5'- GCGGATATCATGGGATTCCAGCAAGGC-3'	Primer #1 for amplification of gene cluster *lipAB* from *C. jeikeium* genome
lipA-Cjk_stop-XbaI		5'- GCGTCTAGATCCTTCGCCATGGATTCAAC-3'	Primer #2 for amplification of gene cluster *lipAB* from *C. jeikeium* genome
lldD1	TlldD_hisD	5'- CCTCCCCACCACCGACGAGGCCTAAAAGTTTCTCTCCTTAGCTATTAAAAG -3'	Amplifying T_{lldD} for pJC4 *purApurB hisD* and pJC4 *hisD*
lldD2	TlldD_rev	5'- CTTCACGAGGCAGACCTCAGCgctagcGATGTCCCAAATTGAAAGTGCTG -3'	Amplifying T_{lldD} for pJC4 *purApurB hisD* and pJC4 *hisD*
pckdel1	pckdel1	5'- GTTGATGGATCCCAGGCTGAGTG-3'	Verification of *pck* deletion
pckdel2	pckdel2	5'- GAACTGGCTGTGAACCTCTGCAG-3'	Verification of *pck* deletion
PgapA1	hisEG_3b	5'- GAAATTATTCGACTAATATCCTCCGATTTTGCATCTGCTGCGAAATCTTTG -3'	Primer #1 for amplification of P_{gapA}
PgapA2	hisEG_4b	5'- CGTACAGCGAGTCAAATGTCTTCATGTTGTGTCTCCTCTAAAGATTGTAGGAAATGC -3'	Primer #2 for amplification of P_{gapA}
pgi1		5'- CCCAAGCTTCAGCGTTGCGTGACGCACTCATTG -3'	Outer primer #1 for introduction of *pgi*^{GTG}, *Hind*III site underlined
pgi2		5'- CCAAACCTGGGTGGTCGAAATGTCCGCCACGAAAACTCCTTTATTGTCG -3'	Inner primer #1 for introduction of *pgi*^{GTG}, nucleotide exchange bold
pgi3		5'- CGACAATAAAGGAGTTTTC**G**TGGCGGACATTTCGACCACCCAGGTTTGG -3'	Inner primer #2 for introduction of *pgi*^{GTG}, nucleotide exchange bold
pgi4		5'- CGCGGATCCCCAATGTTGACGATCTTCTTGATCG -3'	Outer primer #2 for introduction of *pgi*^{GTG}, *BamH*I site underlined
pgiseq		5'- CAAGCGTTGGGTTAAGGAGGA -3'	Sequencing primer for *pgi*^{GTG}
pgm_seq1	pgm_seq1	5'- CAGCCCACAGCGGTGAAG -3'	Sequencing primer for *pgm*^{TTG}
pgm_seq2	pgm_seq2	5'- AGCCACAACGTCAGCGC -3'	Sequencing primer for *pgm*^{TTG}
pgm_seq3	pgm_seq3	5'- CCAAGGATGATGCCATCG -3'	Sequencing primer for *pgm*^{TTG}
pgm1	pgm_1	5'- CAGGAAACAGCTATGACCATGATTACGCCAAGCTTGCTCCACCGCAGAAAGCCTC -3'	Primer #1 for amplification of flank1 for integrating *pgm*^{TTG}
pgm2	pgm_TTG_2	5'- GCGTTCATGTGCCA**A**GTTTGCTCCTTAAAACACCAATACTTTCTC -3'	Primer #2 for amplification of flank1 for integrating *pgm*^{TTG}, nucleotide exchange bold
pgm3	pgm_TTG_3	5'- TTTTAAGGAGCAAAC**T**TGGCACATGAACGCGCCGG -3'	Primer #1 for amplification of flank2 for integrating *pgm*^{TTG}, nucleotide exchange bold
pgm4	pgm_4	5'- CGGCCAGTGAATTCGAGCTCGGTACCCGGGGATCCCATCACGAGGAGGGTTGTGGGATG -3'	Primer #2 for amplification of flank2 for integrating *pgm*^{TTG}
pJC4hisD1	pJC4_hisD1	5'- GCATCTTCCAGGAAATCTCCG -3'	Sequencing primer for pJC4 *purApurB hisD* and pJC4 *hisD*
pJC4hisD2	pJC4_hisD-seq	5'- TGTGCTTCCCATAGTGCAG -3'	Sequencing primer for pJC4 *purApurB hisD* and pJC4 *hisD*
pJC4hisD3	pJC4_hisD2	5'- CTCTCATCAACCGTGGCTC -3'	Sequencing primer for pJC4 *purApurB hisD* and pJC4 *hisD*
pK19-fw	pK19-fw	5'- TAATGCAGCTGGCACGAC -3'	Sequencing primer for pK19*mobsacB* inserts
pK19-rev	pK19-rev	5'- GTAGCTGACATTCATCCG -3'	Sequencing primer for pK19*mobsacB* inserts
prsA_seq1	prsA_seq_1	5'- GAACCGCTGCAGCACAAG -3'	Sequencing primer for *prsA* mutations
prsA_seq2	prsA_seq_2	5'- GGTCGTGCGCACCCAGAACTG -3'	Sequencing primer for *prsA* mutations
prsA_seq3	prsA_seq_3	5'- CACTTCTCTGCAACCTTC -3'	Sequencing primer for *prsA* mutations
prsA1	prsA_for	5'- CGCAAGCTTGTCTTCGTGAACTACGACG -3'	Outer primer #1 for introduction of *prsA* mutations, *Hind*III site underlined
prsA2.1	prsA_R87C_1	5'- CGCGGTGATGCGCTTTGCGGAACCACACTTCAAAGCGTCGATCATCAGC -3'	Inner primer #1 for introduction of *prsA*^{R87C}, affected triplet underlined

Short Name	Working name	Sequence 5' to 3'	Purpose, characteristic(s)
prsA2.2	prsA_D122S_1	5'- CGGTCCGCGCCAGCGGTGAGCATGAGGGA GGCGATGAGGCGAGCAGAAATTGGC -3'	Inner primer #1 for introduction of *prsA*^{D122S}, affected triplet underlined
prsA2.3	prsA_D136A_1	5'- CTGGATCTGATCGGTGTGCAATGCCACGG ACACGATACGGTCCGCGC -3'	Inner primer #1 for introduction of *prsA*^{D136A}, affected triplet underlined
prsA3.1	prsA_R87C_2	5'- GCTGATGATCGACGCTTTGAAGTGTGGTT CCGCAAAGCGCATCACCGCG -3'	Inner primer #2 for introduction of *prsA*^{R87C}, affected triplet underlined
prsA3.2	prsA_D122S_2	5'- GCCAATTTCTGCTCGCCTCATCGCCTCCCT CATGCTCACCGCTGGCGCGGACCG -3'	Inner primer #2 for introduction of *prsA*^{D122S}, affected triplet underlined
prsA3.3	prsA_D136A_2	5'- GCGCGGACCGTATCGTGTCCGTGGCATTG CACACCGATCAGATCCAG -3'	Inner primer #2 for introduction of *prsA*^{D136A}, affected triplet underlined
prsA4	prsA_rev	5'- GAATTCCGGCTGGGTCAGAGAACACAC -3'	Outer primer #2 for introduction of *prsA* mutations, *Eco*RI site underlined
prsArbs1	prsA_1_RBS_ex	5'- CGCAAGCTTGCACCCACGGTTTCGACTCC -3'	Primer #1 for flank1 for modifying the native RBS of *prsA*
prsArbs2	prsA_2_RBS_ex	5'- GTTTCCAGTGAGCAGTCATGGTATGTCCTC CTGCTTAGCCTTCCTGGTTGTGGACG -3'	Primer #2 for flank1 for modifying the native RBS of *prsA*
prsArbs3	prsA_3_RBS_ex	5'- CGTCCACAACCAGGAAGGCTAAGCAGGA GGACATACCATGACTGCTCACTGGAAAC -3'	Primer #1 for flank2 for modifying the native RBS of *prsA*
prsArbs4	prsA_4_RBS_ex	5'- CGCGGATCCCGCAGATGTTGTCCAGGTTG -3'	Primer #2 for flank2 for modifying the native RBS of *prsA*
pup1	dpupcheckfw	5'- TAGTGGTGGCACTTGATACG -3'	Verification primer for deletion of *pup*
pup2	dpupcheckrev	5'- CCTGCAGTACAGCGATATTG -3'	Verification primer for deletion of *pup*
purA1	purA_fw	5'- CGAAGTCCAGGAGGACATACAATGGCTGC AATCGTTATTGTCGGCGCTCAATG -3'	Primer #1 for amplification of *purA* (cg3063)
purA2		5'- GATCTTCTTTTTATCAGCCACTGTATGTCC TCCTGGACTTCCTAGTTGTCAGCTAGTACG -3'	Primer #2 for amplification of *purA* (cg3063)
purArev	purA_rev	5'- GAAAATCTTCTCTCATCCGCCAAAACAGC TAGTTGTCAGCTAGTACGTCATGCAG -3'	Cloning *purA* into pJC4
purAseq	pJC4_rev2	5'- GCTACGCGATTGGGTTC -3'	Cloning *purA* into pJC4
purAseq2	purA_seq1	5'- GCAATCGGCACCACCGGC -3'	Cloning *purA* into pJC4
purB1		5'- CGTACTAGCTGACAACTAGGAAGTCCAGG AGGACATACAGTGGCTGATAAAAAGAAGATC -3'	Primer #1 for amplification of *purB* (cg2876)
purB2		5'- CTTCTCTCATCCGCCAAAACAGTTAAAGA ATCTCACCTGGTCGGTAGTC -3'	Primer #2 for amplification of *purB* (cg2876)
purD1	purD_for	5'- GCGAAGCTTGCCATGGCGTTGCGGAAATC GTAATCG -3'	Primer #1 for flank1 for in-frame deletion of *purD*, *Hind*III site underlined
purD2	purD_del1	5'- GACAAGCCTATCTGCGTACTGCTTGGTTGC ACAGTTTATCCTGCAAAAC -3'	Primer #2 for flank1 for in frame deletion of *purD*
purD3	purD_del2	5'- GTTTTGCAGGATAAACTGTGCAACCAAGC AGTACGCAGATAGGCTTGTC -3'	Primer #1 for flank2 for in frame deletion of *purD*
purD4	purD_rev	5'- CGCGGATCCCCTCCAACATTTGAGCGGTT GGCTG -3'	Primer #2 for flank2 for in-frame deletion of *purD*, *BamH*I site underlined
purF1	purF_for_new	5'- ACATGCATGCGGAGCGGTGTGGATTCTCA CG -3'	Primer #1 for flank1 for in-frame deletion of *purF*, *Pae*I site underlined
purF10	K348Q_1	5'- GGCCAAGGCATGGTCCAGAACGCCTACGT TGGC -3'	Primer #2 for flank1 for *purF*^{K348Q}, affected triplet bold
purF11	K348Q_2	5'- GCCAACGTAGGCGTTCTGGACCATGCCTT GGCC -3'	Primer #1 for flank2 for *purF*^{K348Q}, affected triplet bold
purF12	purFK348Q_rev	5'- CGCGGATCCGACTCCTGCTGCTGCGTATG -3'	Primer #2 for flank2 for *purF*^{K348Q}, *BamH*I site underlined
purF2	purF_del_1	5'- CAACCCCTATCGCCTACCGATCAGGTCAA ATCGTAGTCTGTCGG -3'	Primer #2 for flank1 for in-frame deletion of *purF*
purF3	purF_del_2	5'- CCGACAGACTACGATTTGACCTGATCGGT AGGCGATAGGGGTTG -3'	Primer #1 for flank2 for in-frame deletion of *purF*
purF4	purF_rev	5'- CGCGGATCCCTGCCTGGACACAGCCTTCT GC -3'	Primer #2 for flank2 for in-frame deletion of *purF*, *BamH*I site underlined
purF5	purF_for	5'- CCCAAGCTTGGAGCGGTGTGGATTCTCAC G -3'	Primer #1 for flank1 for *purF*^{TTG}, *Hind*III site underlined

Short Name	Working name	Sequence 5' to 3'	Purpose, characteristic(s)
purF6	purF_GtoT_2	5'- CGTGTGCTGATCAAGTAATGCCA**A**AGGTC AAATCGTAGTCTGTCGG -3'	Primer #2 for flank1 for *purF*^{TTG}, nucleotide exchange bold
purF7	purF_GtoT_3	5'- CCGACAGACTACGATTTGACCT**T**TGGCAT TACTTGATCAGCACACG -3'	Primer #1 for flank2 for *purF*^{TTG}, nucleotide exchange bold
purF8	purF_GtoT_4	5'- CGCGGATCCGGATCGACGAGGCCAAGTTC -3'	Primer #2 for flank2 for *purF*^{TTG}, *BamH*I site underlined
purF9	purFK348Q_for	5'- CCCAAGCTTGATTGCGGACTGGTTAC -3'	Primer #1 for flank1 for *purF*^{K348Q}, *Hind*III site underlined
purH1	purH_fw	5'- GGAAACCTACGAAAGGATTTTTTACCCAT GAGCGATGATCGTAAGGCAATTAAAC -3'	Amplifying gene *purH* for pJC4 *purH*
purH2	purH_rev	5'- CTTCTCTCATCCGCCAAAACAGTTAGTGA GCGAAGTGTCGCGC -3'	Amplifying gene *purH* for pJC4 *purH*
purHseq1	pJC4_purH1new	5'- GGTCGCCCCATTCCAGC -3'	Sequencing primer for pJC4 *purH*
purHseq2	pJC4_purH2	5'- GCTTGCGTTGAGCAGATC -3'	Sequencing primer for pJC4 *purH*
purN1	purN_del1	5'- GCTCTAGAGCGTCTTCAGCGTGCATTCCG -3'	Primer #1 for flank1 for deletion of *purN*, *Xba*I site underlined
purN2	purN_del2	5'- CCTTACGATCATCGCTCATGAAGGATAAC AGATATGTTAACGGTCTTCGGC -3'	Primer #2 for flank1 for deletion of *purN*
purN3	purN_del3	5'- GCCGAAGACCGTTAACATATCTGTTATCCT TCATGAGCGATGATCGTAAGG -3'	Primer #1 for flank2 for deletion of *purN*
purN4	purN_del4	5'- CCGGAATTCCGGTGTGGCGGAAAGCCTC -3'	Primer #2 for flank2 for deletion of *purN*, *EcoR*I site underlined
purNdel1	cg0982_fw	5'- GACGAAGAGGAGCATGTTG -3'	Verification of *purN* deletion
purNdel2	purN_rev	5'- CAGGAATACCAAGCTCAGC -3'	Verification of *purN* deletion
purU1	purU_del1	5'- CCCAAGCTTGCACCAGCAGCAATCAACG -3'	Primer #1 for flank1 for deletion of *purU*, *Hind*III site underlined
purU2	purU_del2	5'- GTTTAGGGTCGCGTCGAAAAGCAAAAAGC CTCGTTGCATTCTACCCTGGAAATTTTCC -3'	Primer #2 for flank1 for deletion of *purU*
purU3	purU_del3	5'- GGAAAATTTCCAGGGTAGAATGCAACGAG GCTTTTTGCTTTTCGACGCGACCCTAAAC -3'	Primer #1 for flank2 for deletion of *purU*
purU4	purU_del4	5'- CGTCTAGACTGTGGCAGATCGGAATCTAC CTCTTCG -3'	Primer #2 for flank2 for deletion of *purU*, *Xba*I site underlined
purUdel1	deoC_fw	5'- GAATCCTGCGACGGTGG -3'	Verification of *purU* deletion
purUdel2	cg0456_rev	5'- CTACAACGACGCACTCATC -3'	Verification of *purU* deletion
R453C2	icd_R453C_2	5'- GGGCATCCTTGACCTGGCATGCAC**A**CCAG ATGTCATTTGCCTCAACGTCG -3'	Primer#2 for flank1 for amino acid exchange R453C in ICD, nucleotide leading to amino acid exchange bold
R453C3	icd_R453C_3	5'- CGACGTTGAGGCAAATGACATCTGG**T**GTG CATGCCAGGTCAAGGATGCCC -3'	Primer#1 for flank2 for amino acid exchange R453C in ICD, nucleotide leading to amino acid exchange bold
RG1	icd_R453C-G407S_for	5'- CCGGAATTCCGTTGTGCGCGCTTACTTCG -3'	Primer #1 for flank1 for amino acid exchange R453C and G407S in ICD, *EcoR*I site underlined
RG2	icd_R453C-G407S_rev	5'- CTAGCTAGCCCTGAACCTGCTGGACGTG -3'	Primer#2 for flank2 for amino acid exchanges R453C and G407S in ICD, *Nhe*I site underlined
RGseq1	R453C-G407S_seq_1	5'- GAGTCCCTGGACAACGGC -3'	Sequencing primer to verify nucleotide exchange leading to G407S and R453C in *icd*
RGseq2	R453C-G407S_seq_2	5'- GAGAGCTGGGTTGCCTC -3'	Sequencing primer to verify nucleotide exchange leading to G407S and R453C in *icd*
RGseq3	R453C-G407S_seq_3	5'- CATCACCAACCTGCATG -3'	Sequencing primer to verify nucleotide exchange leading to G407S and R453C in *icd*
rpi1	rpi_1_ptuf	5'- CGCAAGCTTGCAATCGCTATACCTACGCT G -3'	Primer #1 for flank1 for exchanging native promoter against P_{tuf} in *rpi*, *Hind*III site underlined
rpi2	rpi_2_ptuf	5'- CAAACTACCAGCGTTCACAAATCGCAAAA TAGC -3'	Primer #2 for flank1 for exchanging native promoter against P_{tuf} in *rpi*
rpi3	rpi_3_ptuf	5'- CAGGAGGACATACCATGCGCGTATACCTT GGAGCAG -3'	Primer #1 for flank2 for exchanging native promoter against P_{tuf} in *rpi*

Short Name	Working name	Sequence 5' to 3'	Purpose, characteristic(s)
rpi4	rpi_4_ptuf	5'- CGCGAATTCGGAAAAGAACTTAACCGCCC -3'	Primer #2 for flank2 for exchanging native promoter against P_{tuf} in *rpi*, *EcoR*I site underlined
rrnB1		5'- GACTACCGACCAGGTGAGATTCTTTAACT GTTTTGGCGGATGAGAGAAG -3'	Primer #1 for amplification of terminator region of *rrnB* (*E. coli*)
rrnB2	Trrnb_rev2	5'- CTGCAGATATCCATCACACTGGCGGCCGC AGGAGAGCGTTCACCGACAAACAAC -3'	Primer #2 for amplification of terminator region of *rrnB* (*E. coli*), *Not*I site underlined
rrnb3	Trrnb_purH	5'- GCGCGACACTTCGCTCACTAACTGTTTTGG CGGATGAGAGAAG -3'	Amplifying T_{rrnB} for pJC4 *purH*
rrnb4	Trrnb_rev	5'- ATTTGCGGCCGCAGGAGAGCGTTCACCGA C -3'	Amplifying T_{rrnB} for pJC4 *purH*
seq_int	hisE4	5′- CGCGGATCCGCAACGTAGATGGCGATATC TTTAGG -3′	Sequencing primer for genomic integration of *hisEG* cassette
sodA1		5'- CGTTAAATGAGGAGTACAAGTAAA**TAA**CT GCCAATTATTCCGGGCTTGTGAC -3'	Primer #3 for integration of stop codon and P_{sodA} in front of *hisF*, stop codon bold
sodA2		5'- GAATAACTCGAATTGCCACGCCCATGGGT AAAAAATCCTTTCGTAGGTTTC -3'	Primer #4 for integration of stop codon and P_{sodA} in front of *hisF*
sodA3	PsodA_D	5'- CATCAGTGCCAACATAGTAAGCCAgtatacCT ACTTAGCTGCCAATTATTCCG -3'	Amplifying P_{sodA} for pJC
sodA4	PsodA_hisD	5'- CTCGCAGGTCAGTGACATTCAACATGGGT AAAAAATCCTTTCGTAGG -3'	Amplifying P_{sodA} for pJC4 *purApurB hisD* and pJC4 *hisD*
sodA5	PsodA_fw	5'- GCTCTAGACTACTTAGCTGCCAATTATTC -3'	Amplifying P_{sodA} for pJC4 *purH*
sodA6	PsodA_purH	5'- GTTTAATTGCCTTACGATCATCGCTCATGG GTAAAAAATCCTTTCGTAGGTTTCC -3'	Amplifying P_{sodA} for pJC4 *purH*
tkt 9	tkt 9	5'- CGCGGATCCCAATGACGTAGATGTGGTGG TC -3'	Primer #1 for flank2 for deleting spacer plus RBS region of *tkt* gene
tkt1	tkt 1	5'- CCCAAGCTTCTGCCTGTGACGATTCCGTTA AAG -3'	Primer #1 for modifications of *tkt* gene, *Hind*III site underlined
tkt2	tkt 2	5'- GGAACCAATCCATGCAAGGAACGCAGGTG ACAGCGTCAAGGTGGTC -3'	Primer #2 for flank1 for truncating the *tkt* gene
tkt3	tkt 3	5'- GACCACCTTGACGCTGTCACCTGCGTTCCT TGCATGGATTGGTTCC -3'	Primer #1 for flank2 for truncating the *tkt* gene
tkt4	tkt 4	5'- CGCGGATCCGCTGAGATTGCCGGAAGTAA TGCG -3'	Primer #2 for flank2 for truncating the *tkt* gene, *BamH*I site underlined
tkt5	tkt 5	5'- GACAGCGTCAAGGTGGTCAATCCTGGGTT AAACCGGGACC -3'	Primer #2 for flank1 for deleting spacer region of *tkt* gene
tkt6	tkt 6	5'- GGTCCCGGTTTAACCCAGGATTGACCACC TTGACGCTGTC -3'	Primer #1 for flank2 for deleting spacer region of *tkt* gene
tkt7	tkt 7	5'- CGCGGATCCCAATGACGTAGATGTGGTGG TC -3'	Primer #2 for flank2 for deleting spacer and spacer plus RBS of *tkt* gene, *BamH*I site underlined
tkt8	tkt 8	5'- CGCGGATCCCAATGACGTAGATGTGGTGG TC -3'	Primer #2 for flank1 for deleting spacer plus RBS region of *tkt* gene
tktseq	tktfowseq	5'- CGCGGATCCCAATGACGTAGATGTGGTGG TC -3'	Sequencing primer for deletions tkt^{S} and tkt^{SRbs}
Trrnb_for	Trrnb_for	5'- CCGCATCGCCCGCATCTAGCTGTTTTGGCG GATGAGAGAAG -3'	Primer #1 for amplification of T_{rrnB} terminator from *E. coli*
Trrnb_rev	Trrnb_rev	5'- CTTCCGCATCCAAACTCACTTAGTAGGAG AGCGTTCACCGAC -3'	Primer #2 for amplification of T_{rrnB} terminator from *E. coli*
ttrnbpurA	Trrnb_purA	5'- CATGACGTACTAGCTGACAACTAGCTGTT TTGGCGGATGAGAGAAGATTTTCAG -3'	Cloning *purA* into pJC4
tuf1		5'- AACTGCAGAACCAATGCATCCACAGGGTA GCTGGTAGTTTG -3'	Primer #1 for amplification of P_{tuf}, *Nsi*I site underlined
tuf2		5'- GGGAATTCCATATGATGTCCTCCTGGACTT CGTGGTGGC -3'	Primer #2 for amplification of P_{tuf}, *Nde*I site underlined
tuf2_1	Ptuf_fw2	5'- GATCAGCGACGCCGCAGGGTCTAGACCAC AGGGTAGCTGGTAGTTTGAAAATC -3'	Primer #1 for amplification of P_{tuf}, *Xba*I site underlined
tuf2_2	Ptuf_purA	5'- CATTGAGCGCCGACAATAACGATTGCAGC CATTGTATGTCCTCCTGGACTTCG -3'	Primer #2 for amplification of P_{tuf}
tuf3	ptuf_fw	5'- GATTTGTGAACGCTGGTAGTTTGAAAATC AAC -3'	Amplification of P_{tuf}
tuf4	ptuf_rev	5'- GGTATACGCGCATGGTATGTCCTCCTGGA CTTC -3'	Amplification of P_{tuf}

Short Name	Working name	Sequence 5’ to 3’	Purpose, characteristic(s)
zwf1	zwf_fw	5’- GATCTCTAAGGTACAAGCCG -3’	Primer #1 for introduction of nucleotide exchange in gene *zwf* leading to amino acid exchange A243T
zwf2	zwf_rev	5’- CAACTGGGCTTACTACCTGTCC -3’	Primer #2 for introduction of nucleotide exchange in gene *zwf* leading to amino acid exchange A243T
zwf3	zwf_1_GtoA	5’- CGCAAGCTTGGCGTTGCCAACGCTCAGCG CGC -3’	Primer #1 for flank1 for zwf^{ATG}, *Hind*III site underlined
zwf4	zwf_2_GtoA	5’- CCAGCTGGAGGGGGTCGTGTTTGTGCTCA **T**GATGGTAGTGTCACGATCC -3’	Primer #2 for flank1 for zwf^{ATG}, nucleotide exchange bold
zwf5	zwf_3_GtoA	5’- GGATCGTGACACTACCATC**A**TGAGCACAA ACACGACCCCCTCCAGCTGG -3’	Primer #1 for flank2 for zwf^{ATG}, nucleotide exchange bold
zwf6	zwf_4_GtoA	5’- CGCGGATCCCTTCGGTGGATTCAGCCATG CC -3’	Primer #2 for flank2 for zwf^{ATG}, *BamH*I site underlined
zwfseq	zwf_check	5’- GCGGAGGTTTTATCCAATGG -3’	Sequencing primer for introduction of nucleotide exchange in gene *zwf* leading to amino acid exchange A243T

2.2. Chemicals, Devices, Enzymes, Kits, Materials

2.2.1. *Devices and Materials*

Table 5. Complete list of devices and materials used in this work with their respective product names, distributing companies, purposes, and catalogue numbers.

Product	Company	Purpose	Cat. No.
8-Well Comb	Bio-Rad Laboratories, Inc.	Agarose gel electrophoresis	1704463
15-Well Comb	Bio-Rad Laboratories, Inc.	Agarose gel electrophoresis	1704465
15-Well Comb	Bio-Rad Laboratories, Inc.	Agarose gel electrophoresis	1704446
20-Well Comb	Bio-Rad Laboratories, Inc.	Agarose gel electrophoresis	1704447
8-Well Comb	Bio-Rad Laboratories, Inc.	Agarose gel electrophoresis	1704463
Agilent 1200 Series	Agilent Technologies	HPLC apparatus (amino acid quantification)	
Agilent 1200 Series	Agilent Technologies	HPLC apparatus (adenylate quantification)	
Agilent 1260 Series	Agilent Technologies	HPLC apparatus of the LC MS/MS Q-TOF system	
Agilent 6540 Accurate-Mass LC MS/MS Q-Tof	Agilent Technologies	LC MS/MS Q-TOF system	

Product	Company	Purpose	Cat. No.
BCP-CO2	BlueSens gas sensor GmbH	Exhaust gas CO_2 analysis	
BCP-O2	BlueSens gas sensor GmbH	Exhaust gas O_2 analysis	BCP-02
Benchtop shaker AK 85	Infors AG	Rotary incubation of bacterial cultures	
Centrifuge 5417 R, rotor: FA45-30-11	Eppendorf AG	Tabletop centrifuge for 1.5 mL and 2 mL tubes	
Centrifuge 5427 R, rotor: FA-45-30-11 or F-35-6-30	Eppendorf AG	Tabletop centrifuge for centrifugation of 1.5 mL, 2 mL, 15 mL and 50 mL reaction tubes and DURAN® Centrifuge Tubes Round Bottom	5409000012
Centrifuge 5804 R, rotor: A-4-44 or FA 45-30-11	Eppendorf AG	Tabletop centrifuge for centrifugation of 1.5 mL, 2 mL, 15 mL and 50 mL reaction tubes	5805000327
Centrifuge MiniSpin®, rotor F-45-12-11	Eppendorf AG	Tabletop centrifuge for centrifugation of 0.2 µL, 1.5 mL and 2 mL reaction tubes	5452000018
Centrifuge Tubes Round Bottom (DURAN® 50× 12 ml)	Carl-Roth GmbH	CDW determination	C102.1
Electroporation cuvettes, 2 mm, 40-400 µL	VWR International GmbH	For plasmid transformation	732-1136
Eporator®	Eppendorf AG	Electroporation apparatus	4309000019
Heating circulator	JULABO USA, Inc.	Water bath for several applications	9352506
High performance ZORBAX guard fittings kit	Agilent Technologies	HPLC hardware kit (amino acid quantification)	820999-901
InLab® Easy	Mettler-Toledo GmbH	pH electrode	51343010
InPro® 3100/255 Pt100	Mettler-Toledo GmbH	pH probe bioreactors	52000661
InPro® 6800 Series O_2 Sensors	Mettler-Toledo GmbH	DO probe	52200968
LAS-3000 Imager (Filter: 605DF40)	Fujifilm Medical Systems	Imaging of agarose gels at UV light (320 nm)	
Mass flow controller, 0-2 l min^{-1}	Analyt-MTC GmbH	Mass flow controller for gassing during 30 L cultivations	GFC 171S
Mass flow controller, 0-500 ml min^{-1}	Analyt-MTC GmbH	Mass flow controller for gassing during triple glass reactor cultivations	GFC 171S
MF-Millipore Membrane Filter, mixed cellulose esters, hydrophile, 0,025 µm pore size, 13 mm	Merck Chemicals GmbH	Diafiltration	VSWP01300
Microplate, 96 well, PS	Greiner Bio-One GmbH	Plates for protein analytics	655101
Nano Drop ND-1000 Spectrophotometer	PEQLAB Biotechnologie GmbH	Quantification of purified DNA	
pH meter FiveEasy™ FE20	Mettler-Toledo GmbH	pH meter reaction cup scale	

Product	Company	Purpose	Cat. No.
PARAFILM® M	Carl-Roth GmbH	Plastic shred for pyrolysis water purification	H666.1
Power Pack P25	Biometra GmbH	Power source for agarose gel electrophoresis	846-040-800
Precellys®24	Bertin Instruments	Mechanical cell lysis	
Rotilabo®-syringe filters, CME, 0.22 µm	Carl-Roth GmbH	Filters for stock solution sterilization	KH54.1
Rotilabo®-syringe filters, CME, 0.45 µm	Carl-Roth GmbH	Filters for stock solution sterilization	KH55.1
S20 - SevenEasy™ pH	Mettler-Toledo GmbH	pH meter interface	51302803
Semi-micro cuvette, acrylic	Sarstedt AG & Co	Photometric analysis of enzyme activities	67.740
Semi-micro cuvette, PS	Sarstedt AG & Co	Photometric analysis of OD_{600}	67.742
SeQuant® ZIC-pHILIC	Merck KGaA	LC MS/MS Q-TOF	
SeQuant® ZIC-pHILIC guard column	Merck KGaA	LC MS/MS Q-TOF	
Sub-Cell® GT Cell, Mini-Sub® Cell GT Cell, Wide Mini-Sub Cell GT Cell	Bio-Rad Laboratories, Inc.	Several chambers for agarose gel electrophoresis	
Supelcosil LC-18-T	Agilent Technologies	HPLC column (adenylate quantification)	
Synergy 2 Multi-Mode Reader	BioTek Instruments GmbH	Protein analytics at 560 nm	
TAdvanced thermocycler	Biometra GmbH	Thermocycler for standard and colony PCR and isothermal assembly	
Ultrospec 10 Cell Density Meter (Amersham Biosciences)	GE Healthcare Europe GmbH	OD_{600} analysis	
Ultrospec™ 2100 pro UV/Visible spectrophotometer	GE Healthcare Europe GmbH	Photometric enzyme activity analysis	
UV Transilluminator 312 nm	INTAS Science Imaging Instruments GmbH	UV screen to cut out bands in agarose gels prior to gel elution	
UV Küvetten micro	BRAND GMBH + CO KG	UV cuvettes for MS enzyme assay	
Waters XBridge BEH Amide column	Waters Corp.	LC MS/MS Q-TOF	
Waters XBridge BEH Amide VanGuard Cartridge	Waters Corp.	LC MS/MS Q-TOF	
Watson-Marlow Cased Pump 120U/DV	Watson-Marlow GmbH	Addition of feed, base, acid, STRUKTOL in reactor cultivations	
Zorbax Eclipse Plus C18	Agilent Technologies	HPLC column (amino acid quantification)	959990-902

Product	Company	Purpose	Cat. No.
ZORBAX Eclipse Plus C18	Agilent Technologies	HPLC guard column (amino acid quantification)	820950-936

2.2.2. *Chemicals*

Table 6. Complete list of the chemicals used in this work with their distributing companies and catalogue numbers.

Product	Company	Cat. No.
Acetic acid ROTIPURAN®, 100%	Carl Roth GmbH&Co. KG	3738.2
Acetonitrile	VWR International GmbH	83639 320
Acetonitrile for LC-MS, ≥ 99.9%	Sigma-Aldrich Co. LLC.	34967
Acetyl coenzyme A, sodium salt	Sigma-Aldrich Co. LLC.	A2056-5mg
Adenine, ≥ 99 %	Sigma-Aldrich Co. LLC.	01830
Adenosine-5'-triphosphate, disodium	Carl Roth GmbH&Co. KG	HN35.2
Agar-Agar, Bioscience	Carl Roth GmbH&Co. KG	6494.4
Ammonium acetate for LC-MS, ≥ 99.9%	Sigma-Aldrich Co. LLC.	431311
Ammonium formate for LC-MS,	Agilent Technologies	G1946-85021
Ammonia solution, $NH_3 + H_2O$, ≥ 25%	Carl Roth GmbH&Co. KG	5460.4
Ammonium sulphate, $(NH_4)_2SO_4$, ≥ 99%	Carl Roth GmbH&Co. KG	9218.5
Aspartic acid, L-, ≥ 99%	Sigma-Aldrich Co. LLC.	11190
Bacto™ Brain Heart Infusion	Becton, Dickinson and Company	237500
Biotin, D(+)-, ≥ 98.5%	Carl Roth GmbH&Co. KG	3822.1
Biozym LE Agarose	Biozym Scientific GmbH	840004
Boric acid	Merck Chemicals GmbH	1.00165.0500
Bromophenol blue sodium salt	Sigma-Aldrich Co. LLC.	B8026
Buffer solution, pH 4,00 ± 0,02 (20 °C)	Carl Roth GmbH&Co. KG	A517.1
Buffer solution, pH 7,00 ± 0,02 (20 °C)	Carl Roth GmbH&Co. KG	P713.1
Buffer solution, pH 9,00 ± 0,02 (20 °C)	Carl Roth GmbH&Co. KG	P714.3
Calcium chloride, $CaCl_2$, (discontinued; similar product #1023791000)	Merck Chemicals GmbH	2389
Copper(II) sulfate pentahydrate, $CuSO_4 \cdot 5\ H_2O$, ≥ 99%	Sigma-Aldrich Co. LLC.	61240
1,4-Dithriothreit, ≥ 99%	Carl Roth GmbH&Co. KG	6908.2
DMSO (dimethyl sulfoxide), 100%	Thermo Fisher Scientific Inc.	F-515
Ethanol, denatured,	Carl Roth GmbH&Co. KG	T171.2

Product	Company	Cat. No.
Ethanol ROTIPURAN®, min. 99.8%	Carl Roth GmbH&Co. KG	9065.1
Ethylenediamine tetraacetic acid (EDTA) disodium salt dehydrate, ≥ 99%	Carl Roth GmbH&Co. KG	X986.2
Fmoc chloride	Sigma-Aldrich Co. LLC.	23186
Folic acid, 97%	Sigma-Aldrich Co. LLC.	47620
Formic acid, 85%	Carl Roth GmbH&Co. KG	5355.2
Formic acid for LC-MS, 98%	Sigma-Aldrich Co. LLC.	94318-50ML-F
Fructose, D(-)-, ≥ 99.5%	Carl Roth GmbH&Co. KG	4981.2
GelRed Nucleic Acid Gel Stain, 10,000x in water, 0.5 mL	Biotinum	41003
GeneRuler 1 kb Plus DNA Ladder	Thermo Fisher Scientific Inc.	SM1331
Glass beads, 0.1 mm	Carl Roth GmbH&Co. KG	HH55.1
Glass beads, 4 ± 0.3 mm	Carl Roth GmbH&Co. KG	N029.1
Glucose, α-D(+)-, monohydrate, ≥ 99.5%	Carl Roth GmbH&Co. KG	6780.3
Glutamic acid, L-, ≥ 99%	Sigma-Aldrich Co. LLC.	49450
Glutamine, L-, ≥ 99%	Sigma-Aldrich Co. LLC.	49420
Glycerol, ≥ 98%	Carl Roth GmbH&Co. KG	7530.1
Glcine, ≥ 99%	Sigma-Aldrich Co. LLC.	50049
Hydrochloric acid, HCl, ≥ 32%	Sigma-Aldrich Co. LLC.	84411
Iron(II) sulfate heptahydrate, $FeSO_4 \cdot 7\ H_2O$, 99.0-103.4%	Sigma-Aldrich Co. LLC.	31236
Kanamycin sulphate	Carl Roth GmbH&Co. KG	T832
Magnesium sulphate heptahydrate, $MgSO_4 \cdot 7\ H_2O$, ≥ 99%	Carl Roth GmbH&Co. KG	P027.3
Manganese(II) sulfate monohydrate, $MnSO_4 \cdot H_2O$, ≥ 98%	Sigma-Aldrich Co. LLC.	63555
Mercaptopropionic acid, 3-, ≥ 99%	Sigma-Aldrich Co. LLC.	63768
Methanol	VWR International GmbH	20864 320
Morpholino propane sulphonic acid, 3-N-, MOPS, PUFFERAN®, ≥ 99.5%	Carl Roth GmbH&Co. KG	6979.3
Nickel(II) sulphate hexahydrate, $NiSO_4 \cdot 6\ H_2O$, ≥ 98%	Carl Roth GmbH&Co. KG	7322.1
Nicotinamide adenine dinucleotide phosphate disodium dihydrate, β-, NADP Na_2	GERBU Biotechnik GmbH	1014,1000
Nicotinamide adenine dinucleotide, β-, NAD	GERBU Biotechnik GmbH	1013,0001
Perchloric acid, 70-72%	Sigma-Aldrich Co. LLC.	7601-90-3
Phosphoric acid, *o*-, ROTIPURAN® ≥85 %	Carl Roth GmbH&Co. KG	6366.2
Phthaldialdehyde, *o*-	Sigma-Aldrich Co. LLC.	79760
Ribose, D(-)-, ≥ 98%	Sigma-Aldrich Co. LLC.	R1757-10G-A

Product	Company	Cat. No.
Potassium acetate, 99.0-100.5%	Merck Chemicals GmbH	1048201000
Potassium dihydrogen phosphate, KH_2PO_4, ≥ 98%	Carl Roth GmbH&Co. KG	P018.5
Potassium hydrogen phosphate, di-, K_2HPO_4, anhydrous, ≥ 98%	Carl Roth GmbH&Co. KG	6875.3
Potassium hydroxide, KOH, pellets, ≥ 85%	Carl Roth GmbH&Co. KG	6751.2
Potassium Ds-threo-isocitrate monobasic, 98%	Sigma-Aldrich Co. LLC.	58790
Protocatechuic acid, PCA, 3,4-dihydroxybenzoic acid, ≥ 97%	Carl Roth GmbH&Co. KG	8274.1
Serine, L-, ≥ 99%	Sigma-Aldrich Co. LLC.	84960
Sodium azide, NaN_3, ≥ 99.5%	Sigma-Aldrich Co. LLC.	S2002
Sodium chloride, NaCl, > 99.8%	Carl Roth GmbH&Co. KG	9265.2
Sodium glyoxylate monohydrate, ≥ 95%	Sigma-Aldrich Co. LLC.	G4502
Sodium hydroxide, NaOH, pearls, ≥ 99%	Carl Roth GmbH&Co. KG	9356.2
Sodium sulfite, ≥ 98%, anhydrous	Carl Roth GmbH&Co. KG	8637.1
Sodium tetraborate decahydrate, ≥ 99.5%	Sigma-Aldrich Co. LLC.	S9640
Sorbitol, D-, ≥ 98%	Carl Roth GmbH&Co. KG	6213.1
Spectinomycin dihydrochloride pentahydrate, ≥ 98%	Sigma-Aldrich Co. LLC.	S9007-25G
Struktol™ J 647, 1015 kg $(m^3)^{-1}$, 500 mPa s, combination of polyglycol ethers and aliphatic alcohols, antifoam agent fermentation	Schill+Seilacher GmbH	
Sucrose, D(+)-, ≥ 99.5%	Carl Roth GmbH&Co. KG	4621.2
Tetrabutylammonium hydrogen sulfate, ≥ 99.5%	Sigma-Aldrich Co. LLC.	86868
Tetracycline hydrochloride,	Carl Roth GmbH&Co. KG	0237.1
Thiamine hydrochloride, min. 98.5%	Carl Roth GmbH&Co. KG	T911.2
TRIS PUFFERAN®, ≥ 99,9%	Carl Roth GmbH&Co. KG	4855.2
Tryptone	Becton, Dickinson and Company	211701
Urea, ≥ 99%	Sigma-Aldrich Co. LLC.	51460
Valine, L-, ≥ 99%	Merck Chemicals GmbH	1.08495.0025
Water HiPerSolv CHROMANORM®	VWR International GmbH	83645 320
Xylene Cyanol FF	Sigma-Aldrich Co. LLC.	X4126
Yeast extract	Becton, Dickinson and Company	212730
Zinc sulfate heptahydrate, $ZnSO_4 \cdot 7\ H_2O$, 99.0-103.0%	Sigma-Aldrich Co. LLC.	96501

2.2.3. *Kits*

Table 7. Complete list of the kits used in this work with their respective product names, distributing companies, purpose, and catalogue numbers.

Product	Company	Purpose	Cat. No.
DNeasy Blood & Tissue Kit	QIAGEN	Chromosomal DNA Isolation from *E. coli* and *C. glutamicum*	69504
E.Z.N.A.® Plasmid Mini Kit I	Omega Bio-Tek, Inc.	Plasmid isolation from *E. coli*	D6942-02
NucleoSpin® Gel and PCR Clean-up	Macherey-Nagel GmbH & Co. KG	PCR clean-up and purification of plasmids or PCR fragments from agarose gels	740.609.250
Pierce™ BCA Protein Assay Kit	Thermo Fisher Scientific Inc.	Protein quantification	23227

2.2.4. *Enzymes*

Table 8. Complete list of the enzymes and enzyme related buffers used in this work with their product name, distributing company, purposes, and catalogue number.

Product	Company	Purpose	Cat. No.
PCR-related enzymes/buffers			
Coral Red Buffer Dye solution, 10x	Genaxxon BioScience GmbH	Dye for colony PCR	M3309
dATP Solution (100 mM)	Thermo Fisher Scientific Inc.	For equimolar dNTP mix for PCR	R0141
dCTP Solution (100 mM)	Thermo Fisher Scientific Inc.	For equimolar dNTP mix for PCR	R0151
dGTP Solution (100 mM)	Thermo Fisher Scientific Inc.	For equimolar dNTP mix for PCR	R0161
dTTP Solution (100 mM)	Thermo Fisher Scientific Inc.	For equimolar dNTP mix for PCR	R0171
PCR Buffer S complete, 10x	Genaxxon BioScience GmbH	Buffer for colony PCR	M3454.0015
Phusion GC Buffer, 5x	Thermo Fisher Scientific Inc.	Buffer for standard PCR	F519
Phusion Hot Start II HF DNA Polymerase, 100 U	Thermo Fisher Scientific Inc.	Standard polymerase used in PCR	F-549S
Taq DNA Polymerase S, 250 Units, 5 U mL^{-1}	Genaxxon BioScience GmbH	Polymerase for colony PCR	M3001.0250
Isothermal assembly enzymes and buffers			
FastAP Thermosensitive Alkaline Phosphatase, 1 U mL^{-1}	Thermo Fisher Scientific Inc.	For dephosphorylation of DNA	EF0654

Product	Company	Purpose	Cat. No.
T4 DNA Ligase Buffer, 10x	Thermo Fisher Scientific Inc.	Buffer for ligation	B69
T4 DNA Ligase, 400,000 U mL^{-1}	New England Biolabs	For isothermal assembly mix	M0202S
T4 DNA Ligase, LC, 1 U μL^{-1}	Thermo Fisher Scientific Inc.	For ligation during plasmid cloning	EL0016
T5 Exonuclease, 10,000 U mL^{-1}	New England Biolabs	For isothermal assembly mix	M0363S
Restriction related enzymes and buffers			
*BamH*I, 10 U mL^{-1}	Thermo Fisher Scientific Inc.	Restriction digest	ER0051
*BamH*I-Lsp1109I Buffer, 10x	Thermo Fisher Scientific Inc.	Reaction buffer	B57
Buffer B, 10x	Thermo Fisher Scientific Inc.	Reaction buffer	BB5
Buffer O, 10x	Thermo Fisher Scientific Inc.	Reaction buffer	BO5
Buffer R, 10x	Thermo Fisher Scientific Inc.	Reaction buffer	BR5
Buffer Tango, 10x	Thermo Fisher Scientific Inc.	Reaction buffer	BY5
*EcoR*I Buffer, 10x	Thermo Fisher Scientific Inc.	Restriction digest	B12
*EcoR*I, 10 U μL^{-1}	Thermo Fisher Scientific Inc.	Restriction digest	ER0271
*Hind*III, 10 U μL^{-1}	Thermo Fisher Scientific Inc.	Restriction digest	ER0501
*Nde*I, 10 U μL^{-1}	Thermo Fisher Scientific Inc.	Restriction digest	ER0581
*Nhe*I, 10 U μL^{-1}	Thermo Fisher Scientific Inc.	Restriction digest	ER0971
*Not*I, 10 U μL^{-1}	Thermo Fisher Scientific Inc.	Restriction digest	ER0591
*Nsi*I (Mph1103I), 10 U μL^{-1}	Thermo Fisher Scientific Inc.	Restriction digest	ER0731
*Pae*I (*Sph*I), 10 U μL^{-1}	Thermo Fisher Scientific Inc.	Restriction digest	ER0601
*Xba*I, 10 U μL^{-1}	Thermo Fisher Scientific Inc.	Restriction digest	ER0681
*Xma*I (Cfr9I), 10 U μL^{-1}	Thermo Fisher Scientific Inc.	Restriction digest	ER0171
Enzyme assay related enzymes			
Glucose 6-phosphate dehydrogenase / hexokinase	Sigma-Aldrich Co. LLC.	Enzymatic determination of glucose concentration	10737275001
L-Lactate dehydrogenase from rabbit muscle	Sigma-Aldrich Co. LLC.	Enzymatic determination of ICL activity	

2.3. Media and buffer preparation

For semi-solid cultivations, the medium was prepared and 18 g agar L^{-1} were added before autoclaving.

Table 9. Composition of the 2×yeast extract tryptone (YT) complex medium (Sambrook et al., 2001).

Component	Amount
Tryptone	16 g L^{-1}
Yeast extract	10 g L^{-1}
NaCl	5 g L^{-1}

Table 10. Composition of the Brain Heart Infusion (BHI) medium (Eggeling and Reyes, 2005).

Component	Amount
BHI	37 g L^{-1}

Table 11. Composition and preparation of the Brain Heart Infusion Sorbitol medium (Eggeling and Reyes, 2005).

Component	Amount
BHI	18.5 g
ad dH_2O	250 mL
Sorbitol	45.6 g
ad dH_2O	250 mL

Table 12. Overview of deployed CGXII minimal media in this work. The media in the following table are hybrid media using distinct features of the different published CGXII media (Eikmanns et al., 1991; Keilhauer et al., 1993). The pH of the medium was adjusted with 5 M KOH in shaking flask cultivations. In fermentations, the pH was adjusted after autoclaving by using 25% (v v^{-1}) NH_4OH. $MgSO_4$, $CaCl_2$, trace elements solution (TES; containing $FeSO_4$, $MnSO_4$, $CuSO_4$, $ZnSO_4$, $NiCl_2$; Table 13, p.58), and biotin were prepared as aqueous stock solutions and were added sterilely after the remaining components of the medium had been autoclaved.

	Final concentrations			
	$CGXII^N$	**$CGXII^E$**	**$CGXII^R$**	**Stock concentration**
$(NH_4)_2SO_4$	20 g L^{-1}	5 g L^{-1}	20 g L^{-1}	
Urea	5 g L^{-1}	5 g L^{-1}	-	
MOPS	21 g L^{-1}	21 g L^{-1}	-	
K_2HPO_4	1 g L^{-1}	1 g L^{-1}	1 g L^{-1}	
KH_2PO_4	1 g L^{-1}	1 g L^{-1}	1 g L^{-1}	
$MgSO_4 \times 7\ H_2O$	0.25 g L^{-1}	0.25 g L^{-1}	0.25 g L^{-1}	1000× (250 g L^{-1})
$CaCl_2$	0.01 g L^{-1}	0.01 g L^{-1}	0.01 g L^{-1}	1000× (10 g L^{-1})
$FeSO_4 \times 7\ H_2O$	16.4 mg L^{-1}	16.4 mg L^{-1}	16.4 mg L^{-1}	TES 1000×
$MnSO_4 \times H_2O$	10 mg L^{-1}	10 mg L^{-1}	10 mg L^{-1}	
$CuSO_4 \times 5\ H_2O$*	0.2 mg L^{-1}	0.2 mg L^{-1}	0.2 mg L^{-1}	
$ZnSO_4 \times 7\ H_2O$	1 mg L^{-1}	1 mg L^{-1}	1 mg L^{-1}	
$NiCl_2 \times 6\ H_2O$	0.02 mg L^{-1}	0.02 mg L^{-1}	0.02 mg L^{-1}	
Biotin	0.2 mg L^{-1}	0.2 mg L^{-1}	0.2 mg L^{-1}	1000× (200 mg L^{-1})
pH	7.4	7.4	7.4	
L-glutamate / yeast extract	-	1 mM / 0.5 g L^{-1}	-	
Purpose	**Cultivations of L-histidine producers (PART I)**	**Cultivations of evolution strains (PART II)**	**Reactor cultivations (PART I)**	

Table 13. 1000× trace elements solution (TES) for the CGXII media (Table 12, p.58). The pH of the TES was adjusted to 1 with 32% (w v^{-1}) HCl.

Component	**Amount**
$FeSO_4$ x 7 H_2O	16.4 g L^{-1}
$MnSO_4$ x H_2O	10 g L^{-1}
$CuSO_4$ x 5 H_2O*	0.2 g L^{-1}
$ZnSO_4$ x 7 H_2O	1.0 g L^{-1}
$NiCl_2$ x 6 H_2O	0.02 g L^{-1}

* original publications use water free $CuSO_4$ (Eikmanns et al., 1991; Keilhauer et al., 1993)

Table 14. 50× Tris-acetate-EDTA (TAE) buffer. The 1× working solution was used for agarose gel electrophoresis and had final concentrations of 40 mM Tris-acetate and 1 mM EDTA.

Component	Amount
Tris base	242 g
Acetic acid	57.1 mL
EDTA (0.5 M, pH 8.0)	100 mL
ad dH_2O	1 L

Table 15. 5× Iso reaction buffer for isothermal assembly (Gibson, 2011; Gibson et al., 2009).

Component	**Amount**
PEG-8000	1.5 g
Tris-HCl (1 M, pH 7.5)	3 mL
$MgCl_2$ (2 M)	150 µL
DTT (1 M)	300 µL
dCTP (100 mM)	60 µL
dATP (100 mM)	60 µL
dTTP (100 mM)	60 µL
dGTP (100 mM)	60 µL
NAD^+ (100 mM)	300 µL

Table 16. Iso enzyme reagent mix for isothermal assembly, stored at -20 °C (Gibson, 2011; Gibson et al., 2009)

Component	**Amount**
5× Iso reaction buffer	320 µL
T5 Exonuclease (10 U mL^{-1})	0.64 µL
T4 DNA Ligase (40 U mL^{-1})	160 µL
Phusion Hot Start II HF DNA Polymerase (2 U mL^{-1})	20 µL
ad dH_2O	1200 µL

Table 17. 6× DNA loading dye for agarose gel electrophoresis (Sambrook et al., 2001). The 6× DNA loading dye was mixed with DNA samples, resulting in 1× working concentration.

Component	Amount
Xylene cyanol FF	0.075 g
Bromophenol blue	0.075 g
Glycerol, ≥ 98 %	15 mL
ad dH_2O	50 mL

Table 18. Wash buffer for the preparation of cell free lysates of *C. glutamicum* for enzyme measurements. The pH value of the buffer was adjusted to 7.4 with 32% (w v^{-1}) HCl.

Component	Amount
Tris-HCl (pH 7.4)	0.2 M

Table 19. Lysis buffer for mechanical disruption of *C. glutamicum* to obtain cell free lysates. The pH value of the buffer was adjusted to 7.4 with 32% (w v^{-1}) HCl.

Component	Amount
Tris-HCl (pH 7.4)	0.1 M
Glycerol	10 % (v v^{-1})

Table 20. Lysis buffer for chemical disruption of *C. glutamicum* with perchloric acid to obtain lysates and quench the metabolism. The lysis buffer was chilled to -20 °C before use.

Component	Amount
Perchloric acid (pH 7.4)	35 % (v v^{-1})
EDTA	80 µM

Table 21. Assay buffer for measuring glucose concentration. The pH value of the buffer was adjusted to 7.6 with 32% (w v^{-1}) HCl.

Component	Amount
Tris (pH 7.6)	400 mM
$MgSO_4$	4 mM

Table 22. 2× Assay buffer for measuring enzyme activities of isocitrate dehydrogenase (Eikmanns et al., 1995). The pH value of the buffer was adjusted to 7.6 with 32% (w v^{-1}) HCl. $MnSO_4$ was added after the pH was adjusted, then the pH was controlled again and readjusted if needed.

Component	Amount
Tris (pH 7.6)	100 mM
$MnSO_4 \times H_2O$	0.8 mM
NADP × Na_2	0.5 mM

Table 23. 2× Assay buffer for measuring enzyme activities of isocitrate lyase (Reinscheid et al., 1994a). The pH value of the buffer was adjusted to 7.3 with 1 M NaOH.

Component	Amount
MOPS-NaOH (pH 7.3)	50 mM
Dithriothreit	5 mM
$MgCl_2$	15 mM
EDTA dihydrogen, dinatrium	1 mM
NADH × 2Na	0.2 mM

Table 24. 2× Assay buffer for measuring enzyme activities of malate synthase (Reinscheid et al., 1994b). The pH value of the buffer was adjusted to 7.6 with 32% (w v^{-1}) HCl.

Component	Amount
Tris (pH 7.6)	50 mM
$MgCl_2$	40 mM
Na glyoxylate × H_2O	2 mM

Table 25. Polar phase buffer (A) for amino acid HPLC measurements. The pH value of the buffer was set to 8.2 with 32% (v v^{-1}) HCl.

Component	Amount
Na_2HPO_4 (pH 8.2)	10 mM
$Na_2B_4O_7$	10 mM
NaN_3	0.5 mM

Table 26. Nonpolar phase buffer (B) for amino acid HPLC measurements.

Component	Amount
Methanol	45% (v v^{-1})
Acetonitrile	45% (v v^{-1})
ddH_2O	10% (v v^{-1})

Table 27. Buffer (A) for adenylate HPLC measurements. The pH was adjusted to 6.0 with 1 M KOH.

Component	Amount
KH_2PO_4	0.1 M
K_2HPO_4, pH 6.0	0.1 M
Tetrabutylammonium hydrogen sulfate	4 mM

Table 28. Buffer (B) for adenylate HPLC measurements. The pH was adjusted to 7.2 with 1 M KOH before methanol was added.

Component	Amount
KH_2PO_4	0.1 M
K_2HPO_4, pH 7.2	0.1 M
Tetrabutylammonium hydrogen sulfate	4 mM
Methanol	30% (v v^{-1})

2.4. Cultivations

2.4.1. *General cultivations*

Cultivations in glass reaction tubes (DURAN®, Carl-Roth GmbH, Karlsruhe, Germany) and shaking flasks (500 mL narrow-neck Erlenmeyer flask with 4 baffles, DURAN®, Carl-Roth GmbH, Karlsruhe, Germany) were performed with a rotary shaker (Benchtop shaker AK85, Infors AG, Bottmingen/Basel, Switzerland) at 37 °C for *E. coli* and at 30 °C for *C. glutamicum*,

respectively. The general complex medium for precultivations of both *E. coli* and *C. glutamicum* was 2× yeast extract tryptone (YT; Table 9, p.57) medium (Sambrook et al., 2001). For specified applications, such as preparation of electrocompetent cells or transformations of both *E. coli* or *C. glutamicum*, brain-heart-infusion (BHI; Table 10, p.57) or BHI supplemented with D-sorbitol (BHIS; Table 11, p.57; Sambrook et al., 2001) was used as complex medium, respectively. For semi-solid media cultivations (plating), 18 g agar L^{-1} were added to the medium.

2.4.2. *Storage of bacteria*

The long-time preservation of all strains was achieved by freezing at -70 °C. For this purpose, 5 mL 2xYT (Table 9, p.57) medium were inoculated with a single colony from semi-solid complex medium overnight (o/n). From this culture, 700 µL were monoseptically added to 300 µL sterile glycerol (≥ 98 %, Carl-Roth GmbH, Karlsruhe, Germany), mixed and stored in a screwcap reaction tube at -70 °C. To start an experiment, the glycerol stocks were thawed on ice and cells material was streaked on a suitable agar plate to obtain single colonies.

2.4.3. *Minimal medium*

Shaking flask cultivations of *C. glutamicum* were performed in CGXII medium (Table 12, p.58), which was modified compared to the originally published CGXII medium to match the specific requirements of the respective experimental setup (Eikmanns et al., 1991; Keilhauer et al., 1993). The used medium for PART I standardly contained 20 g $(NH_4)_2SO_4$ L^{-1}, 5 g urea L^{-1}, 21 g 3-morpholinopropanesulfonic acid (MOPS) L^{-1}, 1 g K_2HPO_4 L^{-1}, 1 g KH_2PO_4 L^{-1}, 0.25 g $MgSO_4$ L^{-1}, 0.01 g $CaCl_2$ L^{-1}. Before autoclaving, the pH value of the medium was adjusted to 7.4 with 5 M KOH and afterwards 16.4 mg $FeSO_4 \times 7\ H_2O$ L^{-1}, 10 mg $MnSO_4 \times H_2O$ L^{-1}, 0.2 mg $CuSO_4 \times 5\ H_2O$ L^{-1}, 1 mg $ZnSO_4 \times 7\ H_2O$ L^{-1}, 0.02 mg $NiCl_2 \times 6\ H_2O$ L^{-1}, and 0.2 mg biotin L^{-1} were added sterilely and the medium was named $CGXII^N$. For the evolutionary experiments, the amount of $(NH_4)_2SO_4$ was reduced to 5 g L^{-1} (for PART II) and additionally supplemented with 1 g yeast extract L^{-1} or 1 mM L-glutamate, as indicated. It was named $CGXII^E$. For the fermentation studies, both components MOPS and urea were omitted from the medium, as has been done before for shaking flask experiments (Eikmanns et al., 1991), and the medium was named $CGXII^R$.

2.4.4. *Carbon sources and supplements*

Carbon sources and supplements were either prepared as aqueous solutions, which were filtered sterilely with a sterile filter (MF-Millipore Membrane Filter, 0.025 µm pore size; Merck Chemicals GmbH, Billerica, USA) and added sterilely to the autoclaved medium or weighed out with the remaining media components and autoclaved, as indicated. Both defined and complex components were used as carbon sources in the conducted experiments. For standard cultivations in $CGXII^N$ or $CGXII^E$ (Table 12, p.58), 10 g D-glucose L^{-1} (for PART I) or 20 / 40 g D-glucose L^{-1} (in PART II) were added to the medium sterilely from an aqueous stock solution (500 g L^{-1}) after autoclaving, as indicated, respectively. In specified experiments, 6 g D-ribose L^{-1} (600 g L^{-1}) or 10 g D-fructose L^{-1} were used as carbon source from 600/500 g L^{-1} aqueous stock solution.

Supplements (concentrations of sterile stocks are given in parentheses) included 30 mg protocatechuic acid L^{-1} (PCA, 30 g L^{-1}), 1 / 10 mM L-glutamate (50 mM), 5 mM L-glutamine (50 mM), 20 mM glycine (50 mM), 20 mM L-serine (50 mM), 1 mM / 20 mM L-aspartate (50 mM), 5 mM adenosine triphosphate (ATP, 50 mM), 2 mM adenine (20 mM), 50 µM thiamine (50 mM), 0.36 nM folate (3.6 nm), 1 / 10 mM formate (100 mM), 1 g / 5 g yeast extract L^{-1} (added before autoclaving), 5 g BHI L^{-1} (added before autoclaving). For strains with modifications in the *tkt* gene, additionally 0.5% (w v^{-1}) potassium acetate were added sterilely from an aqueous stock solution (500 g L^{-1}) to liquid and semi-solid media.

Plasmid maintenance was ensured by applying selection pressure via addition of antibiotics (concentration of stock solution is given in parentheses). Therefore, 50 µg kanamycin mL^{-1} (50 mg mL^{-1}, dissolved in dH_2O), 5 µg tetracycline mL^{-1} (50 mg mL^{-1}, dissolved in 50% (v v^{-1}) ethanol), or 250 µg spectinomycin mL^{-1} (250 mg mL^{-1}, dissolved in dH_2O) were added sterilely to the medium, respectively. In case two antibiotics were necessary, concentrations were reduced to 12.5 µg kanamycin mL^{-1} and 2.5 µg tetracycline mL^{-1}.

2.4.5. *Shaking flask cultivations*

Standard shaking flask cultivations were performed in 500 mL glass flasks with four baffles (Erlenmeyer narrow-neck flask, DURAN®, asd). An overview of the seed train is given in Fig. **9** on page 66. Experiments with *C. glutamicum* were initiated by streaking out cell material from a glycerol stock on 2×YT (Table 9, p.57) agar medium, which was incubated for 2 d at

30 °C. A single colony was then inoculated in 5 mL 2×YT in a glass tube, which was incubated for 8 – 10 h at 30 °C. The complete cell suspension was transferred into 50 mL 2×YT in a 500 mL baffled shaking flask with four baffles and incubated o/n (about 12 – 14 h) at 30 °C. The optical density at 600 nm (OD_{600}) of this culture was measured with an Ultrospec 10 Cell Density Meter (GE Healthcare Europe GmbH, Freiburg, Germany), a defined amount of culture suspension was pelleted (4,500 × g, 10 min, room temperature [RT]) with a centrifuge 5804 R (rotor A4-44, Eppendorf AG, Hamburg, Germany) The supernatant was discarded properly and the pellet was resuspended in a defined amount of 0.9% (w v^{-1}) NaCl solution. The main culture was then initiated by transferring this cell solution to the respective 50 mL of $CGXII^{E}$ (Table **12**, p.58) medium, thereby inoculating it to an OD_{600} of about 2.0, if not indicated otherwise.

Evolutionary cultivations were prepared as described above. Main cultures were performed with strains *C. glutamicum* Δ*ppc* Δ*pyc* and *C. glutamicum* Δ*ppc* Δ*pyc* Δ*pck* in 500 mL glass flasks with four baffles (Fig. 9, p.66). Therefore, the cells were pelleted with with a centrifuge 5804 R (rotor A4-44, Eppendorf AG, Hamburg, Germany) at 4,500 × g, 10 min, RT and the pellet was then resuspended in a defined amount of 0.9% (w v^{-1}) NaCl solution, which was then used to inoculate the main culture to an OD_{600} of about 1. The $CGXII^{E}$ (Table 12, p.58) medium contained 40 g D-glucose L^{-1} as carbon source. After 3 – 4 d of incubation at 30 °C, the optical density was determined and a defined amount of cell suspension was pelleted (4,500 × g, 10 min, RT), the pellet was washed once with 10 mL of 0.9% (w v^{-1}) NaCl solution, pelleted again and the supernatant was discarded properly. Then the pellet was resuspended in a defined amount of 0.9% (w v^{-1}) NaCl solution and used to inoculate freshly prepared 50 mL of $CGXII^{E}$ with 40 g D-glucose L^{-1} to an OD_{600} of 1. This was repeated each 3 – 4 d until a distinct increase in OD_{600} was observed, indicating one or more evolutionary event(s). To isolate, i.e. obtaining single colonies, of the evolved strain(s), serial dilutions spanning from 10^{-3} to 10^{-6} in 0.9% (v v^{-1}) NaCl were prepared of the biomass suspension and plated on both 2×YT and

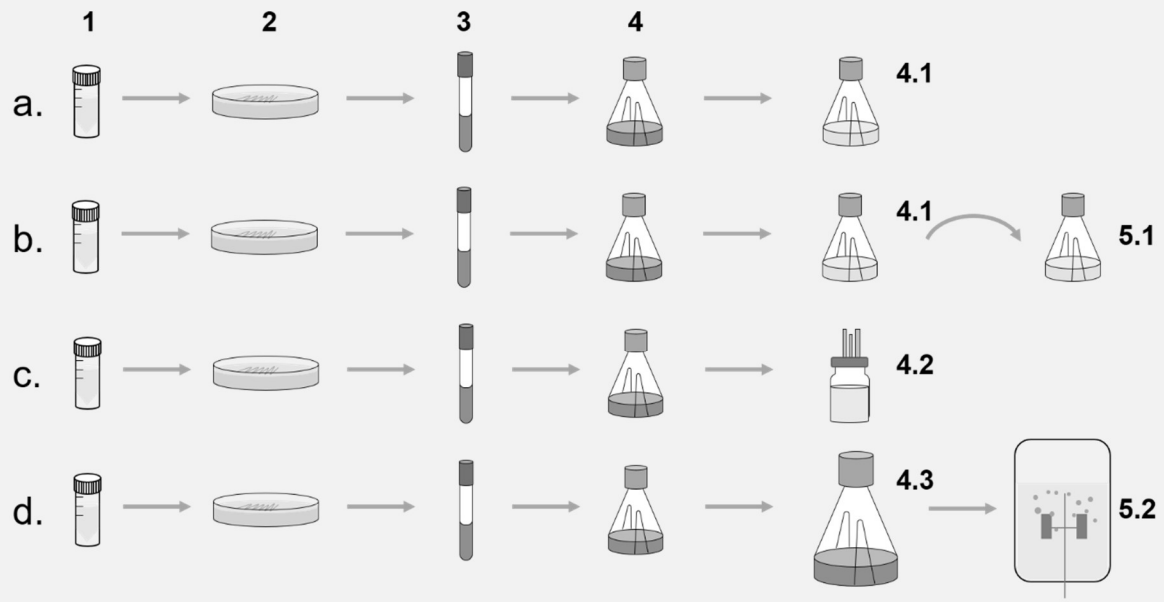

Fig. 9. Overview of the seed trains used for bacterial cultivations in this work: standard cultivations in part I and part II (a.), evolutionary cultivations (b.), small scale fermentations in the glass reactor system (c.), and steel tank reactor cultivations (d.). Seed trains were conducted by thawing a cryo tube culture (1), stored at -70 °C, and streaking cell suspension on 2×YT agar medium (2). After incubation, a single colony was transferred from the semi solid medium into 5 mL 2×YT medium (3) and incubated. After incubation, the complete cell suspension from (3) was transferred into 50 mL 2×YT medium in a 500 mL baffled shaking flask (4). This preculture was then used to inoculate the respective 50 mL CGXII minimal medium in a 500 mL baffled shaking flask (4.1), which was either incubated as main culture in standard growth experiments or from which in the case of evolutionary cultivations cell suspension was transferred regularly into fresh CGXII medium (5.1). In the case of fermentations, the 2×YT culture (4) was either used to inoculate the 200 mL CGXIIR reactor medium (4.2) or in the case of STR fermentations to inoculate a further preculture of 250 mL 2×YT medium in a 2 L baffled shaking flask (4.3). The biomass generated with this preculture (4.3) was then used to inoculate the STR (5.2).

$CGXII^{E}$ agar plates, the latter containing 10 g glucose L^{-1} and 1 g yeast extract L^{-1}. The plates were incubated at 30 °C and checked regularly to identify faster growing colonies. The faster growing ones were transferred onto 2×YT agar plates and their faster growth, compared with the initial strain, was confirmed in subsequent growth experiments.

2.4.6. *Triple glass reactor system*

Reactor cultivations were performed in a triple glass bioreactor system with a working volume of 200 mL (HWS Labortechnik, Mainz, Germany) with 200 mL $CGXII^{R}$ (Table 12, p.58) minimal medium and 10 g D-glucose L^{-1}. To inoculate the medium, the respective strains were prepared as described above (2.4.5 Shaking flask cultivations, p.64) and as shown in Fig**. 9** on page 66. The main culture was inoculated to an OD_{600} of about 1.5. The monitored process

parameters included temperature (T), dissolved oxygen concentration (DO) and pH value, which were monitored with probes (Mettler-Toledo GmbH, Gießen, Germany). Calibration of the DO probe was performed at 30 °C with two setpoints (0% and 100% of saturation). Setpoint one was achieved by gassing with pure N_2 to reduce the DO in the medium to 0%. Setpoint 2 was achieved by gassing with air and calibrating to 100% DO. The pH value was calibrated with commercial buffer solutions for pH 4 and pH 7 (ROTI®CALIPURE, Carl Roth, Karlsruhe, Germany). During the cultivations, the pH value was fixed to 7.4 (unless indicated otherwise) and controlled by addition of 10% (v v^{-1}) o-phosphoric acid and 25% (v v^{-1}) ammonia solution. When foaming occurred, foam development was counteracted by manually adding Struktol™ J 647 (Schill+Seilacher GmbH, Hamburg, Germany). Cultivations were performed at ambient pressure and the initial conditions were agitation at 100 rpm and gassing with 20 mL min^{-1} air flow (0.1 vvm). The DO level was kept above 35% by firstly increasing agitation (gradually up to a maximal value of 450 rpm) and secondly by increasing the gassing (gradually up to a maximal value of 500 mL min^{-1}) with a mass flow controller (Analyt-MTC GmbH, Müllheim, Germany).

2.4.7. *30 L stirred tank reactor cultivations*

For investigation of potential upscaling effects with L-histidine producer strains, cultivations in a 30 L volume steel stirred tank reactor (Bioengineering AG, Wald, Switzerland) were performed. To obtain sufficient amounts of biomass from the precultures, the precultivations were performed as described in 2.4.5 Shaking flask cultivations on page 64. With the purpose to generate sufficient biomass, the seed train was modified as shown in Fig. **9** on page 66 and as described in the following. A second preculture in 250 mL 2× YT (Table 9, p.57) medium in a 2 L baffled shaking flask was inoculated to an OD_{600} = 1.5 by using the first preculture and incubated o/n. To collect the biomass, the cell suspension was centrifuged (8,850 × g, 10 min, RT) with a centrifuge Avanti™ J-25 (rotor JA10, Beckman Coulter, Brea, USA) deploying four beakers à 250 mL. Pellets were resuspended in 200 mL 0.9% (w v^{-1}) NaCl solution and the bioprocess was started by transferring the biosuspension to the STR, containing 40 g D-glucose L^{-1} in a working volume of 10 L CGXII^R medium (Table 12, p.58), and inoculating it to OD_{600}=1.0.

T, DO, and pH were monitored online with standard probes (Mettler-Toledo GmbH, Gießen, Germany). Calibration of the oxygen electrode was done externally at 30 °C at two set points

for the 0% DO level in dH_2O containing sodium sulfite and for 100% in dH_2O with aeration of ambient air. Calibration of the pH electrode was done in buffer solutions at pH 4.0 and pH 7.0. Temperature of the medium during fermentation was fixed at 30 °C and controlled via cooling/heating through the reactor mantle. Excessive foaming was counteracted by manually adding Struktol™ J 647 (Schill+Seilacher GmbH, Hamburg, Germany) when needed. Agitation was set between 200 and 350 rpm at the fermentation start (as indicated) by using a single six blade Rushton turbine and four baffles at the reactor wall. Aeration rates were set to 2.5 L min^{-1} (0.25 vvm for the batch cultivation) at the fermentation start to prevent CO_2 degassing and gradually increased (together with stirrer velocity) as required to keep the DO level above 35% (mass flow controller 0-2 L min^{-1}; Analyt-MTC GmbH, Müllheim, Germany). Aeration was realized through a needle at the bottom of the reactor. The fermentations were run with 0.5 bar overpressure and the exhaust gas composition was analysed with respect to O_2 and CO_2 (BlueSens gas sensor GmbH, Herten, Germany).

For the fermentation in fed-batch mode, a fermentation in batch mode was performed as described above o/n. Changes included the reduction of the starting volume to 8 L and the initial amount of D-glucose to 20 g L^{-1}. After the carbon source was consumed completely from the $CGXII^R$ medium (Table 12, p.58), the fed-batch mode was initiated by switching on the feed. The feed contained 500 g D-glucose L^{-1} and was prepared in a baffled shaking flask with stir bar, which was placed on a magnetic stirrer to prevent precipitation. The initial substrate feed rate was calculated according to Equation 1, the volume of the feed was calculated according to Equation 2. The values for μ and q_S were used as experimentally determined. The μ during the fed-batch phase was set to 0.1 h^{-1} by adding defined amounts of feed.

Equation 1. $$F(t) = \frac{q_S \times V_0 \times c_{x0} \, (e^{\mu t})}{c_{s0}}$$

Equation 2. $$V_{Feed}(t) = \frac{q_S \times V_0 \times c_{x0} \, (e^{\mu t} - 1)}{c_{s0} \times \mu}$$

2.5. Molecular biological methods

The routinely performed molecular biology methods, such as restriction digestions, DNA ligations, and agarose gel electrophoresis were either performed as suggested by Sambrook et al., 2001, or as suggested by the manufacturer. Cloned plasmids and genomic integrations were verified by Sanger sequencing covering the complete altered DNA region, which was commercially performed by GATC Biotech AG, Constance, Germany.

2.5.1. *Isolation/purification of DNA*

For isolation of plasmid DNA from either *E. coli* or *C. glutamicum*, E.Z.N.A.® Plasmid Mini Kit I (Omega Bio-tek, Inc., Norcross, USA) was used according to the manufacturer's specifications. For preparation of plasmid DNA from *C. glutamicum*, a pretreatment with lysozyme (20 mg mL^{-1}) was performed for 60 min at 37 °C. DNA was purified after polymerase chain reaction (PCR) or after excision from agarose gels with NucleoSpin® Gel and PCR Clean-up (Macherey-Nagel GmbH & Co KG, Düren, Germany) according to the manufacturer's specifications. For isolation of genomic DNA from either *E. coli* or *C. glutamicum*, the DNeasy Blood & Tissue Kit (QIAGEN, Hilden, Germany) was used according to the manufacturer's specifications. All Kits used in this work are listed in Table 7, page 55.

2.5.2. *Preparation of electrocompetent cells and transformation*

E. coli

Electrocompetent cells of *E. coli* DH5α were prepared as has been described before (Dower et al., 1988). Therefore, the strain was streaked from a glycerol stock onto a 2×YT (Table 9, p.57) agar plate and incubated o/n at 37 °C. A single colony was used to inoculate 5 mL of 2×YT in a glass tube, which was incubated o/n at 37 °C. From this culture, 500 µL of cell suspension were then used to inoculate 250 mL 2×YT medium in a 1 L shaking flask with three to four baffles. Progress of the increase in OD_{600} was followed with an Ultrospec 10 Cell Density Meter (GE Healthcare Europe GmbH, Freiburg, Germany) and cells were harvested by centrifugation (4,500 × g, 15 min, 4 °C) when an OD_{600} of 0.3 – 0.5 was reached. The deployed centrifuge was a model 5804 R with an A-4-44 rotor (Eppendorf AG, Hamburg, Germany). The

supernatant was discarded properly and cells were washed with 20 mL ice cold water and then pelleted again. This was repeated once again with ice cold water and then two more times with ice cold 10% (v v^{-1}) glycerol. Eventually, the pellet was resuspended in 0.5 mL ice cold 10% (v v^{-1}) glycerol, separated in 50 µL aliquots, frozen instantly in liquid N_2, and stored at -70 °C until needed.

Transformation of electrocompetent *E. coli* DH5α with purified plasmid DNA (0.5 – 1.0 µg of DNA), ligation, or isothermal assembly mixes was performed as has been described before (Dower et al., 1988). This was done in electroporation cuvettes with 2 mm gap width and 400 µL volume (Radnor, Pennsylvania, USA) and with an Eporator® (Eppendorf, Hamburg, Germany). Cells and DNA were mixed, transferred into the cuvettes, and chilled for 5 min on ice. Then a pulse of 2.5 kV was applied (yielding time constants of about 3 – 4 ms). Cells were washed out of the cuvettes with 2×YT medium and regeneration was conducted in 5 mL 2×YT medium for 50 min at 37 °C. After this, cells were plated on 2×YT agar medium containing the appropriate antibiotic (for the respective plasmid) for selection pressure (Table 3, p.39) and incubated o/n at 37 °C.

C. glutamicum

Electrocompetent cells of *C. glutamicum* were prepared as has been described before (Tauch et al., 2002). As a general approach to prepare electrocompetent *C. glutamicum*, a 5 mL BHI (Table 10, p.57) preculture was inoculated with a single colony from a 2×YT (Table 9, p.57) agar plate and incubated for about 6 h at 30 °C. The complete content of this glass tube was then transferred into 50 mL of BHIS (Table 11, p.57) medium in a 500 mL shaking flask and incubated o/n. The main culture of 250 mL BHIS medium in a 1 L baffled shaking flask was then inoculated with 7.5 mL of the preculture and incubated to an OD_{600} of 2.5 (equals a biomass concentration of about 0.55 g CDW L^{-1}). The cells were harvested by centrifugation (4,500 × g, 20 min, 4 °C; model 5804 R with an A-4-44 rotor; Eppendorf AG, Hamburg, Germany), the supernatant was discarded, and the pellet was washed with 100 mL ice cold 10% (v v^{-1}) glycerol. This was repeated three times. The final pellet was then resuspended in 1.6 mL ice cold 10% (v v^{-1}) glycerol, 150 µL aliquots were prepared, directly frozen in liquid N_2, and stored at -70 °C until needed.

For transformations with pJC4-based plasmids, a scaled-down approach of the above described protocol was used. For this purpose, several colonies of the same strain were transferred from a 2×YT agar plate into 5 mL BHI (Table 10, p.57) in a glass tube and incubated for 5 – 6 h at

30 °C. The content of the glass tube was transferred into a 15 mL conical centrifuge tube and centrifuged at 4,500 × g for 10 min at 4 °C (model 5804 R with an A-4-44 rotor (Eppendorf AG, Hamburg, Germany)). The supernatant was discarded, the pellet was resuspended in 1 mL ice cold 10% (v v^{-1}) glycerol and transferred into a 1.5 mL reaction tube. The cells were pelleted (centrigufation at 4,500 × g, 10 min, 4 °C; model 5804 R with an F-45-30-11 rotor [Eppendorf AG, Hamburg, Germany]) and three more washing steps were performed. The final pellet was resuspended in 80 µL ice cold 10% (v v^{-1}) glycerol and either directly applied for transformation (short time storing on ice) or frozen in liquid N_2 and stored at -70 °C until needed.

Transformation of *C. glutamicum* was performed as has been described before (Liebl et al., 1989). For this purpose, electrocompetent cells of *C. glutamicum* were thawed on ice, mixed with the respective plasmid DNA (0.5 - 1.0 µg DNA), transferred into electroporation cuvettes (2 mm gap width, 400 µL volume; Radnor, Pennsylvania, USA), and chilled for 5 min on ice. Electroporation was performed with an Eporator® (Eppendorf, Hamburg, Germany) applying a pulse of 2.5 kV, yielding time constants of 4 – 5 ms. As has been described before, a heat shock for 6 min at 46 °C was performed in 5 mL sterile-filtered BHIS (Table 11, p.57) medium immediately post electroporation (van der Rest et al., 1999). For regeneration purposes, cells were then incubated for 50 min at 30 °C and pelleted afterwards (centrifugation at 4,500 × g for 10 min at RT; model 5804 R with an A-4-44 rotor). The supernatant was discarded and the pellet was resuspended in 50 µL BHIS and plated on BHIS agar plates containing the respective antibiotic for selection purposes (Table 3, p.39).

2.5.3. *Polymerase chain reaction*

For the amplification of DNA, the polymerase chain reaction (Mullis and Faloona, 1987; Saiki et al., 1988) technique was used. Reactions were performed with a Biometra TAdvanced thermocycler (Biometra GmbH, Göttingen, Germany). For cloning purposes, Phusion Hot Start II HF DNA Polymerase (Thermo Fisher Scientific Inc., Waltham, USA) was used with in-house designed primers (synthesized by biomers GmbH, Ulm, Germany). A protocol for the reaction mix and protocol is given in Table 29, page 72. To verify plasmid integrity and genomic DNA integration or deletion, colony PCRs with Taq DNA Polymerase S (Genaxxon BioScience GmbH, Ulm, Germany) were performed. DNA for colony PCRs were prepared by transferring a single colony into 50 µL deionized water (dH_2O) and incubating for 10 min at 95 °C. Cell debris was cleared by centrifugation at 12,100 × g for 3 min (MiniSpin®, rotor F-45-12-11;

Eppendorf AG, Hamburg, Germany). Then, 10 µL of the supernatant were used as template DNA in the colony PCR protocol (Table 30, p.72).

Table 29. Standard PCR reaction composition (A) and thermocycler program (B). The amount of template DNA varied for different PCR reactions.

A

DNA template	**2-5 µL**
DMSO	2 µL
Phusion Hot Start II HF	1 µL
dNTP mix (10 mM)	5 µL
Phusion GC Buffer (5×, + $MgCl_2$)	10 µL
Primer (10 pmol μL^{-1})	2 µL
ad dH_2O	50 µL

B

Denaturation	98 °C	3 min	
Denaturation	98 °C	0.25 min	30-35 cycles
Annealing	55 °C	0.5 min	
Elongation	72 °C	20 s / kb	
Final elongation	72 °C	5 min	
Hold	4 °C	∞	

Table 30. Colony PCR reaction composition (A) and thermocycler program (B).

A

Colony DNA template	**10 µL**
DMSO	1 µL
Taq DNA Polymerase	0.5 µL
dNTP mix (10 mM)	2.5 µL
PCR Buffer S complete (10×)	2.5 µL
Coral Red Buffer Dye (10×)	2.5 µL
Primer (10 pmol μL^{-1})	2 µL
dH_2O	4 µL

B

Denaturation	95 °C	5 min	
Denaturation	95 °C	0.5 min	
Annealing	55 °C	0.5 min	30-35 cycles
Elongation	72 °C	1 min / kb	
Final Elongation	72 °C	8 min	
Hold	4 °C	∞	

2.5.4. *Plasmid construction*

To construct plasmids for overexpression (pJC4-based) or genomic alterations (pK19*mobsacB*-based), either isothermal assembly or SOEing PCR & ligation were performed.

2.5.5. *Isothermal assembly*

The isothermal assembly of one or more DNA fragments with the respective plasmid backbone was performed as has been described before and the protocol is modified after recommendations given in literature (Gibson, 2011; Gibson et al., 2009). DNA fragments were generated via PCR and a minimum of 18 bps of homologous overlap with each other or the plasmid backbone was calculated. The plasmid DNA was linearized with one or two restriction enzymes (Table 8, p.55), purified, and mixed with the DNA fragments in a defined molar ratio

of 1:3 to yield the DNA mix. Then, 5 µL of this DNA mix were added to an iso-enzyme-reagent mix (Table 16, p.59) and isothermal assembly was performed in a Biometra TAdvanced thermocycler (Biometra GmbH, Göttingen, Germany) at 50 °C for 60 min. The assembly mix was then transferred onto a filter membrane (MF-Millipore Membrane Filter, 0.025 µm pore size; Merck Chemicals GmbH, Billerica, USA) and filtered for 10 min against dH_2O. After filtration, 5 µL of the isothermal assembly mix were transformed into electrocompetent *E. coli* DH5α (2.5.2 Preparation of electrocompetent cells and transformation, p.69).

2.5.6. *Splicing by overlap extension PCR and ligation*

Splicing by overlap extension (SOEing) PCR was performed as has been described before (Horton, 1995; Horton et al., 1990). For this purpose, single amplified DNA fragments were generated from the respective template DNA with in-house designed primers. Homologous regions were designed with a minimum of 18 bps overlap. For the SOEing PCR, DNA fragments were deployed in a molecular ratio of 1:1 and Phusion Hot Start II HF DNA Polymerase (Thermo Fisher Scientific Inc., Waltham, USA) was used to amplify the extended product with the two outer primers (Table 4, p.41). The SOEing PCR mix was run on a 1% (w v^{-1}) agarose gel and bands were separated at 80-120 V. The respective band of the SOEing PCR product was cut out on an UV Transilluminator 312 nm (INTAS Science Imaging Instruments GmbH, Göttingen, Germany) and purified with NucleoSpin® Gel and PCR Clean-up Kit (Macherey-Nagel GmbH & Co KG, Düren, Germany). The SOEing PCR product and the adopting plasmid DNA were digested with the two respective restriction enzymes according to the manufacturers specifications (Thermo Fisher Scientific Inc., Waltham, USA), purified after restriction digestion with NucleoSpin® Gel and PCR Clean-up Kit and ligated together with T4 DNA ligase (Thermo Fisher Scientific Inc., Waltham, USA) for 2 h at 22 °C. The ligation mix was then transferred onto a filter membrane (MF-Millipore Membrane Filter, 0.025 µm pore size; Merck Chemicals GmbH, Billerica, USA) and filtered for 10 min against dH_2O. 5 µL of the filtered ligation were then transformed into electrocompetent *E. coli* DH5α (2.5.2 Preparation of electrocompetent cells and transformation, p.69).

2.5.7. *Genomic alterations in C. glutamicum*

For the purpose of modifying the genome (integrations, deletions, base exchanges) of *C. glutamicum*, an already published and well established markerless system was used (Schäfer et al., 1994). This system is based on homologous recombination by applying the mobilizable and integrative vector pK19*mobsacB*. Originally, the vectors pK18 and pK19 were constructed for applications in *E. coli* and constitute the origin of the pK19*mobsacB* system for applications in *C. glutamicum* (Pridmore, 1987). These vectors were combined with the broad host-range transfer machinery of plasmid RP4, a kanamycin resistance cassette, and a modified *sacB* gene from *B. subtilis* for positive selection (Datta et al., 1971; Schäfer et al., 1994; Selbitschka et al., 1993). With the aim to facilitate homologous recombination, the flanking regions were amplified via PCR with a minimum of 500 bps distance, up- and downstream of the genomic area that was intended to be modified.

The pK19*mobsacB* derivatives intended for genomic modifications in *C. glutamicum* were cloned via isothermal assembly (2.5.5 Isothermal assembly, p.72) or SOEing PCR & ligation (2.5.6 Splicing by overlap extension PCR and ligation, p.73). After assembly, the constructs were transformed into *E. coli* DH5α, verified by sequencing, purified, and introduced into the respective *C. glutamicum* strain via electroporation and plating on BHIS (Table 11, p.57) agar plates. The *sacB* gene in pK19*mobsacB* encodes the *B. subtilis* levansucrase, which is responsible for the conversion of sucrose to levan (toxic for *C. glutamicum*), and thus mediates sucrose sensitivity. Selection was therefore carried out on 2×YT (Table 9, p.57) agar plates containing 100 g sucrose L^{-1} thus creating selection pressure to resolve the integrated plasmid by homologous recombination. The pK19*mobsacB* system does not bear an origin of replication (ori) for *C. glutamicum* and counter selection on kanamycin-containing media helps to identify double-crossover events that lead to chromosomal integrations of the complete plasmid. These colonies were discarded and the ones that were not growing on kanamycin-containing agar were tested in colony PCRs (Table 30, p.72) with the appropriate primers and distinguished from the WT.

2.6. Plasmid and strain construction

2.6.1. *Strain Construction – PART I*

In the following, all L-histidine producing strains that were constructed in this work will be described in detail. Oligonucleotides are listed in Table 4, page 41. For an overview of the strain database see Fig. **17** on page 115. All constructed and investigated strains are listed in Table **2** on page 37. If not mentioned otherwise, genomic DNA of *C. glutamicum* ATCC 13032 (WT) was used as template for amplifications via PCR. The ten main strains were named ***C. glutamicum* HIS1 to HIS10** and were constructed proceeding from *C. glutamicum* WT.
The plasmid for exchanging the native HisG variant with the feedback-released $HisG^{G233H-T235Q}$ (Schendzielorz et al., 2014), was implemented into *C. glutamicum* WT by amplifying the flanking genomic regions of *hisG* up- and downstream of the mutations with primer pairs hisG1/hisG2 and hisG3/hisG4 (including the exchanges ggc742cat and acg748cag in *hisG*). Both PCR products were used as templates in a SOEing PCR with primer pair hisG1/hisG4. The SOEing product and pK19*mobsacB* were digested with *BamH*I and fused together in a ligation reaction to give pK19*mobsacB* $hisG^{FB}$. This plasmid was then transformed into *E. coli* DH5α, isolated, and its sequence integrity was verified by DNA sequencing with primers pK19-fw and pK19-rev (GATC Biotech GmbH, Constance, Germany). The verified plasmid was then transformed into *C. glutamicum* WT. The native *hisG* sequence was replaced with the *hisG* sequence containing the nucleotide exchanges leading to $HisG^{G233H-T235Q}$ via a homologous recombination (2.5.7 Genomic alterations in *C. glutamicum*, p.74). For verification of the nucleotide exchanges, a PCR (Table 29, p. 72) with primer pair hisG1/hisG4 was performed and sent for sequencing with primer hisGseq. The resulting strain was named ***C. glutamicum* HIS1**. To construct plasmids for the promoter exchanges in front of the operons containing histidine biosynthesis genes (*C. glutamicum* HIS2, HIS3, HIS4, and HIS6), the flanking regions of the respective promoter was amplified. For the exchange of the native promoter of the operon *hisD-hisC-hisB*-cg2302-cg2301 (Fig. 3, p.16) with the strong promoter of the gene *tuf* (P_{tuf}), encoding the elongation factor TU, the flanking regions were amplified with primer pairs hisD1/hisD2 and hisD3/hisD4. The products of both PCRs were used as templates in a SOEing PCR with primer pair hisD1/hisD4 and the SOEing product and the plasmid pK19*mobsacB* were digested with *BamH*I and *Hind*III and ligated together to give an intermediate plasmid. This plasmid was transformed into *E. coli* DH5α, the plasmid was isolated and sent for sequencing with primers pK19-fw and pK19-rev. In a next step, P_{tuf} was

amplified with primer pair tuf1/tuf2 and the product and the intermediate plasmid were digested with *Nde*I and *Nsi*I. Both were ligated to give plasmid pK19*mobsacB hisD*-P_{tuf}, which was transformed into *E. coli* DH5α, isolated and sent for sequencing with primers pK19-fw and pK19-rev. The verified pK19*mobsacB hisD*-P_{tuf} was transformed into *C. glutamicum* HIS1 and exchange of the native promoter region with the P_{tuf} promoter was again performed on basis of homologous recombination to yield ***C. glutamicum*** **HIS2.** The respective region was amplified with primer pair hisD1/Ptuf2 and verified by sequencing with primer hisD1. The plasmids for exchanging the native promoter with P_{tuf} for operons *hisH-hisA-impA-hisF-hisI-cg2294* and *cg0911-hisN* were constructed in a similar manner. Primer pairs hisH1/hisH2 and hisH3/hisH4 and hisN1/hisN2 and hisN3/hisN4 were used to amplify the flanking regions, respectively. After SOEing PCR, digestion, and ligation, plasmids were transformed into *E. coli* DH5α and prepared. In further steps, the mentioned plasmids were digested with *Nde*I and *Nsi*I and fused with the P_{tuf} region. After sequencing, pK19*mobsacB hisH*-P_{tuf} was implemented in *C. glutamicum* HIS2 to yield ***C. glutamicum*** **HIS3**. The sequence was verified with primers hisH1, hisH4, tuf1, and tuf2. HIS3 served as basis for implementing P_{tuf} in front of *cg0911-hisN* by using pK19*mobsacB hisN*-P_{tuf} to yield ***C. glutamicum*** **HIS4**. HIS4 was verified with primers hisN1, hisN4, tuf1, and tuf2. Since we were not able to implement P_{tuf} for operon *hisE-hisG* in *C. glutamicum* HIS4, we instead used $P_{dapA\text{-A16}}$ (Vašicová et al., 1999), a modified version of the promoter of dihydrodipicolinate synthase, which was amplified with primer pair dapA1/dapA2 from pK18*mobsacB* P*aceE dapA*-A16 (Buchholz et al., 2013). The flanking regions of the *hisE-hisG* promoter were amplified with primer pairs hisE1/hisE2 and hisE3/hisE4, a SOEing PCR was prepared with primer pair hisE1/hisE4. This product and pK19*mobsacB* were digested with *BamH*I and *Hind*III and ligated together. $P_{dapA\text{-A16}}$ and this plasmid were digested with *Nde*I and *Nsi*I and ligated together. Hence, on basis of *C. glutamicum* HIS4, ***C. glutamicum*** **HIS6** was created and verified with primers hisE1, hisE4, dapA1, and dapA2. ***C. glutamicum*** **HIS5** was created by implementing $P_{dapA\text{-A16}}$ in *C. glutamicum* HIS1. To exchange the internal promoter of *hisF* in the operon *hisH-hisA-impA-hisF-hisI-cg2294* with the promoter of manganese superoxide dismutase (encoded by *sodA*), flanking regions and the promoter were amplified with primer pairs hisF1/hisF2, sodA1/sodA2, and hisF3/hisF4 and an additional stop codon (TAA) was integrated upstream of *hisF*. The SOEing PCR (with all three products as template and primer pair hisF1/hisF4) and pK19*mobsacB* were cut with *Hind*III and *BamH*I and ligated together. Integration of P_{sodA} in front of *hisF* in strain *C. glutamicum* HIS6 yielded ***C. glutamicum*** **HIS7**, which was verified

with primers hisF4 and hisFseq. On basis of plasmid pJC4 (Cordes et al., 1992) we constructed pJC4 *purA purB* by amplifying P_{tuf}, *purA*, and *purB* with primer pairs tuf2_1/tuf2_2, purA1/purA2, and purB1/purB2 from the *C. glutamicum* genome. Furthermore, primer pair rrnB1/rrnB2 was used to amplify the T_{rrnB} terminator region of the *rrnB* operon from the *E. coli* K-12 MG1655 genome. Isothermal assembly (2.5.5 Isothermal assembly, p.72) was prepared with these four DNA fragments and pJC4 (Cordes et al., 1992), which had been digested with *Xba*I and *Not*I before. The sequence integrity was verified with primers ABseq1–5. The plasmid pJC4 *purApurB* was transformed into *C. glutamicum* HIS7, to create ***C. glutamicum* HIS8**. The overproduction plasmid for the GCV system from *Corynebacterium jeikeium* was obstained from Evonik Industries AG and was constructed as follows. Plasmid pEC-XT99A (Kirchner and Tauch, 2003) served as basis and was digested with *Ecl*136II and *Xba*I. The gene cluster *gcvPTH* was amplified from the *C. jeikeium* K411 genome (Tauch et al., 2005) with primer pair gcv_Cjk_start_EcoRV/gcv_Cjk_MluI_XbaI and the resulting PCR product was digested with *Eco*RV and *Xba*I and ligated into the cut pEC-XT99A vector. After verification by sequencing, this intermediate plasmid served as basis for the second cloning step. The gene cluster *lipAB* was amplified from the *C. jeikeium* K411 genome with primer pair lipB-Cjk_start-EcoRV/ lipA-Cjk_stop-XbaI and the PCR product was digested with *Ssp*I und *Eco*RV and ligated into the *Xmn*I cut intermediate plasmid to give pEC-XT99A_gcv_OP1-Cjk, which was verified by sequencing. ***C. glutamicum* HIS9** was generated by transforming plasmid pEC-XT99A_gcv_OP1-Cjk into *C. glutamicum* HIS8. The exchange of the translational start codon ATG of gene *pgi* to GTG (Becker et al., 2010) in ***C. glutamicum* HIS10** was done with pK19*mobsacB pgi*^{GTG}. For its construction, the flanking regions were amplified with primer pairs pgi1/pgi2 and pgi3/pgi4, containing the nucleotide exchange. The PCR products were used in a SOEing PCR with primer pair pgi1/pgi4. The SOEing PCR and the vector were digested with *Hind*III and *BamH*I and ligated together. After sequence verification, the plasmid was introduced into *C. glutamicum* HIS9, the base exchange was done as described above, and verified with primer pgiseq.

Besides strains HIS1 to HIS10, the strain database was further extended with accessory strains (Fig. 17, p.115; Table 2, p.37).

Plasmid pK19*mobsacB pgi*^{GTG} was further used to construct strains **CM1** and **HIS7.1**, besides HIS9, which was done as has been described above. Besides *pgi*, genes *gapA* and *pgm* were chosen as targets and their respective translational start codons were changed from the native ATGs to the rarer variants TTG. For this purpose, the respective flanking regions were

amplified from the *C. glutamicum* genome with primer pairs gapA1/gapA2, gapA3/gapA4, pgm1/pgm2 and pgm3/pgm4. Plasmid pK19*mobsacB* was restricted with *Hind*III and *BamH*I and purified. Together with the respective purified PCR products, it was used for isothermal assembly to give pK19*mobsacB gapA*^{TTG} and pK19*mobsacB pgm*^{TTG}. Sequence integritiy was verified by sequencing both with pK19-fw and pK19-rev. These two plasmids were used to create strains **HIS7.2** and **HIS9.1** (for *gapA*^{TTG}) and **HIS7.3** and **HIS9.2** (for *pgm*^{TTG}) and exchange of the respective translational start codon was done by amplifying the surrounding genomic region with primer pairs gapA_seq1/gapA_seq3 and pgm_seq1/pgm_seq3 and sequencing with primers gapA_seq2 and pgm_seq2, respectively.

Plasmid pK18*mobsacB zwf*^{A243T} was obtained from Evonik Industries AG and was used to introduce the amino acid exchange A243T in the G6P DH, to create strain **CM2**. The nucleotide exchange (leading to A243T) was verified by PCR with primers zwf1 and zwf2 and sequencing of the PCR product with primer zwfseq. Besides this amino acid exchange, the *zwf* gene was targeted with another approach. With the purpose to change the translational start codon from the native GTG triplet to the more common variant ATG, the flanking regions of *zwf* were amplified with primer pairs zwf3/zwf4 and zwf5/zwf6. With the two PCR products as templates, a SOEing PCR was performed with primer pair zwf3/zwf6. The SOEing product and pK19*mobsacB* were restricted with *Hind*III and *BamH*I, purified, and ligated together to give pK19*mobsacB zwf*^{ATG}. The resulting plasmid was sequenced with pK19-fw and pK19-rev and used to change the translational start codon of *zwf* in strain CM1. The exchange GTG to ATG in the resulting strain **CM1 *zwf*^{ATG}** was verified by amplifying the respective genomic region with primer pair zwf3/zwf6 and sequencing it with primer zwf3.

Plasmid pK19*mobsacB gnd*^{S361F} was obtained from Evonik Industries AG and was used to introduce the amino acid exchange S361F in the 6PG DH, to create strain **CM2.1**. The nucleotide exchange (leading to S361F) was verified by PCR with primers gnd1 and gnd2 and sequencing of the PCR product with primer gnd_seq.

For the construction of plasmids pK19*mobsacB prsA*^{D122S}, pK19*mobsacB prsA*^{R87C}, and pK19*mobsacB prsA*^{D136A}, flanking regions of the *prsA* gene were amplified with primer pairs prsA1/prsA2.1, prsA1/prsA2.2, or prsA1/prsA2.3 and primer pairs prsA3.1/prsA4, prsA3.2/prsA4, or prsA3.3/prsA4. Then SOEing PCRs with primer pair prsA1/prsA4 were conducted with the respective PCR products from the first PCRs as templates. The three resulting PCR products and the vector pK19*mobsacB* were restricted with *Hind*III and *EcoR*I and ligated together. The resulting plasmid pK19*mobsacB prsA*^{D122S} was sequenced with

primers pK19-fw and pK19-rev and used to create strain **CM3**. The nucleotide exchange leading to *prsA*^{D122S} was verified by amplifying the respective genomic region with primer pair prsA_seq1/prsA_seq3 and sequencing this PCR product with primer prsA_seq2. Despite successful construction of pK19*mobsacB prsA*^{R87C} and pK19*mobsacB prsA*^{D136A}, these amino acid exchanges could not be established in the *C. glutamicum* genome (Table 32, p.122).

Besides amino acid exchanges, the *prsA* gene was also targeted by an exchange of the native RBS (AGGATCCTC) with an improved variant (AGGAGGACATACC). For this purpose, the flanking regions of the *prsA* RBS were amplified with primers containing the improved RBS sequence. These were prsArbs1/prsArbs2 and prsArbs3/prsArbs4. The two PCR products were used as templates in a SOEing PCR with primer pair prsArbs1/prsArbs4. The SOEing product and pK19mobsacB were restricted with HindIII and BamHI, purified, and ligated together to give pK19*mobsacB prsA*^{R}. The resulting plasmid was sequenced with primers pK19-fw and pK19-rev. After implementation of the improved RBS in strain CM1, the sequence identity was verified by amplifying the respective genomic region with primer pair prsArbs1/prsArbs4 and sequencing the product with prsArbs1. The resulting strain was named **CM1 *prsA*^{R}**.

A second genomic integration of the *hisE-hisG* operon was done by constructing a pK19*mobsacB* derivative containing an integration cassette with a modified variant of this operon. The genomic integration site was chosen according to Lange et al., 2017, and was located between genes cg0901 and cg0902 (Lange et al., 2017). The flanking regions of the integration site were amplified with primer pairs cg0901_for/cg0901_rev and cg0902_for/cg0902_rev from the *C. glutamicum* genome. The modified *hisEG* operon (including *hisE*^{ATG} and *hisG*^{FB}) and the P$_{dapA\text{-}A16}$ promoter were amplified from genomic DNA of strain HIS6 with primer pair int1/int2. The Trrnb terminator was amplified with primer pair TrrnB_for/TrrnB_rev from genomic DNA of *E. coli* K-12 MG1655. Plasmid pK19*mobsacB* was restricted with *Xba*I and *Xma*I. All four products and the restricted vector were purified and used in a isothermal assembly reaction to give plasmid pK19*mobsacB* int::P$_{dapA}$*hisE*^{ATG}*hisG*^{FB}. Sequence integrity of this plasmid was verified with primers pK19-fw, int_seq1, int_seq2, int_seq3, int_seq4, and pK19-rev. Integration of the cassette into the CM1 genome to give **HIS$_{int}$** was verified by amplifying the respective genomic region with primer pair int_seq1/seq_int and sequencing this product with primers int_seq1 and int_seq2.

For the in-frame deletion of gene *purF*, the flanking genomic regions were amplified with primer pairs purF1/purF2 and purF3/purF4. Then, a SOEing PCR with both PCR products and primer pair purF1/purF4 was conducted. The SOEing PCR product and pK19*mobsacB* were

restricted with *Pae*I and *BamH*I and ligated together. Integrity of the sequence was verified with primers pK19-fw and pK19-rev. Deletion of *purF* was established in strain CM1 with the resulting plasmid pK19*mobsacB* Δ*purF* and genomic deletion was verified with primer pair purF1/purF4 to create strain **PUR1**. On basis of strain PUR1, *C. glutamicum* **PUR1 Δ*purD*** was constructed, with an additional deletion of the *purD* gene. The flanking regions of the *purD* gene was amplified with primer pairs purD1/purD2 and purD3/purD4, both products were used as templates in a SOEing PCR. This SOEing product and pK19*mobsacB* were restricted with *Hind*III and *BamH*I, purified and ligated together. The resulting pK19*mobsacB* Δ*purD* plasmid was sequenced with primers pK19-fw and pK19-rev. The following deletion of *purD* was verified with primer pair purD1/purD4. Exchange of the translational start codon from the native GTG to the rarer TTG in *purF* was achieved by amplifying the flanking regions with primer pairs purF5/purF6 and purF7/purF8. These two PCR products were used as templates in a SOEing PCR with primer pair purF5/purF8. The SOEing product and pK19*mobsacB* were restricted with *Hind*III and *BamH*I, purified, and ligated together. The sequence integrity of the resulting pK19*mobsacB purF*^{TT}G was verified with primers pK19-fw and pK19-rev. This plasmid was used to create strain **PUR2** and the exchange was verified by amplifying the respective sequence with primers purF5/purF8 and sequencing it with purF5. The plasmid for integration of the nucleotide exchange leading to *purF*^{K348Q} was constructed by amplifying the flanking regions with primer pairs purF9/purF10 and purF11/purF12. The two PCR products were used as templates in a SOEing PCR with primer pair purF9/purF12 and the SOEing product and pK19*mobsacB* were restricted with *Hind*III and *BamH*I, purified, and ligated together. Sequence integrity of pK19*mobsacB purF*^{K348Q} was verified with primers pK19-fw and pK19-rev. In the resulting strain *C. glutamicum* **PUR3**, the nucleotide exchange was verified by amplifying the respective genomic area with primer pair purF9/purF12 and sequencing it with primers K348Qseq1 and K348Qseq2.

Effects of modifications in transketolase availability on L-histidine production was investigated by implementing three different modifications in the *tkt* gene. For the first one, the native genomic *tkt* sequence was replaced with a truncated version. Therefore, the flanking regions of the *tkt* gene were amplified with primer pairs tkt1/tkt2 and tkt3/tkt4. A SOEing PCR was then performed with both PCR products and primer pair tkt1/tkt4 as templates. The SOEing product and pK19*mobsacB* were restricted with *Hind*III and *BamH*I, purified, and ligated together to give pK19*mobsacB* Δ*tkt*. The plasmid was sequenced with primers pK19-fw and pK19-rev and then used to truncate the native *tkt* gene in strains HIS3, HIS4, and HIS6, resulting in strains

HIS3 Δ*tkt*, **HIS4 Δ*tkt***, and **HIS6 Δ*tkt***. The truncation was verified with primer pair tkt1/tkt4. The other modifications in *tkt* constituted the deletion of the region consisting of spacer and spacer plus ribosomal binding site (RBS). The flanking regions were amplified with primer pairs tkt1/tkt5 and tkt6/tkt7 for deletion of the spacer and with primer pairs tkt1/tkt8 and tkt9/tkt7 for the spacer plus the RBS. SOEing PCRs were performed with the products from the preceding PCRs as templates with primer pair tkt1/tkt7. Both SOEing products and pK19*mobsacB* were each restricted with *Hind*III and *BamH*I, purified, and ligated together to result in pK19*mobsacB* Δ*tkt*^{S} (for deletion of the 4 bp spacer region) and pK19*mobsacB* Δ*tkt*^{SRbs} (for deletion of the 8 bp spacer plus RBS region). Sequence indentities were verified by sequencing with primers pK19-fw and pK19-rev. Both were then transformed in strain HIS6, creating **HIS6 *tkt*^{S}** and **HIS6 *tkt*^{SRbs}** and the respective region was amplified with primer pair tkt1/tkt7 for both strains. The PCR product was sequenced with primer tktseq.

The *rpi* gene was targeted by exchanging the native promoter with P_{tuf}. This was done by amplifying the flanking regions with primer pairs rpi1/rpi2 and rpi3/rpi4 and the P_{tuf} region with primer pair tuf3/tuf4. All three PCR products were used as templates in a SOEing PCR with primer pair rpi1/rpi4. The resulting product and pK19*mobsacB* were restricted with *Hind*III and EcoRI, purified, and ligated together, which resulted in pK19*mobsacB* P_{tuf}:*rpi*, which was sequenced with pK19-fw and pK19-rev. The promoter exchange was done with pK19*mobsacB* P_{tuf}:*rpi* in strain CM1 and verified by amplifying the respective region with primer pair rpi1/rp4 and sequencing it with primer rpi1. The resulting strain was named **CM1 P_{tuf}:*rpi***.

The *pup* gene was deleted in the CM1 background with plasmid pK19*mobsacB* Δ*pup*, which was obtained from Lothar Eggeling and Michael Bott (Forschungszentrum Jülich). The genomic deletion of pup in CM1 was verified by amplifying the respective genomic region with primer pair pup1/pup2. The resulting strain was named **CM1 Δ*pup***.

The $P_{dapA\text{-A16}}$ promoter in strain HIS7 was exchanged with the P_{gapA} promoter with pK19*mobsacB* P_{gapA}:*hisE*^{ATG}*hisG*^{FB}. To construct this plasmid, the flanking regions of the modified *hisE-hisG* operon and the P_{gapA} promoter were amplified from genomic DNA of HIS7 with primer pairs hisEG1/hisEG2, PgapA1/PgapA2, and hisEG3/hisEG4. With all three PCR products a SOEing PCR was conducted with primer pair hisEG1/hisEG4, and the SOEing product and pK19mobsacB were restricted with *Hind*III and *BamH*I and purified. Then, restricted plasmid and SOEing product were ligated together, and the resulting pK19*mobsacB* P_{gapA}:*hisE*^{ATG}*hisG*^{FB} was sequenced with primers pK19-fw and pK19-rev. After

implementation in strain HIS7, resulting in **HIS7 P_{gapA}:*hisEG***, the promoter exchange was verified by amplifying the respective genomic region with primer pair hisEGseq1/hisEGseq2 and sequencing with hisEGseq3.

With the purpose to delete the *purN* gene in-frame, the flanking regions were amplified with primer pairs purN1/purN2 and purN3/purN4. The PCR products were used as templates in a SOEing PCR with primer pair purN1/purN4. This product and pK19*mobsacB* were restricted with *Xba*I and *EcoR*I, purified, and ligated together. The resulting plasmid pK19*mobsacB* Δ*purN* was used to delete *purN* in *C. glutamicum* WT. The deletion was verified in the resulting strain ***C. glutamicum* Δ*purN*** with a PCR using primer pair purNdel1/purNdel2. Additionally, the *fdhF* was deleted in strain *C. glutamicum* Δ*purN*. This was done by amplifying the flanking regions of *fdhF* with primer pairs fdhF1/fdhF2 and fdhF3/fdhF4. By using both PCR products as templates in a SOEing PCR and primer pair fdhF1/fdhF4, the flanking regions were connected. The SOEing product and pK19mobsacB were restricted with enzymes *Nhe*I and *BamH*I, purified, and ligated together. The resulting plasmid pK19*mobsacB* Δ*fdhF* was sequenced with pK19-fw and pK19-rev and used to delete the *fdhF* gene in *C. glutamicum* Δ*purN*, to give ***C. glutamicum* Δ*purN* Δ*fdhF***. The deletion was verified in a PCR with primer pair fdhFdel1/fdhFdel2.

Furthermore, the *purU* gene was deleted in-frame in *C. glutamicum* WT and HIS7. This was done by amplifying the flanking regions of the *purU* gene with primer pairs purU1/purU2 and purU3/purU4. The PCR products were used as templates in a SOEing PCR with primer pair purU1/purU4. This SOEing product and pK19*mobsacB* were restricted with *Hind*III and *Xba*I, purified, and ligated together to give pK19*mobsacB* Δ*purU*, whose sequence identity was verified with primers pK19-fw and pK19-rev. The verified plasmid was used to delete *purU* in *C. glutamicum* WT and HIS7, resulting in strains ***C. glutamicum* Δ*purU*** and **HIS7 Δ*purU***. The deletion was verified in both strains by PCR with primers purUdel1/purUdel2.

The two potential L-histidine import systems encoded by *aroP* and cg1305 were also targeted with in-frame deletions. Therefor, the flanking regions were amplified with primer pairs aroP1/aroP2, aroP3/aroP4, cg1305-1/cg1305-2, and cg1305-3/cg1305-4, respectively. Plasmid pK19*mobsacB* was restricted with *Hind*III and *EcoR*I (for *aroP*) and *Xma*I and *EcoR*I (for cg1305), and the purified and restricted plasmids were used with the respective purified PCR products for isothermal assemblies. Sequence identity of both resulting plasmids pK19*mobsacB* Δ*aroP* and pK19*mobsacB* Δcg1305 were verified with pK19-fw and pK19-rev.

The potential purine biosynthesis regulator cg2314 was deleted in strain CM1 by amplifying the flanking regions with primer pairs cg2314-1/cg2314-2 and cg2314-3/cg2314-4. Plasmid pK19*mobsacB* was restricted with *Xba*I and *Nhe*I, purified, and used together with the two purified flanking regions in an isothermal assembly. The resulting plasmid was sequenced pK19*mobsacB* Δcg2314 with primers pK19-fw and pK19-rev and used to delete cg2314 in CM1 to give **CM1 Δcg2314**. The genomic deletion was verified in a PCR with primer pair cg2314-5 and cg2314-4.

The *apt* gene was targeted with an in-frame deletion and an exchange of the translational start codon from GTG to TTG. Therefore, the flanking regions of apt were amplified with primer pairs aptdel1/aptdel2, aptdel3/aptdel4, aptttg1/aptttg2, and aptttg3/aptttg4, respectively. Plasmid pK19*mobsacB* was restricted with *Hind*III and *EcoR*I for both approaches and the purified and restricted plasmid was used together with the respective PCR products in isothermal assemblies. The resulting plasmids pK19*mobsacB* Δ*apt* and pK19*mobsacB* apt^{TTG} were sequenced with primers pK19-fw and pK19-rev.

Overexpressions gene *purA* was achieved with pJC4 as basis. The gene sequence and the P_{tuf} promoter were amplified from the *C. glutamicum* genome with primer pairs tuf2_1/tuf2_2 and purA1/purArev. The T_{rrnB} terminator was amplified from the *E. coli* K-12 MG1655 genome with primer pair trrnbpurA/rrnB2. All three PCR products were fused in a SOEing PCR with primer pair tuf2_1/rrnB2 and purified. Plasmid pJC4 was restricted with *Xba*I and *Not*I and purified. The SOEing product and the restricted plasmid were used for isothermal assembly and the resulting plasmid pJC4 *purA* was sequenced with primers ABseq1, purAseq1, and purAseq2. Transformation into strain CM1 resulted in **CM1 (pJC4 *purA*)**.

Overexpressions of *hisD* was achieved by cloning the *hisD* sequence into pJC4 and into pJC4 *purApurB*. Therefore, P_{sodA} was amplified with primer pair sodA3/sodA4, *hisD* was amplified with primer pair hisD5/hisD6, and the terminator of the lactate dehydrogenase gene *lldD* (cg3227), T_{lldD}, was amplified with primer pair lldD1/lldD2. The T_{lldD} sequence was deduced from Pfeifer-Sancar et al., 2013. With the three PCR products as templates a SOEing PCR was conducted with primer pair sodA3/lldD2 and pJC4 and pJC4 *purApurB* were restricted with *Bst1107*I and *Nhe*I. The purified and restricted plasmids and the purified SOEing product were used in isothermal assemblies to give plasmids pJC4 *hisD* and pJC4 *purApurB hisD*, respectively. Both plasmids were sequenced with primers pJC4hisD1, pJC4hisD2, and pJC4hisD3 and transformed into HIS7 to give **HIS7 (pJC4 *purApurB hisD*)** and **HIS7 (pJC4 *hisD*)**, respectively.

For overexpression of *purH*, P_{sodA} was amplified with primer pair sodA5/sodA6 and *purH* was amplified with primer pair purH1/purH2 from the *C. glutamicum* genome. T_{rrnB} was amplified from the *E. coli* K-12 MG1655 genome with primer pair rrnb3/rrnb4. All three PCR products were used as templates in a SOEing PCR with primer pair sodA5/rrnb4. The resulting product and pJC4 were restricted with *Xba*I and *Not*I, purified, and ligated together. The resulting plasmid pJC4 *purH* was sequenced with primers purHseq1, purHseq2, and purAseq and transformed into CM1 to create *C. glutamicum* **PUR4**.

2.6.2. *Strain Construction – PART II*

For PART II, strains with deletions of genes encoding anaplerotic enzymes were constructed with *C. glutamicum* WT as basis strain. Oligonucleotides are listed in Table 4, page 41. All constructed and investigated strains are listed in Table 2, page 37.

The deletions included genes *ppc*, *pyc*, and *pck*, encoding the phosphoenolpyruvate carboxylase, the pyruvate carboxylase, and the phosphoenolpyruvate carboxykinase. The deletions were done via two-step homologous recombination using the respective pK19*mobsacB* derivative (Table 3, p.39) and all three deletions have been described before (Buchholz et al., 2013; Peters-Wendisch et al., 1998; Riedel et al., 2001). *C. glutamicum* Δ*ppc* (Blombach et al., 2013) was supplied by Bastian Blombach (University of Stuttgart) and served as basis for ***C. glutamicum* Δ*ppc* Δ*pyc***. This strain was constructed with pK*19mobsacB* Δ*pyc* (obtained from Bernhard Eikmanns, University of Ulm) as has been described before (Peters-Wendisch et al., 1998).

Strain ***C. glutamicum* Δ*ppc* Δ*pyc* Δ*pck*** was generated by introducing pK19*mobsacB* Δ*pck* (obtained from Bernhard Eikmanns, University of Ulm) into strain *C. glutamicum* Δ*ppc* Δ*pyc*. After homologous recombination, the *pck* deletion was verified in a PCR with primer pair pckdel1/pckdel2.

The ICD mutations revealed by WGS were re-engineered into the basis strain *C. glutamicum* Δ*ppc* Δ*pyc*. With the purpose to construct plasmids for the introduction of the ICD mutations, the flanking regions of the *icd* gene were amplified from genomic DNA of *C. glutamicum* WT by PCR with primer pairs A94D1/A94D2 and A94D3/A94D4 for amino acid exchange A94D, primer pairs RG1/R453C2 and R453C3/RG2 for amino acid exchange R453C, and primer pairs RG1/G407S2 and G407S3/RG2 for amino acid exchange G407S. The primers already contained the nucleotide exchanges (given in parentheses) leading to the amino acid exchanges A94D (SNP G to T at position 681237 in WT), R453C (SNP G to A at position

680161 in WT), and G407S (SNP T to C at position 680299 in WT), respectively. The two PCR products were fused via SOEing PCRs and the purified product was either cut with *Eco*RI and *BamH*I for A94D or with *Eco*RI and *Nhe*I for G407S and R453C, respectively. Plasmid pK19*mobsacB* was restricted either with *EcoR*I and *BamH*I or *Eco*RI and *Nhe*I. The restricted and purified SOEing products were ligated into pK19*mobsacB* and sequence integrity was verified by DNA sequencing with primers pK19-fw and pK19-rev. After establishing all three amino acid exchanges in *C. glutamicum* Δ*ppc* Δ*pyc*, the respective genomic regions were amplified with primer pairs RGseq1/RGseq2 for G407S and R453C, and A94Dseq1/A94Dseq2 for A94D, and sequenced with primers RGseq3 or A94Dseq3, respectively. This resulted in strains ***C. glutamicum* Δ*ppc* Δ*pyc* ICD^{A94D}**, ***C. glutamicum* Δ*ppc* Δ*pyc* ICD^{R453C}**, and ***C. glutamicum* Δ*ppc* Δ*pyc* ICD^{G407S}**.

For L-valine production, these three strains were each transformed with the L-valine overproduction plasmid pJC4*ilvBNCE* (Radmacher et al., 2002). This resulted in strains ***C. glutamicum* Δ*ppc* Δ*pyc* ICD^{A94D} (pJC4*ilvBNCE*)**, ***C. glutamicum* Δ*ppc* Δ*pyc* ICD^{R453C} (pJC4*ilvBNCE*)**, and ***C. glutamicum* Δ*ppc* Δ*pyc* ICD^{G407S} (pJC4*ilvBNCE*).**

2.7. Disruption of *C. glutamicum*

2.7.1. *Mechanical disruption*

Clear lysates of the respective *C. glutamicum* strains for enzyme assays (2.8.7 Enzyme assays, p.90) was obtained by harvesting cells in the exponential growth phase at an OD_{600} of 7 (about 1.5 g CDW L^{-1}). The cell suspension was centrifuged at 4,500 × g for 10 min at 4 °C (centrifuge 5804 R, rotor: A-4-44, Eppendorf AG, Hamburg, Germany), the supernatant was discarded completely, and the pellet was washed once in wash buffer (0.2 M Tris-HCl pH 7.4; Table 18, p.60), and then resuspended in 0.4 mL lysis buffer (0.1 M Tris-HCl, 10% [v v^{-1}] glycerol, pH 7.4; Table 19, p.60). This solution was then transferred into a screwcap reaction tube filled with 0.25 mL of glass beads (Ø 0.1 mm; Carl Roth GmbH&Co. KG). Mechanical disruption was performed with a Precellys®24 (Bertin Instruments, Montigny-le-Brettonneux, France) device at 6,500 rpm for 3×20 s intervals, intermitted by 5 min breaks, where samples were stored on ice. To obtain cleared lysates, the cell debris was separated by centrifugation at 20,000 × g for 20 min at 4 °C (centrifuge 5804 R, rotor: FA 45-30-11, Eppendorf AG,

Hamburg, Germany). Supernatants were carefully transferred in a new reaction tube and stored on ice until further use (2.8.7 Enzyme assays, p.90).

2.7.2. *Chemical disruption and quenching*

For HPLC analysis of the **intracellular adenylates**, chemical disruption and quenching of the metabolism of *C. glutamicum* was achieved with perchloric acid. The protocol was based on before published approaches (Cserjan-Puschmann et al., 1999; Löffler et al., 2016) and was modified in the following points. The respective strain was cultivated aerobically until the mid-exponential growth phase and cells were harvested at an OD_{600} of 7 (about 1.5 g CDW L^{-1}) and 1 mL of cell suspension was immediately added to 250 µL of -20 °C cold lysis buffer (35% [v v^{-1}] perchloric acid, 80 µM EDTA). This suspension was incubated on an overhead shaker with about 60 rpm at 4 °C. Then, 0.25 mL 1 M K_2HPO_4 followed by 0.19 mL 5 M KOH were added, promoting neutralization (pH 7.0). The suspension was centrifugation (20,800 × g, 5 min, 4 °C; centrifuge 5427 R, rotor: FA 45-30-11, Eppendorf AG, Hamburg, Germany), the supernatant was transferred into a new reaction tube, and the pH value was verified with a pH-meter (pH meter FiveEasy™ FE20, Mettler-Toledo GmbH, Göppingen, Germany). When necessary, 5 M KOH was added in small steps until the desired pH value of 6.95 - 7.00 was reached. The supernatant was analysed directly or stored at -70 °C until further analysis (2.8.6 HPLC measurements, p.89). Alterations of the volume by addition of KOH were noted and considered for recalculations.

For the preparation of **metabolite samples** for SMP measurements (2.8.8 Systems Metabolic Profiling, p.91), the relevant strains were cultivated aerobically in shaking flasks to an OD_{600} of 8.5 (about 1.8 g CDW L^{-1}) for PART I or to an OD_{600} of 12 (about 2.5 g CDW L^{-1}) for PART II. Sampling, quenching, and metabolite extraction were carried out based on a previously described approach (Teleki et al., 2015), including the following minor changes. 2 mL of cell suspension were sampled by fast centrifugation (12,100 × g, 20 s, 30 °C; centrifuge 5427 R, rotor: FA 45 30 11, Eppendorf, Hamburg, Germany), washed with 1.5 mL of 0.9% (w v^{-1}) NaCl solution, and then centrifuged again. Immediately after centrifugation, biomass was quenched in liquid N_2 and stored at -70 °C. Defined amounts of 250 µM L-norvaline solution as internal standard were added to the biomass pellets to obtain an extraction concentration of 20 g CDW L^{-1} for PART I. For PART II, biomass concentrations were adjusted to 30 g L^{-1} by adding defined amounts of H_2O to the pellets. Immediately after addition, samples were preincubated for 1 min at 100 °C in a water bath, homogenized by vortexing for 20 s, and

incubated for either 3 min (for PART I) or 4 min (for PART II) at 100 °C in a water bath. Subsequently, suspensions were chilled on ice, centrifuged (20,800 × g, 10 min, 4 °C; centrifuge 5427 R, rotor: FA 45-30-11, Eppendorf AG, Hamburg, Germany), and supernatants were stored at -70 °C until needed for further analysis (2.8.8 Systems Metabolic Profiling, p.91; Bolten et al., 2007).

2.8. Analytical methods

2.8.1. *Optical density*

Bacterial growth was monitored by determining the turbidity of the cell suspension at a wavelength of 600 nm (OD_{600}) in polystyrolic semi-micro cuvettes (Sarstedt AG & Co. KG, Nümbrecht, Germany). For this purpose, a sample was taken from the cell suspension, diluted in 0.9% (w v^{-1}) NaCl, and analyzed in the Ultrospec 10 Cell Density Meter (GE Healthcare Europe GmbH, Freiburg, Germany) in the linear range of 0.1 - 0.3. A correlation of the turbidity to the cell number was adopted by the correlation of an OD_{600} value of 1 equalling about 10^8 cells.

2.8.2. *Cell dry weight*

To determine the correlation between the OD_{600} values and their respective cell dry weight, the following equation (Equation 3) was used

$$\textbf{Equation 3.} \qquad \mathbf{CDW = \alpha \times OD_{600}} \left[\frac{\mathbf{g}}{\mathbf{L}}\right]$$

The experimental determination of the cell dry weight was done by drying glass test tubes (centrifuge tubes round bottom DURAN®, 12 mL, Carl-Roth GmbH, Karlsruhe, Germany). for 2 d at 105 °C, cooling them to RT in a desiccator, and weighing them. Then, 5 mL of biosuspension from several time points during the bacterial cultivation were taken and centrifuged at 4,000 × g for 10 min at 4 °C (centrifuge 5427 R, rotor: F-35-6-30, Eppendorf AG, Hamburg, Germany). The supernatant was discarded completely, the pellet was washed twice with 5 mL dH_2O, and glass tubes including pellets were dried at 105 °C for 2 d. After cooling to RT in a desiccator, the dry mass of the pellet was determined by subtracting the weight of the empty glass tube from the weight of the filled tube. Representative correlation

coefficients α of CDW with OD_{600} were determined for *C. glutamicum* WT and *C. glutamicum* HIS7 in $CGXII^N$ (Table 12, p.58) minimal medium with 10 g glucose L^{-1} for several OD_{600}/CDW values. The common correlation coefficient α of 0.21 g L^{-1} was determined for the Ultrospec 10 Cell Density Meter (GE Healthcare Europe GmbH, Freiburg, Germany) and both above mentioned strains. This correlation factor was therefore used for all CDW calculations throughout this work.

2.8.3. *Glucose concentration*

The glucose concentration was determined in cleared supernatants of several time points during cultivations according to Equations 2 - 4. Therefore, 1 mL of cell suspension was taken from the bioreactor / shaking flask and centrifuged at 12,100 × g for 5 min at RT (Centrifuge MiniSpin®, rotor F-45-12-11, Eppendorf AG, Hamburg, Germany). The supernatant was transferred in a new reaction tube and directly analysed or frozen at -20 °C until used for further analysis. The photometric quantification of the glucose concentration in the supernatants was performed in acrylic semi-micro cuvettes (Sarstedt AG & Co. KG, Nümbrecht, Germany) with an Ultrospec™ 2100 pro UV/Visible spectrophotometer (GE Healthcare Europe GmbH, Freiburg, Germany). The method was performed as has been described before (Hoffart et al., 2017). For this purpose, 500 µL buffer (400 mM Tris, 4 mM $MgSO_4$, pH 7.6; Table 21, p.60), 100 µL $NADP^+$ (4.4 mg mL^{-1}), 100 µL ATP (9.6 mg mL^{-1}), 190 µL dH_2O, and 100 µL of the prediluted supernatant (concentration in the cuvette < 0.1 mM) were mixed. Then, the initial extinction at a wavelength of 365 nm was determined. The underlying reaction cascade was started by adding 10 µL glucose 6-phosphate dehydrogenase / hexokinase mix (Roche Diagnostics International Ltd) and incubating the reaction mix for 10 min at RT. After incubation, the final extinction was determined and calculation after the Lambert-Beer law was obtained with the following formula (Equations 4, 5, 6), considering ε_{NADPH} at 365 nm.

Equation 4. $$\boldsymbol{\Delta E = \varepsilon \times c \times d}$$

Equation 5. $$\boldsymbol{c = \frac{\Delta E}{\varepsilon \times d}}$$

Equation 6. $$\boldsymbol{\varepsilon_{NADPH} = 3.54 \frac{L}{mmol \times cm}}$$

2.8.4. *DNA*

DNA concentrations and purity of the prepared DNA were determined with a Nano Drop ND-1000 spectrophotometer (PEQLAB Biotechnologie GmbH, Erlangen, Germany) according to the manufacturer's instructions.

2.8.5. *Proteins*

The determination of the total protein content of a sample was done in cleared lysates of *C. glutamicum* (2.7.1 Mechanical disruption, p.85) with the BCA Protein Assay Kit (Thermo Fisher Scientific Inc., Waltham, USA; Table 7, p.55). Quantification of the total protein content was accomplished by analyzing a 9-level standard calibration curve of diluted albumin (BSA; data not shown) at 562 nm in a Synergy 2 microplate reader (BioTek Instruments GmbH, Bad Friedrichshall, Germany) using 96-well plates (Greiner Bio-One GmbH, Frickenhausen, Germany). Samples were diluted 1:10 and 1:20 in dH_2O and reactions were incubated for 30 min at 37 °C.

2.8.6. *HPLC measurements*

For all HPLC measurements HiPerSolv CHROMANORM® water (VWR, Radnor, USA) was used. Concentrations of **amino acids** in the supernatants of cultivated *C. glutamicum* strains were determined as has been described before (Buchholz et al., 2013). For this purpose, 1 mL of cell suspension was harvested by centrifugation (12,100 × g, 5 min, RT; Centrifuge MiniSpin®, rotor F-45-12-11, Eppendorf AG, Hamburg, Germany) and supernatants were used for further analysis. Quantification was performed with an Agilent 1200 series apparatus (Agilent Technologies, Santa Clara, CA, USA) equipped with an Agilent Zorbax Eclipse Plus C_{18} column (250 × 4.6 mm, 5 µm) protected by an Agilent Zorbax Eclipse Plus C_{18} guard column (12.5 × 4.6 mm, 5 µm). Fluorometric detection (excitation at 230 nm and emission at 450 nm) was carried out after automatic precolumn derivatization with *ortho*-phtaldialdehyde. The elution buffer consisted of a polar phase buffer (A) (10 mM Na_2HPO_4, 10 mM $Na_2B_4O_7$, 0.5 mM NaN_3, pH 8.2; Table 25, p.61) and a nonpolar phase buffer (B) (45% (v v^{-1}) methanol, 45% (v v^{-1}) acetonitrile;Table 26, p.62). Quantification of the analytes was conducted by using 200 µM L-ornithine as internal standard to correct variabilities in analytes and a seven-point calibration curve for each component as an external reference standard. For calibration purposes, the Amino Acid Standard (AAS18, Sigma-Aldrich GmbH, Taufkirchen, Germany)

was used, enabling the identification of the following compounds: L-alanine, L-arginine, L-aspartic acid, L-cysteine, L-glutamic acid, glycine, L-histidine, L-isoleucine, L-leucine, L-lysine, L-methionine, L-phenylalanine, L-proline, L-serine, L-threonine, L-tyrosine, and L-valine.

The concentrations of the **adenylates** ATP and ADP were determined with an HPLC system (1200 series, Agilent Technologies, Santa Clara, CA, USA) equipped with a RP-C18 (octadecyl) phase column (Supelcosil LC-18-T, 3 µm, 150 cm × 4.6 mm) and a diode array detector (DAD) and has been described before (Löffler et al., 2016). Samples were prepared as described above (2.7.2 Chemical disruption and quenching, p.86). Buffer A (0.1 M KH_2PO_4, 0.1 M K_2HPO_4, 4 mM TBAS, pH 6.0; Table 27, p.62) and buffer B (0.1 M KH_2PO_4, 0.1 M K_2HPO_4, 4 mM TBAS, pH 7.2 with 30% (v v^{-1}) methanol; Table 28, p.62) were used to generate a gradient (3.5 min, 0% B; 20 min, 30% B, 22 min 35% B; 40 min, 60% B; 48 min, 100% B; 55 min, 100% B, 60 min 0% B) with a flow rate of 1 mL min^{-1}.

2.8.7. *Enzyme assays*

The specific enzyme activities of the tricarboxylic acid (TCA) cycle enzyme isocitrate dehydrogenase (ICD) and of the glyoxylate shunt enzymes isocitrate lyase (ICL) and malate synthase (MS) were determined according to published methods with slight modifications (Eikmanns et al., 1995; Reinscheid et al., 1994b, 1994a). To obtain cleared lysates of the respective strains, they were cultivated, harvested, and disrupted as described above (2.4.1 General cultivations, p. 62; 2.7.1 Mechanical disruption, p.85).

Specific enzyme activities of ICD, ICL, and MS were determined with an Ultrospec™ 2100 pro UV/Visible spectrophotometer (GE Healthcare Europe GmbH, Freiburg, Germany) in acrylic semi-micro cuvettes (Sarstedt AG & Co. KG, Nümbrecht, Germany) or UV cuvettes (UV-Küvetten micro, BRAND GMBH + CO KG, Wertheim, Germany) at 30 °C.

For **ICD**, the cell extracts were diluted 1:50 and 1:100 in lysis buffer (0.1 M Tris, 10% [v v^{-1}] glycerol, pH 7.4; Table 19, p.60) and. 500 µL of assay buffer ICD (100 mM Tris, 0.8 mM $MnSO_4 \times H_2O$, 0.5 mM NADP × 2 Na, pH 7.6; Table 22, p.61), 350 µL dH_2O, and 100 µL prediluted cell extract were mixed and the initial extinction was monitored for 2 min at 30 °C at a wavelength of 340 nm to obtain slope 1 (S1). After 2 min, the reaction was started by adding 50 µL 16 mM Potassium-D_s-threo-isocitrate and the extinction was monitored for 8 min to obtain slope 2 (S2). Both slopes were determined by linear regression.

Specific activities of the **ICL** were determined by diluting the cleared lysates 1:50 and 1:100 in lysis buffer (Table 19, p.60). The content of the cuvette was as follows: 500 µL assay buffer ICL (50 mM MOPS-NaOH, 5 mM dithiothreit, 15 mM $MgCl_2$, 1 mM EDTA, 0.2 mM NADH × 2 Na, pH 7.3; Table 23, p.61), 345 µL dH_2O, 5 µL L-lactate dehydrogenase from rabbit muscle (Sigma-Aldrich GmbH, Taufkirchen, Germany), and 100 µL prediluted lysate. The initial extinction was monitored for 2 min at 30 °C at a wavelength of 340 nm to obtain slope 1 (S1). After 2 min, the reaction was started by adding 50 µL 100 mM Potassium-D_s-threo-isocitrate and the extinction was monitored for 8 min to obtain slope 2 (S2). Both slopes were determined by linear regression.

The **MS** specific activities were determined by prediluting the cleared lysates 1:20 and 1:50 in lysis buffer (Table 19, p.60). Since the alterations in extinction were measured at 232 nm, instead of the acrylic cuvettes, UV cuvettes (UV-Küvetten micro, BRAND GMBH + CO KG, Wertheim, Germany) were used. The cuvettes contained 250 µL assay buffer MS (50 mM Tris, 40 mM $MgCl_2$, 2 mM sodium glyoxylate × H_2O, pH 7.6; Table 24, p.61). The initial extinction was monitored for 2 min at 30 °C at a wavelength of 232 nm to obtain slope 1 (S1). After 2 min, the reaction was started by adding 100 µL 4.8 mM acetyl coenzyme A (acetyl-CoA) and the extinction was monitored for 8 min to obtain slope 2 (S2). Both slopes were determined by linear regression.

2.8.8. *Systems Metabolic Profiling*

Systems Metabolic Profiling (SMP) is an LC-MS/MS Q-TOF-based metabolomics approach, which enables analysis of several interesting metabolites. All SMP measurements conducted for this work were performed by André Feith. For all LC MS/MS Q-TOF-based measurements HiPerSolv CHROMANORM® water (VWR, Radnor, USA) was used. Metabolite samples (2.7.2 Chemical disruption and quenching, p.86) were analyzed on an Agilent 1260 HPLC system coupled to an Agilent 6540 Accurate-Mass LC-MS/MS Q-TOF system with ESI Jet Stream Technology (Agilent Technologies, Santa Clara, USA). Two different hydrophilic interaction chromatography (HILIC) systems were used to get high metabolite coverage.

For PART I, two different hydrophilic interaction chromatography (HILIC) systems were used to get high metabolite coverage. The first method was ammonium acetate based (10 mM, pH 9.2) utilizing a SeQuant ZIC-pHILIC column (150 × 2.1 mm, 5 µm; Merck KGaA, Darmstadt, Germany) with guard column (Sequant ZIC-pHILIC, 20 × 2.1 mm, 5 µm; Merck KGaA, Darmstadt, Germany) at 40 °C, 0.2 mL min 1, and 5 µL injection volume. For details see

(Teleki et al., 2015). an acidic HILIC method was established using ammonium formate buffer (10 mM, pH 2.8) and a Waters XBridge BEH Amide column (150 × 2.1 mm, 3 5 µm; Waters Corp., Milford, MA, USA) coupled to a Waters XBridge BEH Amide VanGuard Cartridge (5 × 2.1 mm, 3.5 µm; Waters Corp., Milford, MA, USA) at 35 °C / 0.2 mL min^{-1} / 5 µL injection volume. Mobile phases were composed as follows: Mobile phase A: 90% acetonitrile / 10% water, 10 mM ammonium formate and mobile phase B: 10% acetonitrile / 90% water, 10 mM ammonium formate. Both adjusted to pH 2.8 with formic acid. Gradient elution was carried out by the following program: Isocratic hold 0% B for 1 min, linear gradient to 62.5% B for 15 min, linear gradient to 100% B for 4 min, column wash at 100% B for 5 min, linear gradient to 0% B for 5 min and column equilibration at 0% B for 15 min. Samples were prepared in 60% (v v^{-1}) acetonitrile and 10 mM ammonium acetate (pH 9.2) or ammonium formate (pH 2.8). All metabolite samples were separated with both HILIC methods in positive and negative MS mode (tuned in extended dynamic range) with following conditions: drying gas flow rate of 8 L min^{-1} with a gas temperature of 325 °C, nebulizer with 40 lb per square inch gauge, sheath gas flow rate of 12 L min^{-1} and sheath gas temperature of 350 °C, capillary voltage of 4000 V and fragmentor voltage of 100 V. Additionally, fragmentation experiments in the targeted MS/MS mode were carried out to investigate and verify structure integrity of IGP, adenylosuccinate, SAICAR, and FGAR. For this, precursor ions [M+H] or [M-H], verified by accurate mass, were selected and fragmented at their characteristic retention times via collision-induced dissociation (CID) at 10, 20, and 30 V. Since analytical standards of those compounds were not commercially available or only by custom synthesis, fragmentation patterns were computationally evaluated with MassHunter Molecular Structure Correlator (B05.00, Agilent Technologies, Santa Clara, USA). By combining accurate mass and plausible fragmentation patterns IGP, adenylosuccinate, SAICAR, and FGAR could be identified.

For PART II, samples were prepared in 60% (v v^{-1}) acetonitrile and 10 mM ammonium acetate buffer (pH 9.2), resulting in 1:20 dilutions. 5 µL of the sample were injected onto a SeQuant® ZIC-pHILIC column (150 × 2.1 mm, 5 µm; Merck KGaA, Darmstadt, Germany) with guard column (SeQuant® ZIC-pHILIC, 20 × 2.1 mm, 5 µm; Merck KGaA, Darmstadt, Germany) at 40 °C with a flow rate of 0.2 mL min^{-1}. Chromatographic separation was based on a previously described method (Teleki et al., 2015), however adapted to a quaternary pump system. Mobile phases were composed as follows: Mobile phase A: 100% acetonitrile, mobile phase B: 90% water / 10% acetonitrile, and mobile phase C: 400 mM ammonium acetate, adjusted to pH 9.2 with 25% (w v^{-1}) ammonium hydroxide. Gradient elution was carried out as follows (2.5% C

was present at all time in the program): isocratic hold 8.2% B for 1 min, linear gradient to 74.2% B for 30 min, linear gradient to 96.2% B for 4 min, column wash at 96.2% B for 5 min, linear gradient to 8.2% B for 10 min, and column equilibration at 8.2% B for 15 min. After separation analytes were detected in negative MS mode (tuned in extended dynamic range) with following conditions: drying gas flow rate of 8 L min^{-1} with a gas temperature of 325 °C, nebulizer with 40 lb per square inch gauge, sheath gas flow rate of 12 L min^{-1} and sheath gas temperature of 350 °C, capillary voltage of 4000 V and fragmentor voltage of 100 V.

2.9. Calculations

2.9.1. *Growth rates*

Growth rates (μ) in h^{-1} were calculated by linear regression in a semi-logarithmic fashion by plotting the biomass concentration (g CDW L^{-1}) over the cultivation time. The exponential growth phase was determined by using a maximization of the coefficient value (R-square). This was done for all calculated growth rates, unless stated otherwise. In some cases, differential growth rates were determined, which were calculated with according to Equation 7.

Equation 7. $$\mu_{diff} = \frac{\Delta c_x}{\Delta t} = \frac{(ln\, c_x^2) - (\ln c_x^1)}{(t^2 - t^1)}\ [h^{-1}]$$

2.9.2. *Yields*

With the aim to thoroughly characterize the constructed strains in detail, several different yields were calculated. The biomass/substrate yield $\mathbf{Y_{X/S}}$ was calculated by linear regression via plotting the biomass concentration (g CDW L^{-1}) over the respective substrate concentration (g glucose L^{-1}).

For all product/substrate yields in PART I and for some in PART II (as indicated), the product and byproduct yields, $\mathbf{Y_{P/S}^{his}}$ for L-histidine, $\mathbf{Y_{P/S}^{gly}}$ for glycine, and $\mathbf{Y_{P/S}^{val}}$ for L-valine were calculated either by plotting the product/byproduct concentration (mM or g L^{-1}) over the respective substrate concentration (mM or g L^{-1}) via linear regression.

For some product/substrate yields in PART I (as indicated), $Y_{P/S}$ was calculated differentially with values obtained after 24 h of cultivation according to Equation 8.

Equation 8. $$Y_{P/S} = \frac{c_P^{24}}{c_S^0 - c_S^{24}} \left[\frac{mol}{mol}\right] \; or \; \left[\frac{g}{g}\right]$$

2.9.3. *Substrate uptake and production rates*

The $Y_{X/S}$ values and the growth rates from above (2.9.1 Growth rates, p.93; 2.9.2 Yields, p.93), were used to calculate the biomass specific substrate uptake rate (q_S) according Equation 9, whereby μ is the growth rate (h^{-1}).

Equation 9. $$q_S = \frac{\mu}{Y_{X/S}} \left[\frac{g}{g_{CDW} \times h}\right]$$

The $Y_{P/S}$ values and the growth rates from above (2.9.1 Growth rates, p.93; 2.9.2 Yields, p.93), were used to calculate the biomass specific product formation rate according Equation 10.

Equation 10. $$q_P = \frac{\mu}{Y_{P/S}} \left[\frac{g}{g_{CDW} \times h}\right] \; or \left[\frac{mmol}{g_{CDW} \times h}\right]$$

Since qP and qS values were calculated from two error-prone values, the standard errors (SE) for qP and qS were determined via Gaussian error propagation using the standard deviations (σ) according to Equation 11. The errors for the energy charges were calculated in the same manner.

Equation 11. $$SE = \sqrt{\left(\frac{1}{Y_{X/S}} \times \sigma_\mu\right)^2 + \left(\mu \times \frac{1}{(Y_{X/S})^2} \times \sigma_{Y_{X/S}}\right)^2}$$

Statistical significances were calculated with Excel v. 2016 (Microsoft Corp., Redmond, USA) as independent two-sample student's t-test to assess the equality of different datasets resulting from biological experiments in triplicates. The confidence interval was set to be $p < 0.05$ and when resulting values were below p, the datasets were assessed as significantly different.

2.9.4. *Specific enzyme activities*

The specific enzyme activities A (U mg^{-1}) of ICD, ICL, and MS enzymes were calculated with the following formula, where S1/S2 are the determined slopes (2.8.7 Enzyme assays, p.90). D is the dilution factor of the sample, V is the volume of the assay (V = 1 mL), ε is the extinction factor for the respective enzyme at the given wave length, d is the diameter of the used cuvette (d = 10 mm), $c_{protein}$ is the protein concentration (2.8.5 Proteins, p.89) of the sample, i.e. cleared bacterial lysate. The used extinction factors for the calculations were ε_{ICD} = 6.28 $(mM\ cm)^{-1}$ for

ICD at 340 nm, ε_{ICL} = 6.28 (mM cm)$^{-1}$ for ICL at 340 nm, and ε_{MS} = 4.50 (mM cm)$^{-1}$ for MS at 232 nm, respectively. Specific enzyme activities were calculated according to Equation 12.

$$\textbf{Equation 12.} \quad \mathbf{A} = \frac{(S_2 - S_1) \times V}{\varepsilon \times d \times c_{protein}} \times \boldsymbol{D} \left[\frac{U}{mg}\right]$$

2.9.5. *Intracellular adenylate concentrations*

The measured concentrations of the adenylate species was related to the biomass concentration. This was done with the following formula, where c_{AxP}^{int} is the intracellular AxP concentration per CDW, c_{AxP} is the measured concentration of the respective adenylate species, c_x is the biomass at the harvest time point, and V is the factor considering volume change during titration in the chemical disruption (2.7.2 Chemical disruption and quenching, p.86). The intracellular adenylate concentration was calculated according to Equation 13.

$$\textbf{Equation 13.} \quad \boldsymbol{c_{AxP}^{int}} = \frac{c_{AxP}}{c_x} \times \boldsymbol{V} \left[\frac{\mu mol\ ATP}{g\ CDW}\right]$$

2.9.6. *Energy charge*

The adenylate energy charge (EC) has been introduced as a measurement to evaluate and compare the energetic state(s) of cells during different phases of microbial growth. This was done based on the originally introduced calculations as were described before and is shown in Equation 14 (Atkinson, 1968; Atkinson and Walton, 1967).

$$\textbf{Equation 14.} \quad \boldsymbol{EC} = \frac{ATP + 0.5 \times ADP}{AMP + ADP + ATP}$$

Owing the fact that ATP is a crucial metabolite in L-histidine production with *C. glutamicum*, the intracellular concentrations of the adenylates were measured (2.9.5 Intracellular adenylate concentrations, p.95) and with the obtained values, energy charges were calculated. Since the absolute concentrations of AMP in all surveyed L-histidine producing mutants were below the detection limit of the applied system (3.1.4 Intracellular ATP & ADP concentrations, p.107), AMP was omitted as factor in these calculations. Equation 15 was used to calculate the ECs.

$$\textbf{Equation 15.} \quad \boldsymbol{EC} = \frac{ATP + 0.5 \times ADP}{ADP + ATP}$$

The omission of AMP from the calculations of the EC for the WT leads to a deviation of about 9%, which was calculated for *C. glutamicum* WT in the exponential growth phase when AMP

was omitted vs. when AMP was considered (data not shown). Since the EC is a relative measurement and since AMP was omitted from EC calculations for all strains, the comparability throughout the strain database is ensured.

2.10. Data analysis

2.10.1. *Systems Metabolic Profiling – Data analysis*

In PART I, peak picking and integration was done in MassHunter ProFinder (B08.00, Agilent Technologies, Santa Clara, USA) by using "batch recursive feature extraction". Subsequently, statistical analysis was performed in Mass Profiler Professional (13.1.1, Agilent Technologies, Santa Clara, CA, USA). Significance testing was done by one-way ANOVA and p-values were filtered ($p < 0.05$). Peaks were identified by accurate mass and with a personal compound data library, containing retention times of authentic standards. Unidentified significant features were searched against the METLIN (Guijas et al., 2018) and MassBank (Horai et al., 2010) database. After identification, peak integration was manually curated via "batch targeted feature extraction".

In PART II, system control and acquisition were performed using MassHunter Data Acquisiton (B06.01, Agilent Technologies, Santa Clara, USA). Peak picking and integration was done in MassHunter ProFinder (B08.00, Agilent Technologies, Santa Clara, USA) by using "*batch targeted feature extraction*" with a personal compound data library, focusing on central carbon metabolism and amino acid biosynthesis. Statistical analysis was performed in Mass Profiler Professional (13.1.1, Agilent Technologies, Santa Clara, USA). Significance testing was done by T-test, p-values were filtered ($p < 0.05$), and fold changes were calculated normalized to *C. glutamicum* WT.

2.10.2. *Flux balance analysis*

Flux Balance Analysis (FBA) was performed to elucidate metabolic flux distributions in *C. glutamicum* WT and to identify alterations in comparison with L-histidine producing mutants (PART I) and the *C. glutamicum* Δ*ppc* Δ*pyc* double deletion mutant strain (PART II). (Becker et al., 2007). All computations were performed with MATLAB 2015b (The MathWorks, Natick, USA) and the COBRA Toolbox v3.0 with glpk solvers (Schellenberger et al., 2011), using the

genome-scale metabolic model (GEM) of *C. glutamicum* ATCC 13032, iCW773 (Zhang et al., 2017).

For PART I, the glucose uptake rate was set to 3.94 mmol g_{CDW}^{-1} h^{-1} for all simulations (Blombach et al., 2013), however objective functions and constraints were changed as follows: a) Maximizing growth rate with no further constraints results in $\mu = 0.36$ h^{-1} and b) maximizing L-histidine production and fixing growth rate to $\mu = 0.1$ h^{-1} results in a yield of 0.51 mol L-histidine mol^{-1} glucose.

In PART II, the pyruvate carboxylase reaction, catalyzed by PCx, was set to irreversible, as opposed to be reversible in the original GEM (Jitrapakdee et al., 2008). Glucose uptake rates were fixed to 4.2 mmol g_{CDW}^{-1} h^{-1} for *C. glutamicum* WT and *C. glutamicum* Δ*ppc* Δ*pyc* resulting in growth rates of 0.390 h^{-1} and 0.389 h^{-1}, respectively. In addition, flux values were constrained to zero for the phosphoenolpyruvate carboxylase (PEPCx) and pyruvate carboxylase reaction (PCx) when computing FBA for the double deletion strain *C. glutamicum* Δ*ppc* Δ*pyc*. The *in vivo* growth rate of 0.27 h^{-1} could also be obtained for the *C. glutamicum* Δ*ppc* Δ*pyc* strain by adjusting glucose uptake rate. However, this did not result in any growth rate dependent changes of metabolic flux distribution.

2.10.3. *Genome sequencing*

The genome sequencing was performed by the Kalinowski Lab at CeBiTec, Bielefeld University. With the aim to identify acquired mutations during the evolutionary cultivations, the genomic DNA of the evolved strains was isolated with the DNeasy Blood & Tissue Kit (QIAGEN, Hilden, Germany; 2.5.1 Isolation/purification of DNA, p.69). An Illumina Nextera sequencing library was prepared according to the manufacturer's instructions and sequenced in a 2 × 150 bp run on a MiSeq Desktop sequencing platform. The reads were mapped to the reference sequence of *C. glutamicum* WT (Kalinowski et al., 2003) using the mapping program SARUMAN (Blom et al., 2011), resulting in a median coverage of the genome between 145.6 to 172.0-fold. Single nucleotide polymorphism (SNP) identification was done using the filtering strategy applied by (Roetzer et al., 2013): SNPs were called for bases with at least 80% reads showing the alternative base with a minimum coverage of 10 reads.

CHAPTER 3: RESULTS

3.1. Results PART I

3.1.1. *Modularizing the L-histidine metabolism*

With the purpose to subdivide the metabolism of *C. glutamicum* around the L-histidine biosynthesis, we classified it in four modules, allowing the separate tackling of each module on the one hand. On the other hand, the holistic combination of the knowledge gained in each module was intended to help balancing the involved pathways on each other. The four created modules comprised the L-histidine biosynthesis, the central carbon metabolism (including glycolysis and pentose phosphate pathway, PPP), the purine biosynthesis (including the *de novo* and salvage parts), and the one carbon metabolism of tetrahydrofolate (THF) species (C_1 metabolism). An overview of this modularization is given in Fig. **10** on page 99 and comprises the selected reactions in the above mentioned pathways with their cofactors, which are important for the detailed contemplation of the following results. This overview is intended to depict and underline the complex, intertwined embedment of the L-histidine biosynthesis in the complete metabolism of *C. glutamicum*. The following paragraphs will illuminate and discuss this embedment.

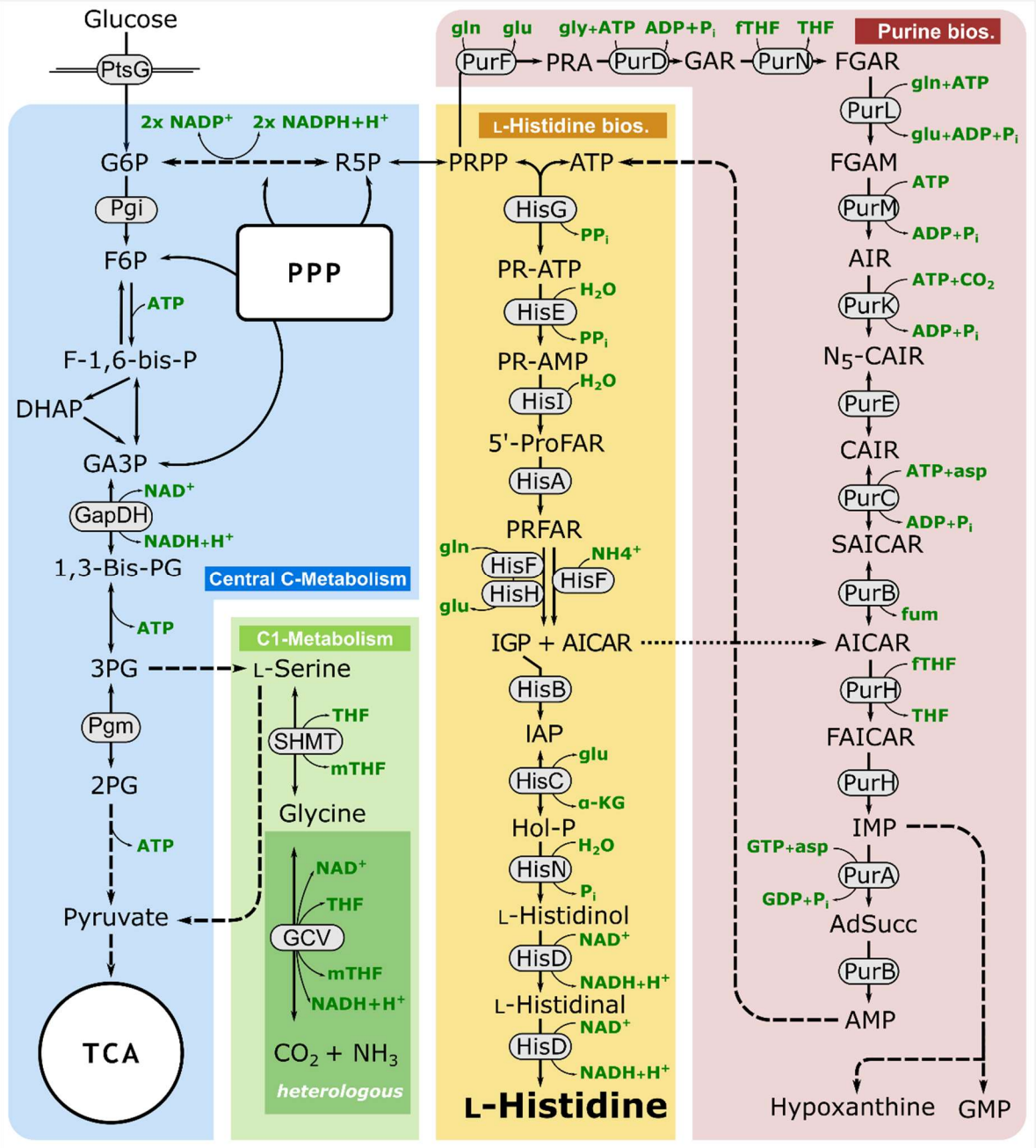

Fig. 10. Overview of the modularized metabolism of *C. glutamicum* with focus on the histidine biosynthesis and the related pathways central carbon metabolism, purine biosynthesis, and one carbon metabolism. The glycine cleavage (GCV) system is not present in *C. glutamicum* WT and was heterologously produced (dark grey). Abbreviations: 2PG, 2-phosphoglycerate; 3PG, 3-phosphoglycerate; 5'-ProFAR, 1-(5-phosphoribosyl)-5-[(5-phosphoribosylamino) methylideneamino] imidazole-4 carboxamide; α KG, α-ketoglutarate; ADP, adenosine diphosphate; AdSucc, adenylosuccinate; AICAR, 1-(5′-phosphoribosyl)-5-amino-4-imidazolecarboxamide; AIR, 5-aminoimidazole ribotide; AMP, adenosine monophosphate; asp; L-aspartate; ATP, adenosine triphosphate; fTHF, 10-formyltetrahydrofolate; F-1,6-Bis-P, fructose-1,6-bisphosphate; F6P, fructose 6-phosphate; FAICAR, 5-formamidoimidazole-4-carboxamide ribotide; fGAM, 5'phosphoribosylformyl-glycineamidine; fGAR, phosphoribosyl-N-formylglcineamide; fum, fumarate; G6P, glucose 6-phosphate; GA3P, glyceraldehyde 3-phosphate; GAR, glycineamide ribonucleotide; GCV, glycine cleavage system; gln, L-glutamine; glu, L-glutamate; GMP, guanosine monophosphate; HisA, 5'ProFAR isomerase; HisB, imidazoleglycerol phosphate dehydratase; HisC, histidinol phosphate aminotransferase;

Legend Fig. 10. continued: HisD, histidinol dehydrogenase; HisE, phosphoribosyl-ATP pyrophosphatase; HisF, synthase subunit of IGP synthase; HisG, ATP phosphoribosyltransferase; HisH, glutaminase subunit of IGP synthase; HisI, phosphoribosyl-AMP cyclohydrolase; HisN, histidinol-phosphate phosphatase; Hol-P, L-histidinol phosphate; IAP, imidazole-acetole phosphate; IGP, imidazole-glycerol phosphate; IMP, inosine monophosphate; mTHF, 5,10-methylenetetrahydrofolate; N_5-CAIR, 5'-phosphoribosyl-4-carboxy-5-aminoimidazole; NAD^+/NADH, oxidized/reduced nicotine amide dinucleotide; $NADP^+$/NADPH, oxidized/reduced nicotine amide dinucleotide phosphate; Pgi, phosphoglucoisomerase; P_i/PP_i, inorganic phosphate/diphosphate; Pgm, phosphoglucomutase; PR-AMP, phosphoribosyl-AMP; PR-ATP, phosphoribosyl-ATP; PRA, phosphoribosylamine; PRFAR, 5-[(5-phospho-1-deoxyribulos-1-ylamino)methylideneamino]-1-(5-phosphoribosyl) imidazole-4-carboxamid; PRPP, phosphoribosyl pyrophosphate; PtsG, phospoenolpyruvate-dependent phosphotransferase system for glucose; PurA, adenylosuccinate synthase; PurB, adenylosuccinate lyase; PurC, phosphoribosylaminoimidazole-succinocarboxamide synthase; PurD, PRA-glycine ligase; PurE, phosphoribosylainoimidazole mutase; PurF, amidophosphoribosyltransferase; PurH, bifunctional AICAR formyltransferase / IMP cyclohydrolase; PurK, phosphoribosylainoimidazole carboxylase; PurL, phosphoribosylformylglycinamide synthase; PurM, phosphoribosylformylglycinamidine cycloligase; PurN, phosphoribosylglycinamide formyltransferase; R5P, ribose 5-phosphate; SAICAR, phosphoribosyl-aminoimidazolesuccinocarboxamide; SHMT, serine hydroxymethyltransferase; TCA, tricarboxylic acid cycle; THF, tetrahydrofolate. **Taken from Schwentner et al., 2019.**

3.1.2. *Flux Balance Analysis*

Flux Balance Analysis (FBA) is a mathematical approach to simulate metabolism based on genome-scale models of metabolic networks (Gianchandani et al., 2009; Orth et al., 2010; Raman and Chandra, 2009). The application of FBAs enables the prediction of systemic phenotypes as fluxes through a reaction network (Gianchandani et al., 2009). André Feith (IBVT, University of Stuttgart) conducted the following FBAs using a genome-scale metabolic model (GEM) of *C. glutamicum* ATCC 13032, iCW773 (Zhang et al., 2017). In two case studies, he a) maximized the growth rate of the model, including no further constraints, which resulted in $\mu = 0.36\ h^{-1}$ and b) maximized L-histidine production, simultaneously fixing the growth rate to $\mu = 0.1\ h^{-1}$, which resulted in a maximal theoretical yield of 0.51 mol L-histidine mol^{-1} glucose (0.44 g L-histidine g substrate). Compared with the case study for growth optimization, the predicted flux distributions for the histidine optimized case study indicated three interesting points:

i) In the L-histidine production scenario, the flux distribution at the junction between glycolysis and PPP (i.e. the reaction catalysed by the phosphoglucoisomerase) changed from a 61:38 ratio to a 34:66 ratio, favouring the PPP over glycolysis and directing increased amounts of carbon towards the L-histidine precursor PRPP, i.e. 74% increased carbon flux (Fig. 11, p.102).

ii) The native ATP recyclization, i.e. conversion from AICAR to AMP/ATP is strongly increased in the L-histidine optimized scenario (compare reactions from AICAR towards AMP; Fig. 11, p.102). Hence, in addition to an increased flux through the L-histidine biosynthesis, an equimolar flux through the purine biosynthesis is emphasized by FBA to be a prerequisite for efficient L-histidine production.

iii) Connected to that, the N10-formyl THF (fTHF) requiring reactions in the purine biosynthesis must be supplied with strongly enhanced pools of loaded THF molecules, which in the L-histidine production scenario is assured by a redistribution of the carbon flux towards L-serine (compare fluxes from 3PG towards Ser; Fig. 11, p.102).

With these hints revealed by FBA in mind, we started to construct L-histidine producing strains, which is described in detail in the following sections.

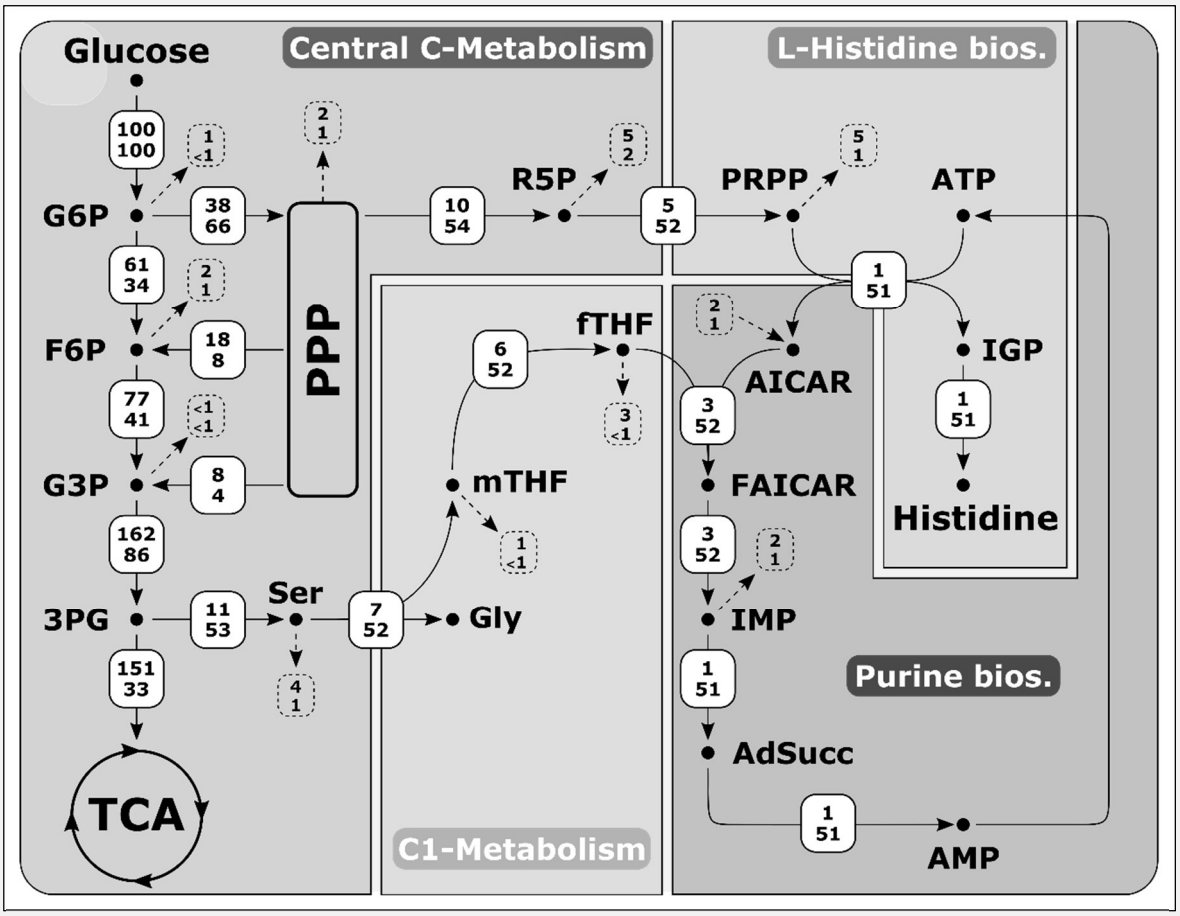

Fig. 11. Flux Balance Analysis (FBA) of a growth optimized (white boxes, upper case) and a L-histidine optimized (white boxes, lower case) strain of *C. glutamicum*. Results are depicted in a schematic overview of the metabolism with focus on the L-histidine biosynthesis and the connected pathways of central carbon metabolism, purine biosynthesis, and one carbon metabolism. White boxes contain fluxes for the growth optimized strain (upper case) and for the L-histidine optimized strain (lower case) and are given in %. Boxes with dashed lines show the carbon flux towards biomass formation. Abbreviations: 3PG, 3-phosphoglycerate; AdSucc, adenylosuccinate; AICAR, 1-(5′-phosphoribosyl)-5-amino-4-imidazolecarboxamide; AMP, adenosine monophosphate; ATP, adenosine triphosphate; bios., biosynthesis; F6P, fructose 6 phosphate; FAICAR, 5-formamidoimidazole-4-carboxamide ribotide; fTHF, 10-formyltetrahydrofolate; G3P, glyceraldehyde 3 phosphate; G6P, glucose 6-phosphate; Gly, glycine; IGP, imidazole-glycerol phosphate; IMP, inosine monophosphate; mTHF, 5,10-methylenetetrahydrofolate; PPP, pentose phosphate pathway; PRPP, phosphoribosyl pyrophosphate; R5P, ribose 5 phosphate; Ser, L-serine; TCA, tricarboxylic acid cycle. **Figure prepared by André Feith. Taken from Schwentner et al., 2019.**

3.1.3. *Optimizing L-histidine biosynthesis*

With the purpose to optimize the L-histidine biosynthesis pathway, several modifications in the operons containing genes encoding L-histidine enzymes, were introduced in the *C. glutamicum* genome. These modifications are shown in Fig. **12** on page 104.

In. a first step, we targeted the ATP phosphoribosyltransferase (HisG), which has been reported before for several organisms (Cho et al., 2003; Pedreño et al., 2012;

Tébar and Ballesteros, 1976), including *C. glutamicum* (Araki and Nakayama, 1974), to be under control of a strong feedback inhibition by the end product of the pathway, L-histidine. Therefore, we aimed to release HisG from its feedback inhibition, which was done by introducing the feedback inhibition released variant $HisG^{G233H-T235Q}$ into *C. glutamicum* WT, i.e. introducing the respective nucleotide exchanges (2.6.1 Strain Construction – PART I, p.75) in the *C. glutamicum* genome (Schendzielorz et al., 2014). It has been shown before, that the $HisG^{G233H-T235Q}$ variant solely is able to cause the excretion of small amounts of L-histidine into the medium (Schendzielorz et al., 2014). The resulting strain *C. glutamicum* HIS1 indeed showed accumulation of L-histidine in the culture supernatant and had a product substrate yield ($Y_{P/S}^{his}$) of 0.015 ± 0.003 mol histidine mol^{-1} glucose (Fig. 13, p.106; Table 31, p.120). Compared to *C. glutamicum* WT, the growth rate μ of *C. glutamicum* HIS1 decreased from 0.38 ± 0.01 h^{-1} to 0.32 ± 0.01 h^{-1}, whereas the biomass substrate yield ($Y_{X/S}$) remained similar with 0.45 ± 0.01 g biomass g^{-1} substrate, compared to 0.46 ± 0.02 g biomass g^{-1} substrate of *C. glutamicum* WT. Beyond this, HIS1 produced glycine as main byproduct besides L-histidine with a $Y_{P/S}^{gly}$ of 0.021 ± 0.003 mol glycine mol^{-1} glucose (Fig. 13, p.106). At this point, the metabolic state of strain *C. glutamicum* HIS1 was analysed in detail by applying Systems Metabolic Profiling (SMP; 2.8.8 Systems Metabolic Profiling, p.91), which revealed increased intracellular peak intensities of D-erythro-1 (imidazole-4-yl)glycerol 3-phosphate (IGP; about 18×) and L-histidinol (about 275×), compared to *C. glutamicum* WT (detailed results see 3.1.9 Systems Metabolic Profiling, p.112). To enable sufficient amounts of enzymes throughout all of the L-histidine pathway, i.e. guaranteeing balanced enzymatic activities of all histidine enzymes, and to prevent accumulations of potentially inhibiting metabolites, we proceeded by exchanging the native promoters of all four canonical operons containing L-histidine genes against stronger ones (compare Fig. 3, p.16 and Fig. 12, p.104). This was done in a first step for the *hisD-hisC-hisB-cg2302-cg2301* operon, where the native promoter sequence was replaced with the promoter of elongation factor TU (encoded by *tuf*), named P_{tuf}. Concomitantly, the sequence in front of the *hisD* gene, which mediates a T-box mediated attenuation mechanism controlling the transcription of this operon, was eliminated (Jung et al., 2010; Kulis-Horn et al., 2014). The resulting strain *C. glutamicum* HIS2 showed similar $Y_{P/S}^{his}$, μ, $Y_{X/S}$, and $Y_{P/S}^{gly}$ with 0.013 ± 0.001 mol L-histidine mol^{-1} glucose, 0.32 ± 0.01 h^{-1}, 0.48 ± 0.01 g biomass g^{-1} substrate, and 0.021 ± 0.01 mol glycine mol^{-1} substrate, respectively (Fig. 13, p.106). In a similar manner, the native promoters of operons *hisH-hisA-impA-hisF-hisI-cg2294* and *cg0911-hisN* were replaced with P_{tuf}. However, the performance characteristics

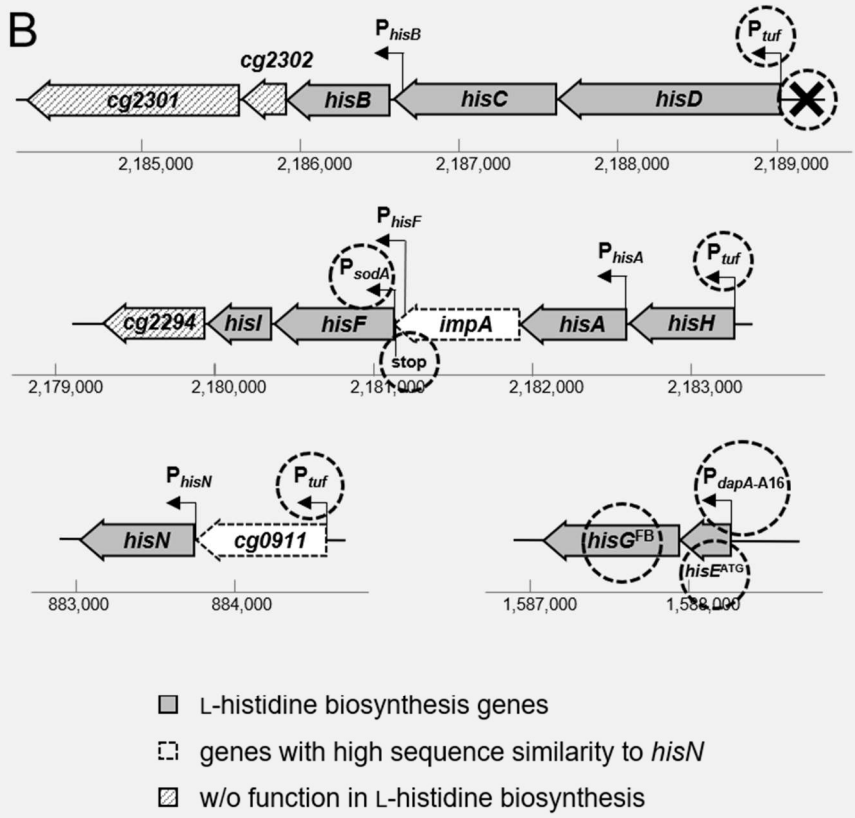

Fig. 12. Modifications in the operons containing L-histidine biosynthetic pathway genes in *C. glutamicum*. Black circles and crosses indicate where modifications were introduced in the *C. glutamicum* genome. Detailed explanations for the modifications is described in 2.6.1 Strain Construction – PART I, page 75. Abbreviations: P, promoter. The ruler indicates the absolute position within the genome of *C. glutamicum* ATCC 13032. Compare with Fig. **3** on page 16. **Taken from Schwentner et al., 2019.**

of the resulting strains *C. glutamicum* HIS3 and HIS4 remained constant, with $Y_{P/S}^{his}$ of 0.013 ± 0.002 and 0.012 ± 0.001 mol L-histidine mol^{-1} glucose, growth rates of 0.33 ± 0.01 and 0.31 ± 0.01 h^{-1}, $Y_{X/S}$ of 0.50 ± 0.02 and 0.45 ± 0.01 g biomass g^{-1} glucose, and $Y_{P/S}^{gly}$ of 0.019 ± 0.001 and 0.017 ± 0.001 mol glycine mol^{-1} glucose, respectively (Fig. 13, p.106). HisG has been reported as being the rate-limiting step in the L-histidine biosynthesis (Mizukami et al., 1994). Therefore, we aimed at replacing the fourth and last remaining native promoter of a histidine operon, which contains genes *hisE* and *hisG*. After several unsuccessful attempts of replacing the native promoter of the *hisEG* operon with P_{tuf} or P_{sodA}, the promoter of manganese superoxide dismutase, encoded by *sodA* (data not shown), we instead implemented $P_{dapA\text{-}A16}$, a mutated variant of the promoter of dihydrodipicolinate synthase, encoded by *dapA* (Vašicová et al., 1999). Simultaneously, the native translational start codon GTG of gene *hisE* was replaced by the more common start codon ATG, to ensure stronger translation efficiency. This has been shown for several genes before to be a potent tool to improve/decrease translation

efficiency (Becker et al., 2010; Kim et al., 2014; Li et al., 2016; Schneider et al., 2012). The resulting strain *C. glutamicum* HIS6 showed improved production behaviour with a $Y_{P/S}^{his}$ of 0.065 ± 0.004 mol L-histidine mol^{-1} glucose, μ of 0.26 ± 0.02 h^{-1}, $Y_{X/S}$ of 0.39 ± 0.05 g biomass g^{-1} glucose, and $Y_{P/S}^{gly}$ of 0.072 ± 0.004 mol glycine mol^{-1} glucose (Fig. 13, p.106).

To reassure the necessity of overexpression of all L-histidine genes, we constructed strain *C. glutamicum* HIS5, which bears the *hisEG* modifications of *C. glutamicum* HIS6, i.e. the $HisG^{G233H-T235Q}$ variant, exchange of the translational start codon from GTG to ATG in *hisE,* and exchange of the native promoter by $P_{dapA\text{-}A16}$. However, this strain does not have P_{tuf} in front of the remaining three L-histidine operons (compare Fig. 12, p.104), thus only overexpressing genes *hisE* and *hisG*. *C. glutamicum* HIS5 showed a $Y_{P/S}^{his}$ of 0.039 ± 0.001 mol L-histidine mol^{-1}glucose, classifying it between *C. glutamicum* HIS4 and HIS6, and thus justifying the overexpression of the remaining L-histidine genes with focus on L-histidine production.

As a further measurement, we implemented P_{sodA} internally inside operon *hisH-hisA-impA-hisF-hisI-cg2294*, directly in front of the *hisF* gene and introduced and additional artificial stop codon upstream of P_{sodA}. The rationale here was to ensure adequate activities of the enzymes encoded by genes *hisF* and *hisI*, which are arranged at the end of a relatively long operon with > 4000 bp (Fig. 12, p.104; Kulis-Horn et al., 2014).

The resulting strain *C. glutamicum* HIS7 showed similar characteristics compared to HIS6, with a $Y_{P/S}^{his}$ of 0.066 ± 0.003 mol L-histidine mol^{-1} glucose, μ of 0.28 ± 0.01 h^{-1}, $Y_{X/S}$ of 0.42 ± 0.02 g biomass g^{-1} glucose, and $Y_{P/S}^{gly}$ of 0.073 ± 0.002 mol glycine mol^{-1} glucose. However, by implementing the internal P_{sodA}, intracellular peak intensities of IGP and L-histidinol in *C. glutamicum* HIS7 were decreased by 88% and 91% compared to *C. glutamicum* HIS1, approaching wildtype like levels and thus re-balancing the connected purine biosynthetic pathway (Fig. 16, p.114). Detailed presentation of the metabolomics data is given in 3.1.9 Systems Metabolic Profiling on page 112.

Fig. 13. Characteristics of strains *C. glutamicum* HIS1 to HIS10 from the strain database including growth rate (h^{-1}) in white, biomass substrate yield $Y_{X/S}$ (g g^{-1}) in dark grey, and (by)product substrate yields for glycine and L-histidine (mol mol^{-1}) with *C. glutamicum* WT as reference. Calculations resulted from results obtained from at least three independently performed experiments per strain and standard deviations are given as error bars. **Taken from Schwentner et al., 2019.**

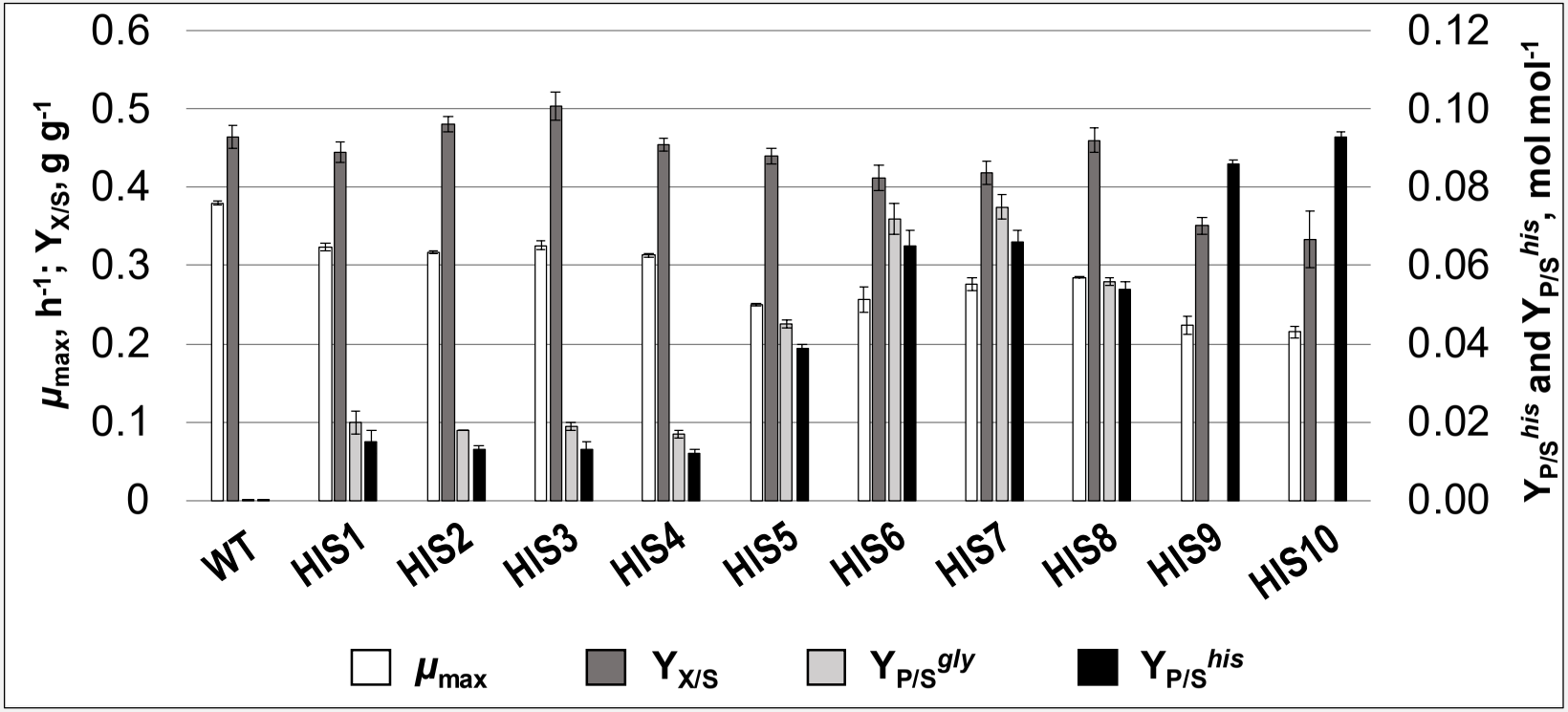

3.1.4. *Intracellular ATP & ADP concentrations*

The tight connection of the biosynthesis pathways for L-histidine and purines manifests a.o. in the form of ATP, as the backbone donor in the HisG-catalysed reaction, and in AICAR, as L-histidine side product and reshuffling molecule for the purine biosynthesis (Fig. 10, p.99). Overproducing L-histidine thus represents a direct intervention in energy metabolism, i.e. purine biosynthesis, and since ATP a.o. is an endproduct of this pathway, cross effects cannot be ruled out *per se*. For this reason, the effect of L-histidine overproductionin the form of overexpression of one or more L-histidine genes, on the intracellular pools of the three adenylates ATP, ADP, and AMP was investigated in more detail. Therefore, intracellular concentrations thereof were determined in strains *C. glutamicum* HIS1 – HIS7 via cell disruption and quenching of the metabolism with perchloric acid (2.7.2 Chemical disruption and quenching, p.86).

For the reference strain *C. glutamicum* WT, intracellular concentrations of 15.7 ± 0.4 µmol ATP g_{CDW}^{-1}, 6.0 ± 0.6 µmol ADP g_{CDW}^{-1} (Fig. **14**, p.108), and 2.1 ± 0.8 µmol AMP g_{CDW}^{-1} were detected when cells were harvested and quenched in the exponential growth phase. This changed, when *C. glutamicum* WT was quenched in the stationary growth phase. Here, AMP was the predominating adenylate species with 17.0 ± 2.4 µmol AMP g_{CDW}^{-1}, followed by 12.9 ± 3.4 µmol ADP g_{CDW}^{-1}, and 1.4 ± 0.3 µmol ATP g_{CDW}^{-1} (data not shown).

For the L-histidine producing strains, cells were quenched in the exponential growth phase. Concentrations of AMP were found to be below the detection limit of the applied system in strains *C. glutamicum* HIS1 – HIS7 (< 300 nm) and were only measurable in *C. glutamicum* WT (data not shown).

In contrast to AMP, ATP and ADP concentrations were traceable in the quenched cell extracts of strains *C. glutamicum* HIS1 – HIS7 and according to the detected concentrations, the mentioned strains can be divided in two groups (Fig. 14, p.108). Compared to *C. glutamicum* WT, the first group (*C. glutamicum* HIS1 – HIS4) exhibited solely diminished ADP levels, showing about half of the concentration of *C. glutamicum* WT, whereas ATP levels remained stable (Fig. **14**, p.108). In contrast to that, the second group (*C. glutamicum* HIS5 - HIS7) exhibited similarly diminished ADP levels compared to *C. glutamicum* WT, however beyond this also ATP levels were strongly affected, showing concentrations as low as 6.6 ± 0.3 µmol ATP g_{CDW}^{-1} and 1.8 ± 0.1 µmol ADP g_{CDW}^{-1} in *C. glutamicum* HIS5 (Fig. 14, p.108). Strikingly, ATP levels were only affected in strains where

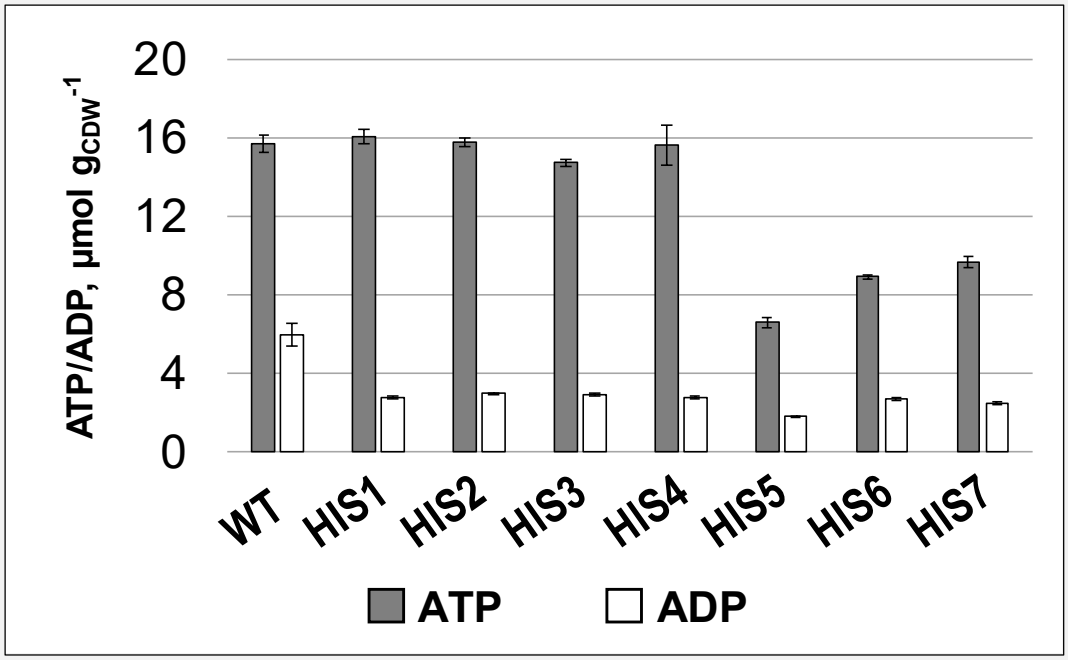

Fig. 14. Intracellular ATP and ADP concentrations during the exponential growth phase for strains *C. glutamicum* HIS1 to HIS7 with *C. glutamicum* WT as reference, as determined via quenching with perchloric acid and HPLC analysis. Intracellular ATP and ADP contents are given in µmol g_{CDW}^{-1} and are shown in dark grey and white, respectively.

the native promoter of the *hisEG* operon had been exchanged with $P_{dapA\text{-}A16}$. As mentioned above, intracellular AMP levels were below the detection limit of the applied HPLC system, and it thus can be concluded that AMP concentrations in strains *C. glutammicum* HIS1 - HIS7 were significantly below the concentrations of *C. glutamicum* WT.

3.1.5. *Energy charges*

The energy charge (EC) has been introduced as a measurement for the energetic state of cells and as a tool to assess cell fitness (Atkinson, 1968; Atkinson and Walton, 1967). The equation for calculating the EC comprises the intracellular concentrations of ATP, ADP, and AMP (2.9.6 Energy charge, p.95). Since AMP concentrations were below the detection limit of the applied HPLC system (2.9.6 Energy charge, p.95), we proceeded by calculating the EC by omitting AMP. Interestingly, despite the absolute intracellular concentrations of ATP and ADP were affected strongly in strains *C. glutamicum* HIS1 - HIS7, the ECs are not affected at all (Fig. 15, p.109). All strains showed very similar ECs compared with *C. glutamicum* WT (0.89 ± 0.04). This indicates that the EC as a critical value is kept stable despite the absolute

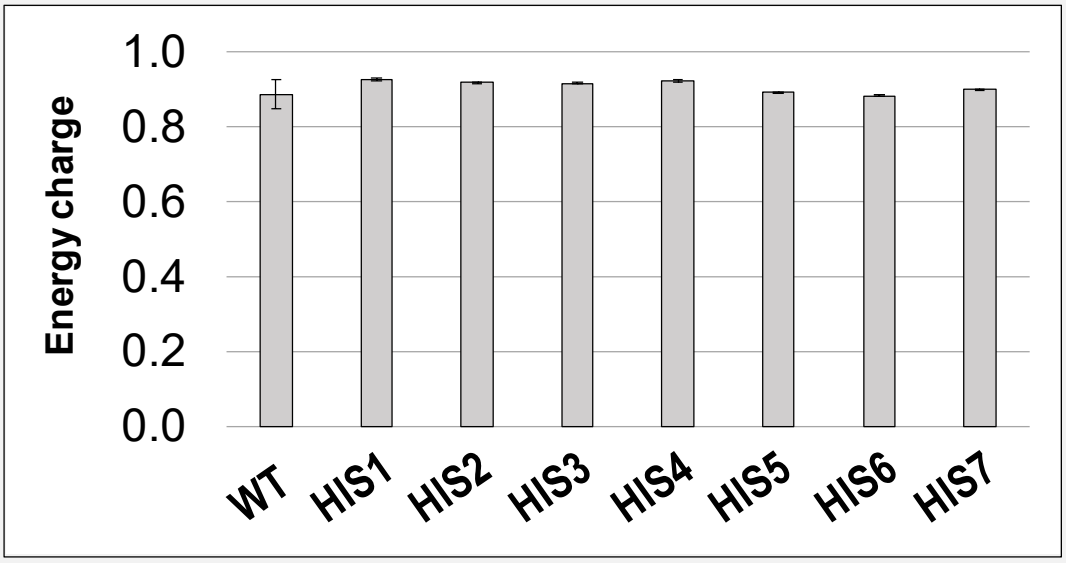

Fig. 15. Energy charges (ECs) of strains *C. glutamicum* HIS1 to HIS7. ECs have been calculated without considering AMP, since AMP concentrations in the L-histidine producing strains were below the detection limit of the applied HPLC system (2.9.6 Energy charge, p.95). Experiments were performed in at least triplicates and standard deviations are given as error bars.

ATP, ADP, and AMP concentrations might vary strongly. Compared to the EC of 0.89 ± 0.04 obtained in the exponential growth phase for *C. glutamicum* WT, the value of the EC determined in the stationary phase was strongly decreased to 0.25 ± 0.03 (data not shown). ECs of the producer strains were not determined during stationary phase.

3.1.6. *Overcoming limitations in ATP recyclization*

At this point, the combined results of FBA (3.1.2 Flux Balance Analysis, p.100), indicating the requirement for an equimolar flux through the purine biosynthesis, and of intracellular ATP measurements (3.1.4 Intracellular ATP & ADP concentrations, p.107), showing that intracellular ATP levels are strongly diminished, pointed towards an increased need for ATP recyclization, i.e. AICAR to AMP/ATP conversion. To support this hypothesis, we aimed at gaining a more holistic overview of the strains optimized in histidine biosynthesis. Therefore, we performed Systems Metabolic Profiling (SMP) of strain *C. glutamicum* HIS7 and identified strongly increased intracellular pool sizes of inosine monophosphate (IMP) and adenylosuccinate (for detailed results see 3.2.10 Systems Metabolic Profiling, p.154; Fig. 16, p.114). Tackling these accumulations and enabling balanced fluxes throughout the L-histidine

connected pathways was done by overexpressing genes *purA* (cg3063) and *purB* (cg2876), encoding the IMP and adenylosuccinate utilizing enzymes adenylosuccinate synthetase and an adenylosuccinate lyase (Fig. 10, p.99). This was achieved by amplifying *purA* and *purB* from the genome of *C. glutamicum* WT and cloning both in the medium copy number plasmid pJC4 under control of promoter P_{tuf} and terminator T_{rrnB}, respectively. The idea behind a combined overexpression of genes *purA* and *purB* was to firstly solve the IMP/adenylosuccinate accumulation and its potentially adverse intracellular effects and secondly to boost the re-cyclization of ATP. The plasmid pJC4*purApurB* was introduced into strain *C. glutamicum* HIS7, and the resulting strain *C. glutamicum* HIS8 was characterized. Surprisingly, *C. glutamicum* HIS8 showed a lower $Y_{P/S}^{his}$ of 0.054 ± 0.002 mol L-histidine mol^{-1} glucose compared to *C. glutamicum* HIS7 (Fig. 13, p.106). The growth rate remained stable with 0.29 ± 0.01 h^{-1} and the biomass substrate yield increased slightly to 0.46 ± 0.02 g biomass g^{-1} glucose. Accordingly, with the decreased L-histidine yield, the glycine yield decreased to 0.056 ± 0.001 mol glycine mol^{-1} glucose (Fig. 13, p.106).

To classify and to reassure the efficacy of the invasion into the energy metabolism (i.e. purine biosynthesis) of the cell by overexpressing *purA* and *purB*, we again performed SMP. Comparison of the metabolomes of strains *C. glutamicum* HIS7 and HIS8 showed that upon introduction of pJC4*purApurB* the intracellular peak intensities of IMP and adenylosuccinate were decreased to wildtype-like levels (Fig. 16, p.114). Additionally, intracellular peak intensities of ATP and ADP were restored to 111% and 96% of the *C. glutamicum* WT levels (Fig. 16, p.114). These findings indicate that despite the $Y_{P/S}^{his}$ was decreased in strain *C. glutamicum* HIS8 compared to HIS7, the accumulations of IMP and adenylosuccinate were re-diminished and the decreased ATP levels could be re-increased. Since the blockages of IMP and/or adenylosuccinate accumulations and ATP re-cyclization were solved properly, it seemed to be most likely that a further limitation that is connected to the highly interlinked L-histidine biosynthesis occurred and superimposed the rearranged ones.

3.1.7. *Reinforcing the native C_1 supply*

The pathway of one-carbon metabolism is a cycle that provides tetrahydrofolate (THF) species as donors of C_1 units for several enzymatic reactions, by reshuffling and regenerating them (1.2.5 L-HISTIDINE related pathways, p.21). The donation of C_1 units is crucial for the synthesis of several metabolites, a.o. for the purine nucleotides and glycine (Sah et al., 2015). As a relevant example, the *de novo* purine biosynthesis requires the supply of two molecules fTHF

as cofactors for reaction steps three (PurN) and ten (PurH). In several organisms, one of the major sources for the generation of C_1 units of the THF cycle is the reaction catalysed by the serine hydroxymethyltransferase (SHMT), converting L-serine to glycine and simultaneously generating 5,10-methylenetetrahydrofolate (mTHF). Interestingly, this fact is also reflected in the FBA with L-histidine overproducing scenario in *C. glutamicum*, where the flux distribution towards glycine was increased (11% to 33%) in a similar manner compared with the distribution towards histidine biosynthesis (5% to 52%) (3.1.2 Flux Balance Analysis, p.100). Furthermore, glycine was experimentally identified as main byproduct being inevitably present in equimolar amounts to L-histidine throughout the generated strain database (3.1.12 Byproduct formation, p.124). Additionally, the SMP data for strain *C. glutamicum* HIS8 showed a strong increase of the intracellular peak intensities of AICAR (+158%), compared to strain HIS7 (3.1.9 Systems Metabolic Profiling, p.112). Interestingly, the peak intensities of AICAR increased even further, despite having solved the IMP/adenylosuccinate accumulations. This shows that the accumulation of AICAR was not due to limited ATP recyclization, but instead might be a problem of cofactor availability. Since one of the two reactions that are required to convert AICAR to IMP is dependent on fTHF, we aimed to improve the fTHF supply. Thus, we identified the glycine cleavage (GCV) system as a solution approach. The GCV system is a multi-enzyme complex converting glycine to CO_2 and NH_3, simultaneously loading THF with a C_1 unit, yielding mTHF, and reducing NAD^+ to NADH (Fujiwara et al., 1984; Kikuchi et al., 2008). The GCV system from *C. jeikeium*, a close relative of *C. glutamicum*, was overproduced via a plasmid-based approach with pEC-XT99A_gcv_ OP1-Cjk (obtained from Andrea Hüser, Evonik Industries AG). This was done to i) eradicate glycine as main byproduct, which has been shown to exhibit adverse effects through above physiological intra- and extracellular concentrations (Hishinuma et al., 1969; Minami et al., 2004), and ii) to supply the cell with additional loaded C_1 units in the form of mTHF (Fig. 10, p.99). Therefore, pEC-XT99A_gcv_ OP1-Cjk was transformed into strain *C. glutamicum* HIS8, resulting in *C. glutamicum* HIS9. *C. glutamicum* HIS9 showed improved L-histidine production with a $Y_{P/S}^{his}$ of 0.086 ± 0.001 mol histidine mol^{-1} glucose, a μ of 0.22 ± 0.01 h^{-1}, and a $Y_{X/S}$ of 0.35 ± 0.01 g biomass g^{-1} glucose (Fig. 13, p.106). The determined glycine concentrations in the medium were negligible (data not shown) and thus $Y_{P/S}^{gly}$ was not calculated. Eradication of glycine in the medium proved the functionality and activity of the GCV system.

3.1.8. *Directing carbon towards L-histidine precursors*

With a rational, purpose-driven approach combined with the indication of the FBA (L-histidine production scenario), the junction of glycolysis and PPP was identified as an additional target for improving strain *C. glutamicum* HIS9 (3.1.2 Flux Balance Analysis, p.100). Thus, *C. glutamicum* HIS9 was engineered to direct increased amounts of carbon towards the crucial L-histidine precursor PRPP. This was done by changing the native translational start codon ATG of the *pgi* (cg0973) gene, encoding the glucose 6-phosphate isomerase (Pgi), to the rarer variant GTG (Pfeifer-Sancar et al., 2013). This has been shown before in *C. glutamicum* to decrease the overall activity of the Pgi enzyme and therefore channelling increased amounts of carbon into the oxidative part of the PPP (Becker et al., 2010, 2009). The generated strain *C. glutamicum* HIS10 showed an improved product yield of 0.093 ± 0.001 mol L-histidine mol^{-1} glucose, while maintaining stable growth rate and biomass substrate yield (Fig. **13**, p.106).

3.1.9. *Systems Metabolic Profiling*

Systems Metabolic Profiling (SMP) is an LC MS/MS Q-TOF-based approach to identify and comparatively analyse peak intensities of intracellular metabolites. This method was developed and tested by André Feith (IBVT, University of Stuttgart), who provided metabolome data for this work (2.8.8 Systems Metabolic Profiling, p.91). Despite results of SMP experiments are incorporated in the above sections, they will be presented in detail in this section.

Strains *C. glutamicum* HIS1, and HIS6 – HIS10, were cultivated and quenched in the mid-exponential growth phase (2.7.2 Chemical disruption and quenching, p.86). The cleared and quenched lysates were then measured on a LC MS/MS Q-TOF system (2.8.8 Systems Metabolic Profiling, p.91) and analysed appropriately (2.10.1 Systems Metabolic Profiling – Data analysis, p.96). Results will not be described in all detail, however the main results from the SMP measurements will be summarized in the following lines.

Upon introduction of the feedback released HisG variant, *C. glutamicum* HIS1 showed altered intracellular peak intensities of several metabolites compared to *C. glutamicum* WT. Among these, D-erythro-1-(imidazol-4-yl)glycerol 3-phosphate (IGP), product of the fifth reaction step in the L-histidine biosynthesis, and L-histidinol, product of the eighth reaction step, were the most prominent ones and resulted in 18× and 275× fold increased intracellular peak intensities (Fig. 16, p.114). Decreased intracellular peak intensities of the TCA cycle (derived)

intermediates α-ketoglutarate, malate, and L-aspartate and slightly increased intensities of the PPP intermediate 6-phosphogluconate indicate that carbon is withdrawn towards the biosynthesis pathways of L-histidine and purines, favouring the oxidative PPP.

The histidine biosynthesis optimized strains *C. glutamicum* HIS6 and HIS7 show, compared to *C. glutamicum* HIS1, relaxed peak intensities of IGP and L-histidinol, indicating that overexpression of all L-histidine genes efficiently balanced the histidine pathway (Fig. 16, p.114). Further, they show a drastic increase in inosine monophosphate (IMP) peak intensities (43× higher than *C. glutamicum* WT), suggesting limitations in the purine biosynthesis. The oxidative part of PPP is further arrogated, which is indicated by the further increasing 6-phosphogluconate peak intensities.

By the overexpression of genes *purA* and *purB* in *C. glutamicum* HIS8 (3.1.6 Overcoming limitations in ATP recyclization, p.109) as reaction to the increased IMP peak intensities, they were re-adjusted to *C. glutamicum* WT like levels. Additionally, ADP and ATP were re-increased to about WT like levels. SMP further revealed strongly increased AICAR peak intensitites in *C. glutamicum* HIS8 compared to *C. glutamicum* WT and *C. glutamicum* HIS7.

As a reaction to the increased AICAR peak intensities in *C. glutamicum* HIS8, the heterologous overproduction of the GCV system from *C. jeikeium* in *C. glutamicum* HIS9 (3.1.7 Reinforcing the native C1 supply, p.110) re-decreased the AICAR peak intensities (reduction of 73% compared to *C. glutamicum* HIS8).

The final strain *C. glutamicum* HIS10 still showed slightly increased peak intensities for AICAR and additionally for FGAR and L-serine, which might be tackled in future experiments and will be discussed below.

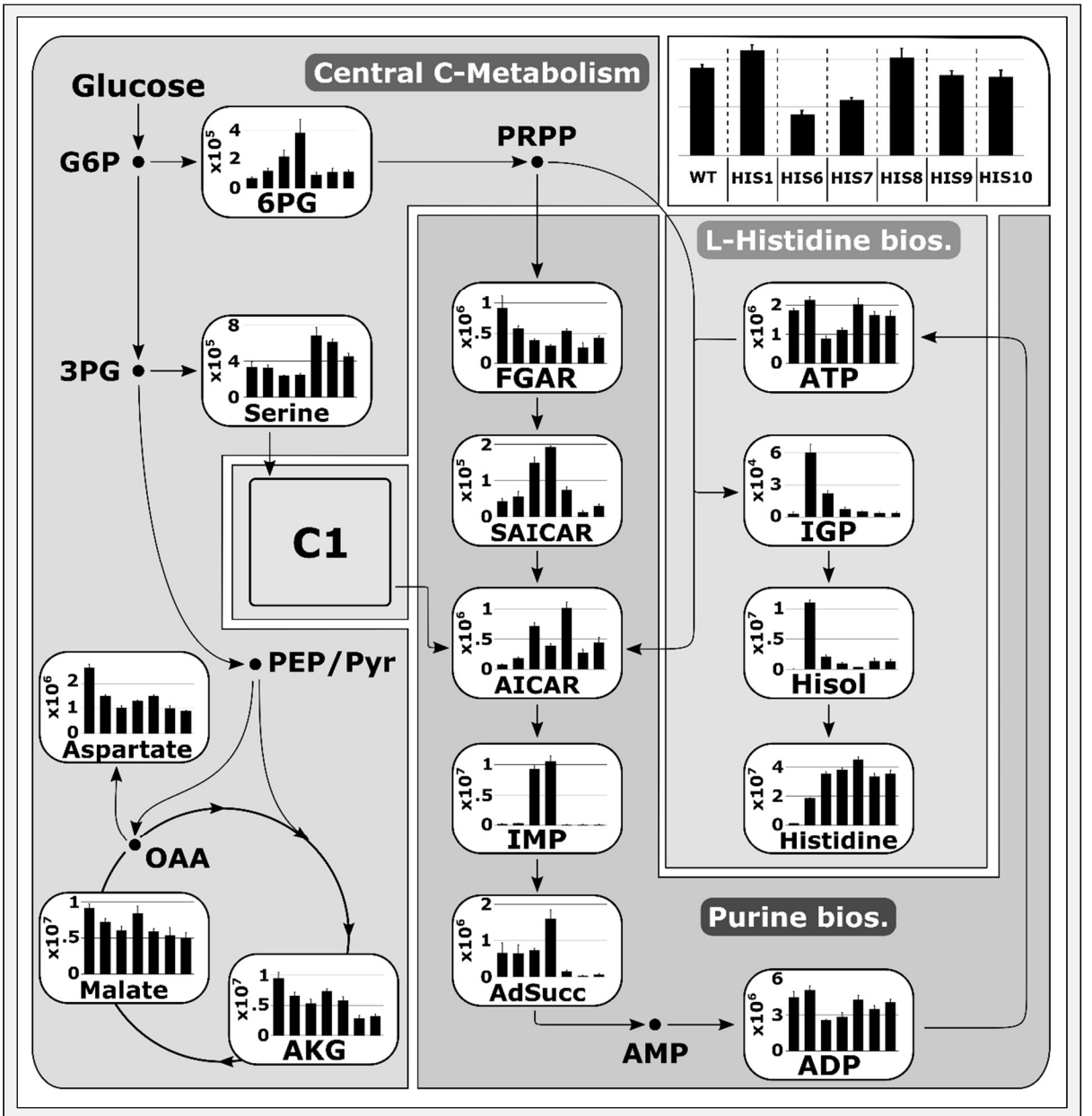

Fig. 16. Systems Metabolic Profiling (SMP) of selected L-histidine producing strains. Results are depicted in a schematic overview of the metabolism with focus on the L histidine biosynthesis and the connected central carbon metabolism, purine biosynthesis, and one carbon metabolism. Selected metabolites originating from these pathways are given as bar diagrams showing intracellular peak intensities. Bars show results for strains *C. glutamicum* WT (WT), HIS1, HIS6, HIS7, HIS8, HIS9, and HIS10, from left to right, respectively. Abbreviations: 3PG, 3-phosphoglycerate; AKG, α-ketoglutarate; ADP, adenosine diphosphate; AdSucc, adenylosuccinate; AICAR, 1-(5′-phosphoribosyl)-5-amino-4-imidazolecarboxamide; AMP, adenosine monophosphate; ATP, adenosine triphosphate; bios., biosynthesis; C1, one carbon metabolism; FGAR, phosphoribosyl-N-formylglcineamide; G6P, glucose 6-phosphate; Hisol, L-histidinol; IGP, imidazole-glycerol phosphate; IMP, inosine monophosphate; OAA, oxaloacetate; PEP, phosphoenolpyruvate; Pyr, pyruvate; PRPP, phosphoribosyl pyrophosphate; SAICAR, phosphoribosyl-aminoimidazolesuccinocarboxamide. **Figure prepared by André Feith. Taken from Schwentner et al., 2019.**

3.1.10. *Extending the strain database*

In addition to strains *C. glutamicum* HIS1 to HIS10, further strains were constructed to extend the strain database and to gain a broader knowledge on the intertwined pathways that are connected to the L-histidine biosynthesis. These strains did not necessarily provide improved histidine yields, they however might provide deeper insights into specific issues, which in the future might ultimately lead to higher yields or at least form a foundation to that.

These strains are quoted in Table 31 on page 120, with their respective growth rates, biomass substrate yields, and histidine and glycine yields. An overview of the modular structure of the strain database and how the strains are based on each other is shown in Fig. **17** on page 115.

After having constructed strain *C. glutamicum* HIS6, with optimized L-histidine biosynthesis pathway, the focus was set on the module of the **central carbon metabolism** (i.e. glycolysis and PPP), where the translational start codon of the *pgi* gene was changed from the native ATG to the rarer variant GTG. The resulting strain was named *C. glutamicum* CM1 (CM for central

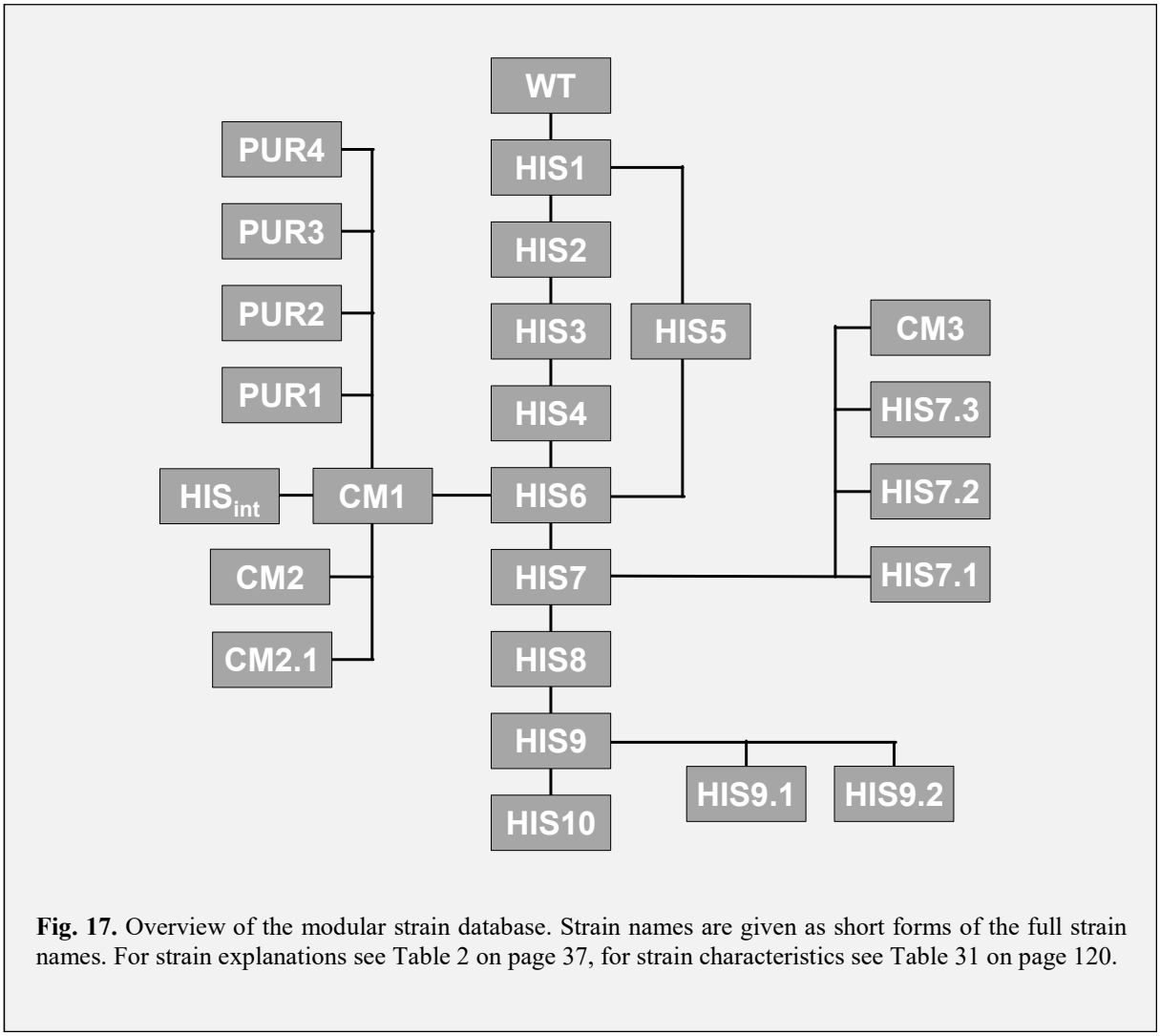

Fig. 17. Overview of the modular strain database. Strain names are given as short forms of the full strain names. For strain explanations see Table 2 on page 37, for strain characteristics see Table 31 on page 120.

carbon metabolism) and showed only slightly altered characteristics (i.e. μ, $Y_{X/S}$, $Y_{P/S}^{his}$, $Y_{P/S}^{gly}$) compared to its basis *C. glutamicum* HIS6. This strain was used a.o. for supplementation studies (3.1.14 Supplementation experiments, p.127) and as a basis for extensive further metabolic engineering studies (see following paragraphs).

Due to the potential overstressing of the oxidative part of the **PPP**, which provides PRPP as L-histidine precursor, and a subsequent increased generation of NADPH (Fig. 10, p.99), the introduction of the published amino acid exchange A243T for the glucose 6-phosphate dehydrogenase (G6P DH) was considered (Georgi et al., 2005). Based on *C. glutamicum* CM1, strain *C. glutamicum* CM2 was constructed, which contains the respective nucleotide exchange in the *zwf* (cg1778) gene, leading to a mutated variant of the G6P DH that is less sensitive to allosteric inhibition by NADPH (Georgi et al., 2005; Moritz et al., 2000). *C. glutamicum* CM2 had a higher $Y_{P/S}^{his}$, it however had a lower growth rate and strongly diminished biomass substrate yield (Table 31, p.120). With the success of the zwf^{A243T} variant, we proceeded by implementing a feedback insensitive variant of the 6-phosphogluconate dehydrogenase (6PG DH), encoded by *gnd* (cg1643) that catalyzes the following reaction. Therefore, the nucleotide exchange of gnd^{S361F} was introduced into the native *gnd* gene, leading to a 6PG DH variant that is less sensitive to allosteric control by fructose-1,6-bisphosphate, glyceraldehyde 3-phosphate, PRPP, ATP, and NADPH (Ohnishi et al., 2005). Based on *C. glutamicum* CM2, the resulting *gnd*-modified strain *C. glutamicum* CM2.1 showed a lower $Y_{P/S}^{his}$ and a lower growth rate.

Another target in the PPP besides *zwf* and *gnd* was the gene *prsA* (cg1075), encoding the PRPP synthetase. It has been described before that this enzyme is the target of allosteric inhibition by mainly ADP, and to lower extents to guanosine diphosphate (GDP), and uridine monophosphate (UMP), in several organisms, a.o. *Bacillus subtilis*, *Salmonella typhimurium*, and *E. coli* (Eriksen et al., 2000; Gibson et al., 1982; Hove-Jensen et al., 1986). In addition to these publications, there is a patent available, where an amino acid exchange in the PRPP synthetase is described, leading to a mutated variant of the PRPP synthetase in *E. coli* that is less sensitive to allosteric inhibition by ADP, which might be harnessed for L-histidine production (Klyachko et al., 2004b). We transferred this amino acid exchange onto the *C. glutamicum* PrsA enzyme resulting in the genetic variant $prsA^{D122S}$ (data not shown). The nucleotide exchange leading to $PrsA^{D122S}$ was introduced in *C. glutamicum* CM1 and resulted in strain *C. glutamicum* CM3. Despite the growth rate and the biomass substrate yield of this strain were similar to those of the progenitor strain, it had higher $Y_{P/S}^{his}$ and $Y_{P/S}^{gly}$ with 0.076 ± 0.002 mol L-histidine

mol^{-1} glucose and 0.093 ± 0.002 mol glycine mol^{-1} glucose, respectively (Table 31, p.120), showing the potential of the PrsA^{D122S} variant.

Based on *C. glutamicum* CM1, one further modification concerning the histidine biosynthesis was investigated. It has been shown e.g. for L-lysine overproducing strains of *C. glutamicum* that additional chromosomal copies of important genes (with respect to the desired product) can improve the product yield (Becker et al., 2011). In this line of thinking, we aimed at implementing an additional copy of the modified *hisE-hisG* operon (HisG$^{G233H-T235Q}$ variant, translational start codon GTG to ATG in *hisE*, and P$_{dapA\text{-A16}}$ in front of *hisE*) into the chromosome of *C. glutamicum* CM1. The resulting strain *C. glutamicum* HIS$_{int}$ showed similar growth rate and $Y_{P/S}^{gly}$ compared with its basis, however $Y_{X/S}$ and $Y_{P/S}^{his}$ decreased to 0.33 ± 0.06 g biomass g^{-1} substrate and 0.063 ± 0.003 mol histidine mol^{-1} glucose, respectively (Table 31, p.120), indicating that additional copies of the *hisE-hisG* operon are adverse for L-histidine production at this point of strain construction.

Beyond the central carbon metabolism, the **purine biosynthesis** was considered as important factor for improving $Y_{P/S}^{his}$. As a first target, the first enzyme of the purine biosynthetic pathway amidophosphoribosyltransferase PurF (encoded by *purF* [cg2857]) was identified. This enzyme competes with a.o. HisG for PRPP as substrate (Fig. 5, p.22) and has been shown to be target of allosteric feedback inhibition by purine nucleotides in *E. coli* and *B. subtilis* (Chen et al., 1997; Zhang et al., 2008; Zhou et al., 1994). With the *purF* gene as target for metabolic engineering, we tested three different modifications. The first one was an in-frame deletion of *purF*, which was performed in strain *C. glutamicum* CM1. The resulting strain *C. glutamicum* PUR1 (for purine biosynthesis) had a strongly diminished growth rate resulting in 0.12 ± 0.01 h^{-1} and $Y_{X/S}$ with 0.18 ± 0.01 g biomass g^{-1} substrate (Table 31, p.120). It further showed lower $Y_{P/S}^{his}$ and $Y_{P/S}^{gly}$, compared to *C. glutamicum* CM1, producing 0.059 ± 0.004 mol L-histidine mol^{-1} glucose and 0.062 ± 0.003 mol glycine mol^{-1} glucose, respectively, indicating the crucial role of the *purF* gene product for the integrity of the cell's (energy) metabolism. Since the product yield was only decreased mildly, despite the very low growth rate and biomass substrate yield, we considered PurF as an interesting target. Instead of abolishing the enzymatic activity of PurF by deleting the encoding gene, we attempted to decrease it in a more sensitive way. Thus, we changed the translational start codon from the native GTG triplet to the rarer variant TTG (Becker et al., 2010, 2009; Pfeifer-Sancar et al., 2013). Interestingly, the resulting strain *C. glutamicum* PUR2 showed very similar characteristics like *C. glutamicum* PUR1, with $\mu = 0.12 \pm 0.01$ h^{-1},

$Y_{X/S}$ = 0.16 ± 0.04 g biomass g^{-1} substrate, $Y_{P/S}^{his}$ = 0.060 ± 0.002 mol L-histidine mol^{-1} glucose and $Y_{P/S}^{gly}$ = 0.068 ± 0.001 mol glycine mol^{-1} glucose (Table 31, p.120). The similar effects of Δ*purF* and *purF*^{TTG} indicate that i) *C. glutamicum* can grow without the *purF* gene and ii) that the TTG exchange has the same effects as a complete deletion of *purF*. However, both modifications seem not to be suitable for L-histidine production with *C. glutamicum* in this manner.

As the third modification concerning PurF, we introduced an amino acid exchange that was described as releasing PurF partially from its allosteric inhibition by AMP and GMP in *E. coli* and *C. glutamicum* (Matsui et al., 2001; Peifer et al., 2012; Shimaoka et al., 2007). The idea behind this step was to reveal the effects of improved purine biosynthesis fluxes on L-histidine production. The resulting strain *C. glutamicum* PUR3 showed decreased characteristics compared to its basis *C. glutamicum* CM1, resulting in μ = 0.21 ± 0.01 h^{-1}, $Y_{X/S}$ = 0.37 ± 0.01 g biomass g^{-1} substrate, $Y_{P/S}^{his}$ = 0.055 ± 0.003 mol L-histidine mol^{-1} glucose and $Y_{P/S}^{gly}$ = 0.067 ± 0.003 mol glycine mol^{-1} glucose (Table 31, p.120).

As another target in the purine biosynthesis besides PurF, the bifunctional enzyme PurH, with functionalities as AICAR formyltransferase and IMP cyclohydrolase (encoded by *purH* [cg0984]) was chosen (Fig. 10, p.99). This enzyme catalyses the reaction steps ten and eleven in the purine biosynthesis and is responsible for processing the AICAR moiety originating from step five of the L-histidine biosynthesis. Since amounts of AICAR coming from the L-histidine pathway most likely are increased in L-histidine overproducing strains, we aimed to withdraw this surplus by overexpressing the *purH* gene. This was done by cloning the native *purH* gene into pJC4 under control of the strong promoter P_{sodA}. The plasmid pJC4-*purH* was introduced into *C. glutamicum* CM1 and resulted in strain *C. glutamicum* PUR4 (Fig. 17, p.115). *C. glutamicum* PUR4 showed improved $Y_{P/S}^{his}$ with 0.075 ± 0.005 mol L-histidine mol^{-1} glucose and $Y_{P/S}^{gly}$ with 0.081 ± 0.006 mol glycine mol^{-1} glucose. The growth rate and $Y_{X/S}$ decreased slightly to 0.19 ± 0.04 h^{-1} and 0.41 ± 0.03 g biomass g^{-1} substrate, respectively. These characteristics indicate the potential of a *purH* overexpression for L-histidine production and might be considered for future strain construction.

In module **glycolysis**, we wanted to test if different points of vantage in this module enable a targeted redirection of carbon fluxes. Three different sites of modification were identified, amongst which the *pgi*^{GTG} modification (leading to CM1; see above) was the first one. *C. glutamicum* HIS7 was used as the basis, and in a first step *pgi*^{GTG} was implemented in this strain to yield *C. glutamicum* HIS7.1 (Fig. 17, p.115). As described above, the attenuation of

the G6P DH activity mediated by *pgi*^{GTG} was intended to direct increased amounts of carbon towards PRPP. Eventually, *C. glutamicum* HIS7.1 showed very similar characteristics compared to its basis, resulting in a growth rate of 0.26 ± 0.01 h^{-1}, $Y_{X/S}$ of 0.44 ± 0.03 g biomass g^{-1} substrate, $Y_{P/S}^{his}$ of 0.064 ± 0.004 mol L-histidine mol^{-1} glucose, and $Y_{P/S}^{gly}$ of 0.078 ± 0.004 mol glycine mol^{-1} glucose (Table 31, p.120). As an alternative to the *pgi*-modification and as the second target in the glycolysis on basis of *C. glutamicum* HIS7, the gene *gapA* (cg1791), encoding the glyceraldehyde 3-phosphate dehydrogenase (GA3P DH), was modified (Fig. 10, p.99; Eikmanns, 1992). In the same manner as for *pgi* and *purF* before, we exchanged the native translational start codon of the *gapA* gene from ATG to TTG, to weaken the GA3P DH activity, thereby directing increased carbon fluxes towards the non-oxidative part of the PPP and eventually to PRPP. The resulting strain *C. glutamicum* HIS7.2 had similar growth rate (0.24 ± 0.01 h^{-1}) and $Y_{X/S}$ (0.40 ± 0.01 g biomass g^{-1} substrate) and increased L-histidine and glycine yields (0.072 ± 0.005 mol L-histidine mol^{-1} glucose, 0.079 ± 0.003 mol glycine mol^{-1} glucose), indicating that carbon is directing towards PRPP rather through the non-oxidative part of PPP instead of the oxidative part and indicating potential of the *gapA*^{TTG} modification for L-histidine production (Table 31, p.120). The phosphoglucomutase (Pgm), encoded by *pgm* (cg2800), was chosen, since a change of the translational start codon from the native ATG to TTG and the putatively connected decrease of the enzymatic activity of Pgm should enable a backlog of carbon into glycolysis/PPP, despite enabling supply of carbon for the crucial SHMT reactions for mTHF generation (Fig. 10, p.99). The resulting strain *C. glutamicum* HIS7.3 had very similar characteristics compared with *C. glutamicum* HIS7, resulting in μ = 0.24 ± 0.01 h^{-1}, $Y_{X/S}$ = 0.41 ± 0.04 g biomass g^{-1} substrate, $Y_{P/S}^{his}$ = 0.064 ± 0.002 mol histidine mol^{-1} glucose and $Y_{P/S}^{gly}$ = 0.073 ± 0.001 mol glycine mol^{-1} glucose (Table 31, p.120). This result indicates either that the *pgm*^{TTG} modification was not strict enough or that the Pgm is not an ideal target for L-histidine production.

To re-evaluate the three modifications of the central carbon metabolism in a strain that was released from the IMP/adenylosuccinate accumulation (3.1.6 Overcoming limitations in ATP recyclization, p.109), we implemented them into strain *C. glutamicum* HIS9. Interestingly, not *gapA*^{TTG} was the most potent one in this background, but *pgi*^{GTG} led to a better performance, yielding strain *C. glutamicum* HIS10 (3.1.8 Directing carbon towards L-HISTIDINE precursors, p.112 and Table 31, p.120). Compared with *C. glutamicum* HIS9, both HIS9.1 (with *gapA*^{TTG}) and HIS9.2 (with *pgm*^{TTG}) each showed a stable growth rate (0.22 ± 0.01 and 0.22 ± 0.01 h^{-1}) and a stable $Y_{X/S}$ (0.32 ± 0.01 and 0.35 ± 0.06 g biomass g^{-1} substrate). However, the

Table 31. Overview of several selected L-histidine producing strains from the modular strain database with their relevant characteristics, including growth rate, substrate specific biomass yield, and substrate specific product yields for the product L-histidine and the main byproduct glycine. Abbreviations: CM, carbon metabolism; HIS, histidine biosynthesis; PUR, purine biosynthesis.

Short	Genotype	μ, h^{-1}	$Y_{X/S}$, g g^{-1}	$Y_{P/S}^{his}$, mol mol^{-1}	$Y_{P/S}^{gly}$, mol mol^{-1}
WT	*C. glutamicum* ATCC 13032	0.38 ± 0.01	0.46 ± 0.02	-	-
HIS1	*C. glutamicum hisG*mut2	0.32 ± 0.01	0.45 ± 0.01	0.015 ± 0.003	0.021 ± 0.003
HIS2	*C. glutamicum hisG*mut2 P_{tuf}*hisD*	0.32 ± 0.01	0.48 ± 0.01	0.013 ± 0.001	0.021 ± 0.001
HIS3	*C. glutamicum hisG*mut2 P_{tuf}*hisD* P_{tuf}*hisH*	0.33 ± 0.01	0.50 ± 0.02	0.013 ± 0.001	0.020 ± 0.002
HIS4	*C. glutamicum hisG*mut2 P_{tuf}*hisD* P_{tuf}*hisH* P_{tuf}*cg0911*	0.31 ± 0.01	0.45 ± 0.01	0.012 ± 0.002	0.019 ± 0.001
HIS5	*C. glutamicum* P_{dapA}*hisEG*mut2	0.25 ± 0.01	0.44 ± 0.01	0.039 ± 0.001	0.045 ± 0.001
HIS6	*C. glutamicum hisG*mut2 P_{tuf}*hisD* P_{tuf}*hisH* P_{tuf}*cg0911* P_{dapA}*hisE*	0.26 ± 0.02	0.39 ± 0.05	0.065 ± 0.001	0.075 ± 0.003
HIS7	*C. glutamicum hisG*mut2 P_{tuf}*hisD* P_{tuf}*hisH* P_{tuf}*cg0911* P_{dapA}*hisE* P_{sodA} *hisFI*	0.28 ± 0.01	0.42 ± 0.02	0.066 ± 0.003	0.073 ± 0.002
HIS8	*C. glutamicum hisG*mut2 P_{tuf}*hisD* P_{tuf}*hisH* P_{tuf}*cg0911* P_{dapA}*hisE* P_{sodA} *hisFI* (pJC4-*purAB*)	0.28 ± 0.01	0.46 ± 0.02	0.054 ± 0.002	0.056 ± 0.001
HIS9	*C. glutamicum hisG*mut2 P_{tuf}*hisD* P_{tuf}*hisH* P_{tuf}*cg0911* P_{dapA}*hisE* P_{sodA} *hisFI* (pJC4-*purAB*) (pEC-*gcv*)	0.22 ± 0.01	0.34 ± 0.01	0.086 ± 0.001	-
HIS10	*C. glutamicum hisG*mut2 P_{tuf}*hisD* P_{tuf}*hisH* P_{tuf}*cg0911* P_{dapA}*hisE* P_{sodA} *hisFI pgi*^{GTG} (pJC4-*purAB*) (pEC-*gcv*)	0.21 ± 0.01	0.33 ± 0.04	0.093 ± 0.001	-
CM1	*C. glutamicum hisG*mut2 P_{tuf}*hisD* P_{tuf}*hisH* P_{tuf}*cg0911* P_{dapA}*hisE pgi*^{GTG}	0.23 ± 0.01	0.44 ± 0.03	0.068 ± 0.001	0.075 ± 0.003
CM2	*C. glutamicum hisG*mut2 P_{tuf}*hisD* P_{tuf}*hisH* P_{tuf}*cg0911* P_{dapA}*hisE pgi*^{GTG} *zwf*^{A243T}	0.19 ± 0.01	0.25 ± 0.02	0.079 ± 0.003	0.098 ± 0.003
CM2.1	*C. glutamicum hisG*mut2 P_{tuf}*hisD* P_{tuf}*hisH* P_{tuf}*cg0911* P_{dapA}*hisE pgi*^{GTG} *zwf*^{A243T} *gnd*^{S361F}	0.16 ± 0.01	0.25 ± 0.02	0.060 ± 0.002	0.074 ± 0.002
CM3	*C. glutamicum hisG*mut2 P_{tuf}*hisD* P_{tuf}*hisH* P_{tuf}*cg0911* P_{dapA}*hisE pgi*^{GTG} *prsA*^{D122S}	0.25 ± 0.01	0.43 ± 0.03	0.076 ± 0.002	0.093 ± 0.002
HIS$_{int}$	*C. glutamicum hisG*mut2 P_{tuf}*hisD* P_{tuf}*hisH* P_{tuf}*cg0911* P_{dapA}*hisE pgi*^{GTG} int:*hisEG*	0.23 ± 0.02	0.33 ± 0.06	0.063 ± 0.003	0.077 ± 0.002
PUR1	*C. glutamicum hisG*mut2 P_{tuf}*hisD* P_{tuf}*hisH* P_{tuf}*cg0911* P_{dapA}*hisE pgi*^{GTG} Δ*purF*	0.12 ± 0.01	0.18 ± 0.01	0.059 ± 0.004	0.062 ± 0.003
PUR2	*C. glutamicum hisG*mut2 P_{tuf}*hisD* P_{tuf}*hisH* P_{tuf}*cg0911* P_{dapA}*hisE pgi*^{GTG} *purF*^{TTG}	0.12 ± 0.01	0.16 ± 0.04	0.060 ± 0.002	0.068 ± 0.001
PUR3	*C. glutamicum hisG*mut2 P_{tuf}*hisD* P_{tuf}*hisH* P_{tuf}*cg0911* P_{dapA}*hisE pgi*^{GTG} *purF*^{K348Q}	0.21 ± 0.01	0.37 ± 0.01	0.055 ± 0.003	0.067 ± 0.003
PUR4	*C. glutamicum hisG*mut2 P_{tuf}*hisD* P_{tuf}*hisH* P_{tuf}*cg0911* P_{dapA}*hisE pgi*^{GTG} (pJC4-*purH*)	0.19 ± 0.04	0.41 ± 0.03	0.075 ± 0.005	0.081 ± 0.006
HIS7.1	*C. glutamicum hisG*mut2 P_{tuf}*hisD* P_{tuf}*hisH* P_{tuf}*cg0911* P_{dapA}*hisE* P_{sodA} *hisFI pgi*^{GTG}	0.26 ± 0.01	0.44 ± 0.03	0.064 ± 0.004	0.078 ± 0.004
HIS7.2	*C. glutamicum hisG*mut2 P_{tuf}*hisD* P_{tuf}*hisH* P_{tuf}*cg0911* P_{dapA}*hisE* P_{sodA} *hisFI gapA*^{TTG}	0.24 ± 0.01	0.40 ± 0.01	0.072 ± 0.005	0.079 ± 0.003
HIS7.3	*C. glutamicum hisG*mut2 P_{tuf}*hisD* P_{tuf}*hisH* P_{tuf}*cg0911* P_{dapA}*hisE* P_{sodA} *hisFI pgm*^{TTG}	0.24 ± 0.01	0.41 ± 0.04	0.064 ± 0.002	0.073 ± 0.001
HIS9.1	*C. glutamicum hisG*mut2 P_{tuf}*hisD* P_{tuf}*hisH* P_{tuf}*cg0911* P_{dapA}*hisE* P_{sodA} *hisFI gapA*^{TTG} (pJC4-*purAB*) (pEC-*gcv*)	0.22 ± 0.01	0.32 ± 0.01	0.076 ± 0.008	-
HIS9.2	*C. glutamicum hisG*mut2 P_{tuf}*hisD* P_{tuf}*hisH* P_{tuf}*cg0911* P_{dapA}*hisE* P_{sodA} *hisFI pgm*^{TTG} (pJC4-*purAB*) (pEC-*gcv*)	0.22 ± 0.01	0.35 ± 0.06	0.081 ± 0.003	-

L-histidine yields were decreased to 0.076 ± 0.008 and 0.081 ± 0.003 mol L-histidine mol^{-1} glucose, respectively (Table 31, p.120).

3.1.11. *A versatile toolbox enables deeper insights*

Due to the highly dynamic and intertwined character of the L-histidine biosynthesis, it is not necessarily given that a certain modification that in the first place proves adverse (i.e. no improvement of $Y_{P/S}^{his}$), still is adverse when a blockage is uncovered. With the following "toolbox" that comprises several pK19*mobsacB*- and pJC4/pEKEx3-based plasmids, a fast and reliable testing of the effects constituted by the respective plasmid, is enabled as soon as a different flux distribution is achieved. The "toolbox" includes mainly plasmids that did not constitute positive effects on $Y_{P/S}^{his}$ in several strain backgrounds or were not implementable in the applied strain basis. However, these constructs might be used for future works and might achieve improvements under the then applied conditions. A list of these plasmids, and if applicable results of their implementation, is given in Table 32 on page 122. The following section will briefly summarize the most relevant results of the toolbox plasmids.

As has been suggested before (Ikeda et al., 1999, 1998; Kamada et al., 2001), gene *tkt* (encoding transketolase) might play an important role for L-histidine production, since it is not elucidated in detail if the carbon flux towards PRPP is channelled through the oxidative or the non-oxidative part of PPP. We chose the *tkt* as target and since promoter engineering (due to the *tkt* gene being part of the operon *tkt-tal-zwf-opcA-pgl*; Kim et al., 2014) and engineering translation initiation (due to the native translational start codon being TTG) were not feasible, we engineered the native RBS. Three approaches were followed, including truncation of the *tkt* gene, deletion of the spacer region of *tkt* (4 bp deletion), and deletion of the extended RBS region of *tkt* (8 bp deletion). Despite supplementing with potassium acetate, the *tkt* modified strains showed no positive effect in growth experiments.

In *E. coli*, the purine regulatory protein PurR has been targeted in a metabolic engineering approach and was deleted from the genome of an L-histidine producing mutant, which led to increased biomass production while maintaining L-histidine production (Doroshenko et al., 2013). Since there is no gene encoding a PurR regulator annotated in the *C. glutamicum* genome, we performed BLAST analysis (data not shown) to identify potential purine regulators in *C. glutamicum*. Therefore, the nucleotide sequences from the genes

Table 32. Overview of plasmids of the toolbox containing plasmids for genomic modifications and plasmids for plasmid-based modifications.

Plasmid	Strain basis	Purpose of plasmid	Idea	Effect
Genomic modifications				
pK19*mobsacB* Δ*tkt*	HIS3,4,6	Chromosomal deletion of gene *tkt* (cg1774)	Investigate effect of deletion of the gene encoding transketolase	n.e.
pK19*mobsacB* Δ*tkt*^{S}	HIS6	Chromosomal deletion of the 4 bp spacer of gene *tkt*	Investigate effect of weakened transcription of the *tkt* gene	n.e.
pK19*mobsacB* Δ*tkt*^{SRbs}	HIS6	Chromosomal deletion of 8 bp spacer and RBS of gene *tkt*	Investigate effect of weakened transcription of the *tkt* gene	n.e.
pK19*mobsacB zwf*^{ATG}	CM1	Change start codon from GTG to ATG for gene *zwf* (cg1778)	Investigate effect of improved translation efficiency for G6P-DH	n.e.
pK19*mobsacB prsA*^{R}	CM1	Modify the RBS of gene *prsA* (cg1075)	Investigate effect of improved translation efficiency for PRPP synthetase	n.e.
pK19*mobsacB prsA*^{D136A}	CM1	Implement nt exchange leading to AA exchange D136A in *prsA*	Investigate effect of mutated variant PrsA^{D136A} (Bower et al., 1989; Shimaoka et al., 2007); amino acid exchange was transferred from the *E. coli* Prs enzyme onto *C. glutamicum* PrsA	n.i.
pK19*mobsacB prsA*^{R87C}	CM1	Implement nt exchange leading to AA exchange R87C in *prsA*	Investigate effect of mutated variant PrsA^{R87C} (Klyachko et al., 2004); amino acid exchange was transferred from the *E. coli* Prs enzyme onto *C. glutamicum* PrsA	n.i.
pK19*mobsacB* P$_{tuf}$*:rpi*	CM1	Chromosomally implement P$_{tuf}$ in front of *rpi* (cg2658)	Investigate effect of improved transcription of *rpi*, encoding phosphopentose isomerase	n.e.
pK19*mobsacB* Δ*pup*	CM1	Chromosomal deletion of gene *pup* (cg1689)	Investigate effect of deletion of the gene encoding the prokaryotic ubiquitin-like protein, potentially responsible for HisC and HisD degradation (Küberl et al., 2014)	n.e.
pK19*mobsacB* P$_{gapA}$*:hisEG*	HIS6	Exchange of P$_{dapA\text{-}A16}$ in front of operon *hisE-hisG* with promoter of gene *gapA*	Testing P$_{gapA}$ as alternative to P$_{dapA\text{-}A16}$; drain higher amounts of carbon into histidine biosynthesis	n.e.
pK19*mobsacB* Δ*cg1305*	-	Chromosomal deletion of gene cg1305	Investigate deletion of cg1305, potentially encoding a histidine import system (Kulis-Horn et al., 2014); prevent histidine reimport into the cell	n.t.
pK19*mobsacB* Δ*aroP*	-	Chromosomal deletion of gene *aroP* (cg1257)	Investigate deletion of *aroP*, potentially encoding a histidine import system (Shang et al., 2013); prevent histidine reimport into the cell	n.t.
pK19*mobsacB* Δ*cg2314*	CM1	Chromosomal deletion of gene cg2314	Investigate deletion of cg2314, potentially encoding a purine regulator	n.e.
pK19*mobsacB* Δ*apt*	-	Chromosomal deletion of gene *apt* (cg1862)	Investigate deletion of *apt*, encoding adenine phosphoribosyltransferase; understanding AMP formation from adenine	n.t.
pK19*mobsacB apt*^{TTG}	-	Change start codon from GTG to TTG for gene *apt* (cg1862)	Investigate effect of decreased translation efficiency for adenine phosphoribosyltransferase	n.t.
Plasmid-based modifications				
pJC4 *purA*	CM1	Overexpression of gene *purA* (cg3063)	Investigate effect of *purA* overexpression, encoding adenylosuccinate synthase; increase adenylate formation	n.e.
pEKEx3 *aspA*	CM1	Overexpression of gene *aspA* (cg1697)	Investigate effect of *aspA* overexpression, encoding aspartate ammonia lyase; provide higher amounts of aspartate for purine biosynthesis	n.e.
pEKEx3 *aspB*	CM1	Overexpression of gene *aspB* (cg0294)	Investigate effect of *aspB* overexpression, encoding aspartate aminotransferase; provide higher amounts of aspartate for purine biosynthesis	n.e.
pJC4 *hisD*	HIS7	Overexpression of gene *hisD* (cg2305)	Investigate effect of *hisD* overexpression, encoding histidinol dehydrogenase; increase enzyme availability of HisD	n.t.
pJC4 *purApurB hisD*	HIS7	Overexpression of genes *purA*, *purB* (cg2876), and *hisD* (cg2305)	Investigate effect of combined *purA*, *purB*, and *hisD* overexpression to solve accumulations in purine and histidine biosynthesis	n.t.

Abbreviations: n.i., not implementable (genomic modification could not be established; n.t., not yet tested; n.e., tested and constituted no phenotypic effect

encoding the PurR proteins of *B. subtilis*, *E. coli*, and *Lactococcus lactis* were obtained (from https://www.ncbi.nlm.nih.gov/; last access 15-08-2018) and the *C. glutamicum* genome was searched for homologous sequences. By this, we identified the following genes (annotations from https://coryneregnet.compbio.sdu.dk/v6/index.html; last access 15-08-2018), encoding (potential) regulatory proteins, given in declining order of amino acid sequence similarity to the *E. coli* PurR protein (amino acid sequence similarity given in parentheses):
cg0210 (29%), cg2314 (27%), cg1410 (25%) annotated as *rbsR* (LacI-family transcriptional regulator), cg2242 (23%), cg2910 (23%) annotated as *ipsA* (transcriptional regulator, LacI family), and cg0221 (20%). Since we were not able to construct a cg0210 deletion plasmid (data not shown), we continued by deleting cg2314 in *C. glutamicum* CM1, which had no effect on the growth phenotype and production behaviour of the resulting strain (Table 32, p.122). The remaining potential regulatory proteins might be considered for further studies concerning purine regulators in *C. glutamicum*.
The prokaryotic ubiquitin like protein (Pup, encoded by *pup*) has been shown to target proteins for further degradation in the proteasome in mycobacteria (Burns et al., 2009; Pearce et al., 2008). Despite not possessing a proteasome, *C. glutamicum* Pup targets proteins, which are potentially degradet or modified in a so far unknown manner (Küberl et al., 2014). Among these pupylated proteins are two enzymes of the L-histidine pathway, namely HisC and HisD (Küberl et al., 2014). To avoid potential cross effects of the pupylation machinery on L-histidine enyzmes, we deleted the *pup* gene in *C. glutamicum* CM1. The resulting strain however showed no effect on the investigated parameters (Table 32, p.122).
The remaining chromosomal- and plasmid-based modifications are given in Table 32 on page 122 and their effects are described by the following abbreviations: not implementable, meaning either the plasmid could not be constructed or the respective modification could not be chromosomally integrated with the constructed plasmid; not (yet) tested, meaning the plasmid has been successfully constructed but due to time / priority reasons the modification has not yet been evaluated; tested and no (phenotypic) effect, meaning the plasmid / chromosomal modification has been implemented but did not constitute any effect on the investigated parameters growth, growth rate, $Y_{X/S}$, $Y_{P/S}^{his}$, and $Y_{P/S}^{gly}$.

3.1.12. *Byproduct formation*

The L-histidine producing strains were analysed for production of L-histidine, which was qualified and quantified. However, as it is a common phenomenon with producer strains of all varieties (a.o. amino acid producers), not only the desired product is excreted into the medium, but also one or more byproducts might occur (Ma et al., 2017; Zhu et al., 2014). The predominating byprodut here was glycine, which was detected in the medium of several strains of the database, including strains *C. glutamicum* HIS1 to HIS7 (Fig. 13, p.106). Interestingly, the amount of glycine was about equimolar with the main product L-histidine in these strains, leading to a strong correlation between $Y_{P/S}^{his}$ and $Y_{P/S}^{gly}$ (Fig. 18, p.124).

Besides glycine, further byproducts were detected in minimal amounts in the supernatant. These included exemplarily for *C. glutamicum* HIS10 after 24 h of cultivation:

L-glutamate (max. 0.4 mM), L-serine (max. 0.2 mM), L-arginine (max. 0.1 mM), L-alanine (max. 0.1 mM), L-lysine (max. 1 mM). For some of these amino acids, concentrations in the

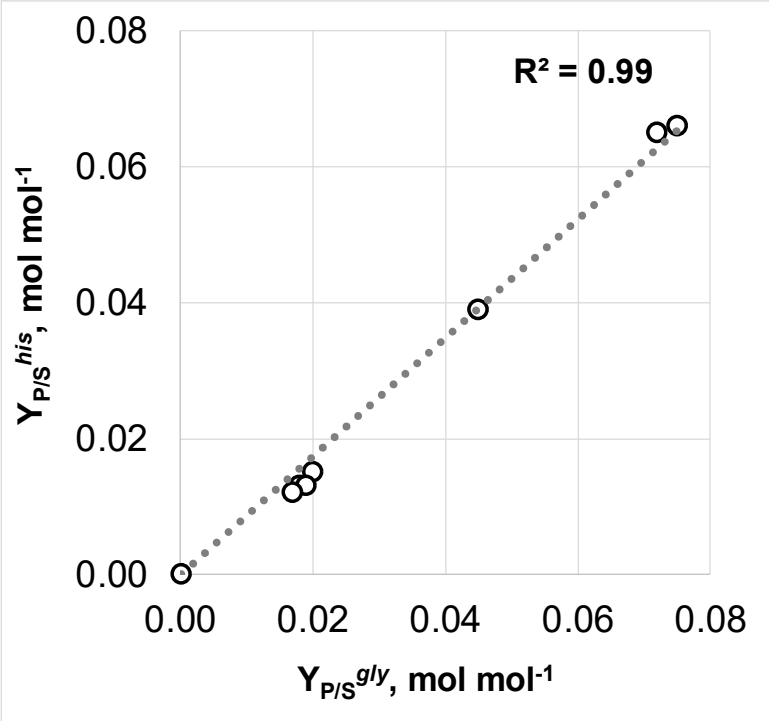

Fig. 18. Correlation of the product substrate yields (mol mol^{-1}) for L-histidine ($Y_{P/S}^{his}$) and glycine ($Y_{P/S}^{gly}$) of strains *C. glutamicum* HIS1 to HIS7 from the strain database, including *C. glutamicum* WT. Given product substrate yields (open circles) are mean values calculated from at least three independent experiments. **Taken from Schwentner et al., 2019.**

medium were lower after 30 h than after 24 h, indicating their re-uptake and degradation, i.e. for L-glutamate. For further improvements of $Y_{P/S}^{his}$, prevention of formation of the detected and other, potentially undetected, byproducts might prevent loss of carbon.

3.1.13. *Studies on purine reactions requiring fTHF*

The purine biosynthesis strongly relies on the supply with C_1 units, since the reaction steps three and ten, which are catalysed by PurN and PurH, both require fTHF as cofactor (Fig. 10, p.99; Zhang et al., 2008). As glycine as the inevitable byproduct indicates, the SHMT reaction is the major source to supply these C_1 units in the form of mTHF (Schirch et al., 1985; Stolz et al., 2007). With the idea in mind to examine, in how far the *de novo* part of the purine biosynthesis can be released from its dependency on fTHF, we conducted preliminary experiments in the *C. glutamicum* WT background. Besides PurN, the ATCC 13032 genome contains a second gene encoding a phosphoribosylglycineamide formyltransferase, which is annotated as PurT, encoded by *purT* (cg3054) (derived from https://coryneregnet.compbio.sdu.dk/v6/index.html). Interestingly PurT catalyses the third reaction step of the purine biosynthesis with formate as C_1 group donor, instead of using fTHF. Thus, we in-frame deleted the *purN* (cg0983) gene from the *C. glutamicum* genome to see if PurT can compensate a *purN* deletion. The resulting strain *C. glutamicum* Δ*purN* showed strongly impaired growth in shaking flask cultivations compared to *C. glutamicum* WT (Fig. **19**, p.126), indicating that PurT is not able to compensate the *purN* deletion.

The PurT reaction was further supported by supplementing 10 mM formate, 0.74 mM adenine, or a combination of both supplements, resulting in elevated growth behaviour, despite being far from WT-like growth behaviour (Fig. **19**, p.126). With the aim to increase the intracellularly available formate, the formate dehydrogenase FDH, encoded by genes *fdhD* (cg0616), cg0617, and *fdhF* (cg0618), was identified as target. This enzyme is known to catalyse the oxidation of formate to CO_2 and it has been shown before for *C. glutamicum* that deletion of *fdhF* prevents formate utilization (Witthoff et al., 2012). Thus, *fdhF* was deleted in-frame in strain *C. glutamicum* Δ*purN* and cultivations of the resulting *C. glutamicum* Δ*purN* Δ*fdhF* showed that *fdhF* deletion was not able to revert the heavy growth defect of *C. glutamicum* Δ*purN*. Since *C. glutamicum* WT was not able to grow with *purN* and/or *fdhF* deletions, we relinquished to test these modifications in a strain with L-histidine production brackground.

The detachment from the dependency on fTHF of the PurN reaction did not work and thus we switched to a different approach: Elimination of potential fTHF-consuming reactions to increase the intracellular fTHF supply for the PurN reaction. It has been shown before that the gene product of *purU* (cg0457), a fTHF deformylase, in *E. coli* constitutes the major source of formate for the PurT reaction by degrading fTHF (Nagy et al., 1993). Therefore, the *purU* gene was deleted in-frame in *C. glutamicum* WT and in HIS7 to prevent potential fTHF degradation. In both strains, no phenotypic effect on growth rate and biomass substrate yields was observable upon *purU* deletion, respectively (data not shown). Furthermore, no effect of *purU* deletion on $Y_{P/S}^{his}$ in *C. glutamicum* HIS7 was observed (data not shown).

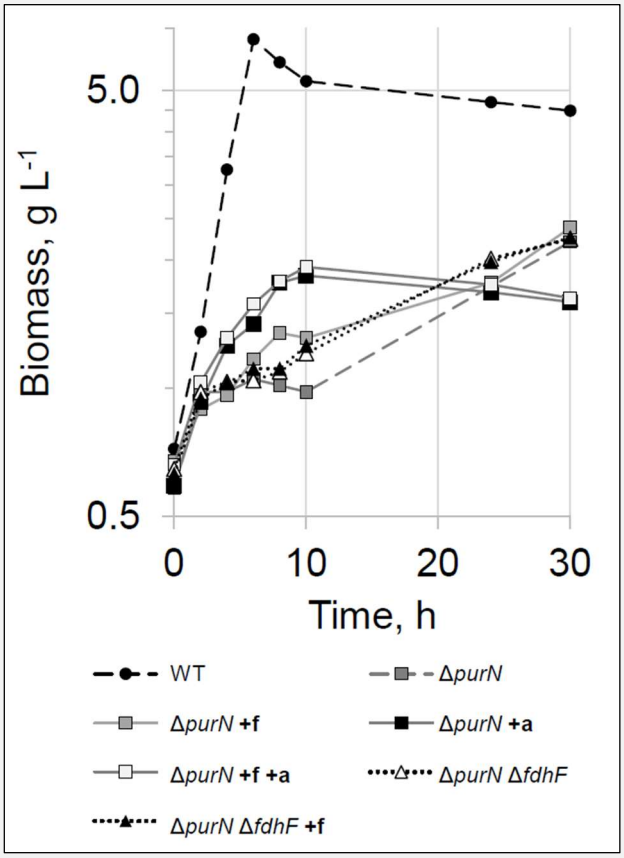

Fig. 19. Shaking flask cultivations of *C. glutamicum* Δ*purN* and *C. glutamicum* Δ*purN* Δ*fdhF* with different supplementations (10 mM formate, 0.74 mM adenine, or a combination of both), including *C. glutamicum* WT as a reference. Abbreviations: +f, medium contained formate; +a, medium contained adenine.

3.1.14. *Supplementation experiments*

In further experiments, selected strains of the strain database (Fig. 17, p.115) were cultivated with a wide range of supplements, focusing on cofactors of the L-histidine connected pathways. These included e.g. amino acids, vitamins, and complex components. The following section describes the idea behind each tested supplement and explains the results that are given in Table **33** on page 129 in a compact form. The results are shown in positive or negative percentages (representing improvement or decline, respectively) for the four characteristics growth rate, $Y_{X/S}$, $Y_{P/S}{}^{his}$, and $Y_{P/S}{}^{gly}$ compared to the cultivations w/o supplementation.

Since we suspected limitations in the purine biosynthesis, we supplemented each cofactor of the *de novo* part of this pathway separately. L-glutamine is the cofactor in enzymatic steps one (PurF) and four (PurL) of the purine biosynthesis and in step five (HisF/HisH) of the L-histidine biosynthesis. Thus, we supplemented *C. glutamicum* CM2 with L-glutamine, which resulted in a slight increase of the growth rate, $Y_{P/S}{}^{his}$ was not affected. We proceeded by supplementing *C. glutamicum* CM1 with glycine, the cofactor of the second step in purine biosynthesis (PurD). This had a slight effect on $Y_{P/S}{}^{his}$, which decreased by about 7%. For the purpose to increase the intracellular fTHF (needed in purine steps three and ten) pool, folate was supplemented to *C. glutamicum* CM1. Folate supplementation showed no effect on the four characteristics of CM1. Reaction steps four, five, and six of the purine biosynthesis (PurM, L, K) require ATP as energy donor. Thus, *C. glutamicum* CM2 was supplemented with ATP, resulting in an increase of μ by 42%, however $Y_{P/S}{}^{his}$ and $Y_{P/S}{}^{gly}$ slightly decreased by 6% and 10%, respectivel, indicating that the ATP surplus is used for faster growth instead of increased product formation. Step eight of the purine pathway requires L-aspartate as cofactor, which was supplemented (20 mM) to *C. glutamicum* CM1. This resulted in an increase of the growth rate (35%) and decreases of $Y_{P/S}{}^{his}$ and $Y_{P/S}{}^{gly}$ by 15% and 13%, respectively. When the concentration of the supplemented L-aspartate was reduced (1 mM), no effect on the four characteristics was observed. Further considering purine biosynthesis, we supplemented *C. glutamicum* CM1 with thiamine, a vitamin whose biosynthesis pathway requires AIR, the product of the PurM reaction (Fig. 4, p.19; Begley et al., 2012; Jurgenson et al., 2009). However, in *C. glutamicum* CM1, thiamine showed no effect. Supplementation of *C. glutamicum* PUR1 and PUR3 showed only an effect on $Y_{P/S}{}^{his}$ (+9%) of the latter one. The purine modified *C. glutamicum* PUR2 with potentially decreased PurF activity was further supplemented with adenine (and a combination of adenine and thiamine), the nucleobase of adenylate nucleotides and nicotinamide adenine dinucleotides, to see if the strongly affected purine biosynthesis in this strain might be sustained

in this way. Experiments showed that adenine and adenine plus thiamine were able to support growth rates (+52% for both) and biomass substrate yields (+155% and +140%), however, $Y_{P/S}^{his}$ were not affected.

In further experiments, we focused on supporting the enhanced requirement of C_1 units. To supply the C_1 metabolism of *C. glutamicum* CM1, L-serine was supplied but showed no effect. Only when *C. glutamicum* CM1 was supplied with L-aspartate in addition to L-serine, an effect on growth rate (+30%), $Y_{P/S}^{his}$ (-19%) and $Y_{P/S}^{gly}$ (-13%) was detected. However, this most likely can be attributed to the effect of L-aspartate (see above). Further, formate was supplied in different concentrations to *C. glutamicum* CM1 to support the PurT catalysed fTHF-independent (and formate-dependent) reaction, thus potentially supporting the PurN catalysed fTHF-dependent reaction (3.1.13 Studies on purine reactions requiring fTHF, p.125). However, formate supplementations showed no effect.

Since protocatechuate (PCA) is a routinely used supplement in cultivations with *C. glutamicum*, we examined its effect on *C. glutamicum* CM1. It was shown before that addition of the iron-complexing compound can mediate accelerated and stable growth of *C. glutamicum* in synthetic media, such as CGXII (Liebl et al., 1989; Unthan et al., 2014). PCA in cultivations with *C. glutamicum* CM1 however did neither increase growth rate nor $Y_{P/S}^{his}$.

Complex media or addition of complex components to synthetic media are well known of being able to support growth of the host strain or to enable increased product formation (Hahn-Hägerdal et al., 2005; Hoffart et al., 2017; Zhang et al., 2003). Thus, strain *C. glutamicum* CM2 was supplemented in shaking flask experiments with one of the two complex components brain-heart-infusion (BHI) or yeast extract (YE), respectively. Interestingly, both components were able to increase growth rates (+163% and +308%, respectively), failed however in supporting $Y_{P/S}^{his}$ (-11% and -8%, respectively).

Table 33. Overview of conducted supplementation experiments with strains of the modular strain database. Effects of the respective supplement(s) on growth rate, substrate specific biomass yield, and substrate specific product/byproduct yield are given in ± % improvement or decline compared to the conditions w/o supplement, respectively. Experiments have been performed in triplicates, unless stated otherwise.

Short	Genotype	Supplement, concentration	μ, h^{-1}	$Y_{X/S}$, g g^{-1}	$Y_{P/S}^{his}$, mol mol^{-1}	$Y_{P/S}^{gly}$, mol mol^{-1}
CM1	*C. glutamicum hisG*mut2 P_{tuf}*hisD* P_{tuf}*hisH* P_{tuf}*cg0911* P_{dapA}*hisE pgi*^{GTG}	* L-Serine, 20 mM	n.e.	n.e.	n.e.	n.e.
CM1	*C. glutamicum hisG*mut2 P_{tuf}*hisD* P_{tuf}*hisH* P_{tuf}*cg0911* P_{dapA}*hisE pgi*^{GTG}	Thiamine, 50 µM	n.e.	n.e.	n.e.	n.e.
CM1	*C. glutamicum hisG*mut2 P_{tuf}*hisD* P_{tuf}*hisH* P_{tuf}*cg0911* P_{dapA}*hisE pgi*^{GTG}	L-Aspartate, 20 mM	+35%	n.e.	-15%	-13%
CM1	*C. glutamicum hisG*mut2 P_{tuf}*hisD* P_{tuf}*hisH* P_{tuf}*cg0911* P_{dapA}*hisE pgi*^{GTG}	* L-Aspartate, 1 mM	n.e.	n.e.	n.e.	n.e.
CM1	*C. glutamicum hisG*mut2 P_{tuf}*hisD* P_{tuf}*hisH* P_{tuf}*cg0911* P_{dapA}*hisE pgi*^{GTG}	* L-Aspartate, 20 mM L-Serine, 20 mM	+30%	n.e.	-19%	-13%
CM1	*C. glutamicum hisG*mut2 P_{tuf}*hisD* P_{tuf}*hisH* P_{tuf}*cg0911* P_{dapA}*hisE pgi*^{GTG}	Glycine, 20 mM	n.e.	n.e.	-7%	n.d.
CM1	*C. glutamicum hisG*mut2 P_{tuf}*hisD* P_{tuf}*hisH* P_{tuf}*cg0911* P_{dapA}*hisE pgi*^{GTG}	Folate, 0,36 nM	n.e.	n.e.	n.e.	n.e.
CM1	*C. glutamicum hisG*mut2 P_{tuf}*hisD* P_{tuf}*hisH* P_{tuf}*cg0911* P_{dapA}*hisE pgi*^{GTG}	Formate, 1 mM / 10 mM	n.e.	n.e.	n.e.	n.e.
CM1	*C. glutamicum hisG*mut2 P_{tuf}*hisD* P_{tuf}*hisH* P_{tuf}*cg0911* P_{dapA}*hisE pgi*^{GTG}	Protocatechuate, 30 mg L^{-1}	n.e.	n.e.	n.e.	n.e.
CM2	*C. glutamicum hisG*mut2 P_{tuf}*hisD* P_{tuf}*hisH* P_{tuf}*cg0911* P_{dapA}*hisE pgi*^{GTG} *zwf*^{A243T}	L-Glutamine, 5 mM	+16%	n.e.	n.e.	n.e.
CM2	*C. glutamicum hisG*mut2 P_{tuf}*hisD* P_{tuf}*hisH* P_{tuf}*cg0911* P_{dapA}*hisE pgi*^{GTG} *zwf*^{A243T}	Yeast extract, 5 g L^{-1}	+163%	+308%	-11%	-16%
CM2	*C. glutamicum hisG*mut2 P_{tuf}*hisD* P_{tuf}*hisH* P_{tuf}*cg0911* P_{dapA}*hisE pgi*^{GTG} *zwf*^{A243T}	Brain heart infusion, 5 g L^{-1}	+132%	+200%	-8%	-17%
CM2	*C. glutamicum hisG*mut2 P_{tuf}*hisD* P_{tuf}*hisH* P_{tuf}*cg0911* P_{dapA}*hisE pgi*^{GTG} *zwf*^{A243T}	ATP, 5 g L^{-1}	+42%	n.d.	-6%	-10%
PUR1	*C. glutamicum hisG*mut2 P_{tuf}*hisD* P_{tuf}*hisH* P_{tuf}*cg0911* P_{dapA}*hisE pgi*^{GTG} Δ*purF*	Thiamine, 50 µM	n.e.	n.e.	n.e.	n.e.
PUR2	*C. glutamicum hisG*mut2 P_{tuf}*hisD* P_{tuf}*hisH* P_{tuf}*cg0911* P_{dapA}*hisE pgi*^{GTG} *purF*^{TTG}	Adenine, 2 mM	+52%	+155%	n.e.	n.e.
PUR2	*C. glutamicum hisG*mut2 P_{tuf}*hisD* P_{tuf}*hisH* P_{tuf}*cg0911* P_{dapA}*hisE pgi*^{GTG} *purF*^{TTG}	Adenine, 2 mM Thiamine, 50 µM	+52%	+140%	n.e.	n.e.
PUR3	*C. glutamicum hisG*mut2 P_{tuf}*hisD* P_{tuf}*hisH* P_{tuf}*cg0911* P_{dapA}*hisE pgi*^{GTG} *purF*^{K348Q}	Thiamine, 50 µM	n.e.	n.e.	+9%	n.e.

Abbreviations: *, experiments have been performed in duplicates; ATP, adenosine triphosphate; n.d., not determined; n.e., no effect (effect of the supplementations was below 5%).

3.1.15. *Redox balance*

The metabolic cofactors and reducing equivalents NADH and NADPH play important roles in a wide variety of cellular processes. Imbalances in the NADPH pool of *C. glutamicum* have been shown to be adverse for product formation in certain cases and balancing these pools increased product formation, e.g. in L-arginine production with *C. glutamicum* (Park et al., 2014). A major cellular source in *C. glutamicum* for the generation of the reducing equivalent NADPH under glycolytic conditions are the two initial reactions of the oxidative part of the PPP, constituted by the G6P DH and the 6PG DH, and others, such as the reactions of isocitrate dehydrogenase and malic enzyme (Spaans et al., 2015). All these reactions in *C. glutamicum* use $NADP^+$ as a cofactor and reduce it to NADPH, which is needed as reducing equivalent for several reductive biosynthetic reactions (Moritz et al., 2000). The modification of the redox pool constituted by NADPH has been studied intensively, especially in the case of industrial producer strains, since several products require increased provision of NADPH (Lee et al., 2013; Papagianni, 2012). Such a product with relevance to *C. glutamicum* is L-lysine, whose biosynthesis requires 4 mol of NADPH for the generation of 1 mol L-lysine (Kiefer et al., 2004; Takeno et al., 2010) and thus efforts have been made to increase NADPH supply (Becker et al., 2005; Bommareddy et al., 2014; Georgi et al., 2005; Takeno et al., 2010). L-Histidine, on the other side, is a product that theoretically generates increased amounts of NADPH, meaning by providing increased amounts of the L-histidine precursor PRPP, the oxidative part of the PPP is overused, compared to growth of *C. glutamicum* WT (Fig. 10, p.99). However, the metabolic model (Zhang et al., 2017) used for FBA (3.1.2 Flux Balance Analysis, p.100) did not indicate any imbalances connected with increased formation of NADPH in the L-histidine overproduction study (personal communication with André Feith, IBVT, University of Stuttgart). For the purpose to investigate the redox state of the L-histidine producing strains, we constructed a multi-copy plasmid based on pJC4, expressing the *sthA* gene from *E. coli* K-12 MG1655 under control of P_{tuf}. The *sthA* gene encodes a soluble transhydrogenase from *E. coli*, which can transfer reducing equivalents between NAD^+ and $NADP^+$ (Boonstra et al., 1999; Cao et al., 2011; Sauer et al., 2004). This hydrogenase has been applied successfully for balancing NAD/NADP ratios in producer strains before (Jan et al., 2013; Sánchez et al., 2008). The plasmid pJC4 *sthA* was introduced in strains *C. glutamicum* HIS6 and CM1 and the resulting strains were cultivated and characterised. Since both strains showed strongly impaired growth and very low $Y_{P/S}^{his}$, we concluded that expression of *sthA* from *E. coli* is not beneficial for L-histidine production at this point of the strain construction. It

however remains to be elucidated if the soluble transhydrogenase from *E. coli* is produced functionally in *C. glutamicum* from the pJC4 plasmid.

3.1.16. *Alternative carbon source(s)*

The L-histidine biosynthesis pathway precursor molecule PRPP originates from the PPP and chemically is a C5 sugar phosphate. Thus, D-ribose (i.e. ribose 5-phosphate) suggested itself to be tested as an alternative carbon source to glucose, due to its spatiotemporal proximity to the L-histidine biosynthesis, compared to glucose (Fig. 4, p.19). Additionally, *C. glutamicum* has been shown to be able to grow on D-ribose as sole carbon source (Blombach and Seibold, 2010; Wendisch, 2003). Therefore, strains *C. glutamicum* HIS7 and CM2 were cultivated in $CGXII^N$ supplemented with 12 g D-ribose L^{-1}. Where *C. glutamicum* WT was able to grow ($\mu = 0.22 \pm 0.02\ h^{-1}$), both *C. glutamicum* HIS7 and CM2 surprisingly showed no growth. We proceeded by cultivating *C. glutamicum* CM2 with a mixture of 6 g D-ribose L^{-1} and 5 g glucose L^{-1}, where it was able to grow ($\mu = 0.20 \pm 0.02\ h^{-1}$). Since the ribose concentration was not determined, the $Y_{P/S}^{his}$ and $Y_{P/S}^{gly}$ were not available. However, *C. glutamicum* CM2 with mixed glucose and ribose substrates excreted 4.8 ± 0.4 mM L-histidine and 5.6 ± 0.4 mM glycine into the medium after 30 h of cultivation, which equals approximately what *C. glutamicum* CM2 excreted when growing on glucose as sole carbon source (data not shown). However, despite not being able to grow (and produce) on D-ribose as sole carbon source, *C. glutamicum* CM2 takes up, metabolizes, and produces L-histidine from D-ribose when glucose is simultaneously present.

3.1.17. *MGE – Decoupling purine biosynthesis from L-histidine biosynthesis*

In a evolutionary approach, we aimed at decoupling the two tightly interlinked pathways of purine biosynthesis and L-histidine biosynthesis (1.2.5 L-HISTIDINE related pathways, p.21). The method chosen for this task, Metabolic engineering to Guide Evolution (MGE), is described in PART II of this work in detail (3.2 Results PART II – Metabolic engineering to guide evolution, p.142). The principle idea for this experiment was to switch off a part of the *de novo* purine biosynthesis, namely the reactions originating from PurF and ending with PurB, yielding the purine intermediate AICAR (Fig. 10, p.99). This metabolically expensive part of the *de novo* purine biosynthesis consists of nine enzymatic reactions that require five molecules of ATP and

several other cometabolites, such as L-glutamine, fTHF, and L-aspartate (Fig. 10, p.99). By shutting down this part of the metabolism and by trying to evolve a cell that can grow without using this branch of the purine pathway and instead coupling the L-histidine biosynthesis to the generation of required purine intermediates in the form of AICAR, we hoped to boost the L-histidine production in *C. glutamicum*.

In a first MGE experiment, *C. glutamicum* PUR1 with in-frame deleted *purF* gene was cultivated in $CGXII^{E}$ with 20 g glucose L^{-1} and 1 g yeast extract L^{-1} and regularly transferred into fresh medium. After about 14 d of continuous cultivation with intermitted transfers, evolutionary events occurred in three independent MGE approaches in parallel, which were identified by strongly increased biomass formation (data not shown). The faster growing strains were isolated and their cultivation showed that the growth rates were the same as for the basis strain ($\mu = 0.1\ h^{-1}$ for all). However, the three evolved strains showed increased biomass formation after 24 h, reaching above 200% increased biomass concentrations (data not shown). To reveal the underlying mutations, we sequenced genes that encode potential isoenzymes. Such a potential isoenzyme for amidophosphoribosyltransferase PurF is the anthranilate phosphoribosyltransferase (TrpD, encoded by *trpD*), which has been connected to this circumstance before in *S. enterica* (Lambrecht and Downs, 2013; Ramos et al., 2008). Surprisingly, we found an intact *trpD* gene, however, sequencing of the *trp* operon revealed single nucleotide polymorphisms (SNPs) in the *trpCF* gene, encoding the the bifunctional indole-3-glycerol-phosphate synthase (TrpC)/ phosphoribosylanthranilate isomerase (TrpF) in two of the evolved strains (Ikeda, 2006). The first SNP resulted in an isoleucine to threonine exchange (I422T), the other in a tryptophan to arginine exchange (W405R), both manifesting in the *trpF* encoded part of the enzyme. It was shown in *E. coli* that a *trpF* deletion can be compensated by a secondary function of PurF (Patrick and Matsumura, 2008). It appears that in the presented case, it was *vice versa*.

Since MGE of *C. glutamicum* PUR1 resulted in evolved strains that were able to evolve a potential isoenzyme of PurF, we additionally deleted gene *purD*, catalysing the PurF following reaction to ensure inhibited flux through the *de novo* purine branch (Fig. 10, p.99). As *C. glutamicum* PUR1 before, the newly constructed *C. glutamicum* PUR1 Δ*purD* was deployed in an MGE approach using $CGXII^{E}$ with 20 g glucose L^{-1} and 1 g yeast extract L^{-1} and was regularly transferred into fresh medium. However, after 90 d of consecutively passaging, the strain showed no increasing biomass formation, meaning no evolutionary event could be observed in three independent cultivations.

3.1.18. *Preliminary Fermentation studies*

For each producer strain with the potential to be used as host strain in industrial scale production processes, the transfer from a laboratory scale over a pilot scale towards an industrial scale are critical steps and eventually determine the implementability of a strain (Delvigne and Noorman, 2017; Reisman, 1993; Thiry and Cingolani, 2002). The suitability of *C. glutamicum* for the large-scale production of industrially relevant products in general as a production host is out of question, since several established processes are based on this organism. Especially the processes for amino acid production, e.g. L-glutamate, L-lysine, and L-methionene are economically lucrative (Becker and Wittmann, 2012; Ikeda, 2003; Wendisch et al., 2016). It is a well-known phenomenon that producer strains, despite performing well in a laboratory scale, fail to deliver the same or similar performances in a bigger scale (Delvigne et al., 2017; Gonçalves et al., 2014). With the purpose to anticipate such issues, we conducted preliminary fermentation studies with selected strains of the strain database of L-histidine producing mutants (Fig. 17, p.115). These experiments were intended to reveal potentially emerging critical points for scale-up experiments in future projects. However, one needs to keep in mind that all conducted fermentation experiments were performed as single experiments and in order to confirm the obtained results, repetitions are urgently needed. The purpose of the subsequently presented experiments was to gain swift insights in potential issues connected with scale-up, allowing the opportunity to counteract such potential issues during strain construction.

A 1. Glass reactor system

With the purpose to investigate the growth and production behaviour of L-histidine producing strains in bioreactor systems and compare these to the standardly used shaking flask system, selected strains were cultivated in a glass reactor system (2.4.6 Triple glass reactor system, p.66). All results of fermentations in this system are summarized in Table 34 on page 134.

Comparison between shaking flask and fermentation cultivations. Strains *C. glutamicum* HIS7 and *C. glutamicum* CM2 were chosen as a basis for the fermentation experiments in the small-scale bioreactor system. Both were cultivated in a laboratory scale fermentation with a working volume of 200 mL in the fermentation minimal medium ($CGXII^R$; Table 12, p.58).

Table 34. Overview of preliminary fermentation studies with strains of the modular strain database under various conditions. As evaluation characteristics the growth rate, the substrate specific biomass yield ($Y_{X/S}$), and the product yields for L-histidine ($Y_{P/S}^{his}$) and glycine ($Y_{P/S}^{gly}$) were calculated.

Strain	Medium	Condition	μ, h^{-1}	$Y_{X/S}$, g g^{-1}	$Y_{P/S}^{his}$, mol mol^{-1}	$Y_{P/S}^{gly}$, mol mol^{-1}
HIS7	CGXII^{R}	std	0.31§	0.41§	0.035§§	0.038§
CM2	CGXII^{R}	std	0.26§	0.44§	0.055§§	0.064§
HIS7	CGXII^{R*}	std	0.30	0.43	0.032	0.033
HIS7	CGXII$^{R\neq}$	std	0.32	0.46	0.035	0.038
CM2	CGXII^{N}	std	0.30	0.42	0.043	0.054
CM2	CGXII^{N}	pH regulation disabled	0.21	0.27	0.052	0.069
CM2	CGXII^{R}	O_2-limitation at t=4h	0.23	0.42	0.034	0.038
CM2	CGXII^{R}	O_2-limitation at t=6h	0.26	0.46	0.029	0.034
CM2	CGXII^{R}	O_2-limitation at t=8h	0.27	0.52	0.023	0.030
CM2	CGXII^{R}	pH fixed to 6.25	0.30	0.44	0.041	0.055
CM2	CGXII^{R}	pH fixed to 8.00	0.17	0.47	0.055	0.068
CM2	CGXII^{R}	pH fixed to 8.25	< 0.1	< 0.1	n.d.	n.d.

Fermentations performed as single experiments, unless marked with §, then values are mean values of two experiments (SD <5%).
Media: CGXII^{R*}, CGXII^{R} containing 5 g urea L^{-1}; CGXII$^{R\neq}$, CGXII^{R} containing 21 g MOPS L^{-1}
Abbreviations: std, standard conditions; n.d., not determined

The results showed that the growth rate of both *C. glutamicum* HIS7 and CM2 increased from 0.28 h^{-1} and 0.19 h^{-1} in shaking flasks to 0.31 h^{-1} and 0.26 h^{-1} in the reactor system, respectively. Interestingly, the $Y_{X/S}$ of *C. glutamicum* HIS7 remained stable (0.42 ± 0.02 vs. 0.41 g biomass g^{-1} substrate), whereas the $Y_{X/S}$ of *C. glutamicum* CM2 strongly increased during fermentation from 0.25 ± 0.02 to 0.44 g biomass g^{-1} substrate (compare Table 31, p.120, and Table 34, p.134). Compared to the shaking flask cultivations, the growth profile of both strains was continuously exponential until the glucose was completely consumed. In the

shaking flask cultivations, this was different. Here, the growth profile was characterized by a first phase of exponential growth, which then slowed down and slowly approached a maximal biomass concentration, instead of a wildtype-like exponential growth until reaching the stationary phase (exemplarily shown for *C. glutamicum* CM2; Fig. 33, p.231).

The $Y_{P/S}^{his}$ in contrast to the growth rate decreased in both strains from 0.066 ± 0.003 to 0.035 mol L-histidine mol^{-1} glucose for *C. glutamicum* HIS7 and from 0.079 ± 0.003 to 0.057 mol L-histidine mol^{-1} glucose for *C. glutamicum* CM2, respectively. The same holds true for $Y_{P/S}^{gly}$, which decreased from 0.073 ± 0.002 to 0.038 mol glycine mol^{-1} glucose for *C. glutamicum* HIS7 and from 0.098 ± 0.003 to 0.058 mol glycine mol^{-1} glucose for *C. glutamicum* CM2, respectively. These results indicate (i) that the scaling-up from shaking flasks to a small-scale fermentations holds challenges, which need to be considered preferably early on in strain construction. And (ii), glycine remains an equimolar byproduct to L-histidine, as was observed in the shaking flask cultivations (Table 31, p.120 and Fig. 18, p.124).

Mimicking shaking flask cultivations in small-scale fermentations: medium composition. With the purpose to investigate the differences in $Y_{P/S}^{his}$ between shaking flask and reactor cultivations in more detail, the media compositions were examined in more detail. Since the fermentation medium $CGXII^{R}$ (Table 12, p.58) compared to $CGXII^{N}$ (standardly used in shaking flask cultivations) lacks the two components urea and 3-(N-morpholino) propanesulfonic acid (MOPS), we performed reactor cultivations and added these components separately (*C. glutamicum* HIS7) and combined (*C. glutamicum* CM2) to the medium to investigate if these components are responsible for the decreased $Y_{P/S}^{his}$ in shaking flask cultivations compared to the initially conducted reactor cultivations. These reactor cultivations resulted in similar growth rates, biomass substrate yields, and product yields for *C. glutamicum* HIS7 compared to small scale reactor cultivations in $CGXII^{R}$ medium (Table **34**, p.134). Preliminary experiments for cultivations of *C. glutamicum* CM2 in reactor cultivations using the shaking flask medium (including urea and MOPS) indicate similar circumstances. The decrease of the $Y_{P/S}^{his}$ here needs closer investigations, however.

Mimicking shaking flask cultivations in small-scale fermentations: pH. Besides the differences in the composition of the medium, there are further factors that behave differently in reactor and shaking flask cultivations, e.g. the absolute value of the pH and its progress over the cultivation time. While the pH value in reactor cultivations is fixed to a certain value (by adding acid/base), constituting the optimal value for the deployed organism, shaking flask cultivations show a gradient of pH values ranging from the starting value of 7.4 to a maximal

value of 8.6 (after 24 h) over the cultivation duration (Fig. 34, p.229; Follmann et al., 2009; Lange et al., 2018). Thus, we disabled the standardly used automated pH regulation (with 10% H_3PO_4 and 25% NH_4OH; 2.4.6 Triple glass reactor system, p.66) and cultivated *C. glutamicum* CM2 in $CGXII^N$ medium. In this scenario, the pH steadily increased to a maximal value of 8.79, which was reached after about 10 h of cultivation and slowly re-decreased to about 8.60 after 24 h, exceeding the maximal pH value of the shaking flask cultivations (Fig. 34, p.231). The growth rate and the $Y_{X/S}$ of *C. glutamicum* CM2 both strongly decreased to 0.21 h^{-1} and 0.27 g biomass g^{-1} substrate, compared to the cultivation with active pH regulation. Interestingly, $Y_{P/S}^{his}$ (and $Y_{P/S}^{gly}$) increased to 0.052 mol L-histidine mol^{-1} glucose (and 0.069 mol glycine mol^{-1} glucose), indicating that the pH unregulated process promotes increased formation or export of L-histidine and underlining an important role of the extracellular pH for further fermentation cultivations.

We proceeded by cultivating *C. glutamicum* CM2 at different fixed pH values, including 6.25, 8.0, and 8.25, and compared results to standard cultivations at a fixed pH of 7.4 (see above). When cultivated at a pH of 6.25, the growth rate slightly increased to 0.30 h^{-1} and the $Y_{X/S}$ remained stable with 0.44 g biomass g^{-1} substrate. However, $Y_{P/S}^{his}$ and $Y_{P/S}^{gly}$ decreased to 0.042 mol L-histidine mol^{-1} glucose and 0.055 mol glycine mol^{-1} glucose, respectively, indicating that slightly acidic fermentation conditions might have adverse effects for L-histidine production with *C. glutamicum*. Next, *C. glutamicum* CM2 was cultivated with a fixed pH value of 8.0 and under this condition, performed better than at pH 6.25. Despite the growth rate strongly decreased to 0.17 h^{-1}, $Y_{X/S}$, $Y_{P/S}^{his}$, and $Y_{P/S}^{gly}$ remained stable compared to pH 7.4, resulting in 0.47 g biomass g^{-1} substrate, 0.053 mol L-histidine mol^{-1} glucose and 0.065 mol glycine mol^{-1} glucose. When cultivated at pH 8.25, the growth and production behaviour of *C. glutamicum* CM2 decreased strongly. The growth rate was below 0.1 h^{-1}, the $Y_{X/S}$ was below 0.1 g biomass g^{-1} substrate, and $Y_{P/S}^{his}$ and $Y_{P/S}^{gly}$ were not calculated due to the low extracellular concentrations of L-histidine and glycine, respectively. Despite the pH values in shaking flask cultivations increased above values of 8.6 (Fig. 34, p.231), it seems that the starting phase of the cultivation (at about pH 7.4) where *C. glutamicum* starts to build biomass is important to bear the burden of increased pH values in a later phase of cultivation.

Mimicking shaking flask cultivations in small-scale fermentations: oxygen limitation. Beyond the mentioned differences, shaking flask cultivations in general differ from reactor cultivations in the option of controlled aeration. For aerobic cultivations, oxygen needs to be transferred from the gas phase into the liquid phase. In aerobic bioreactor cultivations this is

actively facilitated via aeration through sterile filters and controlling air bubble sizes with frits. The simpler shaking flask system on the other hand relies on passive aeration via natural oxygen transfer at the interface of liquid and gas phases, which might be increased by using baffled flasks. Despite its many advantages e.g. for fast screening of producer strains, it is known that oxygen limitations in the shaking flask system occur and probabilities of these increase with increasing biomass concentrations (Klöckner and Büchs, 2012; Lange et al., 2018; Losen et al., 2004; McDaniel and Bailey, 1969). For the purpose to investigate if these potential limitations in the shaking flask system have impacts on the L-histidine producing strains, we conducted small-scale fermentations with strain *C. glutamicum* CM2 and induced oxygen limitations after 4, 6, and 8 h of cultivation time. This was done by restricting the velocity of the stirrer and the aeration to fixed values (100 rpm, 0.1 vvm) after 4, 6, or 8 h of cultivation to decrease the pO_2 in a controlled manner. Results showed that compared with the fermentations with controlled oxygen supply, the limitations did not lead to significantly different values for growth rates and biomass substrate yields. With an oxygen limitation after 4 h of cultivation, *C. glutamicum* CM2 showed a slightly decreased growth rate, whereas with an oxygen limitation after 8 h it had an increased $Y_{X/S}$ of 0.52 g biomass g^{-1} substrate. The $Y_{P/S}^{his}$ and $Y_{P/S}^{gly}$ in all three scenarios decreased strongly to 0.034, 0.029, and 0.023 mol L-histidine mol^{-1} glucose and 0.038, 0.034, and 0.030 mol glycine mol^{-1}, indicating that the cells need an optimal oxygen supply for L-histidine production. However, since these are results from mostly preliminary single experiments, repetitions are urgently needed to substantiate these first findings.

A 2. STR batch fermentation

With the purpose to conduct initial and preliminary fermentation studies in increasingly larger volumes, the process was transferred from the glass reactor system with 200 mL working volume to a stirred tank steel reactor (STR) with a working volume of 30 L (2.4.7 30 L stirred tank reactor cultivations, p.67). To generate sufficient amounts of biomass, the seed train was modified (Fig. 9, p.66) and 10 L CGXII^{R} medium were inoculated with *C. glutamicum* CM2 in the STR. In a first study, *C. glutamicum* CM2 performed poor and showed a growth rate of < 0.1 h^{-1} and $Y_{X/S}$ of <0.1 g biomass g^{-1} substrate (data not shown). We monitored growth for 8 h, where the strain had accumulated 0.67 g biomass L^{-1} (from the initial 0.27 g biomass L^{-1}). Since protocatechuic acid (PCA) is known to be a crucial supplement for reactor cultivations in certain scenarios with *C. glutamicum* (personal communication with Bastian Blombach, Michaela Graf; both IBVT, University of Stuttgart), 30 mg L^{-1} were added sterilely to the medium. Indeed, the cells showed increasing differential growth rates after addition of PCA

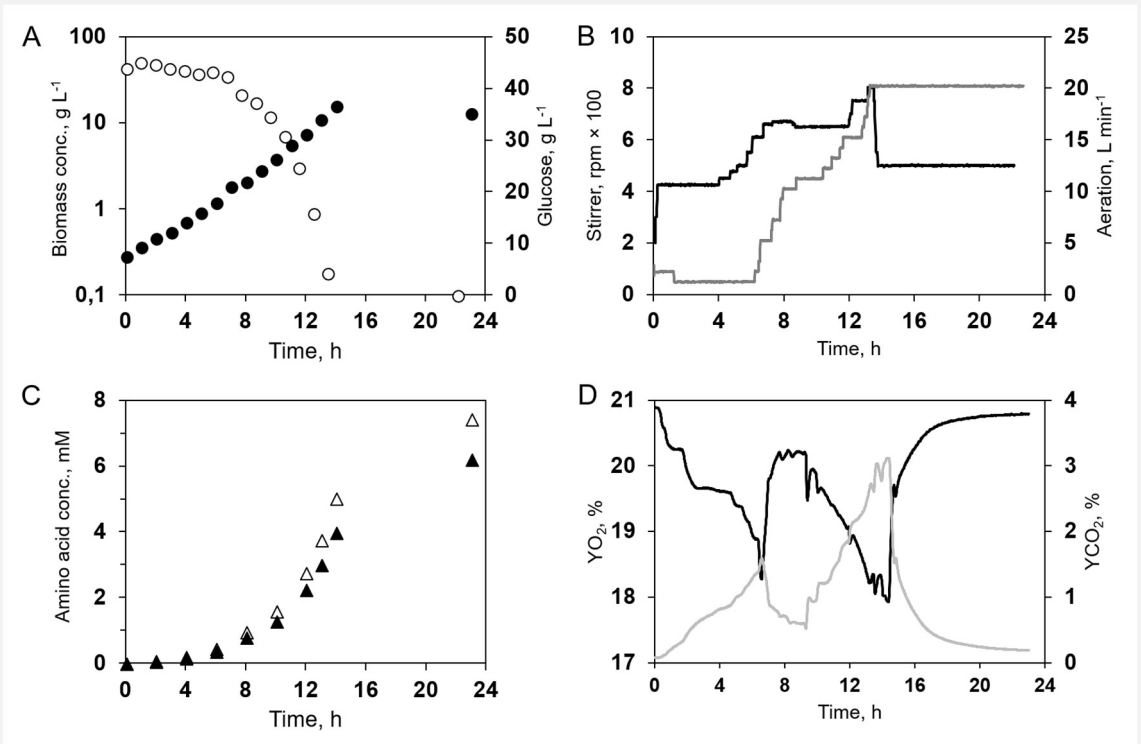

Fig. 20. Representative stirred tank reactor fermentation in batch mode of strain *C. glutamicum* CM2 in 10 L working volume in CGXII^{R} medium with 30 mg protocatechuate L^{-1} and 45 g glucose L^{-1}. (A) biomass concentration (filled circles) and glucose concentration (open circles), (B) process data velocity of the stirrer (black line) and aeration with sterile air (grey line), (C) amino acid concentrations for L-histidine (black triangles) and glycine (white triangles), (D) proportion of the exhaust gas in percentage for O_2 (black line) and CO_2 (grey line).

and the strain increased its biomass significantly to 17.6 g biomass L^{-1} after 22 h of cultivation (data not shown). Thus,PCA was identified as an essential ingredient for bioreactor cultivations with the L-histidine producing *C. glutamicum* CM2 in scales above 200 mL working volume.
A further bioreactor cultivation was conducted and *C. glutamicum* CM2 was cultivated with the same conditions as before, with the difference that PCA was included in all applied minimal media (seed train and main culture). When PCA was present, *C. glutamicum* CM2 grew exponentially with a growth rate of 0.29 h^{-1} and had a $Y_{X/S}$ of 0.39 g biomass g^{-1} substrate. The $Y_{P/S}^{his}$, and $Y_{P/S}^{gly}$ decreased compared to the standard cultivation conditions in shaking flasks (Table 31, p.120) and in the small-scale fermentations in glass reactors (Table 34, p.134), to 0.025 mol L-histidine mol^{-1} glucose and 0.035 mol glycine mol^{-1} glucose, respectively. Despite $Y_{P/S}^{his}$ was in the end diminished compared to cultivations in shaking flasks and small-scale fermentations, the strain showed exponential growth (with PCA) until it reached the stationary phase, consumed the glucose steadily and showed no strain instabilities, at least in this scenario (Fig. 20, p.138).

A 3. STR fed-batch fermentation

In a final reactor cultivation, we performed a preliminary fed-batch fermentation with a starting volume of 8 L in the 30 L stirred STR with *C. glutamicum* CM2. The required biomass for the fed-batch mode was generated with a batch fermentation, which was run o/n with the same conditions as used above, with slight changes (A 2 STR batch fermentation, p.138). As soon as the initially supplied 20 g glucose L^{-1} in the medium were consumed, the fed-batch mode was initiated and the growth rate of *C. glutamicum* CM2 was adjusted to $\mu = 0.1$ h^{-1} by adding defined amounts of glucose feed (Fig. 21, p.141). At the end of the batch phase, *C. glutamicum* CM2 had reached a biomass concentration of 9.2 g biomass L^{-1}, which corresponds to a $Y_{X/S}$ of 0.43 g biomass g^{-1} substrate. It had grown with a growth rate of 0.26 h^{-1}, similar to the small-scale fermentations (Table 34, p.134). During the batch phase, *C. glutamicum* CM2 had excreted 2.48 mM L-histidine and 3.37 mM glycine into the medium, resulting in $Y_{P/S}^{his}$ and $Y_{P/S}^{gly}$ of 0.022 mol L-histidine mol^{-1} glucose and 0.029 mol glycine mol^{-1} glucose.
C. glutamicum CM2 had consumed the initial 20 g glucose L^{-1} in the o/n batch phase after about 13 h of process duration (Fig. 21A, p.141). At this point, the process was switched to fed-batch mode, where μ was set to be 0.1 h^{-1}. The overall growth rate during the fed-batch phase ultimately was about 0.09 h^{-1}, slightly below the intended μ (data not shown).

The bioprocess was aborted after about 28 h, after the oxygen content in the exhaust gas started to increase significantly (data not shown) and after glucose concentration in the medium started to increase drastically (Fig. 21A, p.141) after about 22.3 h. Both findings indicate that one of the medium components was limiting at this point, since glucose was present in excess. However, medium components were not fed, which might be considered for future fermentation studies. The extension of the fed-batch process after glucose in the medium and oxygen in the exhaust gas increased, was performed to investigate whether *C. glutamicum* CM2 under these conditions also produced L-histidine one of the medium components limited, as was observed in the shaking flask cultivations when glucose limited (data not shown). Indeed, *C. glutamicum* CM2 kept producing L-histidine (and glycine) after one ore more components limited, between hours 22.3 and about 26 h (Fig. 21B, p.141).

During the fed-batch phase a maximal CDW of 25.6 g biomass L^{-1} was reached after about 25 h of cultivation. The substrate specific biomass yield and the glucose uptake rate were 0.89 g biomass g^{-1} substrate and 0.90 g substrate g^{-1} biomass h^{-1}. $Y_{P/S}^{his}$ was 0.014 mol histidine mol^{-1} glucose.

The batch and fed-batch phases combined resulted in 2.6 g histidine L^{-1} and in 1.4 g glycine as main byproduct. Interestingly, 86% of L-histidine were produced in the fed-batch phase, whereas only 64% of biomass were built. $Y_{P/S}^{his}$ was 30% lower in the fed-batch phase compared to the batch phase.

Between about 18 h and 22 h of cultivation, there is an increase in L-histidine and glycine production (Fig. 21B, p.141). In this phase, $Y_{P/}$ was 0.022 mol L-histidine mol^{-1} glucose. The process data show an upregulation of the stirrer speed to maintain the DO level above a critical value of 35% (Fig. 21C, p.141). After about 12 h of cultivation at the end of the batch phase, strong foaming occurred, which most likely resulted in accumulation of the base NH_4OH on top of the foam layer. Manual addition of antifoam destroyed the accumulated foam. However, the accumulated base led to an increase of the pH to about 8.7 (data not shown). We counteracted this by adding 20 mL 10% (v v^{-1}) phosphoric acid followed by 20 mL 80% (v v^{-1}) phosphoric acid, readjusting the pH to 7.4. Determination of the anorganic phosphate in the medium revealed that due to the addition of phosphoric acid, phosphate was not the growth limiting component in the medium (data not shown).

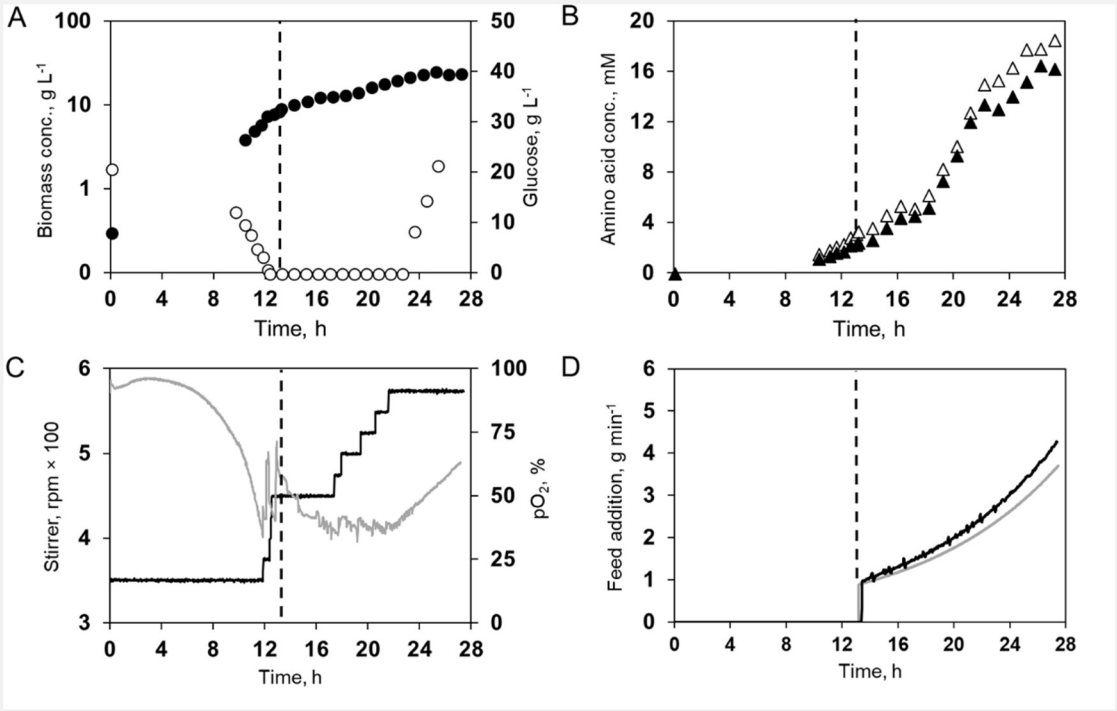

Fig. 21. Fed-batch fermentation of strain *C. glutamicum* CM2 in a stirred tank steel reactor with 8 L starting volume of CGXII^{R} medium with 30 mg protocatechuate $^{-1}$1 and 20 g glucose L^{-1} starting concentration. First about 13 h show fermentation in batch mode, then the fed-batch was switched on and defined amounts of glucose were added to the medium. (A) biomass concentration (filled circles) and glucose concentration (open circles), (B) amino acid concentrations for L-histidine (black triangles) and glycine (white triangles), (C) process data velocity of the stirrer (black line) and oxygen partial pressure (grey line), (D) actual feed addition during the fed-batch phase of the fermentation (black line) and calculated feed addition (grey line). The dashed line indicates the start of the fed-batch mode, i.e. when the feed was switched on.

3.2. Results PART II – Metabolic engineering to guide evolution

3.2.1. *Idea*

The ideas behind the development of an evolutionary method in addition to the multiple available evolutionary approaches, such as adaptive laboratory evolution (ALE) or directed evolution was

i) to develop an evolutionary approach that yields only a minimal set of mutational background, thus enabling simple screening for the desired mutations and

ii) to create a novel metabolic mode for production of L-valine with this evolutionary approach. This novel metabolic mode was intended to expand the the available modes for L-valine production, which classically focus on inactiving or attenuating the pyruvate dehydrogenase complex (PDHC; Blombach et al., 2009, 2008, 2007; Buchholz et al., 2013; Oldiges et al., 2014). Therefore, in a first step, we applied metabolic engineering and inactivated PEPCx and PCx enzymes with the aim to increase carbon fluxes over the PDHC thereby supplying increased amounts of pyruvate, which might then be drawn towards L-valine (Fig. 7, p.32). Strain *C. glutamicum* Δ*ppc* Δ*ppc* constituted the basis for the evolutionary approach.

3.2.2. *Flux Balance Analysis*

We intended to construct a double deletion mutant strain with deletions of the genes *ppc*, encoding PEP carboxylase, and *pyc*, encoding pyruvate carboxylase, to harness the potentially higher flux over the PDHC for L-valine production. However, the double deletion mutant had been described before as being unable to grow on glucose as sole carbon source (Peters-Wendisch et al., 1998). Therefore, in a first step, André Feith (IBVT, University of Stuttgart) conducted a Flux balance analysis (FBA) with a recently published model of *C. glutamicum* (Zhang et al., 2017). This was done to predict compensatory flux distributions that might enable the growth of *C. glutamicum* Δ*ppc* Δ*pyc* on glucose, as a potential result of an evolutionary experiment (Fig. 22, p.143).

In the *C. glutamicum* WT scenario, the FBA predicted a μ of 0.39 h^{-1}, which fits the experimental data quite well (compare Table 36, p.151). FBA further predicted a flux distribution between PPP and glycolysis of 39:60 for *C. glutamicum* WT and no flux into the glyoxylate shunt during growth on glucose (Fig. 22A, p.143), as is known from experimental

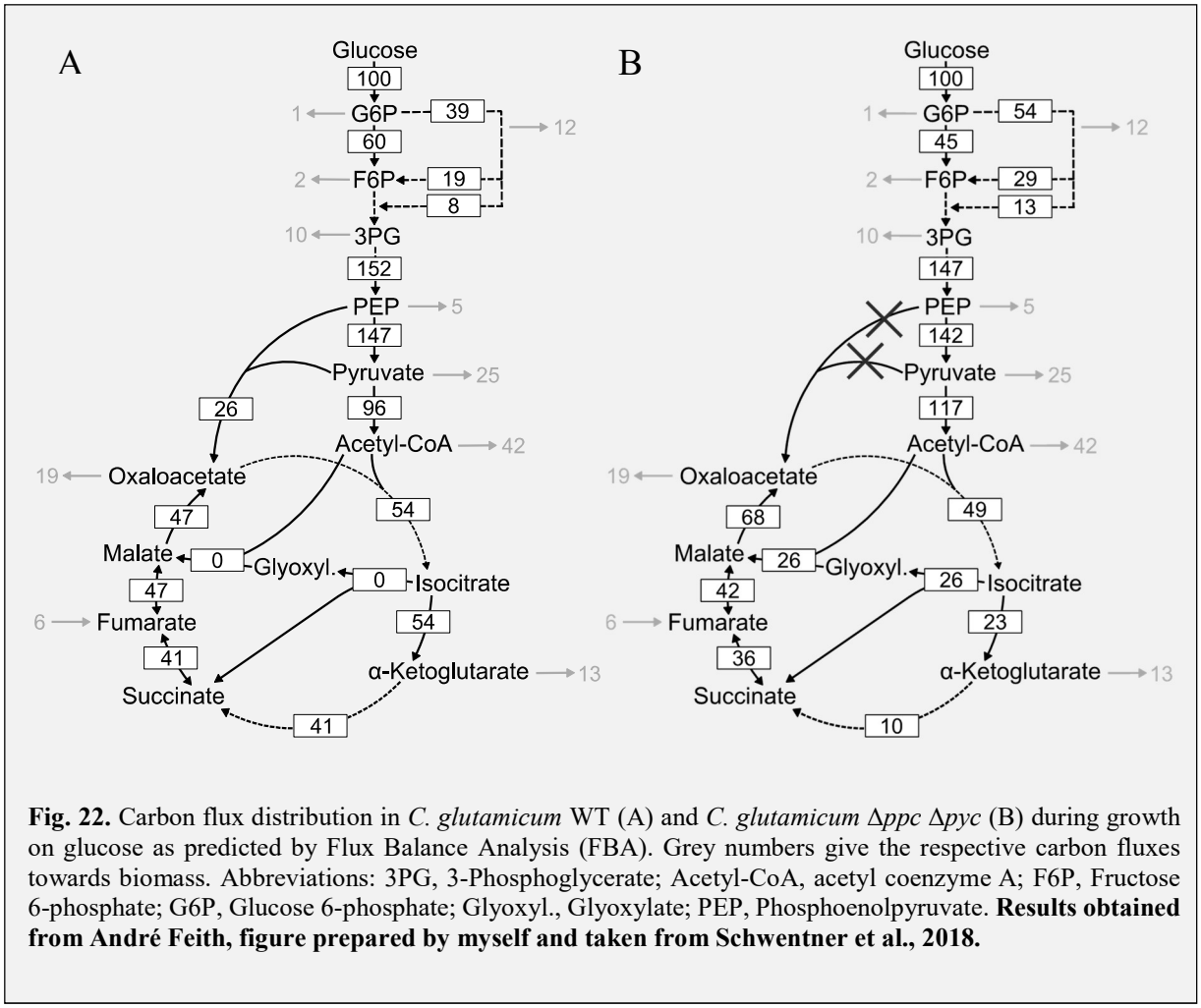

Fig. 22. Carbon flux distribution in *C. glutamicum* WT (A) and *C. glutamicum* Δ*ppc* Δ*pyc* (B) during growth on glucose as predicted by Flux Balance Analysis (FBA). Grey numbers give the respective carbon fluxes towards biomass. Abbreviations: 3PG, 3-Phosphoglycerate; Acetyl-CoA, acetyl coenzyme A; F6P, Fructose 6-phosphate; G6P, Glucose 6-phosphate; Glyoxyl., Glyoxylate; PEP, Phosphoenolpyruvate. **Results obtained from André Feith, figure prepared by myself and taken from Schwentner et al., 2018.**

data, since the glyoxylate shunt enzymes isocitrate lyase (ICL) and malate synthase (MS) are inactive on glucose as sole carbon source (Wendisch et al., 2000).

In contrast to that, the flux distributions changed when the two anaplerotic reactions of PEPCx and PCx were deleted from the model (Fig. 22B, p.143). Here, the glyoxylate shunt became active with a split ratio of 23:26 between the ICD and ICL reactions, resulting in an identical μ compared to *C. glutamicum* WT. Furthermore, the flux distribution between PPP and glycolysis changed to 54:45, favouring the NADPH-forming reactions in the PPP as compensation for the diminished flux through the NADPH-forming ICD reaction.

In sum, the FBA predicted that growth of a *C. glutamicum* Δ*ppc* Δ*pyc* mutant should be feasible on glucose as sole carbon source, when the glyoxylate shunt is activated.

3.2.3. *Metabolic engineering of the anaplerotic reactions*

With the result from the FBA indicating that a *C. glutamicum* mutant with deficiencies in the PCx and PEPCx reactions might potentially be able to grow on glucose, we constructed the

basis strain for the evolutionary approach *C. glutamicum* Δ*ppc* Δ*pyc*. In addition to *C. glutamicum* Δ*ppc* Δ*pyc*, we constructed *C. glutamicum* Δ*ppc* Δ*pyc* Δ*pck*, based on the afore mentioned strain, with an additional deletion of the *pck* gene, encoding PEP carboxykinase. In general, the PEPCk reaction is a gluconeogenic enzyme and directed towards pyruvate generation, rather than consumption (Riedel et al., 2001). It however has been demonstrated that PEPCk activity in *C. glutamicum* during growth on glucose is present (Riedel et al., 2001) and that the PEPCk reaction is reversible in principle (Jetten and Sinskey, 1993; Klaffl et al., 2013). Thus, by deploying a PEPCk deficient strain in the evolutionary approach, PEPCk should be omitted as potential target acquiring mutations.

Firstly, the growth behaviour of both basis strains *C. glutamicum* Δ*ppc* Δ*pyc* and *C. glutamicum* Δ*ppc* Δ*pyc* Δ*pck* was monitored in shaking flask experiments in CGXII^{E} (Table **12**, p.58) medium w/o yeast extract or L-glutamate with 20 g glucose L^{-1}, where none of the two strains was able to grow (data not shown). We proceeded by cultivating *C. glutamicum* Δ*ppc* Δ*pyc* and *C. glutamicum* Δ*ppc* Δ*pyc* Δ*pck* in CGXII^{E} medium, containing 20 g glucose L^{-1} and 1 g yeast extract L^{-1}. Compared with the growth of *C. glutamicum* WT (growth rate 0.39 ± 0.01 h^{-1}), both *C. glutamicum* Δ*ppc* Δ*pyc* and *C. glutamicum* Δ*ppc* Δ*pyc* Δ*pck*, showed strong growth deficits, as was expected (Fig. **23**, p.144). However, addition of 1 g yeast extract L^{-1} into the medium enabled minimal growth,

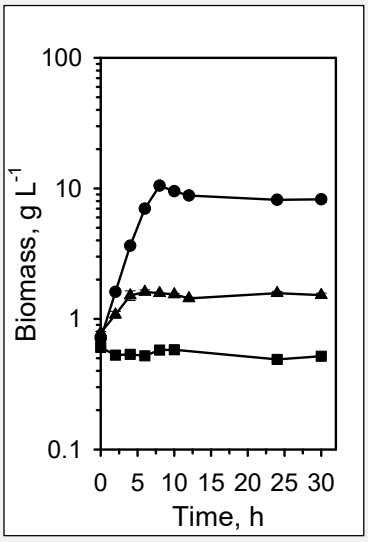

Fig. 23. Shaking flask cultivations of strains *C. glutamicum* WT (circles), *C. glutamicum* Δ*ppc* Δ*pyc* (triangles), and *C. glutamicum* Δ*ppc* Δ*pyc* Δ*pck* (squares) in CGXII^{E} minimal medium with 20 g glucose L^{-1} and 1 g yeast extract L^{-1}. Experiments were performed in triplicates and error bars show standard deviation. **Figure taken from Schwentner et al., 2018**

which is considered as prerequisite for an evolutionary approach relying on growth, i.e. increasing biomass concentration, as the screening indicator. In CGXII^{E} medium w/o yeast extract, neither *C. glutamicum* Δ*ppc* Δ*pyc* nor *C. glutamicum* Δ*ppc* Δ*pyc* Δ*pck* showed an increase in biomass concentration at all (data not shown).

3.2.4. *Evolutionary Approach*

Both strains *C. glutamicum* Δ*ppc* Δ*pyc* and *C. glutamicum* Δ*ppc* Δ*pyc* Δ*pck* were deployed in evolutionary experiments in CGXII^{E} minimal medium with 40 g glucose L^{-1}, inoculated and incubated for 3-4 days, and then transferred into fresh medium (Fig. 24, p.145; 2.4.5 Shaking flask cultivations, p.64). The evolutionary cultures were monitored each day for increasing biomass, simply by observing the density of the biosuspension. Increased biomass formation indicating an evolutionary event was observed two times independently for strain *C. glutamicum* Δ*ppc* Δ*pyc* after 14 and 15 days (exemplarily shown for one culture in Fig. **24**, p.145), and once for strain *C. glutamicum* Δ*ppc* Δ*pyc* Δ*pck* after 33 days.

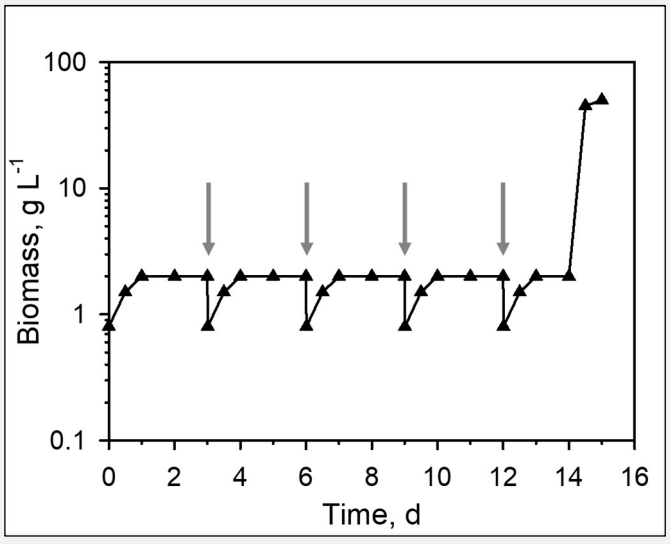

Fig. 24. Exemplary growth profile of *C. glutamicum* Δ*ppc* Δ*pyc* in CGXII^{E} medium with 40 g glucose L^{-1} and 1 g yeast extract L^{-1} during the shaking flask cultivations of the evolutionary experiment. Arrows indicate transfers of biomass into fresh CGXII^{E} medium. **Figure taken from Schwentner et al., 2018.**

3.2.5. *Evolved Strains*

Of each shaking flask containing evolved cultures, cell suspension was plated in serial dilutions on semi-solid complex and minimal medium ($CGXII^E$) with the aim to identify faster growing cells, i.e. colonies, and extract them from the mixed culture containing the initial strains *C. glutamicum* Δ*ppc* Δ*pyc* or *C. glutamicum* Δ*ppc* Δ*pyc* Δ*pck*. The agar plates were incubated for 1-3 days and examined regularly to identify faster growing colonies. The fastest growing ones were isolated and characterized in shaking flask cultivations with $CGXII^E$ containing 20 g glucose L^{-1} and 1 g yeast extract L^{-1}. The two evolved strains proceeding from *C. glutamicum* Δ*ppc* Δ*pyc* were named Evo1.1 and Evo1.2 and showed distinctly faster growth compared to the initial strain (Fig. 25, p.146), with growth rates of 0.23 ± 0.01 h^{-1} and 0.22 ± 0.01 h^{-1}, respectively (compare Table 36, p.151). The evolved strain proceeding from *C. glutamicum* Δ*ppc* Δ*pyc* Δ*pck* was named Evo2 and showed a distinctly lower growth rate of 0.08 ± 0.01 h^{-1}, compared with Evo1.1 and Evo 1.2. However, the growth of Evo2 was indeed enhanced compared to the initial strain (compare Table 36, p.151).

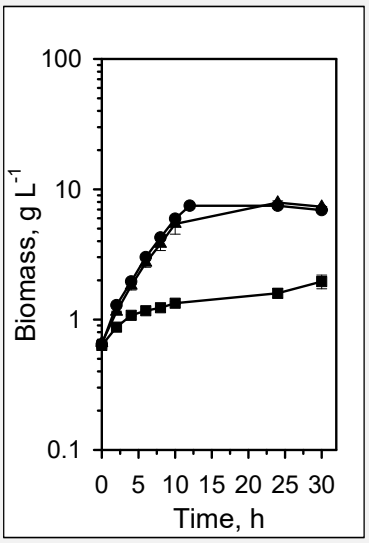

Fig. 25. Shaking flask cultivations of the evolved strains *C. glutamicum* Δ*ppc* Δ*pyc* Evo1.1 (circles), *C. glutamicum* Δ*ppc* Δ*pyc* Evo1.2 (triangles), and *C. glutamicum* Δ*ppc* Δ*pyc* Δ*pck* Evo2 (squares) obtained from the evolutionary experiments. Cultivations were performed in $CGXII^E$ minimal medium with 20 g glucose L^{-1} and 1 g yeast extract L^{-1}. Experiments were performed in triplicates and error bars show standard deviation. **Figure taken from Schwentner et al., 2018**

3.2.6. *Whole genome sequencing and mutational intersection*

With the evolved and verified strains in hands, it remained to elucidate what enables the faster growth of the evolved strains. With the purpose to identify chromosomal alterations as an outcome of the evolutionary experiment, the genomic DNA of strains Evo1.1, Evo1.2, and Evo2 was extracted and analysed at the Center for Biotechnology (CeBiTec), Bielefeld University, in the working group of Prof. J. Kalinowski (Microbial Genomics and Biotechnology). Whole genome sequencing (WGS) was performed with *C. glutamicum* WT as basis of comparison to identify the genomic alterations of strains Evo1.1, Evo1.2, and Evo2. As a result, three alterations in two of the evolved strains (Evo1.1 and Evo2) and six alterations in one evolved strain (Evo1.2) were identified (for a complete overview of the genomic alterations see Table **35**, p.148). These alterations comprise several single nucleotide polymorphisms (SNPs), synonymous as well as nonsynonymous SNPs, a nucleotide insertion, and a deletion of 12 bps. From this pool of mutations, we built the mutational intersection of the three evolved strains and visualized it in a Venn-diagram (Fig. 26, p.149). The result of the mutational intersection showed that only one target gene was mutationally affected in all three strains, which was the *icd* gene (cg0766), encoding the isocitrate dehydrogenase (ICD). The SNPs T to C (pos. 680299) in Evo1.1, G to A (pos. 680161) in Evo1.2, and G to T (pos. 681237) in Evo2 in the *icd* gene constituted nonsynonymous missense SNPs led to the three amino acid exchanges A94D, R453C, and G407S in the ICD enzyme, respectively, and were named ICD^{A94D}, ICD^{R453C}, and ICD^{G407S}. The genome positions given refer to the genome sequence of Kalinowski et al., 2003. Other mutational targets comprised PtsF (cg2120) and BenR (cg2641) in Evo1.1, cg0466, GlgE (cg1382), PtsF (cg2120), BenR (cg2641), and an ABC-type sugar transport system ATPase component (cg2708) in Evo1.2, and GlgE (cg1382) and cg1793 in Evo2 (Table 35, p.148).

Table 35. Overview of the mutations in the genomic background of the evolved strains that were created with Metabolic engineering to guide evolution. Given genomic targets were mutated in evolved strains Evo1.1, Evo1.2, or Evo2, compared to *C. glutamicum* WT, respectively. **Table taken from Schwentner et al., 2018**.

Gene	Gene product	COG category	Alteration on genome level	Effect on AA level
***C. glutamicum* Δ*ppc* Δ*pyc* Evo1.1**				
cg0766	ICD, isocitrate dehydrogenase	Carbohydrate metabolism and transport	SNP T to C (pos. 680299)	G407S
cg2120	PtsF, sugar specific PTS system, fructose/mannitol-specific transport protein	Carbohydrate metabolism and transport	Deletion of 12 bp (pos. 2015184 to 2015197)	-
cg2641	BenR, bacterial regulatory protein, LuxR-family	Carbohydrate metabolism and transport	SNP G to C (pos. 2522231)	G262A
***C. glutamicum* Δ*ppc* Δ*pyc* Evo1.2**				
cg0466	Conserved secreted protein	Function unknown	SNP G to C (pos. 410981)	none
cg0766	ICD, isocitrate dehydrogenase	Carbohydrate metabolism and transport	SNP G to A (pos. 680161)	R453C
cg1382	GlgE, potential maltosyltransferase[1]	Carbohydrate metabolism and transport	SNP A to C (pos. 1291535)	L491W
cg2120	PtsF, sugar specific PTS system, fructose/mannitol-specific transport protein	Carbohydrate metabolism and transport	SNP G to A (pos. 2013605)	G17S
cg2641	BenR, bacterial regulatory protein, LuxR-family	Carbohydrate metabolism and transport	SNP A to C (pos. 2523745)	T767P
cg2708	ABC-type sugar transport system, ATPase component	Carbohydrate metabolism and transport	SNP C to T (pos. 2582187)	G43D
***C. glutamicum* Δ*ppc* Δ*pyc* Δ*pck* Evo2**				
cg0766	ICD, isocitrate dehydrogenase	Carbohydrate metabolism and transport	SNP G to T (pos. 681237)	A94D
cg1382	GlgE, potential maltosyltransferase[1]	Carbohydrate metabolism and transport	SNP A to G (pos. 1291707)	S434P
cg1793	Hypothetical protein	Function unknown	Insertion G (pos. 1687061)	-

Source for information on genes and gene products: https://coryneregnet.compbio.sdu.dk/v6/index.html (last access: 2017-08-08)

[1] Seibold, G.M., Breitinger, K.J., Kempkes, R., Both, L., Krämer, M., Dempf, S., Eikmanns, B.J., 2011. The *glgB*-encoded glycogen branching enzyme is essential for glycogen accumulation in *Corynebacterium glutamicum*. Microbiology 157, 3243–3251. doi:10.1099/mic.0.051565-0.

Abbr.: AA, amino acid; COG, clusters of orthologous categories; pos., position; PTS, phosphoenolpyruvate-dependent phosphotransferase system; SNP, single nucleotide polymorphism

Since the *ptsF* gene was affected by mutations in strains Evo1.1 and Evo1.2, both strains were cultivated in CGXII^{E} minimal medium with fructose instead of glucose. Here, both strains showed impaired growth compared to growth on glucose (data not shown) other than C. glutamicum WT, which is able to grow on fructose as sole carbon source

Fig. 26. Venn-diagram showing the mutational background of the evolved strains *C. glutamicum* Δ*ppc* Δ*pyc* Evo1.1, *C. glutamicum* Δ*ppc* Δ*pyc* Evo1.2, and *C. glutamicum* Δ*ppc* Δ*pyc* Δ*pck* Evo2. Genomic targets that were altered compared to the genome of *C. glutamicum* WT were revealed by (comparative) whole genome sequencing and are given as cg numbers (according to https://coryneregnet.compbio.sdu.dk/v6/index.html; last access 15-06-2018). WGS unveiled gene cg0766 (icd, encoding isocitrate dehydrogenase) as mutational intersection, i.e. only consistent target in all three evolved strains. For an overview of all targets of the evolutionary approach see Table 35 on page 148. **Figure taken from Schwentner et al., 2018.**

(Dominguez et al., 1998, 1997). This indicates that the mutations in the *ptsF* gene indeed affect the PtsF protein in Evo1.1 and Evo1.2.

3.2.7. *Re-engineering*

Having identified *icd* as the sole mutational intersection, we proceeded by re-engineering the three nucleotide exchanges into *C. glutamicum* Δ*ppc* Δ*pyc*, resulting in the re-engineered strains *C. glutamicum* Δ*ppc* Δ*pyc* ICD^{A94D}, *C. glutamicum* Δ*ppc* Δ*pyc* ICD^{R453C}, and *C. glutamicum* Δ*ppc* Δ*pyc* ICD^{G407S}. With the aim to confirm the ICD mutations as definitive factor for the enhanced growth of the evolved strains, the re-engineered strains were cultivated in $CGXII^{E}$ minimal medium containing 20 g glucose L^{-1} and 1 g yeast extract L^{-1} (Fig. **27**, p.150). *C. glutamicum* Δ*ppc* Δ*pyc* ICD^{A94D}, *C. glutamicum* Δ*ppc* Δ*pyc* ICD^{R453C}, and *C. glutamicum* Δ*ppc* Δ*pyc* ICD^{G407S} showed growth rates of 0.24 ± 0.03 h^{-1}, 0.22 ± 0.01 h^{-1}, and 0.31 ± 0.02 h^{-1}, respectively, accounting to 62%, 56%, and 80% of the growth rate of *C. glutamicum* WT (Table 36, p.151).

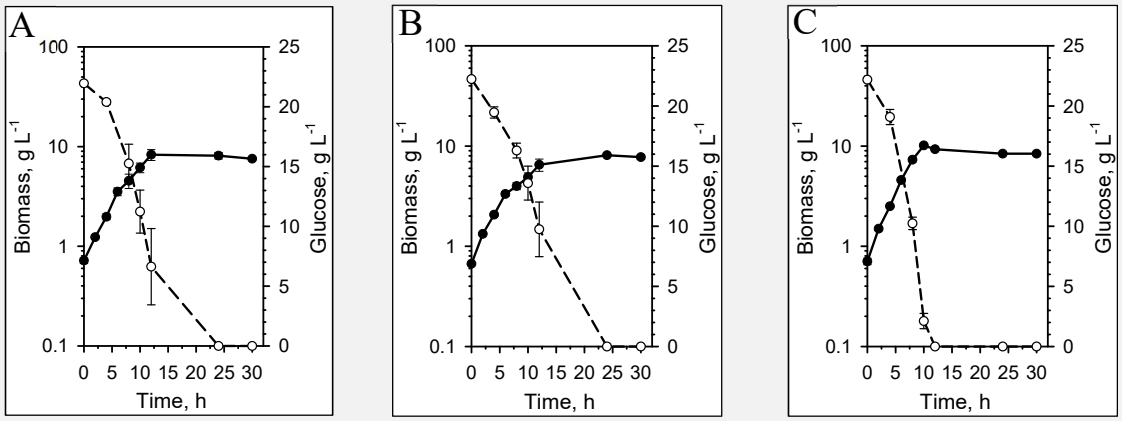

Fig. 27. Shaking flask cultivations of the re-engineered strains *C. glutamicum* Δ*ppc* Δ*pyc* ICD^{A94D} (A), *C. glutamicum* Δ*ppc* Δ*pyc* ICD^{R453C} (B), and *C. glutamicum* Δ*ppc* Δ*pyc* ICD^{G407S} (C) in CGXII^{E} minimal medium with 20 g glucose L^{-1} and 1 g yeast extract L^{-1}. Filled circles represent biomass formation, empty circles represent glucose concentration. Experiments were performed in triplicates and error bars show standard deviation. **Figure taken from Schwentner et al., 2018.**

Under these conditions, substrate specific biomass yields slightly decreased to 0.56 ± 0.03, 0.56 ± 0.02, and 0.55 ± 0.03 g biomass per g substrate, respectively, compared to 0.60 ± 0.01 g biomass per g substrate of *C. glutamicum* WT (Table 36, p.151).

Biomass specific glucose consumption rates q_S decreased from 0.64 ± 0.01 g glucose per g biomass per h for *C. glutamicum* WT to 0.43 ± 0.05, 0.40 ± 0.02, and 0.56 ± 0.04 g glucose per g biomass per h in *C. glutamicum* Δ*ppc* Δ*pyc* ICD^{A94D}, *C. glutamicum* Δ*ppc* Δ*pyc* ICD^{R453C}, and *C. glutamicum* Δ*ppc* Δ*pyc* ICD^{G407S} (Table 36, p.151). By re-engineering the ICD mutations into the initial strain *C. glutamicum* Δ*ppc* Δ*pyc*, we created a strain that is deficient in the reactions catalysed by PCx and PEPCx and despite this can grow on the glycolytic substrate glucose. ICD mutations were identified as the one factor enhancing the growth phenotype of the initial strain and enabled the evolved strains to grow, where *C. glutamicum* Δ*ppc* Δ*pyc* was not able to.

3.2.8. *Media investigations*

In further experiments, we investigated the requirements of the re-engineered strains concerning media composition in more detail. Therefore, yeast extract, which enabled minimal growth of the initial strain *C. glutamicum* Δ*ppc* Δ*pyc* (3.2.3 Metabolic engineering of the anaplerotic reactions, p.143), was omitted from the CGXII^{E} medium. Interestingly, none of the re-engineered strains was able to grow in this environment, indicating that evolution strongly selects according to surrounding conditions (data not shown; Nevo, 2011), since Evo1.1, Evo1.2, and Evo2 had evolved in the presence of yeast extract. To see whether the yeast extract complex component could be replaced by a more defined component, we supplemented the CGXII^{E} medium (w/o yeast extract) with 1 mM or 10 mM L-glutamate. This was intended to enable the re-engineered strains to take up L-glutamate, incorporate carbon into the TCA cycle via the reaction of *gdh* (cg2280) encoded L-glutamate dehydrogenase (Gdh), and potentially close their oxaloacetate-forming gap due to the deletions of *ppc* and *pyc*. Both 1 mM (Fig. **28**, p.152) and 10 mM (data not shown) of supplemented L-glutamate were able to mediate growth of the re-engineered strains. Exemplarily, the consumption of 1 mM L-glutamate was monitored for *C. glutamicum* Δ*ppc* Δ*pyc* ICD^{G407S}, which had consumed all present L-glutamate in the medium post 8 h of cultivation start (data not shown). Further, it continued to grow after depletion of L-glutamate and showed an overall growth rate of 0.27 ± 0.01 h^{-1}, which corresponds to 87% compared to conditions with yeast extract. The other two

Table 36. Overview of growth rates, substrate specific biomass yields, and biomass specific substrate uptake ratess of *C. glutamicum* WT, the initial strains for the evolutionary experiment, and the re-engineered strains in CGXII^{E} medium with 20 g glucose L^{-1} and 1 g yeast extract L^{-1}.

Strain	μ, h^{-1}	$Y_{X/S}$, g g^{-1}	qs, g g^{-1} h^{-1}
C. glutamicum WT	0.39 ± 0.01	0.60 ± 0.01	0.64 ± 0.01
C. glutamicum Δ*ppc* Δ*pyc*	n.s.g.	n.s.g.	n.s.g.
C. glutamicum Δ*ppc* Δ*pyc* Δ*pck*	n.s.g.	n.s.g.	n.s.g.
C. glutamicum Δ*ppc* Δ*pyc* Evo1.1	0.23 ± 0.01	n.d.	n.d.
C. glutamicum Δ*ppc* Δ*pyc* Evo1.1	0.22 ± 0.01	n.d.	n.d.
C. glutamicum Δ*ppc* Δ*pyc* Δ*pck* Evo2	0.08 ± 0.01	n.d.	n.d.
C. glutamicum Δ*ppc* Δ*pyc* ICD^{A94D}	0.24 ± 0.03	0.56 ± 0.03	0.43 ± 0.05
C. glutamicum Δ*ppc* Δ*pyc* ICD^{R453C}	0.22 ± 0.01	0.56 ± 0.02	0.40 ± 0.02
C. glutamicum Δ*ppc* Δ*pyc* ICD^{G407S}	0.31 ± 0.02	0.55 ± 0.03	0.56 ± 0.04

Abbr.: n.d., not determined; n.s.g, no significant growth

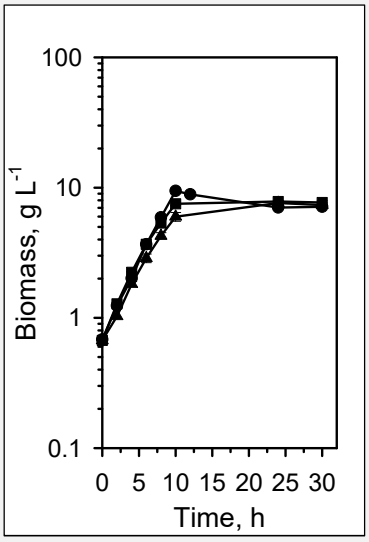

Fig. 28. Shaking flask cultivations of the re engineered strains *C. glutamicum* Δ*ppc* Δ*pyc* ICD^{A94D} (triangles), *C. glutamicum* Δ*ppc* Δ*pyc* ICD^{R453C} (squares), and *C. glutamicum* Δ*ppc* Δ*pyc* ICD^{G407S} (circles) in CGXII^{E} minimal medium with 20 g glucose L^{-1} and 1 mM L-glutamate, instead of yeast extract. Experiments were performed in triplicates and error bars show standard deviation. **Figure taken from Schwentner et al., 2018.**

re-engineered strains, *C. glutamicum* Δ*ppc* Δ*pyc* ZICD^{A94D} and *C. glutamicum* Δ*ppc* Δ*pyc* ICD^{R453C}, showed growth rates of 0.24 ± 0.01 h^{-1} and 0.26 ± 0.01 h^{-1} in the presence of 1 mM L-glutamate, which corresponds to 100% and 118% compared to when supplemented with yeast extract, respectively.

3.2.9. *ICD mutations impair ICD activities*

After having verified ICD mutations as growth-enabling factors of the re-engineered strains on glucose and having identified L-glutamate as required supplement, we proceeded by investigating the effects of the ICD mutations in more detail. Therefore, the specific ICD enzyme activities (2.8.7 Enzyme assays, p.90) of all three ICD variants were measured. This was done by generating cell-free lysates of strains *C. glutamicum* Δ*ppc* Δ*pyc* ICD^{A94D}, *C. glutamicum* Δ*ppc* Δ*pyc* ICD^{R453C}, *C. glutamicum* Δ*ppc* Δ*pyc* ICD^{G407S}, and *C. glutamicum* WT, grown in CGXII^{E} with 20 g glucose L^{-1} and 1 mM L-glutamate.

The three ICD variants ICD^{A94D}, ICD^{R453C}, and ICD^{G407S} showed specific ICD activities of 0.11 ± 0.01, 0.31 ± 0.03, and 0.58 ± 0.06 U (mg protein)$^{-1}$, accounting to about 10%, 29%, and 55% of the specific ICD activity of the wildtype enzyme, respectively (Fig. 29, p.153). The measurement of the specific enzyme activities of the ICD variants, ICD^{A94D}, ICD^{R453C}, and

ICD^{G407S}, showed that the specific activities of the mutated variants was significantly lower than the one of the native enzyme.

Since the FBA (3.2.2 Flux Balance Analysis, p.142) predicted that growth of the double deletion mutant *C. glutamicum* Δ*ppc* Δ*pyc* on glucose in principle is possible, but that activation of the glyoxylate shunt - i.e. presence of enzymatic activities of ICL and MS – is needed, we proceeded by investigating activities of these enzymes. Lysates were prepared as described for ICD and measurements showed that in glucose-grown *C. glutamicum* WT specific activities of ICL and MS were negligible, resulting in 0.03 ± 0.05 and below 0.01 U (mg protein)$^{-1}$ specific activity (Fig. 29, p.153). It is known that both enzymes are typically inactive when *C. glutamicum* is growing on glucose as sole carbon source (Wendisch et al., 2000, 1997). In contrast, specific ICL and MS activities in the re-engineered strains were significantly higher than in *C. glutamicum* WT, reaching 0.33 ± 0.06, 0.32 ± 0.05, and 0.53 ± 0.07 U (mg protein)$^{-1}$ for ICL and 0.44 ± 0.07, 0.42 ± 0.08, and 0.39 ± 0.03 U (mg protein)$^{-1}$ for MS in *C. glutamicum* Δ*ppc* Δ*pyc* ICD^{A94D}, *C. glutamicum* Δ*ppc* Δ*pyc* ICD^{R453C}, and *C. glutamicum* Δ*ppc* Δ*pyc* ICD^{G407S}, respectively (Fig. 29, p.153). Thus, ICD mutations indeed activated the glyoxylate shunt, manifesting in ICL and MS activity.

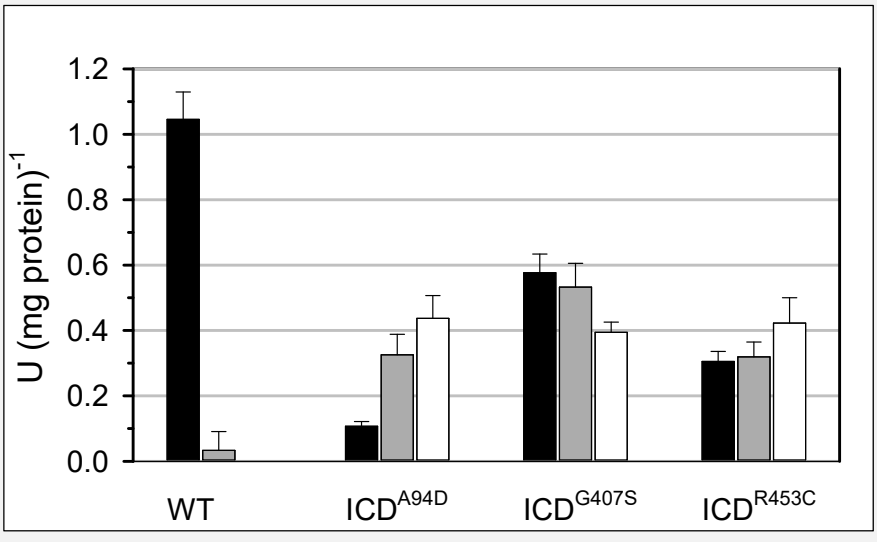

Fig. 29. Specific enzyme activities of isocitrate dehydrogenase (black bars), isocitrate lyase (gray bars), and malate synthase (white bars) in strains *C. glutamicum* WT, *C. glutamicum* Δ*ppc* Δ*pyc* ICD^{A94D}, *C. glutamicum* Δ*ppc* Δ*pyc* ICD^{G407S}, and *C. glutamicum* Δ*ppc* Δ*pyc* ICD^{R453C}. All experiments were performed in triplicates and error bars show standard deviation. **Figure taken from Schwentner et al., 2018.**

3.2.10. *Systems Metabolic Profiling*

With the purpose to gain a more detailed insight into the metabolic state of the re-engineered mutants, André Feith (IBVT, Univeristy of Stuttgart) exemplarily performed a comparative metabolome analysis, entitled SMP (2.8.8 Systems Metabolic Profiling, p.91), with *C. glutamicum* Δ*ppc* Δ*pyc* ICD^{G407S} as representative of the re-engineered strains on an LC-MS/MS Q-TOF system and evaluated fold changes (FCs) normalized on the metabolome levels of *C. glutamicum* WT. In four independent cultivations, *C. glutamicum* Δ*ppc* Δ*pyc* ICD^{G407S} showed altered intracellular pool sizes of several metabolites compared to *C. glutamicum* WT (Fig. 30, p.154). Amongst these, *cis*-aconitate (FC+13.2), citrate (FC+12.1), isocitrate (FC+6.4), and L-valine (FC+1.9) were the most prominent ones in relation to increased intracellular pool sizes. Several metabolites showed decreased intracellular pool sizes, amongst these were besides others acetyl-CoA (FC-0.9), -1,6-bisphosphate (FC-1.2), glucose 6-phosphate (FC-1.4), fructose, and as most prominent member glycerate-2/3-phosphate (FC-3.8).

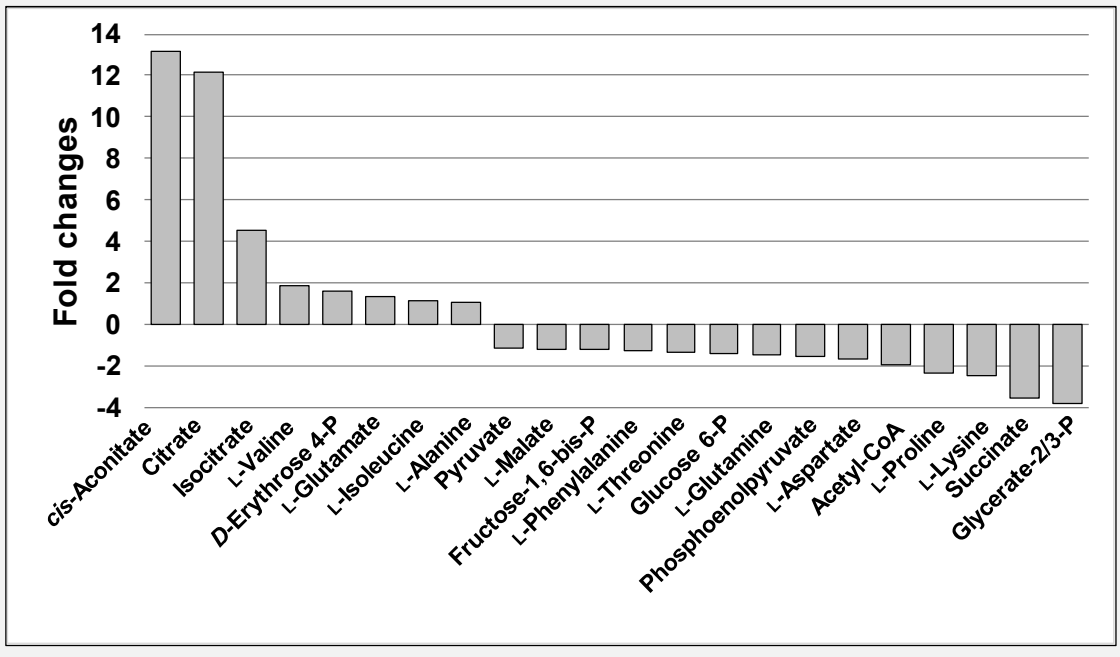

Fig. 30. Comparative metabolomics between *C. glutamicum* WT and *C. glutamicum* Δ*ppc* Δ*pyc* ICD^{G407S} showing the identified metabolites that had increased or decreased fold changes (FCs) in the latter strain. Abbreviations: P, -phosphate. **Results and figure obtained from André Feith. Results published partially in Schwentner et al., 2018.**

3.2.11. *L-Valine production*

As has been intended with the deletions of genes *pyc* and *ppc*, *C. glutamicum* Δ*ppc* Δ*pyc* might have an increased carbon flux over the PDHC and towards the TCA cycle. Such an increased carbon flux might be harnessed for the generation of pyruvate-derived products.

This potentially higher PDHC flux has been indicated by the results of FBA of *C. glutamicum* Δ*ppc* Δ*pyc* (3.2.2 Flux Balance Analysis, p.142) and our plan to apply L-valine as a product was further underlined by the result of the metabolomics, showing that *C. glutamicum* Δ*ppc* Δ*pyc* ICD^{G407S} exhibited increased intracellular pool sizes of L-valine. This indicated its potential as L-valine producer. Thus, we transformed the L-valine overproduction plasmid

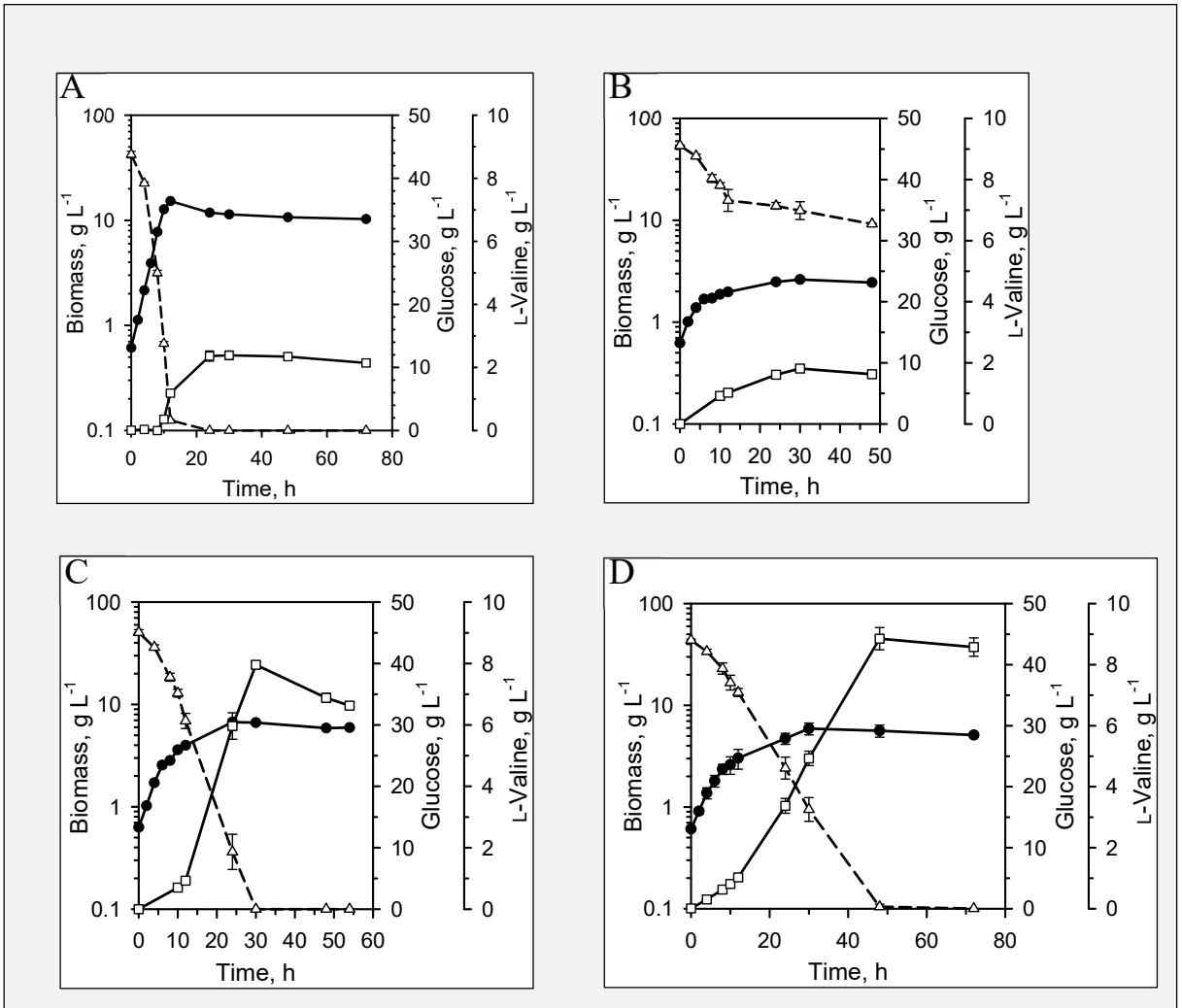

Fig. 31. Shaking flask cultivations for L-valine production of strains *C. glutamicum* (pJC4*ilvBNCE*) (A), *C. glutamicum* Δ*ppc* Δ*pyc* ICD^{R453C} (pJC4*ilvBNCE*) (B), *C. glutamicum* Δ*ppc* Δ*pyc* ICD^{A94D} (pJC4*ilvBNCE*) (C), and *C. glutamicum* Δ*ppc* Δ*pyc* ICD^{G407S} (pJC4*ilvBNCE*) (D). Filled circles represent biomass formation, empty triangles represent glucose concentration, and empty squares represent L-valine concentration. Experiments were performed in triplicates, error bars show standard deviation. **Figure taken from Schwentner et al., 2018.**

pJC4*ilvBNCE* (Radmacher et al., 2002) into *C. glutamicum* Δ*ppc* Δ*pyc* ICD^{A94D}, *C. glutamicum* Δ*ppc* Δ*pyc* ICD^{R453C}, and *C. glutamicum* Δ*ppc* Δ*pyc* ICD^{G407S}. Additionally, pJC4*ilvBNCE* was transformed into *C. glutamicum* WT, which does not excrete L-valine under the applied growth conditions (data not shown), to serve as a control strain. The plasmid pJC4*ilvBNCE* has been applied for L-valine production before and contains the L-valine biosynthesis genes *ilvB* (cg1435), encoding the large SU of acetohydroxyacid synthase (AHAS), *ilvN* (cg1436), encoding the small SU of AHAS, *ilvC* (cg1437), encoding acetohydroacid isomeroreductase (AHAIR), and *ilvE* (cg2418), encoding transaminase B (TA) (Fig. 7, p.31; Leyval et al., 2003; McHardy et al., 2003; Radmacher et al., 2002).

The three re-engineered strains and *C. glutamicum* WT, each containing pJC4*ilvBNCE*, were cultivated in CGXII^{E} supplemented with 40 g glucose L^{-1} and 1 mM L-glutamate (Fig. **31**, p.155). Here, *C. glutamicum* (pJC4*ilvBNCE*) showed a growth rate of 0.32 ± 0.01 h^{-1}, a $Y_{X/S}$ of 0.38 ± 0.02 g_{CDW} per g glucose and reached a maximal concentration of 2.4 ± 0.1 g L-valine L^{-1} in the medium, which corresponds to a product yield of 0.05 ± 0.01 g L-valine per g glucose. *C. glutamicum* Δ*ppc* Δ*pyc* ICD^{R453C} (pJC4*ilvBNCE*) showed a growth rate of 0.17 ± 0.01 h^{-1} in the first 6 h of cultivation, however, reached only a maximal biomass concentration of 2.6 ± 0.1 g_{CDW} per L, and was unable to consume the glucose completely within 48 h of fermentation. In contrast, *C. glutamicum* Δ*ppc* Δ*pyc* ICD^{A94D} (pJC4*ilvBNCE*) and *C. glutamicum* Δ*ppc* Δ*pyc* ICD^{G407S} (pJC4*ilvBNCE*) metabolized the glucose efficiently and showed a growth rate of 0.20 ± 0.01 h^{-1} and 0.17 ± 0.01 h^{-1} and a $Y_{X/S}$ of 0.30 ± 0.01 and 0.37 ± 0.03 g_{CDW} per g glucose, respectively. Besides L-valine, all strains secreted between 2.4 to 3.7 mM L-alanine (data not shown). *C. glutamicum* Δ*ppc* Δ*pyc* ICD^{A94D} (pJC4*ilvBNCE*) and *C. glutamicum* Δ*ppc* Δ*pyc* ICD^{G407S} (pJC4*ilvBNCE*) produced maximal 8.0 ± 0.1 and 8.9 ± 0.4 g L-valine per L, which corresponds to an overall $Y_{P/S}$ of 0.20 ± 0.01 and 0.22 ± 0.01 g L-valine per g glucose, respectively.

Taken together, the re-engineered strains showed a solid L-valine production performance, which demonstrates their potential for further modifications. MGE thus proved to be functional to identify a non-rational target to improve producer strains by identifying ICD mutations as a novel mode for L-valine production with *C. glutamicum*. Table 37 on page 157, gives a brief comparison of the best here constructed L-valine producer strain with other, in literature available, L-valine producers based on *C. glutamicum* and *E. coli*.

Table 37. Brief comparison of selected *E. coli* and *C. glutamicum* L-valine producer strains. Table modified after Oldiges et al., 2014 and Wang et al., 2018.

Strain	Titer, mM	$Y_{P/S}$§	Fermentation	Source
C. glutamicum				
Δ*ppc* Δ*ppc* ICD^{G407S} (pJC4*ilvBNCE*)	75	0.22 g g^{-1}	Shaking flask	(This work, Schwentner et al., 2018)
Δ*panBC* Δ*ilvA* (pJC1*ilvBNCD*)	92	0.27 g g^{-1}*	Shaking flask	(Radmacher et al., 2002)
Δ*ilvA* Δ*panB ilvN*M13 (pECKA*ilvBNC*)	130	0.38 g g^{-1}*	Shaking flask	(Elišáková et al., 2005)
*ilvN*M13 Δ*panB* P-*ilvA*M1CG P-*ilvD*M7 P-*ilvE*M6	136	0.40 g g^{-1}*	Shaking flask	(Holátko et al., 2009)
Δ*aceE* Δ*pqo* Δ*pgi* (pJC4*ilvBNCE*)	410	0.49 g g^{-1}	Fed-batch	(Blombach et al., 2008)
aceE A16 Δ*pqo* Δ*ppc* (pJC4*ilvBNCE*)	738	0.36 mol mol^{-1}	Fed-batch	(Buchholz et al., 2013)
E. coli				
VAMF (pKBRilvBNCED) (pTrc184ygaZHlrp)	65	0.38 g g^{-1}	Batch	(Park et al., 2007)
WLA (pKBRilvBN^{mut}CED) (pTrc184ygaZHlrp)	518	0.34 mol mol^{-1}	Fed-batch	(Park et al., 2011)

§$Y_{P/S}$ either given in g L-valine per g glucose or mol L-valine per mol glucose, as indicated.
*neither $Y_{P/S}$ calculation nor glucose concentration given in reference. Therefore glucose concentration was assumed to be 40 g glucose L^{-1}, as given in the general reference of the used CGXII medium (Keilhauer et al., 1993). Additional supplements like L-isoleucine or L-valine were omitted from the calculations. $Y_{P/S}$, if not given in the cited publications, were calculated as described in the Materials and methods part of this work. Data taken from Oldiges et al., 2014 and Wang et al., 2018.

CHAPTER 4: DISCUSSION

4.1. Part I

L-Histidine is an attractive amino acid for various applications in several sectors, such as feed supplement for salmon and chicken breeding (Han et al., 1991; Haug et al., 2008; Park et al., 2013; Waagbø et al., 2010), food supplement (https://www.lambertshealthcare.co.uk/l-histidine-hcl-500mg-p8313/; last access 25-07-2018; https://www.bulkpowders.co.uk/histidine.html; last access 25-07-2018), and medical applications, e.g. against obesity (Du et al., 2017; Feng et al., 2013; Keller et al., 2000; Kimura et al., 2013; Tuttle et al., 2012; Watanabe et al., 2008). In 2003 the annual fermentative production of L-histidine was estimated to be 400 t per year (Ikeda, 2003). Nowadays, L-histidine is produced in large scale via fermentation processes by several companies, e.g. Ajinomoto K.K. (https://www.ajiaminoscience.com/Products/histidine; last access 25-07-2018) and DAESANG Corp. (http://www.businesskorea.co.kr/news /articleView.html?idxno=19569; last access 25-07-2018). However, current numbers for the annual worldwide production of L-histidine are not available.

Most efficient producer strains that are described in scientific literature have been obtained by classical mutagenesis and show maximal $Y_{P/S}^{his}$ values of about 0.15 - 0.20 g L-histidine per g substrate (Becker and Wittmann, 2012; Mizukami et al., 1994), which is about 2.5 fold lower than the maximum theoretical growth coupled ($\mu = 0.1\ h^{-1}$) yield of 0.44 g per g calculated by André Feith (IBVT, University of Stuttgart) in the context of the underlying project (3.1.2 Flux Balance Analysis, p.100). Knowledge for the targeted engineering of *C. glutamicum* for L-histidine production so far is limited on the deregulation of the biosynthesis and improving precursor availability (Ikeda, 2003; Kulis-Horn et al., 2015; Mizukami et al., 1994; Zhang et al., 2012). The moderate success to develop efficient production strains might be attributed to the demanding biosynthesis of L-histidine, which is reflected by its tight connection to the energy and C_1 metabolism (1.2.5 L-HISTIDINE related pathways, p.21).

Therefore, to gain a more holistic understanding in the metabolic limitations for L-histidine production, we performed a modularized metabolic engineering approach, including flux balance analysis and LC MS/MS Q-TOF based systems metabolic profiling (SMP). Especially, the applied untargeted metabolomics workflow proofed as effective tool to monitor intracellular levels of key metabolites in the engineered strain genealogy.

In the first module, the biosynthesis pathway of L-histidine, we introduced two allele exchanges in the *hisG* gene (ggc742cat and acg748cag), entitled *hisG*^{FB}, leading to amino acid exchanges G233H and T235Q in the native amino acid sequence of the ATP phosphoribosyltransferase (HisG) (Schendzielorz et al., 2014). HisG has been described in several organisms, such as *S. typhimurium* (Wainscott and Ferretti, 1978), *M. tuberculosis* (Pedreño et al., 2012), *E. coli* (Dall-Larsen, 1988), and *C. glutamicum* (Araki and Nakayama, 1974) to be the target of a potent feedback inhibition mediated by the endproduct of the pathway, L-histidine, demonstrating the universality of this principle. For *S. typhimurium*, a synergistic inhibition of HisG by guanosine tetraphosphate (ppGpp), an intermediate of the stringent response (Traxler et al., 2008), and L-histidine has been demonstrated (Morton and Parsons, 1977). With the purpose to circumvent this feedback regulation in *C. glutamicum*, we implemented the mentioned mutated HisG variant from Schendzielorz et al. and the resulting strain *C. glutamicum* HIS1 indeed produced L-histidine, with a product subtrate yield for L-histidine ($Y_{P/S}^{his}$) of 0.015 ± 0.003 mol L-histidine per mol glucose. Simultaneously with L-histidine, this strain produced glycine in about equimolar amounts, which was the main detected byproduct and accompanied L-histidine throughout the strain history (Table 31, p.120). The coproduction of glycine and L-histidine had been observed in other L-histidine producing mutants of *C. glutamicum* (Araki and Nakayama, 1971; Ishino et al., 1986) and related strains (Shimizu et al., 2002) before, indicating inevitability in these organisms. Most likely, the glycine by-production can be ascribed to the requirement of the *de novo* purine biosynthesis steps three (PurN) and ten (PurH) for each one molecule of fTHF, serving as donor of a C_1 unit in the form of a formyl group. However, glycine by-production was not observed in L-histidine producing *E. coli* (Doroshenko et al., 2013; Malykh et al., 2018) and *Streptomyces coelicolor* (Korajlija and Delíc, 1977), showing the presence of a functional GCV system in these organisms, compared to *C. glutamicum*. It might be speculated that the presence of a GCV system led to the evolution of a different network and embedment of the L-histidine biosynthesis in these organisms.

The introduced modifications in strains *C. glutamicum* HIS1 to HIS7 concerning the L-histidine biosynthesis (feedback release of HisG, promoter exchanges in front of all four operons containing L-histidine genes, exchange of translational start codon, integration of an internal promoter, elimination of a potential translational regulatory domain) enabled L-histidine overproduction. However, the characteristics (growth rate, biomass substrate yield, product substrate yield of L-histidine) remained stable in strains *C. glutamicum* HIS1 – HIS4. As soon as the *hisEG* promoter was improved, $Y_{P/S}^{his}$ increased dramatically in *C. glutamicum* HIS6. This clearly shows that in addition to the feedback release of HisG the overexpression of *hisEG* is crucial for improved $Y_{P/S}^{his}$. This is most presumably due to overexpression of *hisG* (since it encodes the first enzyme in the pathway) to initially withdraw PRPP (and ATP) precursor(s) into the L-histidine biosynthesis, away from the competing PRPP-consuming reactions (Fig. 5, p.22; Hove-Jensen et al., 2016). Overproduction of desensitized HisG variants has been performed before in a plasmid-based approach and was shown to be beneficial for increasing L-histidine production (Mizukami et al., 1994).

The transitional strain *C. glutamicum* HIS5 that was solely modified in the *hisEG* operon (feedback release of HisG, promoter exchange from P_{hisE} to $P_{dapA\text{-}A16}$, exchange of translational start codon of *hisE* from GTG to ATG) was constructed to prove the necessity of overexpressing all L-histidine operons, i.e. genes. *C. glutamicum* HIS5 resulted in an intermediate $Y_{P/S}^{his}$ of 0.039 ± 0.001 mol L-histidine per mol glucose (compared to 0.012 ± 0.002 and 0.065 ± 0.001 mol L-histidine per mol glucose of *C. glutamicum* HIS4 and HIS6, respectively), thus showing that overexpression of all L-histidine operons, i.e. genes, is beneficial for improving $Y_{P/S}^{his}$. To my knowledge, this has not been shown before and represents the first approach to improve L-histidine production with a holistic strategy considering all relevant genes.

Relative metabolome measurements (entitled SMP) to determine the intracellular peak intensities of key metabolites showed that IGP and L-histidinol, two intermediates in L-histidine biosynthesis, drastically increased upon feedback release of HisG (in *C. glutamicum* HIS1). The increased IGP and L-histidinol peak intensities were re-decreased to wildtype like levels in *C. glutamicum* HIS7. In contrast, the intracellular peak intensities of L-histidine increased stepwise (reaching maximal levels in *C. glutamicum* HIS8 where intensities were 33 times higher compared to the WT), indicating an export limitation. Concerning export of L-histidine, to my knowledge no export system has been identified in *C. glutamicum* so far, nor in any other organism. Concerning L-histidine import, the gene product of gene cg1305 was proposed to be

involved in histidine import (Kulis-Horn et al., 2014). A strategy pursued in future experiments should include the deletion of potential L-histidine import systems, such as the one encoded by cg1305 (deletion construct available; Table 32, p.122). By this, re-import of L-histidine might be prevented, decreasing the high intracellular peak intensities of L-histidine detected in the L-histidine producing mutants and potentially easing regulatory/inhibiting effects. Positive effects for such a scenario were demonstrated for production of L-tryptophan with *C. glutamicum*, where the respective L-tryptophan uptake system was modified (Ikeda et al., 1994; Ikeda and Katsumata, 1995).

In a further approach to optimize the L-histidine biosynthesis, we implemented second copies of the genes *hisE* and *hisG* into the chromosome of *C. glutamicum* CM1, in the form of a modified *hisEG* operon (containing genes $hisE^{ATG}$ and $hisG^{FB}$) under control of P_{dapA} and T_{rrnB}. The chromosomal integration of multiple copies of the gene encoding the first enzyme of a pathway with the aim to withdraw carbon, has been proven beneficial for e.g. L-lysine production with *C. glutamicum* (Becker et al., 2011). However, in the case of L-histidine production, the introduction of a second copy of the *hisEG* operon did not manifest in increased $Y_{P/S}^{his}$, in fact it decreased $Y_{P/S}^{his}$ by 7% in *C. glutamicum* HIS_{int}, indicating that the amount of carbon withdrawn into the L-histidine biosynthesis is not the limiting step in this strain. Instead, withdrawal of increased amounts of PRPP or ATP seemed to have adverse effects on $Y_{P/S}^{his}$, probably by withdrawing the precursors from other reactions. Nevertheless, implementation of a second *hisEG* copy might be expedient in strain *C. glutamicum* HIS10, where important pathways are more balanced, and should be considered for future experiments.

The reaction catalysed by HisG withdraws one molecule of ATP from the general ATP pool of the cell by condensing it to PRPP (Alifano et al., 1996). With the purpose to investigate potential effects of this condensation, i.e. withdrawal, on the energy metabolism in an L-histidine overproduction scenario, we measured intracellular concentrations of the three adenylate species ATP, ADP, and AMP. Adenylates were quenched with perchloric acid and quantified via HPLC measurements and showed that intracellular concentrations of AMP in L-histidine producers were below the detection limit of the applied system (< 300 nM, data not shown). Since AMP concentrations in *C. glutamicum* WT were determined to be about 2.1 µmol AMP g_{CDW}^{-1}, intracellular AMP concentrations in the L-histidine producing mutants probably are far below the WT's levels.

Determination of the intracellular ADP concentrations showed that they were decreased in the analysed strains *C. glutamicum* HIS1 - HIS7 to roughly about half the value of *C. glutamicum*

WT. For the third and energy densest species, ATP, we found that overexpression of operon *hisEG* in strains *C. glutamicum* HIS5 – HIS7 drained ATP efficiently into L-histidine biosynthesis and led to strongly diminished concentrations of ATP, which was not observed when *hisEG* was not overexpressed. This effect might most likely be addressed to the overexpression of *hisG*, encoding ATP phosphoribosyltransferase, which is responsible for the covalent binding of ATP to PRPP, rather than to an effect mediated by *hisE* overexpression. Overexpression of the *hisG* gene has been shown before to be an important step in bacterial L-histidine production (Cheng et al., 2013; Mizukami et al., 1994; Zhang et al., 2012), but has not yet been connected to perturbations in the energy metabolism in *C. glutamicum*. However, HisG has been connected to perturbations in energy metabolism in *S. typhimurium* before, where low levels of HisG enzyme activity led to adenine auxotrophic mutants and reverting clones thereof were found to bear mutations in the *hisG* gene (Johnston and Roth, 1979).

From the absolute concentrations of ATP and ADP (AMP was omitted since concentrations were below the detection limit) we calculated the energy charge (EC), a measure for the energetic state of the cell that considers the phosphate groups per adenosine moiety and thus the energy delivering potential of each adenylate species. Interestingly, the perturbation of the energy metabolism in the L-histidine producers did not manifest in altered ECs, despite the ATP (in some strains) and ADP (in all strains) concentrations were diminished strongly. Typical ECs of exponentially and aerobically growing *E. coli* range from about 0.80 – 0.95 and revolve in this range. This was studied in *E. coli* in detail and it was shown that the EC declined upon carbon starvation, i.e. in the stationary growth phase, however, it was kept stable when nitrogen was the limiting factor (Chapman et al., 1971). An increase in EC is connected to (i) the activation of enzymes that are controlling anabolic, i.e. ATP requiring, pathways, such as PRPP synthetase, and to (ii) the inhibition of enzymes controlling amphibolic pathways, i.e. ATP generating, such as PDHC and phosphofructokinase (Atkinson and Walton, 1967, 1965). It thus appears that control of these enzymes (and their pathways) has evolved to maintain the EC within tight boundaries resembling an energy buffering system (Nelson and Cox, 2009). This might be reflected in the here presented ECs that are kept stable despite strongly altered absolute concentrations of ATP, ADP, and AMP. Reported conditions that result in diminished ECs are connected with nutrient starvation, i.e. stationary growth phase (Strange et al., 1963) and for example resting states, such as sporulation (Setlow and Kornberg, 1970), small decreases in EC also occurred in *E. coli* when cells were transitioned from aerobic to anaerobic conditions (Chapman et al., 1971).

This underpins the relevance of a balanced energy state in the regulatory hierarchy of the cell (Atkinson, 1968; Walker-Simmons and Atkinson, 1977).

The FBA (conducted by André Feith) already pointed to the requirement of a high ATP regeneration, i.e. AICAR to AMP/ATP recycling, capacity of the cell for efficient L-histidine production. Additionally, the SMP approach (also conducted by André Feith) finally hinted to PurA and/or PurB as limiting step(s), since the intracellular peak intensities of IMP and adenylosuccinate were strongly increased in *C. glutamicum* HIS6 and HIS7, compared to *C. glutamicum* WT. One of the IMP converting reactions is the one catalysed by adenylosuccinate synthethase (PurA, encoded by *purA*), which converts IMP to adenylosuccinate, which is then further converted to AMP by the action of adenylosuccinate lyase (PurB, encoded by *purB*). Beyond that, IMP might also be converted to xanthosine monophosphate (XMP), inosine, and hypoxanthine. However, intracellular accumulation of IMP and adenylosuccinate indicated limitations in PurA and PurB capacities. Therefore, we plasmid-based oxerexpressed *purA* and *purB*, which not only reduced the intracellular peak intensities of IMP and adenylosuccinate but also readjusted the ADP and ATP peak intensitites to *C. glutamicum* WT niveau. This demonstrated that the natural capacity of the cell is not suited to regenerate ATP on top of the growth demands in an L-histidine overproduction scenario.

Further SMP studies in the resulting *C. glutamicum* HIS8 strain revealed increased peak intensities of AICAR compared to *C. glutamicum* WT. In a recent work, where *E. coli* was engineered for L-histidine production, an observed intracellular accumulation of AICAR was overcome by introduction of an additional copy of the *purA* gene into the chromosome (Malykh et al., 2018). Since overexpression of *purA* and *purB* positively impacted the energy state of the cell but did not improve $Y_{P/S}^{his}$, we speculated that the increased intracellular AICAR peak intensities feedback on the upper part of L-histidine biosynthesis and indicate a further bottleneck in the metabolism of *C. glutamicum*. In accordance, Malykh et al. (2018) suggested a competitive inhibitory influence of AICAR on HisG in *E. coli*. However, this regulatory effect has not yet been proven for *C. glutamicum* or other bacteria and might be different in Actinobacteria compared to Enterobacteria.

AICAR (also termed ZMP) was shown to accumulate upon folate limitation and to bind to a specific, conserved riboswitch, which negatively controls expression of several purine genes (Kim et al., 2015). This riboswitch also binds 5-aminoimidazole-4-carboxamide-riboside-5-triphosphate (ZTP), which was shown to accumulate in *S. typhimurium* and *E. coli* upon

artificial shortage of folates (Bochner and Ames, 1982; Rohlman and Matthews, 1990) and thus was proposed as an alarmone for C_1 / folate shortage (Bochner and Ames, 1982). Interstingly, ZTP is directly synthesized in one reaction catalysed by PRPP synthetase, which transfers pyrophosphate onto ZMP, and not like other triphosphate ribonucleotides, whose formation is catalysed in two reactions by mono- and diphosphate kinases, in e.g. *B. subtilis* (Sabina et al., 1985, 1984). However, the presence of ZTP in *C. glutamicum* or other Actinobacteria is unclear and has not yet been investigated. Further, the availability of fTHF in *S. typhimurium* was connected to an influence on the mode of derepression of the L-histidine genes, indicating farreaching connections of the C_1 metabolism and the L-histidine biosynthesis (Berberich et al., 1966; Petersen et al., 1976a, 1976b). In *B. subtilis*, folate shortage has been shown to initiate sporulation (Freese et al., 1979; Heinze et al., 1978).

AICAR is converted to FAICAR and IMP, both reactions are catalysed by PurH. As mentioned, the first of them depends on the crucial cofactor fTHF. Therefore, we interpreted the AICAR accumulations in *C. glutamcium* HIS8 as potential limitations in the supply with C_1 units. This hypothesis was additionally supported by the results of FBA, proposing a requirement for higher flux over the serine hydroxymethyltransfere (SHMT) reaction, thereby supplying increased amounts of C_1 units. Additionally, strains *C. glutamicum* HIS1 - HIS8 secreted glycine as inevitable equimolar byproduct to L-histidine (see above), pointing in the same direction, since the required fTHF for purine biosynthesis is supplied by the reaction of the SHMT, converting L-serine to glycine. In this reaction, THF is loaded with a C_1 unit to yield mTHF (Green and Matthews, 2007; Huennekens, 1969; Schweitzer et al., 2009; Simic et al., 2002). Unfortunately, the various THF-species of the C_1 metabolism are not accessible with the applied analytical system, due to low pool sizes caused by interconversion, polyglutamylation, and degradation (Lu et al., 2007). However, the C_1 cycle is a complex network of several oxidised/reduced forms of C_1 units with THF as carrier molecule and has been investigated before for L-methionine and L-serine overproducing *C. glutamicum* strains (Bolten et al., 2010; Harvey and Dev, 1975; Krömer et al., 2006; Stolz et al., 2007). Interconversion of the different THF species has been elucidated in detail (Green and Matthews, 2007) and thus we speculated in supplying the cell with increased amounts of mTHF and rely on the interconversion potential of the cell.

With this purpose, we plasmid-based overproduced a glycine cleavage (GCV) system from the close *C. glutamicum* relative *C. jeikeium* in *C. glutamicum* HIS8. Upon this, only minimal amounts of glycine were detectable during the cultivation (< 0.2 mM; data not shown) and were

eradicated from the medium at the end of the cultivation, indicating re-uptake. In combination with the *purA* and *purB* overexpression, overexpression of the GCV genes led to a significant reduction of the intracellular AICAR peak intensities in the resulting *C. glutamicum* HIS9 and a significantly increased $Y_{P/S}^{his}$. This was attributed to the combined effects of (i) balanced pool sizes of IMP, adenylosuccinate, AICAR, and the adenylates (due to *purA*/*purB* overexpression) and (ii) the eradication of glycine from the medium with the simultaneous improved supply of the purine biosynthesis with fTHF, enabling a higher ATP recycling capacity, i.e. AICAR to AMP/ATP regeneration (due to overexpression of the GCV genes). Glycine has been demonstrated to effectively inhibit bacterial growth above certain concentrations (Hammes et al., 1973; Hishinuma et al., 1969; Strominger and Birge, 1965). In several bacterial species, e.g. *S. typhimurium*, the GCV system is the main source for C_1 units *in vivo*, however SHMT is the main source *in vitro* (Jelsbak et al., 2016). In a recent approach, a GCV system from *E. coli* has been applied in a metabolic engineering approach in *C. glutamicum*, where it enabled increased L-serine accumulation in a *glyA* (encoding SHMT) attenuated strain, by generating improved amounts of C_1 units for incorporation in the purine biosynthesis (Zhang et al., 2018). Consistent with these data, the GCV system from *C. jeikeium* seems to be able to at least partially satisfy the need for loaded THF molecules in the here investigated L-histidine producing *C. glutamicum*. However, SMP revealed still slightly increased intracellular AICAR peak intesities in *C. glutamicum* HIS9 and HIS10. This either indicates an even higher demand for fTHF or points to limiting AICAR formyltransferase/IMP cyclohydrolase activity. In the former case, an overproduction of the SHMT (or overexpression of the coding *glyA*) might counteract the still increased intracellular peak intensities in these strains by converting the surplus to glycine, thereby providing increased amounts of fTHF. In the case that the AICAR formyltransferase/IMP cyclohydrolase constitutes a limiting factor, the overproduction of PurH (or overexpression of *purH*) might be pursued in future experiments. In fact, the plasmid-based overexpression of the *purH* gene in the *C. glutamicum* CM1 background (resulting in *C. glutamicum* PUR4) improved $Y_{P/S}^{his}$ by 10%, indicating that increased PurH activity can solve AICAR accumulations and that this is beneficial for L-histidine production. Depending on the potency of a feedback inhibition of AICAR on HisG, as was identified in *E. coli* (Malykh et al., 2018), the balancing of still increased AICAR levels back to *C. glutamicum* WT niveau might reveal further beneficial effects on L-histidine formation in *C. glutamicum* HIS10. This might include studying the AICAR inhibition on HisG in more detail.

The $Y_{P/S}^{his}$ was further increased by exchanging the translational start codon of *pgi* from the native ATG triplet to GTG, thereby decreasing the translational efficiency and leading to a decrease in enzyme activity of the phosphoglucoisomerase by about 40% (Becker et al., 2010). This modification has proven beneficial for production of L-lysine (Becker et al., 2010) and L-ornithine (Kim et al., 2014) with *C. glutamicum*, since it favours the pentose phosphate pathway (PPP) over glycolysis, thus generating increased amounts of NADPH, which are required for both mentioned amino acid pathways. Since pgi^{GTG} was able to improve $Y_{P/S}^{his}$ in the *C. glutamicum* HIS10 background, however not in strain *C. glutamicum* CM1, the increase in $Y_{P/S}^{his}$ most likely is connected to a combination of improved PRPP precursor supply (as result of pgi^{GTG}) together with the PurA/PurB and GCV overproduction background. It appears that in strain *C. glutamicum* CM1 the beneficial effect of pgi^{GTG} was superimposed by the graver fTHF and IMP/adenylosuccinate limitations. To my knowledge, it has not been advised whether flux towards PRPP in *C. glutamicum* is provided via the oxidative (NADPH-generating) part of the PPP or via the non-oxidative part. In an inosine producing mutant of the close *C. glutamicum* relative *C. ammoniagenes*, *zwf* was interrupted in order to provide increased amounts of ribose 5-phosphate via the non-oxidative PPP, which led to decreased production of inosine (Kamada et al., 2003). Overproduction of transketolase (Tkt, encoded by *tkt*) and transaldolase could not improve production in the *zwf* deficient background (Kamada et al., 2003). In contrast to that, deletion of the *tkt* gene improved production of inosine (Kamada et al., 2001). Consistent with that, it was shown that increased activity of Tkt is beneficial for production of aromatic amino acids (Ikeda et al., 1999) and it was suggested that diminished activity or deficiency of Tkt might be beneficial for L-histidine production (Ikeda, 2003), requiring the same precursor as inosine production. However, several modifications aiming at decreasing Tkt activity (in strains *C. glutamicum* HIS3, HIS4, HIS6) including *tkt* deletion, deletion of the RBS, and deletion of the extended RBS did not improve L-histidine production. Again, these modifications might be expedient when applied in the *C. glutamicum* HIS10 background.

Since it remained unclear to what exact extent the carbon flux towards PRPP is directed through the oxidative vs. the non-oxidative PPP, we constructed several mutant strains with attenuations most likely leading to different flux patterns. As alternative to the pgi^{GTG} variant (described above), the translational start codons of the *gapA* (encoding glyceraldehyde 3-phosphate dehydrogenase) and the *pgm* (encoding phosphoglucomutase) genes (Omumasaba et al., 2005; Seibold and Eikmanns, 2013) were exchanged from the native ATG to the rare variant TTG.

Compared to *pgi*^{GTG}, *gapA*^{TTG} was intended to direct carbon through the non-oxidative PPP towards PRPP, whereas *pgm*^{TTG} was intended to retain carbon downstream of the junction towards the SHMT reaction, leaving sufficient carbon for C_1 generation. These modifications were tested in different strain backgrounds. All three were introduced in the *C. glutamicum* HIS7 background, resulting in strains HIS7.1, HIS7.2, and HIS7.3. In this scenario, only the *gapA*^{TTG} exchange manifested in improved $Y_{P/S}^{his}$ (+9%), whereas *pgi*^{GTG} and *pgm*^{TTG} did not improve $Y_{P/S}^{his}$. When the exchanges were implemented in the *C. glutamicum* HIS9 background, only *pgi*^{GTG} improved $Y_{P/S}^{his}$ (+8%), whereas *gapA*^{TTG} and *pgm*^{TTG} resulted in lower $Y_{P/S}^{his}$ (-11% and -6%, respectively). It seems that these different results in the different strain backgrounds reflect the complexity of carbon fluxes in the generated L-histidine production scenario. The finding that the *purApurB* overexpression in *C. glutamicum* HIS8 balanced the intermediates in the purine pathway and that this did not increase $Y_{P/S}^{his}$, whereas $Y_{P/S}^{his}$ was only increased after combined overproduction of PurA/PurB and the GCV system indicates the complexity of limitations in L-histidine production. Limitations seem to superimpose each other and solving one must not necessarily solve a knot but rather expose further limitations.

One of these limitations, however, is the supply with C_1 units. For future experiments, the allocation of C_1 units might be generated by attenuating or deleting the gene encoding L-serine dehydratase (L-serDH, encoded by *sdaA*), which converts L-serine to pyruvate, thus competing with the C_1 generating SHMT for L-serine (Netzer et al., 2004). Additionally, cystathionine β-lyase was identified to consume L-serine (Kim et al., 2001; Netzer et al., 2004), however, to a lesser extent than L-serDH, which should be considered for future L-histidine producer strains. Generating a surplus of L-serine by supplementing the amino acid in growth experiments with strain *C. glutamicum* CM1 did not result in altered growth and production characteristics, despite the amino acid was consumed from the medium (data not shown), which has been demonstrated before, where *C. glutamicum* cometabolized L-serine with glucose (Netzer et al., 2004). As mentioned above, overexpression of *glyA* might be more expedient in this case.

In further studies, modifications in the two PPP enzymes glucose 6-phosphate dehydrogenase (G6P DH, encoded by *zwf*) and 6-phosphogluconate dehydrogenase (6PG DH, encoded by *gnd*) were examined for their suitability for L-histidine production. It has been shown that G6P DH is allosterically inhibited mainly by NADPH, however, oxaloacetate, fructose-1,6-bisphosphate, and PRPP were also identified as inhibitors (Eggeling and Bott,

2005). 6PG DH was shown to be inhibited by NADPH, fructose-1,6-bisphosphate, ribulose 5-phosphate, glyceraldehyde 3-phosphate, and erythrose 4-phosphate (Eggeling and Bott, 2005). For both enzymes, desensitized variants are available in *C. glutamicum*, namely *zwf*^{A243T} and *gnd*^{S361F}, which both have been deployed for amino acid production with the aim to strengthen the flux through the oxidative PPP before (Georgi et al., 2005; Ohnishi et al., 2005). In a sequential approach we first implemented *zwf*^{A243T}, which increased $Y_{P/S}^{his}$ in *C. glutamicum* CM2 compared to the parental strain by 16%. Most likely this can be attributed to the release from feedback inhibition of G6P DH from NADPH and PRPP, since by strengthening the PPP flux via *pgi*^{GTG}, these two molecules are generated in increased amounts. The *zwf*^{A243T} modification represents an interesting regulating screw to be modified in *C. glutamicum* HIS10, where energy metabolism and C_1 supply are optimized. The second modification, *gnd*^{S361F}, however, did not prove beneficial, since the resulting strain *C. glutamicum* CM2.1 had 24% lower $Y_{P/S}^{his}$ compared to its parental strain *C. glutamicum* CM2. It remains unclear why a combination of both desensitized variants is not beneficial for L-histidine production. So far, these two oxidative PPP modifications have not been implemented in row, wherefore a comparison is not possible.

Besides *zwf* and *gnd*, the *prsA* gene, encoding the PRPP synthetase, was targeted. PRPP synthetase is a key enzyme since it provides PRPP for several reactions (reviewed in Hove-Jensen et al., 2016 and Jensen et al., 2008). The *C. glutamicum* enzyme has not yet been investigated in detail, however, there are intensive data for PRPP synthetases from other bacteria available, such as *E. coli* (Hove-Jensen et al., 1986), *S. typhimurium* (Post and Switzer, 1991; Switzer and Gibson, 1978), and the *C. glutamicum* relative *M. tuberculosis* (Alderwick et al., 2011). PRPP synthetase transfers the diphosphoryl group from ATP onto ribose 5-phosphate, releasing AMP and PRPP in a Mg^{2+} and P_i dependent manner and is allosterically inhibited by ADP as the most potent allosteric inhibitor in all these bacterial species. PRPP synthetase obviously has the potential of a regulating screw since it provides the crucial L-histidine precursor PRPP. Thus, we aimed to release PRPP synthetase from its regulatory mechanisms. There are mutant variants of PRPP synthetase available in different organisms wherefrom we chose the three amino acid exchanges R78C, elevating the K_m towards ATP and ribose 5-phosphate and reducing sensitivity for ADP inhibition , D115S, desensitizing PRPP synthetase against purine nucleotide inhibition, and D128A, leading to higher K_m value towards ATP and releasing PRPP synthetase from AMP inhibition (Klyachko et al., 2004b). These patents applied the PRPP synthetase variants for L-histidine

production with *Entereobacteriacea*. Therefore, the amino acid exchanges were transferred from the *E. coli* enzyme onto the *C. glutamicum* enzyme via BLAST analysis (data not shown), which led to the three amino acid exchanges R87C, D122S, and D136A. After several attempts to implement the respective nucleotide exchanges in the *prsA* gene of *C. glutamicum*, only the one leading to D122S could be established, indicating that amino acids arginine at position 87 and aspartate at position 136 are essential for PRPP synthetase functionality in *C. glutamicum*. The D122S variant was established in *C. glutamicum* CM1, resulting in *C. glutamicum* CM3, which had stable growth rate and biomass substrate yield and improved $Y_{P/S}^{his}$ by 11%. This underlines the potential of PRPP synthetase as target for L-histidine production with *C. glutamicum* and mutations thereof might be introduced in *C. glutamicum* HIS10 with balanced purine and L-histidine pathways and improved C_1 supply in future experiments.

Further modifications were introduced in the purine biosynthesis with the objective to elucidate the potential of this pathway for increasing $Y_{P/S}^{his}$. Since PurF, the first enzyme in the purine pathway, competes with HisG for the common precursor PRPP, we intended to decrease the overall PurF activity to leave increased amounts of PRPP for the HisG reaction. Therefore, we pursued two approaches in which we firstly deleted the *purF* gene and exchanged its translational start codon from GTG to TTG. The resulting strains *C. glutamicum* PUR1 and PUR2 showed very similar phenotypes and were characterized by strong decreases in growth rate (half the one of *C. glutamicum* CM1) and biomass substrate yield (below half the one of *C. glutamicum* CM1). However, the $Y_{P/S}^{his}$ only decreased by about 12% and 13%, respectively. In bacteria, an important moiety for thiamine biosynthesis originates from the purine intermediate AIR (Begley et al., 2012). To exclude thiamine interferences caused by modifying the entry flux into the purine pathway by a *purF* deletion/attenuation, we supplemented *C. glutamicum* PUR1 with thiamine, which was not able to compensate the growth defect. Supplementations of *C. glutamicum* PUR2 with adenine (plus thiamine) increased the growth rate by 52% (52%) and strongly increased biomass substrate yield by 155% (140%). However, no effect on $Y_{P/S}^{his}$ was detected. These experiments indicate that (i) the exchange of the translational start codon from GTG to the rarest variant TTG in *purF* is an intrusion that resembles an in-frame deletion of the gene, heavily impacting cells, and (ii) that *purF* is not essential since *C. glutamicum* PUR1 can grow in minimal medium w/o supplementations. ATG is the most common translational start codon in *C. glutamicum*, being present in 72% of all cases, whereas GTG (21%) and TTG (7%) occur less often (Becker et al., 2010). For *purF* deletion mutants of *S. typhimurium* it was suggested that an alternative way to form PRA, the

product of PurF, exists (Downs and Roth, 1991). This potential alternative route might also exist in *C. glutamicum*. Interestingly, the supplementation of *C. glutamicum* PUR2 with adenine did not result in increased $Y_{P/S}^{his}$ but increased growth rate and biomass substrate yield strongly, indicating that the additonal carbon provided by adenine is directly used for biomass formation and not for product formation. Adenine supplementation for a butanol producing *Clostridium saccharoperbutylacetonicum* strain was shown to strongly increase the growth and simultaneously increasing product formation (Kiyoshi et al., 2017). The third *purF* modification included the feedback released variant K348Q (K326Q in *E. coli*) that had been characterized in *C. glutamicum* (Peifer et al., 2012) and *E. coli* (Zhou et al., 1993) before. The mutant strain *C. glutamicum purF*^{K348Q} had been deployed for IMP production and resulted in increased intracellular concentrations of AMP and adenine by about 25%, respectively (Peifer et al., 2012). The here constructed strain *C. glutamicum* PUR3 was characterized by a lower growth rate, biomass substrate yield, and $Y_{P/S}^{his}$ compared to its progenitor *C. glutamicum* CM1, suggesting that the potentially increased adenine and AMP concentrations where not a limiting factor in this strain background. This might have to do with increased amounts of PRPP that are withdrawn into purine biosynthesis, instead of L-histidine biosynthesis and renders *purF*^{K348Q} uninteresting for L-histidine production.

Further studies in the *de novo* part of the purine pathway focused on the fTHF requiring reactions of PurN and PurH. In an attempt to circumvent the PurN reaction, the respective *purN* gene was deleted in *C. glutamicum* WT to investigate if PurT (performing the reaction step w/o fTHF, instead using formate as formyl group donor) is able to take over the PurN reaction (Nagy et al., 1993; Nygaard and Smith, 1993; Saxild et al., 1995). Radioactive tracing experiments had revealed that when both PurN and PurT are present in an organism, here in *E. coli*, the completely synthesized purine molecule in 50% of the cases contained a carbon atom at position C8 originating from the PurN reaction, in the other 50% of the cases it originated from the PurT reaction (Dev and Harvey, 1982), suggesting an even usage between both reactions in *E. coli*.

However, the resulting strain *C. glutamicum* Δ*purN* showed a strong growth defect in minimal medium. Supplementation with adenine was partially able to compensate the growth defect, however, failed to revert growth to *C. glutamicum* WT niveau. To support PurT with its cofactor, *C. glutamicum* Δ*purN* was supplemented with formate, which was not able to compensate the strong growth defect. This either indicates that the PurT activity is too low to compensate a *purN* deletion or that formate as cofactor for PurT is limiting. In *S. typhimurium*

it had been shown that a *purN* deletion caused a 50% reduced *in vivo* multiplication rate, whereas a *purT* deletion did not (Jelsbak et al., 2016). With the purpose to increase intracellularly available formate, we deleted the formate dehydrogenase gene *fdhF* in *C. glutamicum* Δ*purN*, which was shown in *C. glutamicum* to abolish formate dehydrogenase activity (Witthoff et al., 2012). Since *C. glutamicum* Δ*purN* Δ*fdhF* had a similar growth phenotype as its parental strain, even with formate supplementation, we concluded that supply with the cofactor is not limiting the PurT reaction. Further studies in this direction might include overexpression of the PurT gene in *C. glutamicum* Δ*purN* Δ*fdhF* and if feasible, apply this scenario in a strain with L-histidine production background. Besides PurT, another source for the formate dependent generation of fTHF exists in some bacteria, constituted by formate-THF ligase (Fhs), encoded by the *fhs* gene (Aluri et al., 2015; Sah et al., 2015). Both genes *purT* and *fhs* are anticorrelatively present in bacterial genomes, meaning only one of both is encoded in the vast majority of bacteria (Aluri et al., 2015). Fhs catalyses the transfer of a C_1 unit from formate to THF, requiring ATP (Celeste et al., 2012; McGuire and Rabinowitz, 1978). A potential idea for further studies could be the heterologous expression of a (codon optimized) *fhs* gene in an L-histidine producer with *purN* deletion, to enforce the allocation of additional C_1 units.

Besides the PurN reaction in the third step of the purine biosynthesis, the tenth step is also fTHF dependent in bacteria, where the formylation of AICAR to FAICAR is catalysed by PurH (which also performs a cyclohydrolase reaction in step eleven). In archaea, steps ten and eleven in the purine biosynthesis are not mediated by one enzyme, but rather by two (reviewd in Brown et al., 2011). In the tenth step, the formylation of AICAR is mediated in absence of folates instead relying on formate as formyl group donor by an enzyme entitled PurP (Zhang et al., 2008) and then the cyclohydrolase reaction is performed by an enzyme entitled PurO (Graupner et al., 2002; Ownby et al., 2005). In the case that the supply with C_1 units indeed is one of the limiting factors for L-histidine production in *C. glutamicum*, future approaches might include the deletion of the native *purH* gene in *C. glutamicum* and the heterologous (codon-optimized) expression of archaeal *purO* and *purP* genes. Cumulatively, this could be done on top of the deletion of *purN* combined with the heterologous expression of a *fhs* gene in an L-histidine production background and could enable a complete relief of the purine *de novo* biosynthesis from the SHMT (and GCV system) reactions in *C. glutamicum* (and *C. glutamicum* HIS10), thus decoupling L-histidine biosynthesis from L-serine/glycine, i.e. C_1 metabolism.

Purine biosynthesis in *E. coli* is regulated by a purine regulatory protein, named PurR, that specifically binds to a motif in the operator region of the *purF* gene, repressing its expression, and in this way controlling the entry flux into *de novo* part of the purine biosynthesis, further autoregulating its own synthesis (He et al., 1990; Meng et al., 1990; Rolfes and Zalkin, 1988). Moreover, high-resolution chromatin immunoprecipitation (ChIP)–chip experiments revealed that genes beyond the purine pathway are regulated by PurR, e.g. genes encoding enzymes of the pyrimidine pathway (Cho et al., 2011). Existence of purine regulatory proteins has also been revealed in Gram-positive organisms, such as *B. subtilis* (Bera et al., 2003; Saxild et al., 2001; Shin et al., 1997) and *Lactococcus lactis* (Beyer et al., 2003; Kilstrup and Martinussen, 1998). Due to the interconnectivity of the purine pathway and its strong influence on energy metabolism and other pathways, PurR is an attractive target for strain engineering. Logically, PurR has been chosen as target for, e.g. riboflavin production with *B. subtilis* (Shi et al., 2014) and interestingly also for L-histidine production with *E. coli* (Doroshenko et al., 2013). In the latter case, the *purR* gene was deleted leading to increased biomass formation while maintaining stable L-histidine production (Doroshenko et al., 2013). However, a gene encoding a purine regulatory protein has not been identified in *C. glutamicum* to my knowledge. BLAST analysis (data not shown) with the purine regulators of *B. subtilis*, *L. lactis*, and *E. coli* with *C. glutamicum* regulatory proteins identified potential candidates, among them cg2314 (annotated as transcriptional regulator, LacI family; annotation from https://coryneregnet.compbio.sdu.dk/v6/index.html, last access 15-08-2018). The respective gene was deleted in *C. glutamicum* CM1, but the resulting strain did not show an altered growth phenotype or production behaviour. The task to identify further potential purine regulators in *C. glutamicum* and exploring their potential for L-histidine production should be tackled in future experiments and might consider the additional identified regulatory proteins (3.1.11 A versatile toolbox enables deeper insights, p.121).

The best producer strain in a laboratory scale is useless for industrial demands if it does not perform in a larger scale, which commonly includes the transfers to a pilot and further to an industrial scale (Delvigne and Noorman, 2017; Reisman, 1993; Thiry and Cingolani, 2002). *C. glutamicum* is well known as industrial production host and several processes with industrial scales are established, such as for the production of L-glutamate, L-lysine, and L-methionine (Becker and Wittmann, 2012; Ikeda, 2003; Wendisch et al., 2016). However, the phenomenon that production hosts show poor performances in a larger scale, despite performing well in a laboratory scale, is known (Delvigne and Noorman, 2017; Gonçalves et al., 2014).

Since the L-histidine producers constructed in this work were standardly evaluated in a shaking flask approach, we transferred this process to small scale fermentations in glass reactors and further into medium scale steel tank reactors (STR), to enable first insights in the performance potential of these strains. It has to be mentioned that several conducted processes were not performed as triplicates, meaning that to secure the obtained results of the here presented preliminary experiments, they need to be replicated and reproduced in upcoming experiments. Nevertheless, these preliminary fermentations enabled fast insights into the performance characteristics of the L-histidine producers. In the standard reactor medium, $CGXII^{R}$, *C. glutamicum* HIS7 and CM2 showed increased growth rates (by 11% and 37%), whereas the $Y_{P/S}^{his}$ of both strains decreased (by 47% and 28%) in reactor cultivations compared to shaking flask cultivations. The faster growth in the reactor might be attributed to the increased supply with oxygen, which has been shown to constitute a limiting factor in shaking flask cultivations (Klöckner and Büchs, 2012; Losen et al., 2004; McDaniel and Bailey, 1969). With the purpose to elucidate the influencing factor(s) responsible for the decreased product formation in reactor cultivations, we conducted experiments investigating the composition of the medium, the pH value, and the oxygen supply.

Cultivations with different media compositions, including the components urea and MOPS into the $CGXII^{R}$ reactor medium, showed that both had no influence on the examined characteristics growth rate, $Y_{X/S}$, $Y_{P/S}^{his}$, and $Y_{P/S}^{gly}$, when included as sole addition or in a combination of both (equalling the $CGXII^{N}$ medium). Consecutively, urea and MOPS were ruled out as influencing factor(s) for decreased $Y_{P/S}^{his}$. Cultivations with different pH values and with disabled pH regulation indicated that *C. glutamicum* can grow and produce at pH values of 6.25 and 8.00. Growth was strongly affected at pH value 8.25. These findings only partially match published data, where stable pH homeostasis of *C. glutamicum* was found at pH values between 6 and 9 (Follmann et al., 2009). The same study revelead 2.3× increased amounts of intracellular L-histidine in *C. glutamicum* grown in medium with pH 6 compared to pH 7.5 (Follmann et al., 2009). Interstingly, the reactor cultivation performed at a fixed pH value of 8.00 revealed a strongly diminished growth rate and however stable $Y_{P/S}^{his}$, compared to the standard $CGXII^{R}$ cultivation with a pH value at 7.4, indicating potential applications of high pH values for further fermentations. Nevertheless, $Y_{P/S}^{his}$ was diminished in all reactor cultivations in whiche the pH as influencing factor was investigated, pointing towards other factor(s) that are responsible for the altered behaviour in reactor cultivations vs. shaking flask cultivations.

The third investigated factor was oxygen supply, a known limiting factor in the shaking flask system (as mentioned above). To mimick the shaking flask cultivations, oxygen limitations where induced after defined time points during cultivation. However, the results showed that limiting the oxygen supply is not beneficial for L-histidine production at all. Despite the growth rate and $Y_{X/S}$ of *C. glutamicum* CM2 were stable in all these experiments and resembled the values obtained in the standard reactor cultivation, the $Y_{P/S}^{his}$ decreased significantly (as low as by 58%). However, it might as well be that the induced oxygen deprivations were to harsh and that the oxygen limitations potentially occurring in the shaking flask system are less severe and occur in a more fluent manner.

The factor(s) that are responsible for the higher $Y_{P/S}^{his}$ in the shaking flask system remain unknown and will have to be revealed in further experiments. Nevertheless, we were able to establish a functional seed train and first bioprocesses with selected strains of the strain database constructed in this work. It might as well be that the combination of these factors leads to the different production behaviour in the shaking flask system.

With the knowledge of the small scale fermentations and with the established seed train as basis, we performed first STR fermentations in a steel tank reactor with a medium volume of 10 L and cultivated *C. glutamicum* CM2 in batch mode. Here, we identified protocatechuic acid (PCA) as an essential component for growth of *C. glutamicum* CM2 in this scenario, in contrast to shaking flask and small scale fermentation scales.

Why PCA addition is required for the 10 L cultivations and not in the small scale cultivations remains unknown. PCA has been shown to increase growth rates in reactor cultivations, which was connected to the iron metabolism, however, it is not an essential component in *C. glutamicum* WT for growth in reactor cultivations (Liebl et al., 1989; Unthan et al., 2014).

Unfortunately, fermentation data for L-histidine producing strains of *C. glutamicum* are lacking in the available literature. The available data focusing on cultivations in reaction tubes / shaking flasks of L-histidine producers however show that all deployed strains require expensive and complex components for growth and production, such as yeast and meat extract (Araki and Nakayama, 1974; Cheng et al., 2013; Doroshenko et al., 2013), uracil (Chim-Anage et al., 1991), or adenosine (Doroshenko et al., 2013; Malykh et al., 2018). Therein lies an advantage of the constructed strains in this work, since they do not require additional supplements besides glucose as carbon source in the deployed CGXII minimal medium to grow and produce L-histidine. Since the batch and fed-batch processes represent preliminary bioprocesses, they will not be discussed thoroughly. They are ment to represent a basis for

potential expansion of the L-histidine project and might serve as first points of references for future experiments. Nevertheless, it became obvious that the strains we cultivated in bioprocesses were not able to achieve the same product substrate yields found in shaking flask cultivations. To elucidate where these differences come from and how to tackle them will remain tasks for future experimenters.

Taken together, the applied interplay of strain engineering, metabolomics (SMP), and model-based analysis (FBA) enabled a comprehensive view on the complex metabolic network of the L-histidine biosynthesis. Engineering of the purine pathway identified and reinforced the intrinsic low ATP regeneration capacity to maintain the balanced energy state of the cell. To utilize the readjusted ATP levels for L-histidine production, it was essential to provide C_1 units in adequate amounts, which was accomplished by overproduction of a GCV system. Further, AICAR, which seems to be a potent effector molecule to control the entry flux into L-histidine biosynthesis, was identified as future regulating screw.

4.2. Part II

Genetic variation i.e. the variability of an organism's genetic information is one of biology's basic principles and a source for new life forms and a major factor of influence for what is known as evolution in the sense of Charles Darwin. This principle has been exploited since the beginnings of modern biotechnology for the breeding and selection of prokaryotic and eukaryotic unicellular producer organisms. In the classical way, mutagenizing substances, such as N-methyl-N'-nitro-N-nitrosoguanidine (NTG) and ethylmethanesulfonate (EMS), or radiation, such as ultraviolet (UV) light, were/are used to stimulate such genetic variations in this way accelerating evolution (Burns et al., 1986; Delić et al., 1970; Doudney and Young, 1962; Ekwall and Thon, 2017; Foster, 1991; Sega, 1984; van Zeeland et al., 1983). By this, the natural spontaneous mutation frequency (4×10^{-10} for *E. coli*) can be accelerated to magnitudes above this (Parkhomchuk et al., 2009). The creation of genetic diversity in huge libraries of mutants are the results of these experiments and single cells often bear up to hundreds of mutations after mutagenic treatment (Harper et al., 2011; Parkhomchuk et al., 2009). With the purpose to identify the mutations responsible for the phenotype of the mutant, e.g. improved concentrations of the desired product, sophisticated and often time-consuming screening strategies are needed (Harper et al., 2011; Zhou and Alper, 2018). These undirected and random mutagenesis approaches were in the last decades further developed towards more directed and targeted approaches, often entitled as directed evolution, due to the acceleration of the Darwinian principle of evolution without resorting to mutagenizing substances (Cobb et al., 2013b; Harper et al., 2011). Combined with new techniques of improved screening technologies, such as biosensor strains or high-throughput screenings, undirected and directed evolution approaches have made great progress (Dietrich et al., 2010; Eggeling et al., 2015; Lin et al., 2017; Zhou and Alper, 2018). However, most available evolution approaches create a variety of mutations per cell, requiring intense screenings.

We here conceived a method we entitled Metabolic engineering to Guide Evolution (MGE) that relies on creating intrinsic evolutionary pressure and deliberately omits mutagenizing agents. By this we intended to generate a minimal set of mutations to enable a simplified identification of the phenotype-generating mutation(s), which is the most time-consuming and laborious step in evolution approaches (Harper et al., 2011). In a first step, we conceived how to generate the evolutionary pressure. An abundance of methods for generating genetic diversity in single cell

organisms is available, which comprise beyond the mentioned mutagenizing approaches also methods like error-prone PCR (McCullum et al., 2010; Wilson and Keefe, 2001), DNA shuffling (Cohen, 2001; Zhao and Arnold, 1997), sequence saturation mutagenesis (Wong et al., 2004), synthetic shuffling (Ness et al., 2002; Zha et al., 2008), just to name some of the available ones (reviewed in Kumar and Singh, 2013). These methods allow the targeted improvement of traits like biocatalysts (Turner, 2009), biosynthetic pathways (Atsumi and Liao, 2008), and regulatory networks (Yokobayashi et al., 2002).

We here relied on the generation of an intrinsic evolutionary pressure by applying metabolic engineering in *C. glutamicum* and aimed at identifying and evolving a novel metabolic mode for production of L-valine. The production of L-valine with *C. glutamicum* has been intensively studied and exploited to generate producer strains (reviewed in Oldiges et al., 2014; Wang et al., 2018). So far, metabolic engineering of the L-valine biosynthesis in *C. glutamicum* mainly relied on redirecting carbon fluxes towards the endproduct by targeting the pyruvate dehydrogenase complex (PDHC), which generates acetyl-coenzyme A (acetyl-CoA) from pyruvate (Oldiges et al., 2014). This was either achieved by a complete inactivation or an attenuation of the PDHC, by deletion of the *aceE* gene or reduction of its promoter activity (Blombach et al., 2009, 2008, 2007; Buchholz et al., 2013). Further strategies comprised the application of anaerobic conditions to reduce tricarboxylic acid (TCA) cycle activity (Hasegawa et al., 2013; Satoshi Hasegawa et al., 2012) and the inactivation or attenuation of pantothenate biosynthesis to limit availability of coenzyme A, which is required for acetyl-CoA formation through the PDHC (Bartek et al., 2008; Elišáková et al., 2005; Holátko et al., 2009; Radmacher et al., 2002).

With the purpose to generate a basis strain for the following evolutionary experiments, we created the double deletion mutant strain *C. glutamicum* Δ*ppc* Δ*pyc*. By deleting the genes for PEP carboxylase and pyruvate carboxylase, we aimed at increasing the flux over the PDHC to the disadvantage of oxaloacetate formation. Generally, during growth on glycolytic substrates (such as the standardly used glucose), the glyoxylate shunt is inactive in *C. glutamicum* and the anaplerotic carboxylation of either PEP or pyruvate to replenish the TCA with oxaloacetate is mediated by PEPCx and/or PCx (Sauer and Eikmanns, 2005). In contrast to several other bacteria like *E. coli* (Morikawa et al., 1980) and *Bacillus subtilis* (Diesterhaft and Freese, 1973), *C. glutamicum*, possesses both a PEPCx and a PCx. Although PEPCk activity is present in *C. glutamicum* during growth on glucose (Riedel et al., 2001) and is in principle reversible (Jetten and Sinskey, 1993; Klaffl et al., 2013), *C. glutamicum* Δ*ppc* Δ*pyc* is unable to grow on

glucose (Peters-Wendisch et al., 1998). However, since the PEPCk reaction has been shown to be bifunctional in some organisms, e.g. *Alcaligenes eutrophus* (Schobert and Bowien, 1984) and since a mutated PEPCk enabled growth of an evolved *Saccharomyces cerevisiae* Δ*pyc1* Δ*pyc2* strain on glucose (Zelle et al., 2010), we additionally constructed *C. glutamicum* Δ*ppc* Δ*pyc* Δ*pck* as a second basis strain. This was done to avoid potentially occurring mutations in the *pck* gene during evolution, i.e. to eliminate the *pck* gene as evolutionary target in this scenario. However, mutated variants of the *pck* gene in the two evolved *C. glutamicum* Δ*ppc* Δ*pyc* strains (Evo1.1 and Evo1.2) were not observed.

Evolution strives to optimize growth, which basically restricts the outcome of evolutionary experiments and enables the prediction of theoretical flux distributions by FBA (Motter et al., 2008) or its variants such as MOMA (Segrè et al., 2002) and OptReg (Pharkya and Maranas, 2006). With the purpose to predict the evolvability of the constructed basis strains, André Feith conducted FBAs of *C. glutamicum* Δ*ppc* Δ*pyc*. Therefore, the reactions of PEPCx and PCx were deleted from the metabolic model (Zhang et al., 2017) and optimized for growth. Indeed, in the here presented study, FBA predicted the most expectable result of the evolution, i.e. the activation of the glyoxylate shunt to compensate for the missing oxaloacetate-forming carboxylase reactions, thereby enabling growth of *C. glutamicum* Δ*ppc* Δ*pyc*. Thus, our study is one of the rare examples exploiting the potential of evolution by constraining solutions with target-oriented metabolic engineering approaches (Auriol et al., 2011).

With the anticipation that growth of *C. glutamicum* Δ*ppc* Δ*pyc* in general should be possible, we performed preliminary growth experiments in minimal media to identify a suitable evolutionary environment, which potentially plays a role for the outcome of the experiment (Dykhuizen, 1990). In minimal medium with glucose as sole carbon source, both *C. glutamicum* Δ*ppc* Δ*pyc* and *C. glutamicum* Δ*ppc* Δ*pyc* Δ*pck* were not able to grow, as has been reported before (Peters-Wendisch et al., 1998). However, when a small amount of yeast extract was added to the medium, at least the double deletion mutant showed minimal growth. It needs to be clarified in further experiments, why the triple deletion mutant showed stronger impaired growth compared to the double deletion mutant, since a *C. glutamicum* Δ*pck* mutant has been reported to show no growth defect on minimal medium with glucose (Riedel et al., 2001). We regarded growth as prerequisite for evolutionary experiments, since we intended to deploy increasing biomass concentrations, i.e. reproduction, as the screening indicator. Having defined the boundaries of the planned scenario, we cultivated the double and

triple deletion mutants in minimal medium with glucose and yeast extract and transferred defined amounts of biomass every three to four days, respectively, to clear the medium from potentially growth inhibiting compounds and supply the cells with all factors needed for growth. Increasing biomass concentrations (as the results of evolutionary events) were observed for the double deletion mutant after 14 and 15 d, respectively, and for the triple deletion mutant after 33 d. The delayed occurrence of increasing biomass concentrations for the triple deletion mutant compared to the double deletion mutant might reflect the stronger impaired growth of the basis strain. The evolved strains were isolated by plating dilutions on semi-solid agar media and tested for improved growth characteristics in the evolutionary medium. Evo1.1 and Evo1.2 showed distinctly faster growth compared to their initial strain *C. glutamicum* Δ*ppc* Δ*pyc*. Compared to Evo1.1 and Evo1.2, Evo2 showed slower growth, although it now was able to grow, compared to its basis strain *C. glutamicum* Δ*ppc* Δ*pyc* Δ*pck*. Having isolated the evolved strains and having confirmed their improved growth phenotypes, we proceeded by re-sequencing their genomes. This was done in a whole genome sequencing (WGS) approach at the CeBiTec (Bielefeld University) and allowed us to compare the genomes of *C. glutamicum* WT and the evolved strains. By deliberately omitting the application of mutagenic agents, the evolutionary approach resulted in a neat set of mutations per cell (as was intended), yielding two strains with each three mutations and one strain with six mutations (Table 35, p.148). These numbers are far below the numbers of mutations per single cell that are generated with classical evolutionary approaches, which often result in >100 mutations per single cell (Harper et al., 2011; Parkhomchuk et al., 2009). With this neat set of mutations, we built the mutational intersection of the three evolved strains to identify shared targets of the evolutionary approach. The mutational intersection in our case only yielded one relevant target that was affected by mutations in Evo1.1, Evo1.2, and Evo2, namely the *icd* (cg0766) gene, encoding the isocitrate dehydrogenase (ICD). ICD is a key enzyme of the TCA cycle, generating NADPH from $NADP^+$ by oxidatively decarboxylating isocitrate to α-ketoglutarate and CO_2, thus supporting the cell with reducing equivalents and precursors (Eikmanns et al., 1995). The genomic alterations (i.e. single nucleotide polymorphisms [SNPs]) in *icd* led to three amino acid exchanges in ICD, respectively. These SNPs were then introduced in the basis strain *C. glutamicum* Δ*ppc* Δ*pyc* and resulted in three re-engineered strains, with the three different amino acid exchanges A94D, R453C, and G407S. With the purpose to understand the underlying effects of these exchanges (mutations), we measured the specific enzyme activities of the three ICD variants and found that all three variants showed

drastically lower activities than the native enzyme. It has been reported that the specific enzyme activity of ICD is 1 U mg^{-1} protein, regardless of the carbon source (Eikmanns et al., 1995; Wendisch et al., 1997), reflecting the value we obtained for *C. glutamicum* WT. In a metabolic engineering approach Becker et al. targeted the TCA cycle by exchanging the native translational start codon of ICD (ATG) with GTG, which resulted in about 70% decreased ICD activity and increased L-lysine production (Becker et al., 2009). However, this was correlated to a shift of the TCA cycle towards anaplerotic carboxylation and not to connected with a potential activation of the glyoxylate shunt (Becker et al., 2009). The idea that isocitrate might be metabolized via the glyoxylate shunt in an strain with low ICD activity, i.e. *C. glutamicum* Δ*icd* mutant, has been mentioned before (Baumgart et al., 2011). With the purpose to test this hypothesis in relation to the re-engineered strains and nurtured by the FBA result, we measured isocitrate lyase (ICL) and malate synthase (MS) activites. Results for *C. glutamicum* WT showed that no activities for both enzymes were present in minimal medium with glucose (and L-glutamate). This is in accordance with published data, since it was shown before that ICL and MS activities are absent in *C. glutamicum* in glucose-based minimal medium (Reinscheid et al., 1994b, 1994a). In contrast, specific activities of ICL and MS were present in all three re-engineered strains, thus showing that ICD mutations activate the glyoxylate shunt.

Besides the *icd* gene as shared target in the three evolved strains, mutations were found in two genes with yet unknown function (cg0466, cg1793) and four genes (*glgE*, *msiK1*, *benR*, *ptsF*) encoding enzymes of the carbohydrate metabolism. Interestingly, we found a SNP and a 12 bp deletion in *ptsF* (cg2120), encoding the fructose-specific EIIABC permease of the PEP-dependent phosphotransferase system for fructose (PTS^{Fru}), which had evolved independently. Both mutations led to a defective PTS^{Fru}, since strains Evo1.1 and Evo1.2 (in both *ptsF* was affected) showed impaired growth on fructose compared to glucose (data not shown). Recently, Δ*pfkB*-suppressor mutants were characterized with a deletion of the *ptsF*-operon gene *pfkB,* which regained growth on sucrose (Wang et al., 2016). Subsequently, they found a 12 bp deletion in *ptsF*, which overlaps with our identified 12 bp *ptsF* deletion in 8 bp. Quantification of intracellular sugar phosphates of a sucrose grown *ptsF* mutant revealed strongly reduced levels of glucose 6-phosphate (72 %), fructose 6-phosphate (84 %) and fructose 1-phosphate (below detection limit) compared to the wildtype strain (Wang et al., 2016). Interestingly, our re-engineered strain *C. glutamicum* Δ*ppc* Δ*pyc* ICD^{G407S} also showed significant reduced intracellular glucose 6-phosphate (40%) and

fructose-1,6-bisphosphate (20%) pools compared to the wildtype strain. These sugar phosphates represent most relevant effector molecules regulating microbial metabolism and are typically present in low intracellular concentrations during growth on gluconeogenic carbon sources (Engels and Wendisch, 2007; Görke and Stülke, 2008). However, elevated transcriptional levels of genes related to acetate metabolism (e.g. *aceA*, *aceB*, *pta*, *ack*) were not observed in the *ptsF* mutant (Wang et al., 2016). This indicates a different or more complex regulatory pattern to explain the activation of the glyoxylate shunt during growth on glucose in the evolved and re-engineered *C. glutamicum* Δ*ppc* Δ*pyc* strains and might be more likely attributed to the increased intracellular pool sizes of *cis*-aconitate, citrate, and isocitrate, which were exemplary observed in *C. glutamicum* Δ*ppc* Δ*pyc* ICD^{G407S} compared to *C. glutamicum* WT. In accordance with the results of the FBA from André Feith and the determination of significant ICL and MS activities in strains with reduced ICD activity, Baumgart et al. proposed an activation of the glyoxylate shunt in a *C. glutamicum* Δ*icd* mutant to metabolize accumulating isocitrate from glucose (Baumgart et al., 2011). However, since the effector molecules or activity modulating effects of the most relevant regulators of acetate metabolism, RamA and RamB (Cramer et al., 2006; Gerstmeir et al., 2004; Teramoto et al., 2011), are still unknown and since other transcriptional regulators such as GlxR (Kim et al., 2004; Teramoto et al., 2011) and SugR (Engels and Wendisch, 2007; Gaigalat et al., 2007; Tanaka et al., 2008; Teramoto et al., 2011) are involved (Toyoda et al., 2013), the regulatory interplay remains puzzling and requires further investigation to explain the altered flux distributions in the evolved and re-engineered strains.

All three re-engineered strains and the basis strain *C. glutamicum* Δ*ppc* Δ*pyc* needed yeast extract for (minimal) growth in minimal medium. Interestingly, the yeast extract was replaceable by L-glutamate, which was used as a more defined component, compared to yeast extract. In our understanding, this is facilitated by the conversion of L-glutamate by the reaction of glutamate dehydrogenase, which (reversibly) channels the carbon from glutamate into the TCA cycle, in this way enabling the formation of α-ketoglutarate (Börmann et al., 1992). By this, α-ketoglutarate might be further converted in the TCA cycle thus providing initial molecules of oxaloacetate, which serve as acceptor molecules for acetyl-CoA, provided by the PDHC (Bott, 2007). Eventually, the lack of the two oxaloacetate-forming reactions of PEPCx and PCx in the basis and re-engineered strains can be compensated. Since the re-engineered strain had consumed all available L-glutamate after 8 h of cultivation and did not stop growing thereafter, we hypothesized that L-glutamate is needed

to kickstart the TCA cycle in absence of PEPCx and PCx. Accompanied by a decreased activity of the ICD enzyme (in ICD^{G407S}) in combination with the PEPCx and PCx deficiencies, we observed decreased intracellular concentrations of oxaloacetate-derived products, such as L-aspartate, L-lysine, and L-threonine, whereas TCA intermediates upstream of the ICD reaction were increased, such as isocitrate, *cis*-aconitate, and citrate.

For future evolutionary studies it would be interesting to use a *C. glutamicum* Δ*ppc* Δ*pyc* Δ*aceA* Δ*aceB* deletion mutant in an MGE approach. With the additional deletions of the genes encoding ICL and MS, the basis strain for MGE would be deprived of the possibility to activate the glyoxylate shunt by acquiring glyoxylate shunt-activating mutations. It would be fascinating to explore if the metabolism of *C. glutamicum* holds ready other options to compensate for a combined PEPCx and PCx deficiency, besides the here acquired ICD mutations. Options therefor could be the evolution of a native carboxylase enzyme adopting the PEPCx or PCx reaction. This might be facilitated by a carboxylase that forms oxaloacetate but uses different substrates than PEP or pyruvate, respectively. A further evolutionary target in such a scenario could be a decarboxylating enzyme, which gains a mutation that reverts its reaction mechanism.

A further interesting topic for future investigations concerning the re-engineered strains might be the evaluation of the intracellular balances of reducing equivalents, i.e. $NADP^+$/NADPH. In the re-engineered strains, the carbon flux over the NADH- / NADPH-forming reactions catalysed by ICD and 2-oxoglutarate dehydrogenase complex is weakend due to the ICD mutations and thus less NADH / NADPH might be formed due to the active glyoxylate bypass. In several studies *C. glutamicum* has been engineered for production of L-valine and strains are readily available which operate close to the maximal theoretical yield (Blombach et al., 2008; Hasegawa et al., 2012). Besides the overexpression of L-valine biosynthesis genes and mutated variants thereof, a common feature of efficient producer strains is a direct or indirect inactivation or attenuation of the PDHC to improve pyruvate availability for L-valine production (Eikmanns and Blombach, 2014; Oldiges et al., 2014). To engineer a novel basis strain which does not rely on reduced or absent PDHC activity, we applied MGE to evolve *C. glutamicum* Δ*ppc* Δ*pyc* to grow on glucose. The FBA predicted growth of the double deletion mutant by activation of the glyoxylate shunt and an increased flux through the PDHC compared to *C. glutamicum* WT, which might be rerouted towards L-valine. To test this hypothesis, we transformed the strains *C. glutamicum* Δ*ppc* Δ*pyc* carrying the re-engineered *icd* variants with the plasmid pJC4*ilvBNCE*, which was previously applied for L-valine production with

C. glutamicum (Oldiges et al., 2014; Radmacher et al., 2002). *C. glutamicum* Δ*ppc* Δ*pyc* ICDG^{A94D} (pJC4*ilvBNCE*) and *C. glutamicum* Δ*ppc* Δ*pyc* ICDG^{G407S} (pJC4*ilvBNCE*) efficiently produced L-valine from glucose with product yields of 0.20 ± 0.01 and 0.22 ± 0.01 g L-valine per g glucose, respectively, which are about 4 times higher compared to the $Y_{P/S}$ of *C. glutamicum* (pJC4*ilvBNCE*). The $Y_{P/S}$ values of the novel engineered strains compete with already published data for L-valine producers, which are based on reduced or absent PDHC activity (Buchholz et al., 2013) or on an H^+-ATPase deficiency (Wada et al., 2008) but are still improvable. However, we here identified with modulating ICD activity an alternative mode for L-valine production with *C. glutamicum* and created the basis for further research in this direction. To further advance the performance of the presented strains, future work might focus on an adjustment of the NADPH supply, an improvement of the export capacity, or a rescue from feedback inhibition of acetohydroxy acid synthase (AHAS) as previously proved beneficial for L-valine production with *C. glutamicum* and *E. coli* (Oldiges et al., 2014; Park and Lee, 2010).

After having presented and discussed the idea and results of MGE, I want to complete this discussion with an evaluation of MGE as method. Ultimately, MGE relies on an ancient and well-described evolutionary principle, which is called genetic suppression. Genetic suppression is a phenomenon, which reverts phenotypic effects of an already existing mutation by an acquired second mutation at a site distinct from the first one, and is applied to explore gene expression, function, and interaction (Hodgkin, 2005). Even lethal phenotypes might thus be rescued by either a loss-of-function or a gain-of-function mutation (Motter et al., 2008). This process has been described as synthetic rescue (Motter et al., 2008) and represented a driving force to utilize this concept for the here described method of MGE. MGE introduces targeted deletions, thereby generating a suboptimal metabolic state for the cell and reducing or abolishing growth of the microbial host with the aim to create intrinsic selection pressure. This eventually is supposed to guide evolution to create a new metabolic state of the cell, which is beneficial for the synthesis of the target molecule by optimizing precursor availability and/or creating an alternative metabolic mode. Typically, the evolutionary readjusted metabolism increases the previously low growth rate or even revives the cell. Increasing biomass concentrations constitute a straightforward indicator that facilitates simplified screening and easily identifies relevant evolving clones. The application of mutagenizing agents or radiation might accelerate evolution, it however potentiates the number of mutations, which requires laborious re-engineering to identify relevant ones (Harper et al., 2011). We deliberately omitted

mutagens in MGE and relied on intrinsic selection pressure created via metabolic engineering, which worked out and resulted in a neat set of mutations (seven genomic targets in sum, separated in strains with each three, three or six mutations; Table 35, p.148).

Other evolution approaches, such as adaptive laboratory evolution (ALE), have also been applied with focus on improving L-valine production with *C. glutamicum* in combination with an L-valine responsive biosensor (Mahr et al., 2015). Identified genomic targets in this approach comprised *ureD*, *glxR*, *prpD2*, *rpsP*, and *lepA* (Mahr et al., 2015).

Beyond this, parallel, independent, and timesaving evolution experiments further simplify the identification of relevant mutations, since they enable forming an intersection of the mutational pool. In our experiments this yielded one shared, i.e. relevant, target gene (*icd*) with three mutated variants, which could be swiftly re-engineered and identified as growth-mediating factors. Combined with the technology of comparative metabolomics, in the form of SMP, evolved strains could readily be screened for potential production applications. In our case, MGE worked out as planned and cells were indeed suitable for L-valine production, which was underlined by the revelation of increased intracellular L-valine pools in *C. glutamicum* Δ*ppc* Δ*pyc* ICDG^{G407S}.

MGE has proven to be able to identify novel targets with the purpose to improve existing producer strains. This might prove exceptionally useful when rational strain design comes to its limits. However, applying MGE requires intense and profound knowledge of the hosts metabolism including underlying regulation networks and accessibility of the targeted genes/enzymes. It is indispensable to predict potential outcomes of an evolutionary experiment, which however might be encouraged by applying FBA, with the aim to evaluate the prospect of success prior starting. Nevertheless, a profound knowledge of the deployed methods and technologies, such as FBA, strain construction, and SMP, and importantly a synergy thereof is required from the experimenter.

Taken together, the application of MGE identified and created a novel metabolic mode for L-valine production with *C. glutamicum*, which represents a suitable alternative to already existing approaches.

CHAPTER 5: LITERATURE

Abe, S., Takayama, K.-I., Kinoshita, S., 1967. Taxonomical studies on glutamic acid-producing bacteria. J. Gen. Appl. Microbiol. 13, 279–301. https://doi.org/10.2323/jgam.13.279

Adachi, N., Takahashi, C., Ono-Murota, N., Yamaguchi, R., Tanaka, T., Kondo, A., 2013. Direct L-lysine production from cellobiose by *Corynebacterium glutamicum* displaying beta-glucosidase on its cell surface. Appl. Microbiol. Biotechnol. 97, 7165–7172. https://doi.org/10.1007/s00253-013-5009-4

Agresti, J.J., Antipov, E., Abate, A.R., Ahn, K., Rowat, A.C., Baret, J.-C., Marquez, M., Klibanov, A.M., Griffiths, A.D., Weitz, D.A., 2010. Ultrahigh-throughput screening in drop-based microfluidics for directed evolution. Proc. Natl. Acad. Sci. U.S.A. 107, 4004–4009. https://doi.org/10.1073/pnas.0910781107

Ajinomoto Co., 2016. FY2015 Market and other information. https://www.ajinomoto.com/en/ir/event/presentation/main/09/teaserItems1/00/linkList/02/link/FY15_Data_E.pdf (last access 2018-07-18)

Alderwick, L.J., Dover, L.G., Seidel, M., Gande, R., Sahm, H., Eggeling, L., Besra, G.S., 2006. Arabinan-deficient mutants of *Corynebacterium glutamicum* and the consequent flux in decaprenylmonophosphoryl-d-arabinose metabolism. Glycobiology 16, 1073–1081. https://doi.org/10.1093/glycob/cwl030

Alderwick, L.J., Lloyd, G.S., Lloyd, A.J., Lovering, A.L., Eggeling, L., Besra, G.S., 2011. Biochemical characterization of the *Mycobacterium tuberculosis* phosphoribosyl-1-pyrophosphate synthetase. Glycobiology 21, 410–425. https://doi.org/10.1093/glycob/cwq173

Alifano, P., Fani, R., Liò, P., Lazcano, A., Bazzicalupo, M., Carlomagno, M.S., Bruni, C.B., 1996. Histidine biosynthetic pathway and genes: structure, regulation, and evolution. Microbiol. Rev. 60, 44–69

Aluri, S., Rex, K., Varshney, U., 2015. Simultaneous presence of *fhs* and *purT* genes is disadvantageous for the fitness of *Escherichia coli* growth. FEMS Microbiol. Lett. 362:14. https://doi.org/10.1093/femsle/fnv101

Ames, B.N., Martin, R.G., Garry, B.J., 1961. The first step of histidine biosynthesis. J. Biol. Chem. 236, 2019-2026

Araki, K., Kato, F., Arai, Y., Nakayama, K., 1974. Histidine production by auxotrophic histidine analog-resistant mutants of *Corynebacterium glutamicum*. Agric. Biol. Chem. 38, 189–194. https://doi.org/10.1080/00021369.1974.10861132

Araki, K., Nakayama, K., 1975. Accumulation of L-histidinol by a histidine auxotroph of *Corynebacterium glutamicum* and its conversion into L-histidine by an *Escherichia coli* strain. Agric. Biol. Chem. 39, 127–132. https://doi.org/10.1271/bbb1961.39.127

Araki, K., Nakayama, K., 1974. Feedback-resistant phosphoribosyl-ATP pyrophosphorylase in L-histidine-producing mutants of *Corynebacterium glutamicum*. Agric. Biol. Chem. 38, 2209-2218. https://doi.org/10.1271/bbb1961.38.2209

Araki, K., Nakayama, K., 1971. Studies on histidine fermentation Part I. L-Histidine production by histidine analog-resistant mutants from several bacteria. Agric. Biol. Chem. 35, 2081–2088. https://doi.org/10.1080/00021369.1971.10860195

Arinze, I.J., 2005. Facilitating understanding of the purine nucleotide cycle and the one-carbon pool: Part II: Metabolism of the one-carbon pool. Biochem. Mol. Biol. Educ. 33, 255–259. https://doi.org/10.1002/bmb.2005.49403304255

Arndt, A., Auchter, M., Ishige, T., Wendisch, V.F., Eikmanns, B.J., 2008. Ethanol catabolism in *Corynebacterium glutamicum*. J. Mol. Microbiol. Biotechnol. 15, 222–233. https://doi.org/10.1159/000107370

Arndt, A., Eikmanns, B.J., 2007. The alcohol dehydrogenase gene *adhA* in *Corynebacterium glutamicum* is subject to carbon catabolite repression. J. Bacteriol. 189, 7408–7416. https://doi.org/10.1128/JB.00791-07

Atkinson, D.E., 1968. The energy charge of the adenylate pool as a regulatory parameter. Interaction with feedback modifiers. Biochemistry 7, 4030–4034. https://doi.org/10.1021/bi00851a033

Atkinson, D.E., Fall, L., 1967. Adenosine triphosphate conservation in biosynthetic regulation. *Escherichia coli* phosphoribosylpyrophosphate synthase. J. Biol. Chem. 242, 3241–3242

Atkinson, D.E., Walton, G.M., 1967. Adenosine triphosphate conservation in metabolic regulation. Rat liver citrate cleavage enzyme. J. Biol. Chem. 242, 3239–3241

Atkinson, D.E., Walton, G.M., 1965. Kinetics of regulatory enzymes. *Escherichia coli* phosphofructokinase. J. Biol. Chem. 240, 757–763

Atsumi, S., Liao, J.C., 2008. Directed Evolution of *Methanococcus jannaschii* citramalate synthase for biosynthesis of 1-propanol and 1-butanol by *Escherichia coli*. Appl. Environ. Microbiol. 74, 7802–7808. https://doi.org/10.1128/AEM.02046-08

Auchter, M., Cramer, A., Hüser, A., Rückert, C., Emer, D., Schwarz, P., Arndt, A., Lange, C., Kalinowski, J., Wendisch, V.F., Eikmanns, B.J., 2011. RamA and RamB are global transcriptional regulators in *Corynebacterium glutamicum* and control genes for enzymes of the central metabolism. J. Biotechnol. 154, 126–139. https://doi.org/10.1016/j.jbiotec.2010.07.001

Auerbach, V.H., DiGeorge, A.M., Baldridge, R.C., Tourtellotte, C.D., Brigham, M.P., 1962. Histidinemia: A deficiency in histidase resulting in the urinary excretion of histidine and of imidazolepyruvic acid. J. Pediatr. 60, 487–497. https://doi.org/10.1016/S0022-3476(62)80109-7

Auriol, C., Bestel-Corre, G., Claude, J.-B., Soucaille, P., Meynial-Salles, I., 2011. Stress-induced evolution of *Escherichia coli* points to original concepts in respiratory cofactor selectivity. Proc. Natl. Acad. Sci. U.S.A. 108, 1278–1283

Baritugo, K.-A., Kim, H.T., David, Y., Choi, J., Hong, S.H., Jeong, K.J., Choi, J.H., Joo, J.C., Park, S.J., 2018. Metabolic engineering of *Corynebacterium glutamicum* for fermentative production of chemicals in biorefinery. Appl. Microbiol. Biotechnol. 102, 3915–3937. https://doi.org/10.1007/s00253-018-8896-6

Barrett, E., Stanton, C., Zelder, O., Fitzgerald, G., Ross, R.P., 2004. Heterologous expression of lactose- and galactose-utilizing pathways from lactic acid bacteria in *Corynebacterium glutamicum* for production of lysine in whey. Appl. Environ. Microbiol. 70, 2861–2866. https://doi.org/10.1128/AEM.70.5.2861-2866.2004

Barriuso-Iglesias, M., Schluesener, D., Barreiro, C., Poetsch, A., Martín, J.F., 2008. Response of the cytoplasmic and membrane proteome of *Corynebacterium glutamicum* ATCC 13032 to pH changes. BMC Microbiol 8, 225. https://doi.org/10.1186/1471-2180-8-225

Bartek, T., Blombach, B., Lang, S., Eikmanns, B.J., Wiechert, W., Oldiges, M., Nöh, K., Noack, S., 2011. Comparative ^{13}C metabolic flux analysis of pyruvate dehydrogenase complex-deficient, L-valine-producing *Corynebacterium glutamicum*. Appl. Environ. Microbiol. 77, 6644–6652. https://doi.org/10.1128/AEM.00575-11

Bartek, T., Makus, P., Klein, B., Lang, S., Oldiges, M., 2008. Influence of L-isoleucine and pantothenate auxotrophy for L-valine formation in *Corynebacterium glutamicum* revisited by metabolome analyses. Bioprocess Biosyst. Eng. 31, 217–225. https://doi.org/10.1007/s00449-008-0202-z

Bassalo, M.C., Liu, R., Gill, R.T., 2016. Directed evolution and synthetic biology applications to microbial systems. Curr. Opin. Biotechnol. 39, 126–133. https://doi.org/10.1016/j.copbio.2016.03.016

Bäumchen, C., Knoll, A., Husemann, B., Seletzky, J., Maier, B., Dietrich, C., Amoabediny, G., Büchs, J., 2007. Effect of elevated dissolved carbon dioxide concentrations on growth of *Corynebacterium glutamicum* on D-glucose and L-lactate. J. Biotechnol. 128, 868–874. https://doi.org/10.1016/j.jbiotec.2007.01.001

Baumgart, M., Mustafi, N., Krug, A., Bott, M., 2011. Deletion of the aconitase gene in *Corynebacterium glutamicum* causes strong selection pressure for secondary mutations inactivating citrate synthase. J. Bacteriol. 193, 6864–6873. https://doi.org/10.1128/JB.05465-11

Bayan, N., Houssin, C., Chami, M., Leblon, G., 2003. Mycomembrane and S-layer: two important structures of *Corynebacterium glutamicum* cell envelope with promising biotechnology applications. J. Biotechnol. 104, 55–67. https://doi.org/10.1016/S0168-1656(03)00163-9

Becker, J., Buschke, N., Bücker, R., Wittmann, C., 2010. Systems level engineering of *Corynebacterium glutamicum* – Reprogramming translational efficiency for superior production. Eng. Life Sci. 10, 430–438. https://doi.org/10.1002/elsc.201000008

Becker, J., Klopprogge, C., Schröder, H., Wittmann, C., 2009. Metabolic engineering of the tricarboxylic acid cycle for improved lysine production by *Corynebacterium glutamicum*. Appl. Environ. Microbiol. 75, 7866–7869. https://doi.org/10.1128/AEM.01942-09

Becker, J., Klopprogge, C., Zelder, O., Heinzle, E., Wittmann, C., 2005. Amplified expression of fructose 1,6-bisphosphatase in *Corynebacterium glutamicum* increases *in vivo* flux through the pentose phosphate pathway and lysine production on different carbon sources. Appl. Environ. Microbiol. 71, 8587–8596. https://doi.org/10.1128/AEM.71.12.8587-8596.2005

Becker, J., Wittmann, C., 2015. Advanced biotechnology: metabolically engineered cells for the bio-based production of chemicals and fuels, materials, and health-care products. Angew. Chem., Int. Ed. 54, 3328–3350. https://doi.org/10.1002/anie.201409033

Becker, J., Wittmann, C., 2012. Bio-based production of chemicals, materials and fuels – *Corynebacterium glutamicum* as versatile cell factory. Curr. Opin. Biotechnol. 23, 631–640. https://doi.org/10.1016/j.copbio.2011.11.012

Becker, J., Zelder, O., Häfner, S., Schröder, H., Wittmann, C., 2011. From zero to hero - Design-based systems metabolic engineering of *Corynebacterium glutamicum* for L-lysine production. Metab. Eng. 13, 159–168. https://doi.org/10.1016/j.ymben.2011.01.003

Becker, S.A., Feist, A.M., Mo, M.L., Hannum, G., Palsson, B.Ø., Herrgard, M.J., 2007. Quantitative prediction of cellular metabolism with constraint-based models: the COBRA Toolbox. Nat. Protoc. 2, 727–738. https://doi.org/10.1038/nprot.2007.99

Begley, T.P., Ealick, S.E., McLafferty, F.W., 2012. Thiamin biosynthesis - still yielding fascinating biological chemistry. Biochem. Soc. Trans. 40, 555–560. https://doi.org/10.1042/BST20120084

Begley, T.P., Kinsland, C., Mehl, R.A., Osterman, A., Dorrestein, P., 2001. The biosynthesis of nicotinamide adenine dinucleotides in bacteria. Vitam. Horm. (N.Y.) 61, 103–119. https://doi.org/10.1016/S0083-6729(01)61003-3

Bender, R.A., 2012. Regulation of the histidine utilization (Hut) system in bacteria. Microbiol. Mol. Biol. Rev. 76, 565–584. https://doi.org/10.1128/MMBR.00014-12

Bennett, B.D., Kimball, E.H., Gao, M., Osterhout, R., Van Dien, S.J., Rabinowitz, J.D., 2009. Absolute metabolite concentrations and implied enzyme active site occupancy in *Escherichia coli*. Nat. Chem. Biol. 5, 593–599. https://doi.org/10.1038/nchembio.186

Bentley, S.D., Chater, K.F., Cerdeño-Tárraga, A.-M., Challis, G.L., Thomson, N.R., James, K.D., Harris, D.E., Quail, M.A., Kieser, H., Harper, D., Bateman, A., Brown, S., Chandra, G., Chen, C.W., Collins, M., Cronin, A., Fraser, A., Goble, A., Hidalgo, J., Hornsby, T., Howarth, S., Huang, C.-H., Kieser, T., Larke, L., Murphy, L., Oliver, K., O'Neil, S., Rabbinowitsch, E., Rajandream, M.-A., Rutherford, K., Rutter, S., Seeger, K., Saunders, D., Sharp, S., Squares, R., Squares, S., Taylor, K., Warren, T., Wietzorrek, A., Woodward, J., Barrell, B.G., Parkhill, J., Hopwood, D.A., 2002. Complete genome sequence of the model actinomycete *Streptomyces coelicolor* A3(2). Nature 417, 141–147. https://doi.org/10.1038/417141a

Bera, A.K., Zhu, J., Zalkin, H., Smith, J.L., 2003. Functional dissection of the *Bacillus subtilis pur* operator site. J. Bacteriol. 185, 4099–4109. https://doi.org/10.1128/JB.185.14.4099-4109.2003

Berberich, M.A., Venetianer, P., Goldberger, R.F., 1966. Alternative modes of derepression of the histidine operon observed in *Salmonella typhimurium*. J. Biol. Chem. 241, 4426–4433.

Betz, A., Moore, C., 1967. Fluctuating metabolite levels in yeast cells and extracts, and the control of phosphofructokinase activity *in vitro*. Arch. Biochem. Biophys. 120, 268–273. https://doi.org/10.1016/0003-9861(67)90238-X

Beyer, N.H., Roepstorff, P., Hammer, K., Kilstrup, M., 2003. Proteome analysis of the purine stimulon from *Lactococcus lactis*. Proteomics 3, 786–797. https://doi.org/10.1002/pmic.200300416

Blom, J., Jakobi, T., Doppmeier, D., Jaenicke, S., Kalinowski, J., Stoye, J., Goesmann, A., 2011. Exact and complete short-read alignment to microbial genomes using graphics processing unit programming. Bioinformatics 27, 1351–1358. https://doi.org/10.1093/bioinformatics/btr151

Blombach, B., Arndt, A., Auchter, M., Eikmanns, B.J., 2009. L-Valine Production during growth of pyruvate dehydrogenase complex-deficient *Corynebacterium glutamicum* in the presence of ethanol or by inactivation of the transcriptional regulator SugR. Appl. Environ. Microbiol. 75, 1197–1200. https://doi.org/10.1128/AEM.02351-08

Blombach, B., Buchholz, J., Busche, T., Kalinowski, J., Takors, R., 2013. Impact of different CO_2/HCO_3^- levels on metabolism and regulation in *Corynebacterium glutamicum*. J. Biotechnol. 168, 331–340. https://doi.org/10.1016/j.jbiotec.2013.10.005

Blombach, B., Riester, T., Wieschalka, S., Ziert, C., Youn, J.-W., Wendisch, V.F., Eikmanns, B.J., 2011. *Corynebacterium glutamicum* tailored for efficient isobutanol production. Appl. Environ. Microbiol. 77, 3300–3310. https://doi.org/10.1128/AEM.02972-10

Blombach, B., Schreiner, M.E., Bartek, T., Oldiges, M., Eikmanns, B.J., 2008. *Corynebacterium glutamicum* tailored for high-yield L-valine production. Appl. Microbiol. Biotechnol. 79, 471–479. https://doi.org/10.1007/s00253-008-1444-z

Blombach, B., Schreiner, M.E., Holatko, J., Bartek, T., Oldiges, M., Eikmanns, B.J., 2007. L-Valine production with pyruvate dehydrogenase complex-deficient *Corynebacterium glutamicum*. Appl. Environ. Microbiol. 73, 2079–2084. https://doi.org/10.1128/AEM.02826-06

Blombach, B., Seibold, G.M., 2010. Carbohydrate metabolism in *Corynebacterium glutamicum* and applications for the metabolic engineering of L-lysine production strains. Appl. Microbiol. Biotechnol. 86, 1313–1322. https://doi.org/10.1007/s00253-010-2537-z

Bochner, B. R., Ames, B.N., 1982. Complete analysis of cellular nucleotides by two-dimensional thin layer chromatography. J. Biol. Chem. 257, 9759–9769.

Bochner, Barry R., Ames, B.N., 1982. ZTP (5-amino 4-imidazole carboxamide riboside 5′-triphosphate): A proposed alarmone for 10-formyl-tetrahydrofolate deficiency. Cell 29, 929–937. https://doi.org/10.1016/0092-8674(82)90455-X

Bolten, C.J., Kiefer, P., Letisse, F., Portais, J.-C., Wittmann, C., 2007. Sampling for metabolome analysis of microorganisms. Anal. Chem. 79, 3843–3849. https://doi.org/10.1021/ac0623888

Bolten, C.J., Schröder, H., Dickschat, J., Wittmann, C., 2010. Towards methionine overproduction in *Corynebacterium glutamicum* - methanethiol and dimethyldisulfide as reduced sulfur sources. J. Microbiol. Biotechnol. 20, 1196–1203.

Bommareddy, R.R., Chen, Z., Rappert, S., Zeng, A.-P., 2014. A *de novo* NADPH generation pathway for improving lysine production of *Corynebacterium glutamicum* by rational design of the coenzyme specificity of glyceraldehyde 3-phosphate dehydrogenase. Metab. Eng. 25, 30–37. https://doi.org/10.1016/j.ymben.2014.06.005

Boonstra, B., French, C.E., Wainwright, I., Bruce, N.C., 1999. The *udhA* gene of *Escherichia coli* encodes a soluble pyridine nucleotide transhydrogenase. J. Bacteriol. 181, 1030–1034.

Börmann, E.R., Eikmanns, B.J., Sahm, H., 1992. Molecular analysis of the *Corynebacterium glutamicum gdh* gene encoding glutamate dehydrogenase. Mol.r Microbiol. 6, 317–326. https://doi.org/10.1111/j.1365-2958.1992.tb01474.x

Bott, M., 2007. Offering surprises: TCA cycle regulation in *Corynebacterium glutamicum*. Trends Microbiol. 15, 417–425. https://doi.org/10.1016/j.tim.2007.08.004

Bott, M., Eikmanns, B.J., 2013. TCA cycle and glyoxylate shunt of *Corynebacterium glutamicum*, in: Yukawa, H. and Inui, M. (Eds) *Corynebacterium glutamicum*: Biology and Biotechnology. Springer Berlin Heidelberg, p. 281–313.

Brockmann-Gretza, O., Kalinowski, J., 2006. Global gene expression during stringent response in *Corynebacterium glutamicum* in presence and absence of the *rel* gene encoding (p)ppGpp synthase. BMC Genomics 7, 230. https://doi.org/10.1186/1471-2164-7-230

Brown, A.M., Hoopes, S.L., White, R.H., Sarisky, C.A., 2011. Purine biosynthesis in archaea: variations on a theme. Biol. Direct 6, 63. https://doi.org/10.1186/1745-6150-6-63

Brückner, R., Titgemeyer, F., 2002. Carbon catabolite repression in bacteria: choice of the carbon source and autoregulatory limitation of sugar utilization. FEMS Microbiol. Lett. 209, 141–148. https://doi.org/10.1111/j.1574-6968.2002.tb11123.x

Buchholz, J., Schwentner, A., Brunnenkan, B., Gabris, C., Grimm, S., Gerstmeir, R., Takors, R., Eikmanns, B.J., Blombach, B., 2013. Platform engineering of *Corynebacterium glutamicum* with reduced pyruvate dehydrogenase complex activity for improved production of L-lysine, L-valine, and 2-ketoisovalerate. Appl. Environ. Microbiol. 79, 5566–5575. https://doi.org/10.1128/AEM.01741-13

Bückle-Vallant, V., Krause, F.S., Messerschmidt, S., Eikmanns, B.J., 2013. Metabolic engineering of *Corynebacterium glutamicum* for 2-ketoisocaproate production. Appl. Microbiol. Biotechnol. 98, 297–311. https://doi.org/10.1007/s00253-013-5310-2

Burkovski, A., 2013. Cell envelope of Corynebacteria: Structure and Influence on Pathogenicity. ISRN Microbiol. 2013. https://doi.org/10.1155/2013/935736

Burns, K.E., Liu, W.-T., Boshoff, H.I.M., Dorrestein, P.C., Barry, C.E., 2009. Proteasomal protein degradation in Mycobacteria is dependent upon a prokaryotic ubiquitin-like protein. J. Biol. Chem. 284, 3069–3075. https://doi.org/10.1074/jbc.M808032200

Burns, P.A., Allen, F.L., Glickman, B.W., 1986. DNA sequence analysis of mutagenicity and site specificity of ethyl methanesulfonate in Uvr^+ and $UvrB^-$ strains of *Escherichia coli*. Genetics 113, 811–819.

Buschke, N., Becker, J., Schäfer, R., Kiefer, P., Biedendieck, R., Wittmann, C., 2013. Systems metabolic engineering of xylose-utilizing *Corynebacterium glutamicum* for production of 1,5-diaminopentane. Biotechnol. J. 8, 557–570. https://doi.org/10.1002/biot.201200367

Cadwell, R.C., Joyce, G.F., 1992. Randomization of genes by PCR mutagenesis. Genome Res. 2, 28–33. https://doi.org/10.1101/gr.2.1.28

Cao, Z., Song, P., Xu, Q., Su, R., Zhu, G., 2011. Overexpression and biochemical characterization of soluble pyridine nucleotide transhydrogenase from *Escherichia coli*. FEMS Microbiol. Lett. 320, 9–14. https://doi.org/10.1111/j.1574-6968.2011.02287.x

Celeste, L.R., Chai, G., Bielak, M., Minor, W., Lovelace, L.L., Lebioda, L., 2012. Mechanism of N^{10}-formyltetrahydrofolate synthetase derived from complexes with intermediates and inhibitors. Protein Sci. 21, 219–228. https://doi.org/10.1002/pro.2005

Chapman, A.G., Fall, L., Atkinson, D.E., 1971. Adenylate energy charge in *Escherichia coli* during growth and starvation. J. Bacteriol. 108, 1072–1086.

Chen, S., Tomchick, D.R., Wolle, D., Hu, P., Smith, J.L., Switzer, R.L., Zalkin, H., 1997. Mechanism of the synergistic end-product regulation of *Bacillus subtilis* glutamine phosphoribosylpyrophosphate amidotransferase by nucleotides. Biochemistry 36, 10718–10726. https://doi.org/10.1021/bi9711893

Cheng, Y., Zhou, Y., Yang, L., Zhang, C., Xu, Q., Xie, X., Chen, N., 2013. Modification of histidine biosynthesis pathway genes and the impact on production of L-histidine in *Corynebacterium glutamicum*. Biotechnol. Lett. 35, 735–741. https://doi.org/10.1007/s10529-013-1138-1

Chim-Anage, P., Shioya, S., Suga, K., 1991. Maximum histidine production by fed-batch culture of *Brevibacterium flavum*. J. Ferment. and Bioeng. 71, 186–190. https://doi.org/10.1016/0922-338X(91)90107-R

Cho, B.-K., Federowicz, S.A., Embree, M., Park, Y.-S., Kim, D., Palsson, B.Ø., 2011. The PurR regulon in *Escherichia coli* K-12 MG1655. Nucleic Acids Res. 39, 6456–6464. https://doi.org/10.1093/nar/gkr307

Cho, Y., Sharma, V., Sacchettini, J.C., 2003. Crystal structure of ATP phosphoribosyltransferase from *Mycobacterium tuberculosis*. J. Biol. Chem. 278, 8333–8339. https://doi.org/10.1074/jbc.M212124200

Chou, H.H., Keasling, J.D., 2013. Programming adaptive control to evolve increased metabolite production. Nature Commun. 4, 2595. https://doi.org/10.1038/ncomms3595

Cobb, R.E., Chao, R., Zhao, H., 2013a. Directed evolution: Past, present, and future. AIChE J. 59, 1432–1440. https://doi.org/10.1002/aic.13995

Cobb, R.E., Sun, N., Zhao, H., 2013b. Directed evolution as a powerful synthetic biology tool. Methods 60, 81–90. https://doi.org/10.1016/j.ymeth.2012.03.009

Cohen, J., 2001. How DNA shuffling works. Science 293, 237–237. https://doi.org/10.1126/science.293.5528.237

Cole, S.T., Brosch, R., Parkhill, J., Garnier, T., Churcher, C., Harris, D., Gordon, S.V., Eiglmeier, K., Gas, S., Iii, C.E.B., Tekaia, F., Badcock, K., Basham, D., Brown, D., Chillingworth, T., Connor, R., Davies, R., Devlin, K., Feltwell, T., Gentles, S., Hamlin, N., Holroyd, S., Hornsby, T., Jagels, K., Krogh, A., McLean, J., Moule, S., Murphy, L., Oliver, K., Osborne, J., Quail, M.A., Rajandream, M.-A., Rogers, J., Rutter, S., Seeger, K., Skelton, J., Squares, R., Squares, S., Sulston, J.E., Taylor, K., Whitehead, S., Barrell, B.G., 1998. Deciphering the biology of *Mycobacterium tuberculosis* from the complete genome sequence. Nature 393, 537–544. https://doi.org/10.1038/31159

Cordes, C., Möckel, B., Eggeling, L., Sahm, H., 1992. Cloning, organization and functional analysis of *ilvA*, *ilvB* and *ilvC* genes from *Corynebacterium glutamicum*. Gene 112, 113–116. https://doi.org/10.1016/0378-1119(92)90311-C

Cramer, A., Auchter, M., Frunzke, J., Bott, M., Eikmanns, B.J., 2007. RamB, the transcriptional regulator of acetate metabolism in *Corynebacterium glutamicum* is subject to regulation by RamA and RamB. J. Bacteriol. 189, 1145–1149. https://doi.org/10.1128/JB.01061-06

Cramer, A., Eikmanns, B.J., 2007. RamA, the transcriptional regulator of acetate metabolism in *Corynebacterium glutamicum*, is subject to negative autoregulation. J. Mol. Microbiol. Biotechnol. 12, 51–59. https://doi.org/10.1159/000096459

Cramer, A., Gerstmeir, R., Schaffer, S., Bott, M., Eikmanns, B.J., 2006. Identification of RamA, a novel LuxR-type transcriptional regulator of genes involved in acetate metabolism of *Corynebacterium glutamicum*. J. Bacteriol. 188, 2554–2567. https://doi.org/10.1128/JB.188.7.2554-2567.2006

Cserjan-Puschmann, M., Kramer, W., Duerrschmid, E., Striedner, G., Bayer, K., 1999. Metabolic approaches for the optimisation of recombinant fermentation processes. Appl. Microbiol. Biotechnol. 53, 43–50.

Dahod, S.K., Greasham, R., Kennedy, M., 2010. Raw materials selection and medium development for industrial fermentation processes, in: Baltz, R.H., Demain, A.L., Davies, J.E., Bull, A.T., Junker, B., Katz, L., Lynd, L.R., Masurekar, P., Reeves, C.D., Zhao, H. (Eds.) Manual of Industrial Microbiology and Biotechnology. ASM Press Washington D.C., p. 659–668. https://doi.org/10.1128/9781555816827.ch46

Dall-Larsen, T., 1988. Regulation of the first step of the histidine biosynthesis in *Escherichia coli*. Int. J. Biochem. 20, 231–235. https://doi.org/10.1016/0020-711X(88)90346-1

Datta, N., Hedges, R.W., Shaw, E.J., Sykes, R.B., Richmond, M.H., 1971. Properties of an R factor from *Pseudomonas aeruginosa*. J. Bacteriol. 108, 1244–1249.

De la Fuente, I.M., Cortés, J.M., Valero, E., Desroches, M., Rodrigues, S., Malaina, I., Martínez, L., 2014. On the dynamics of the adenylate energy system: Homeorhesis vs homeostasis. PLoS One 9. https://doi.org/10.1371/journal.pone.0108676

Delić, V., Hopwood, D.A., Friend, E.J., 1970. Mutagenesis by N-methyl-N′-nitro-N-nitrosoguanidine (NTG) in *Streptomyces coelicolor*. Mutat. Res. 9, 167–182. https://doi.org/10.1016/0027-5107(70)90055-2

Delvigne, F., Noorman, H., 2017. Scale-up/Scale-down of microbial bioprocesses: a modern light on an old issue. Microb. Biotechnol. 10, 685–687. https://doi.org/10.1111/1751-7915.12732

Delvigne, F., Takors, R., Mudde, R., Gulik, W. van, Noorman, H., 2017. Bioprocess scale-up/down as integrative enabling technology: from fluid mechanics to systems biology and beyond. Microb. Biotechnol. 10, 1267–1274. https://doi.org/10.1111/1751-7915.12803

Dev, I.K., Harvey, R.J., 1982. Sources of one-carbon units in the folate pathway of *Escherichia coli*. J. Biol. Chem. 257, 1980–1986.

Diesterhaft, M.D., Freese, E., 1973. Role of pyruvate carboxylase, phosphoenolpyruvate carboxykinase, and malic enzyme during growth and sporulation of *Bacillus subtilis*. J. Biol. Chem. 248, 6062–6070.

Dietrich, J.A., McKee, A.E., Keasling, J.D., 2010. High-throughput metabolic engineering: advances in small-molecule screening and selection. Annu. Rev. Biochem. 79, 563–590. https://doi.org/10.1146/annurev-biochem-062608-095938

DiNicolantonio, J.J., McCarty, M.F., OKeefe, J.H., 2018. Role of dietary histidine in the prevention of obesity and metabolic syndrome. Open Heart 5. https://doi.org/10.1136/openhrt-2017-000676

Dominguez, H., Cocaign-Bousquet, M., Lindley, N.D., 1997. Simultaneous consumption of glucose and fructose from sugar mixtures during batch growth of *Corynebacterium glutamicum*. Appl. Microbiol. Biotechnol. 47, 600–603. https://doi.org/10.1007/s002530050980

Dominguez, H., Lindley, N.D., 1996. Complete sucrose metabolism requires fructose phosphotransferase activity in *Corynebacterium glutamicum* to ensure phosphorylation of liberated fructose. Appl. Environ. Microbiol. 62, 3878–3880.

Dominguez, H., Rollin, C., Guyonvarch, A., Guerquin-Kern, J.-L., Cocaign-Bousquet, M., Lindley, N.D., 1998. Carbon-flux distribution in the central metabolic pathways of *Corynebacterium glutamicum* during growth on fructose. Eur. J.Biochem. 254, 96–102. https://doi.org/10.1046/j.1432-1327.1998.2540096.x

Doroshenko, V.G., Lobanov, A.O., Fedorina, E.A., 2013. The directed modification of *Escherichia coli* MG1655 to obtain histidine-producing mutants. Appl. Biochem. Microbiol. 49, 130–135. https://doi.org/10.1134/S0003683813020026

Doudney, C.O., Young, C.S., 1962. Ultraviolet light induced mutation and deoxyribonucleic acid replication in bacteria. Genetics 47, 1125–1138.

Dower, W.J., Miller, J.F., Ragsdale, C.W., 1988. High efficiency transformation of *E. coli* by high voltage electroporation. Nucleic Acids Res. 16, 6127–45.

Downs, D.M., Roth, J.R., 1991. Synthesis of thiamine in *Salmonella typhimurium* independent of the *purF* function. J. Bacteriol. 173, 6597–6604.

Du, Q., Wang, H., Xie, J., 2011. Thiamin (Vitamin B1) biosynthesis and regulation: A rich source of antimicrobial drug targets? Int. J. Biol. Sci. 7, 41–52.

Du, S., Sun, S., Liu, L., Zhang, Q., Guo, F., Li, C., Feng, R., Sun, C., 2017. Effects of histidine supplementation on global serum and urine ^{1}H NMR-based metabolomics and serum amino acid profiles in obese women from a randomized controlled study. J. Proteome Res. 16, 2221–2230. https://doi.org/10.1021/acs.jproteome.7b00030

Dykhuizen, D.E., 1990. Experimental studies of natural selection in bacteria. Annu. Rev. Ecol. Syst. 21, 373–398.

Eggeling, L., Bott, M., 2005. Handbook of *Corynebacterium glutamicum*. CRC Press, Boca Raton, USA.

Eggeling, L., Bott, M., Marienhagen, J., 2015. Novel screening methods - biosensors. Curr. Opin. .Biotechnol. 35, 30–36. https://doi.org/10.1016/j.copbio.2014.12.021

Eggeling, L., Reyes, O., 2005. Experiments., in: Handbook of *Corynebacterium Glutamicum*. CRC Press, Boca Raton, USA, p. 421–422.

Eikmanns, B.J., 2005. Central metabolism: tricarboxylic acid cycle and anaplerotic reactions, in: Eggeling, L. and Bott, M. (Eds) Handbook of *Corynebacterium Glutamicum*. CRC Press, Boca Raton, USA, p. 241–276.

Eikmanns, B.J., 1992. Identification, sequence analysis, and expression of *a Corynebacterium glutamicum* gene cluster encoding the three glycolytic enzymes glyceraldehyde-3-phosphate dehydrogenase, 3-phosphoglycerate kinase, and triosephosphate isomerase. J. Bacteriol. 174, 6076–6086.

Eikmanns, B.J., Blombach, B., 2014. The pyruvate dehydrogenase complex of *Corynebacterium glutamicum*: An attractive target for metabolic engineering. J. Biotechnol. 192, 339–345. https://doi.org/10.1016/j.jbiotec.2013.12.019

Eikmanns, B.J., Metzger, M., Reinscheid, D., Kircher, M., Sahm, H., 1991. Amplification of three threonine biosynthesis genes in *Corynebacterium glutamicum* and its influence on carbon flux in different strains. Appl. Microbiol. Biotechnol. 34, 617–622. https://doi.org/10.1007/BF00167910

Eikmanns, B.J., Rittmann, D., Sahm, H., 1995. Cloning, sequence analysis, expression, and inactivation of the *Corynebacterium glutamicum icd* gene encoding isocitrate dehydrogenase and biochemical characterization of the enzyme. J. Bacteriol. 177, 774–782.

Ekwall, K., Thon, G., 2017. Ethyl methanesulfonate mutagenesis in *Schizosaccharomyces pombe*. Cold Spring Harbor Protoc. 2017. https://doi.org/10.1101/pdb.prot091736

Elišáková, V., Pátek, M., Holátko, J., Nešvera, J., Leyval, D., Goergen, J.-L., Delaunay, S., 2005. Feedback-resistant acetohydroxy acid synthase increases valine production in *Corynebacterium glutamicum*. Appl. Environ .Microbiol. 71, 207–213. https://doi.org/10.1128/AEM.71.1.207-213.2005

Engels, V., Wendisch, V.F., 2007. The DeoR-type regulator SugR represses expression of *ptsG* in *Corynebacterium glutamicum*. J. Bacteriol. 189, 2955–2966. https://doi.org/10.1128/JB.01596-06

Eriksen, T.A., Kadziola, A., Bentsen, A.-K., Harlow, K.W., Larsen, S., 2000. Structural basis for the function of *Bacillus subtilis* phosphoribosyl-pyrophosphate synthetase. Nat. Struct. Biol. 7, 303–308. https://doi.org/10.1038/74069

Fani, R., Liò, P., Lazcano, A., 1995. Molecular evolution of the histidine biosynthetic pathway. J. Mol. Evol. 41, 760–774. https://doi.org/10.1007/BF00173156

Feng, R.N., Niu, Y.C., Sun, X.W., Li, Q., Zhao, C., Wang, C., Guo, F.C., Sun, C.H., Li, Y., 2013. Histidine supplementation improves insulin resistance through suppressed inflammation in obese women with the metabolic syndrome: a randomised controlled trial. Diabetologia 56, 985–994. https://doi.org/10.1007/s00125-013-2839-7

Follmann, M., Ochrombel, I., Krämer, R., Trötschel, C., Poetsch, A., Rückert, C., Hüser, A., Persicke, M., Seiferling, D., Kalinowski, J., Marin, K., 2009. Functional genomics of pH homeostasis in *Corynebacterium glutamicum* revealed novel links between pH response, oxidative stress, iron homeostasis and methionine synthesis. BMC Genomics 10, 621. https://doi.org/10.1186/1471-2164-10-621

Fondi, M., Emiliani, G., Liò, P., Gribaldo, S., Fani, R., 2009. The evolution of histidine biosynthesis in archaea: insights into the *his* genes structure and organization in LUCA. J. Mol. Evol. 69, 512. https://doi.org/10.1007/s00239-009-9286-6

Foster, J.W., Moat, A.G., 1980. Nicotinamide adenine dinucleotide biosynthesis and pyridine nucleotide cycle metabolism in microbial systems. Microbiol. Rev. 44, 83–105.

Foster, P.L., 1991. *In vivo* mutagenesis. Methods Enzymol. 204, 114–125.

Franzen, J.S., Binkley, S.B., 1961. Comparison of the acid-soluble nucleotides in *Escherichia coli* at different growth rates. J. Biol. Chem. 236, 515–519.

Freese, E., Heinze, J.E., Galliers, E.M., 1979. Partial purine deprivation causes sporulation of *Bacillus subtilis* in the presence of excess ammonia, glucose and phosphate. J. Gen. Microbiol. 115, 193–205. https://doi.org/10.1099/00221287-115-1-193

Freudl, R., 2017. Beyond amino acids: Use of the *Corynebacterium glutamicum* cell factory for the secretion of heterologous proteins. J. Biotechnol. 258, 101–109. https://doi.org/10.1016/j.jbiotec.2017.02.023

Frezza, C., 2018. Histidine metabolism boosts cancer therapy. Nature 559, 484. https://doi.org/10.1038/d41586-018-05573-4

Fujiwara, K., Okamura-Ikeda, K., Motokawa, Y., 1984. Mechanism of the glycine cleavage reaction. Further characterization of the intermediate attached to H-protein and of the reaction catalyzed by T-protein. J. Biol. Chem. 259, 10664–10668.

Gaigalat, L., Schlüter, J.-P., Hartmann, M., Mormann, S., Tauch, A., Pühler, A., Kalinowski, J., 2007. The DeoR-type transcriptional regulator SugR acts as a repressor for genes encoding the phosphoenolpyruvate:sugar phosphotransferase system (PTS) in *Corynebacterium glutamicum*. BMC Molecul. Biol. 8, 104. https://doi.org/10.1186/1471-2199-8-104

Georgi, T., Rittmann, D., Wendisch, V.F., 2005. Lysine and glutamate production by *Corynebacterium glutamicum* on glucose, fructose and sucrose: Roles of malic enzyme and fructose-1,6-bisphosphatase. Metab. Eng. 7, 291–301. https://doi.org/10.1016/j.ymben.2005.05.001

Gerstmeir, R., Cramer, A., Dangel, P., Schaffer, S., Eikmanns, B.J., 2004. RamB, a novel transcriptional regulator of genes involved in acetate metabolism of *Corynebacterium glutamicum*. J. Bacteriol. 186, 2798–2809. https://doi.org/10.1128/JB.186.9.2798-2809.2004

Gerstmeir, R., Wendisch, V.F., Schnicke, S., Ruan, H., Farwick, M., Reinscheid, D., Eikmanns, B.J., 2003. Acetate metabolism and its regulation in *Corynebacterium glutamicum*. J. Biotechnol. 104, 99–122. https://doi.org/10.1016/S0168-1656(03)00167-6

Gianchandani, E.P., Chavali, A.K., Papin, J.A., 2009. The application of flux balance analysis in systems biology. Wiley Interdiscip. Rev. Syst. Biol. Med. 2, 372–382. https://doi.org/10.1002/wsbm.60

Gibson, D.G., 2011. Chapter fifteen - Enzymatic assembly of overlapping DNA fragments, in: Voigt, C. (Ed.), Methods in Enzymology, Synthetic Biology, Part B Computer Aided Design and DNA Assembly. Academic Press, p. 349–361. https://doi.org/10.1016/B978-0-12-385120-8.00015-2

Gibson, D.G., Young, L., Chuang, R.-Y., Venter, J.C., Hutchison, C.A., Smith, H.O., 2009. Enzymatic assembly of DNA molecules up to several hundred kilobases. Nat. Meth. 6, 343–345. https://doi.org/10.1038/nmeth.1318

Gibson, K.J., Schubert, K.R., Switzer, R.L., 1982. Binding of the substrates and the allosteric inhibitor adenosine 5'-diphosphate to phosphoribosylpyrophosphate synthetase from *Salmonella typhimurium*. J. Biol. Chem. 257, 2391–2396.

Gonçalves, G.A.L., Prather, K.L.J., Monteiro, G.A., Prazeres, D.M.F., 2014. Engineering of *Escherichia coli* strains for plasmid biopharmaceutical production: Scale-up challenges. Vaccine 32, 2847–2850. https://doi.org/10.1016/j.vaccine.2014.02.023

Görisch, H., Hölke, W., 1985. Binding of histidinal to histidinol dehydrogenase. Eur. J. Biochem. 150, 305–308. https://doi.org/10.1111/j.1432-1033.1985.tb09021.x

Görke, B., Stülke, J., 2008. Carbon catabolite repression in bacteria: many ways to make the most out of nutrients. Nat. Rev. Micro. 6, 613–624. https://doi.org/10.1038/nrmicro1932

Gourdon, P., Baucher, M.-F., Lindley, N.D., Guyonvarch, A., 2000. Cloning of the malic enzyme gene from *Corynebacterium glutamicum* and role of the enzyme in lactate metabolism. Appl. Environ. Microbiol. 66, 2981–2987.

Graupner, M., Xu, H., White, R.H., 2002. New class of IMP cyclohydrolases in *Methanococcus jannaschii*. J. Bacteriol. 184, 1471–1473. https://doi.org/10.1128/JB.184.5.1471-1473.2002

Green, J.M., Matthews, R.G., 2007. Folate biosynthesis, reduction, and polyglutamylation and the interconversion of folate derivatives. EcoSal Plus 2. https://doi.org/10.1128/ecosalplus.3.6.3.6

Grünberger, A., van Ooyen, J., Paczia, N., Rohe, P., Schiendzielorz, G., Eggeling, L., Wiechert, W., Kohlheyer, D., Noack, S., 2012. Beyond growth rate 0.6: *Corynebacterium glutamicum* cultivated in highly diluted environments. Biotechnol. Bioeng. 110, 220–228. https://doi.org/10.1002/bit.24616

Guijas, C., Montenegro-Burke, J.R., Domingo-Almenara, X., Palermo, A., Warth, B., Hermann, G., Koellensperger, G., Huan, T., Uritboonthai, W., Aisporna, A.E., Wolan, D.W., Spilker, M.E., Benton, H.P., Siuzdak, G., 2018. METLIN: A technology platform for identifying knowns and unknowns. Anal. Chem. 90, 3156–3164. https://doi.org/10.1021/acs.analchem.7b04424

Hahn-Hägerdal, B., Karhumaa, K., Larsson, C.U., Gorwa-Grauslund, M., Görgens, J., van Zyl, W.H., 2005. Role of cultivation media in the development of yeast strains for large scale industrial use. Microb. Cell Fact. 4, 31. https://doi.org/10.1186/1475-2859-4-31

Hammes, W., Schleifer, K.H., Kandler, O., 1973. Mode of action of glycine on the biosynthesis of peptidoglycan. J. Bacteriol. 116, 1029–1053.

Han, Y., Suzuki, H., Baker, D.H., 1991. Histidine and tryptophan requirement of growing chicks. Poult. Sci. 70, 2148–2153. https://doi.org/10.3382/ps.0702148

Hara, K.Y., Kondo, A., 2015. ATP regulation in bioproduction. Microb. Cell Fact. 14, 198. https://doi.org/10.1186/s12934-015-0390-6

Harada, K., 1963. Asymmetric synthesis of α-amino-acids by the Strecker synthesis. Nature 200, 1201. https://doi.org/10.1038/2001201a0

Harper, M.A., Chen, Z., Toy, T., Machado, I.M.P., Nelson, S.F., Liao, J.C., Lee, C.J., 2011. Phenotype sequencing: Identifying the genes that cause a phenotype directly from pooled sequencing of independent mutants. PLoS One 6. https://doi.org/10.1371/journal.pone.0016517

Harvey, R.J., Dev, I.K., 1975. Regulation in the folate pathway of *Escherichia coli*. Adv. Enzyme Regul. 13, 97–124. https://doi.org/10.1016/0065-2571(75)90010-2

Hasegawa, S., Ichiyama, T., Sonaka, I., Ohsaki, A., Hirano, R., Haneda, Y., Fukano, R., Hara, M., Furukawa, S., 2011. Amino acids exhibit anti-inflammatory effects in human monocytic leukemia cell line, THP-1 cells. Inflamm. Res. 60, 1013. https://doi.org/10.1007/s00011-011-0362-1

Hasegawa, S, Ichiyama, T., Sonaka, I., Ohsaki, A., Okada, S., Wakiguchi, H., Kudo, K., Kittaka, S., Hara, M., Furukawa, S., 2012. Cysteine, histidine and glycine exhibit anti-inflammatory effects in human coronary arterial endothelial cells. Clin. Exp. Immunol. 167, 269–274. https://doi.org/10.1111/j.1365-2249.2011.04519.x

Hasegawa, S., Suda, M., Uematsu, K., Natsuma, Y., Hiraga, K., Jojima, T., Inui, M., Yukawa, H., 2013. Engineering of *Corynebacterium glutamicum* for high-yield L-valine production under oxygen deprivation conditions. Appl. Environ. Microbiol. 79, 1250–1257. https://doi.org/10.1128/AEM.02806-12

Hasegawa, Satoshi, Uematsu, K., Natsuma, Y., Suda, M., Hiraga, K., Jojima, T., Inui, M., Yukawa, H., 2012. Improvement of the redox balance increases L-valine production by *Corynebacterium glutamicum* under oxygen deprivation conditions. Appl. Environ. Microbiol. 78, 865–875. https://doi.org/10.1128/AEM.07056-11

Haug, A., Rødbotten, R., Mydland, L.T., Christophersen, O.A., 2008. Increased broiler muscle carnosine and anserine following histidine supplementation of commercial broiler feed concentrate. Acta Agric. Scand. A Anim. Sci. 58, 71–77. https://doi.org/10.1080/09064700802213545

He, B., Shiau, A., Choi, K.Y., Zalkin, H., Smith, J.M., 1990. Genes of the *Escherichia coli pur* regulon are negatively controlled by a repressor-operator interaction. J. Bacteriol. 172, 4555–4562.

Heider, S.A.E., Peters-Wendisch, P., Netzer, R., Stafnes, M., Brautaset, T., Wendisch, V.F., 2014. Production and glucosylation of C_{50} and C_{40} carotenoids by metabolically engineered *Corynebacterium glutamicum*. Appl. Microbiol. Biotechnol. 98, 1223–1235. https://doi.org/10.1007/s00253-013-5359-y

Heider, S.A.E., Wendisch, V.F., 2015. Engineering microbial cell factories: Metabolic engineering of *Corynebacterium glutamicum* with a focus on non-natural products. Biotechnol. J. 10, 1170–1184. https://doi.org/10.1002/biot.201400590

Heinze, J.E., Mitani, T., Rich, K.E., Freese, E., 1978. Induction of sporulation by inhibitory purines and related compounds. Biochim. Biophys. Acta 521, 16–26. https://doi.org/10.1016/0005-2787(78)90245-9

Hishinuma, F., Izaki, K., Takahashi, H., 1969. Effects of glycine and D-amino acids on growth of various microorganisms. Agric. Biol. Chem. 33, 1577–1586. https://doi.org/10.1080/00021369.1969.10859511

Hodgkin, J., 2005. Genetic suppression. WormBook. https://doi.org/10.1895/wormbook.1.59.1

Hoffart, E., Grenz, S., Lange, J., Nitschel, R., Müller, F., Schwentner, A., Feith, A., Lenfers-Lücker, M., Takors, R., Blombach, B., 2017. High substrate uptake rates empower *Vibrio natriegens* as production host for industrial biotechnology. Appl. Environ. Microbiol. 83, e01614-17. https://doi.org/10.1128/AEM.01614-17

Holátko, J., Elišáková, V., Prouza, M., Sobotka, M., Nešvera, J., Pátek, M., 2009. Metabolic engineering of the L-valine biosynthesis pathway in *Corynebacterium glutamicum* using promoter activity modulation. J. Biotechnol. 139, 203–210. https://doi.org/10.1016/j.jbiotec.2008.12.005

Horai, H., Arita, M., Kanaya, S., Nihei, Y., Ikeda, T., Suwa, K., Ojima, Y., Tanaka, Kenichi, Tanaka, S., Aoshima, K., Oda, Y., Kakazu, Y., Kusano, M., Tohge, T., Matsuda, F., Sawada, Y., Hirai, M.Y., Nakanishi, H., Ikeda, K., Akimoto, N., Maoka, T., Takahashi, H., Ara, T., Sakurai, N., Suzuki, H., Shibata, D., Neumann, S., Iida, T., Tanaka, Ken, Funatsu, K., Matsuura, F., Soga, T., Taguchi, R., Saito, K., Nishioka, T., 2010. MassBank: a public repository for sharing mass spectral data for life sciences. J. Mass Spectrom. 45, 703–714. https://doi.org/10.1002/jms.1777

Horton, R.M., 1995. PCR-mediated recombination and mutagenesis. SOEing together tailor-made genes. Mol. Biotechnol. 3, 93–99. https://doi.org/10.1007/BF02789105

Horton, R.M., Cai, Z.L., Ho, S.N., Pease, L.R., 1990. Gene splicing by overlap extension: tailor-made genes using the polymerase chain reaction. BioTechniques 8, 528–535.

Hoskisson, P.A., 2018. Microbe Profile: *Corynebacterium diphtheriae* – an old foe always ready to seize opportunity. Microbiology 164, 865–867. https://doi.org/10.1099/mic.0.000627

Hove-Jensen, B., Andersen, K.R., Kilstrup, M., Martinussen, J., Switzer, R.L., Willemoës, M., 2016. Phosphoribosyl diphosphate (PRPP): Biosynthesis, enzymology, utilization, and metabolic significance. Microbiol. Mol. Biol. Rev. 81. https://doi.org/10.1128/MMBR.00040-16

Hove-Jensen, B., Harlow, K.W., King, C.J., Switzer, R.L., 1986. Phosphoribosylpyrophosphate synthetase of *Escherichia coli*. Properties of the purified enzyme and primary structure of the prs gene. J. Biol. Chem. 261, 6765–6771.

Huennekens, F.M., 1969. Folic acid coenzymes in the biosynthesis of purines and pyrimidines, in: Harris, R.S., Wool, I.G., Loraine, J.A., Thimann, K.V. (Eds.), Vitamins & Hormones. Academic Press, p. 375–394. https://doi.org/10.1016/S0083-6729(08)60762-1

Hüser, A.T., Chassagnole, C., Lindley, N.D., Merkamm, M., Guyonvarch, A., Elišáková, V., Pátek, M., Kalinowski, J., Brune, I., Pühler, A., Tauch, A., 2005. Rational design of a *Corynebacterium glutamicum* pantothenate production strain and its characterization by metabolic flux analysis and genome-wide transcriptional profiling. Appl. Environ. Microbiol. 71, 3255–3268. https://doi.org/10.1128/AEM.71.6.3255-3268.2005

Hwang, J.-H., Hwang, G.-H., Cho, J.-Y., 2008. Effect of increased glutamate availability on L-ornithine production in *Corynebacterium glutamicum*. J. Microbiol. Biotechnol. 18, 704–710.

Ikeda, M., 2006. Towards bacterial strains overproducing L-tryptophan and other aromatics by metabolic engineering. Appl. Microbiol. Biotechnol. 69, 615–626. https://doi.org/10.1007/s00253-005-0252-y

Ikeda, M., 2003. Amino acid production processes, in: Faurie, R., Thommel, J., Bathe, B., Debabov, V.G., Huebner, S., Ikeda, M., Kimura, E., Marx, A., Möckel, B., Mueller, U., Pfefferle, W. (Eds.), Microbial Production of L-Amino Acids. Springer-Verlag Berlin Heidelberg, p. 1–35.

Ikeda, M., Katsumata, R., 1999. Hyperproduction of tryptophan by *Corynebacterium glutamicum* with the modified pentose phosphate pathway. Appl. Environ. Microbiol. 65, 2497–2502.

Ikeda, M., Katsumata, R., 1995. Tryptophan production by transport mutants of *Corynebacterium glutamicum*. Biosci. Biotechnol. Biochem. 59, 1600–1602. https://doi.org/10.1271/bbb.59.1600

Ikeda, M., Katsumata, R., 1992. Metabolic engineering to produce tyrosine or phenylalanine in a tryptophan-producing *Corynebacterium glutamicum* strain. Appl. Environ. Microbiol. 58, 781–785.

Ikeda, M., Nakagawa, S., 2003. The *Corynebacterium glutamicum* genome: features and impacts on biotechnological processes. Appl. Microbiol. Biotechnol. 62, 99–109. https://doi.org/10.1007/s00253-003-1328-1

Ikeda, M., Nakanishi, K., Kino, K., Katsumata, R., 1994. Fermentative production of tryptophan by a stable recombinant strain of *Corynebacterium glutamicum* with a modified serine-biosynthetic pathway. Biosci. Biotechnol. Biochem. 58, 674–678. https://doi.org/10.1271/bbb.58.674

Ikeda, M., Okamoto, K., Katsumata, R., 1999. Cloning of the transketolase gene and the effect of its dosage on aromatic amino acid production in *Corynebacterium glutamicum*. Appl. Microbiol. Biotechnol. 51, 201–206.

Ikeda, M., Okamoto, K., Katsumata, R., 1998. A transketolase mutant of *Corynebacterium glutamicum*. Appl Microbiol Biotechnol 50, 375–378. https://doi.org/10.1007/s002530051307

Ingle, R.A., 2011. Histidine biosynthesis. Arabidopsis Book 9. https://doi.org/10.1199/tab.0141

Ishino, S., Kuga, T., Yamaguchi, K., Shirahata, K., Araki, K., 1986. ^{13}C NMR studies of histidine fermentation with a *Corynebacterium glutamicum* mutant. Agric. Biol. Chem. 50, 307–310. https://doi.org/10.1080/00021369.1986.10867392

Ivanov, K., Stoimenova, A., Obreshkova, D., Saso, L., 2013. Biotechnology in the production of pharmaceutical industry ingredients: Amino acids. Biotechnol. Biotechnol. Equip. 27, 3620–3626. https://doi.org/10.5504/BBEQ.2012.0134

Jan, J., Martinez, I., Wang, Y., Bennett, G.N., San, K.-Y., 2013. Metabolic engineering and transhydrogenase effects on NADPH availability in *Escherichia coli*. Biotechnol. Prog. 29, 1124–1130. https://doi.org/10.1002/btpr.1765

Jelsbak, L., Mortensen, M.I.B., Kilstrup, M., Olsen, J.E., 2016. The *in vitro* redundant enzymes PurN and PurT are both essential for systemic infection of mice in *Salmonella enterica* Serovar Typhimurium. Infect. Immun. 84, 2076–2085. https://doi.org/10.1128/IAI.00182-16

Jensen, J.V.K., Eberhardt, D., Wendisch, V.F., 2015. Modular pathway engineering of *Corynebacterium glutamicum* for production of the glutamate-derived compounds ornithine, proline, putrescine, citrulline, and arginine. J. Biotechnol. 214, 85–94. https://doi.org/10.1016/j.jbiotec.2015.09.017

Jensen, K.F., Dandanell, G., Hove-Jensen, B., WillemoËs, M., 2008. Nucleotides, Nucleosides, and Nucleobases. EcoSal Plus 3. https://doi.org/10.1128/ecosalplus.3.6.2

Jensen, R.A., 1969. Metabolic interlock - Regulatory interactions exerted between biochemical pathways. J. Biol. Chem. 244, 2816–2823.

Jetten, M.S.M., Sinskey, A.J., 1993. Characterization of phosphoenolpyruvate carboxykinase from *Corynebacterium glutamicum*. FEMS Microbiol. Lett. 111, 183–188. https://doi.org/10.1111/j.1574-6968.1993.tb06383.x

Jitrapakdee, S., Maurice, M.S., Rayment, I., Cleland, W.W., Wallace, J.C., Attwood, P.V., 2008. Structure, mechanism and regulation of pyruvate carboxylase. Biochem. J. 413, 369–387. https://doi.org/10.1042/BJ20080709

Jo, J.-H., Seol, H.-Y., Lee, Y.-B., Kim, M.-H., Hyun, H.-H., Lee, H.-H., 2012. Disruption of genes for the enhanced biosynthesis of α-ketoglutarate in *Corynebacterium glutamicum*. Can. J. Microbiol. 58, 278–286. https://doi.org/10.1139/w11-132

Jo, S.-J., Leong, C.R., Matsumoto, K., Taguchi, S., 2009. Dual production of poly(3-hydroxybutyrate) and glutamate using variable biotin concentrations in *Corynebacterium glutamicum*. J. Biosci. Bioeng. 107, 409–411. https://doi.org/10.1016/j.jbiosc.2008.12.003

Johnston, H.M., Roth, J.R., 1979. Histidine mutants requiring adenine: Selection of mutants with reduced *hisG* expression in *Salmonella typhimurium*. Genetics 92, 1–15.

Jojima, T., Fujii, M., Mori, E., Inui, M., Yukawa, H., 2010. Engineering of sugar metabolism of *Corynebacterium glutamicum* for production of amino acid L-alanine under oxygen deprivation. Appl. Microbiol. Biotechnol. 87, 159–165. https://doi.org/10.1007/s00253-010-2493-7

Jojima, T., Noburyu, R., Sasaki, M., Tajima, T., Suda, M., Yukawa, H., Inui, M., 2014. Metabolic engineering for improved production of ethanol by *Corynebacterium glutamicum*. Appl. Microbiol. Biotechnol. 1165–1172. https://doi.org/10.1007/s00253-014-6223-4

Joo, Y.-C., Hyeon, J.E., Han, S.O., 2017. Metabolic design of *Corynebacterium glutamicum* for production of L-cysteine with consideration of sulfur-supplemented animal feed. J. Agric. Food Chem. 65, 4698–4707. https://doi.org/10.1021/acs.jafc.7b01061

Jung, S., Chun, J.-Y., Yim, S.-H., Lee, S.-S., Cheon, C.-I., Song, E., Lee, M.-S., 2010. Transcriptional regulation of histidine biosynthesis genes in *Corynebacterium glutamicum*. Can. J. Microbiol. 56, 178–187. https://doi.org/10.1139/w09-115

Jurgenson, C.T., Begley, T.P., Ealick, S.E., 2009. The structural and biochemical foundations of thiamin biosynthesis. Annu. Rev. Biochem. 78, 569–603. https://doi.org/10.1146/annurev.biochem.78.072407.102340

Kafarski, P., 2012. Rainbow code of biotechnology. CHEMIK 66, 811-816.

Kalinowski, J., Bathe, B., Bartels, D., Bischoff, N., Bott, M., Burkovski, A., Dusch, N., Eggeling, L., Eikmanns, B.J., Gaigalat, L., Goesmann, A., Hartmann, M., Huthmacher, K., Krämer, R., Linke, B., McHardy, A.C., Meyer, F., Möckel, B., Pfefferle, W., Pühler, A., Rey, D.A., Rückert, C., Rupp, O., Sahm, H., Wendisch, V.F., Wiegräbe, I., Tauch, A., 2003. The complete *Corynebacterium glutamicum* ATCC 13032 genome sequence and its impact on the production of L-aspartate-derived amino acids and vitamins. J. Biotechnol. 104, 5–25. https://doi.org/10.1016/S0168-1656(03)00154-8

Kamada, N., Yasuhara, A., Ikeda, M., 2003. Significance of the non-oxidative route of the pentose phosphate pathway for supplying carbon to the purine-nucleotide pathway in *Corynebacterium ammoniagenes*. J. Ind. Microbio. Biotechnol. 30, 129–132. https://doi.org/10.1007/s10295-002-0014-0

Kamada, N., Yasuhara, A., Takano, Y., Nakano, T., Ikeda, M., 2001. Effect of transketolase modifications on carbon flow to the purine-nucleotide pathway in *Corynebacterium ammoniagenes*. Appl. Microbiol. Biotechnol. 56, 710–717. https://doi.org/10.1007/s002530100738

Kanarek, N., Keys, H.R., Cantor, J.R., Lewis, C.A., Chan, S.H., Kunchok, T., Abu-Remaileh, M., Freinkman, E., Schweitzer, L.D., Sabatini, D.M., 2018. Histidine catabolism is a major determinant of methotrexate sensitivity. Nature 559, 632–636. https://doi.org/10.1038/s41586-018-0316-7

Kasai, T., 1974. Regulation of the expression of the histidine operon in *Salmonella typhimurium*. Nature 249, 523–527. https://doi.org/10.1038/249523a0

Kawaguchi, H., Sasaki, M., Vertès, A.A., Inui, M., Yukawa, H., 2008. Engineering of an L-arabinose metabolic pathway in *Corynebacterium glutamicum*. Appl. Microbiol. Biotechnol. 77, 1053–1062. https://doi.org/10.1007/s00253-007-1244-x

Kawai, Y., Moriyama, A., Asai, K., Coleman-Campbell, C.M., Sumi, S., Morishita, H., Suchi, M., 2005. Molecular characterization of histidinemia: identification of four missense mutations in the histidase gene. Hum. Genet. 116, 340–346. https://doi.org/10.1007/s00439-004-1232-5

Keilhauer, C., Eggeling, L., Sahm, H., 1993. Isoleucine synthesis in *Corynebacterium glutamicum*: molecular analysis of the *ilvB-ilvN-ilvC* operon. J. Bacteriol. 175, 5595–5603.

Keller, K.A., Chu, Y., Grider, A., Coffield, J.A., 2000. Supplementation with L-Histidine during Dietary Zinc Repletion Improves Short-Term Memory in Zinc-Restricted Young Adult Male Rats. J Nutr 130, 1633–1640. https://doi.org/10.1093/jn/130.6.1633

Kiefer, P., Heinzle, E., Wittmann, C., 2002. Influence of glucose, fructose and sucrose as carbon sources on kinetics and stoichiometry of lysine production by *Corynebacterium glutamicum*. J. Ind. Microbiol. Biotechnol. 28, 338–343. https://doi.org/10.1038/sj/jim/7000252

Kiefer, P., Heinzle, E., Zelder, O., Wittmann, C., 2004. Comparative metabolic flux analysis of lysine-producing *Corynebacterium glutamicum* cultured on glucose or fructose. Appl. Environ. Microbiol. 70, 229–239. https://doi.org/10.1128/AEM.70.1.229-239.2004

Kikuchi, G., Motokawa, Y., Yoshida, T., Hiraga, K., 2008. Glycine cleavage system: reaction mechanism, physiological significance, and hyperglycinemia. Proc. Jpn. Acad. Ser. B Phys. Biol. Sci. 84, 246–263. https://doi.org/10.2183/pjab/84.246

Kilstrup, M., Martinussen, J., 1998. A transcriptional activator, homologous to the *Bacillus subtilis* PurR repressor, is required for expression of purine biosynthetic genes in *Lactococcus lactis*. J. Bacteriol. 180, 3907–3916.

Kim, H.-J., Kim, T.-H., Kim, Y., Lee, H.-S., 2004. Identification and characterization of *glxR*, a gene involved in regulation of glyoxylate bypass in *Corynebacterium glutamicum*. J. Bacteriol. 186, 3453–3460. https://doi.org/10.1128/JB.186.11.3453-3460.2004

Kim, H.J., Lee, H.S., C., 1997. Gene amplification of *aceA* and *aceB* in lysine-producing *Corynebacterium glutamicum* ssp. lactofermentum ATCC21799. J. Microbiol. Biotechnol. 7, 287–292.

Kim, J.W., Kim, H.J., Kim, Y., Lee, M.S., Lee, H.S., 2001. Properties of the *Corynebacterium glutamicum metC* gene encoding cystathionine beta-lyase. Mol. Cells 11, 220–225.

Kim, P.B., Nelson, J.W., Breaker, R.R., 2015. An ancient riboswitch class in bacteria regulates purine biosynthesis and one-carbon metabolism. Mol. Cell 57, 317–328. https://doi.org/10.1016/j.molcel.2015.01.001

Kim, S.Y., Lee, J., Lee, S.Y., 2014. Metabolic engineering of *Corynebacterium glutamicum* for the production of L-ornithine. Biotechnol. Bioeng. https://doi.org/10.1002/bit.25440

Kimura, K., Nakamura, Y., Inaba, Y., Matsumoto, M., Kido, Y., Asahara, S., Matsuda, T., Watanabe, H., Maeda, A., Inagaki, F., Mukai, C., Takeda, K., Akira, S., Ota, T., Nakabayashi, H., Kaneko, S., Kasuga, M., Inoue, H., 2013. Histidine augments the suppression of hepatic glucose production by central insulin action. Diabetes 62, 2266–2277. https://doi.org/10.2337/db12-1701

Kinoshita, S., Nakayama, K., Akita, S., 1958. Taxonomical study of glutamic acid accumulating bacteria, *Micrococcus glutamicus* nov. sp. Bull. Chem. Soc. Jpn. 22, 176–185.

Kinoshita, S., Udaka, S., Shimono, M., 2004. Studies on the amino acid fermentation. Part 1. Production of L-glutamic acid by various microorganisms. J. Gen. Appl. Microbiol. 50, 331–343.

Kinoshita, S., Udaka, S., Shimono, M., 1957. Studies on the amino acid fermentation: I. Production of L-glutamic acid by various microorganisms. J. Gen. Appl. Microbiol. 3, 193–205.

Kirchner, O., Tauch, A., 2003. Tools for genetic engineering in the amino acid-producing bacterium *Corynebacterium glutamicum*. J. Biotechnol. 104, 287–299. https://doi.org/10.1016/S0168-1656(03)00148-2

Kiyoshi, K., Kawashima, S., Nobuki, K., Kadokura, T., Nakazato, A., Suzuki, K., Nakayama, S., 2017. Adenine addition restores cell viability and butanol production in *Clostridium saccharoperbutylacetonicum* N1-4 (ATCC 13564) cultivated at 37°C. Appl. Environ. Microbiol. 83. https://doi.org/10.1128/AEM.02960-16

Klaffl, S., Brocker, M., Kalinowski, J., Eikmanns, B.J., Bott, M., 2013. Complex regulation of the phosphoenolpyruvate carboxykinase gene *pck* and characterization of its GntR-type regulator IolR as a repressor of *myo*-inositol utilization genes in *Corynebacterium glutamicum*. J. Bacteriol. 195, 4283–4296. https://doi.org/10.1128/JB.00265-13

Klaffl, S., Eikmanns, B.J., 2010. Genetic and functional analysis of the soluble oxaloacetate decarboxylase from *Corynebacterium glutamicum*. J. Bacteriol. 192, 2604–2612. https://doi.org/10.1128/JB.01678-09

Klöckner, W., Büchs, J., 2012. Advances in shaking technologies. Trends Biotechnol. 30, 307-314. https://doi.org/10.1016/j.tibtech.2012.03.001

Klyachko, E., Shakulov, R., Kozlov, Y., 2004a. Method for producing L-histidine using Enterobacteriaceae bacteria which has an enhanced *purH* gene produced, patent US7785860B2 (https://patents.google.com/patent/US7785860B2/en?oq=US7785860B2; last access 2018-10-16)

Klyachko, E., Shakulov, R., Kozlov, Y., 2004b. Mutant phosphoribosylpyrophosphate synthetase and method for producing L-histidine. US8071339B2 (https://patents.google.com/patent/US8071339B2/en; last access 2018-10-16)

Kopple, J.D., Swendseid, M.E., 1975. Evidence that histidine is an essential amino acid in normal and chronically uremic man. J. Clin. Invest. 55, 881–891.

Korajlija, J., Delíc, V., 1977. Histidine production by a regulatory mutant of *Streptomyces coelicolor*. Appl. Environl. Microbiol. 34, 621–625.

Krause, F.S., Blombach, B., Eikmanns, B.J., 2010. Metabolic engineering of *Corynebacterium glutamicum* for 2-ketoisovalerate production. Appl. Environ. Microbiol. 76, 8053–8061. https://doi.org/10.1128/AEM.01710-10

Krömer, J.O., Wittmann, C., Schröder, H., Heinzle, E., 2006. Metabolic pathway analysis for rational design of L-methionine production by Escherichia coli and *Corynebacterium glutamicum*. Metab. Eng. 8, 353–369. https://doi.org/10.1016/j.ymben.2006.02.001

Küberl, A., Fränzel, B., Eggeling, L., Polen, T., Wolters, D.A., Bott, M., 2014. Pupylated proteins in *Corynebacterium glutamicum* revealed by MudPIT analysis. Proteomics 14, 1531-1542. https://doi.org/10.1002/pmic.201300531

Kubota, K., Shiro, T., Okumura, S., 1971. Fermentative production of L-histidine. J. Gen. Appl. Microbiol. 17, 1–12. https://doi.org/10.2323/jgam.17.1

Kulis-Horn, R.K., Persicke, M., Kalinowski, J., 2015. *Corynebacterium glutamicum* ATP-phosphoribosyl transferases suitable for L-histidine production – Strategies for the elimination of feedback inhibition. J. Biotechnol. 206, 26–37. https://doi.org/10.1016/j.jbiotec.2015.04.001

Kulis-Horn, R.K., Persicke, M., Kalinowski, J., 2014. Histidine biosynthesis, its regulation and biotechnological application in *Corynebacterium glutamicum*. Microb. Biotechnol. 7, 5–25. https://doi.org/10.1111/1751-7915.12055

Kulis-Horn, R.K., Rückert, C., Kalinowski, J., Persicke, M., 2017. Sequence-based identification of inositol monophosphatase-like histidinol-phosphate phosphatases (HisN) in *Corynebacterium glutamicum*, Actinobacteria, and beyond. BMC Microbiol. 17. https://doi.org/10.1186/s12866-017-1069-4

Kumar, A., Singh, S., 2013. Directed evolution: tailoring biocatalysts for industrial applications. Crit. Rev. Biotechnol. 33, 365–378. https://doi.org/10.3109/07388551.2012.716810

Lai, S., Zhang, Y., Liu, S., Liang, Y., Shang, X., Chai, X., Wen, T., 2012. Metabolic engineering and flux analysis of *Corynebacterium glutamicum* for L-serine production. Sci. China Life Sci. 55, 283–290. https://doi.org/10.1007/s11427-012-4304-0

Lambrecht, J.A., Downs, D.M., 2013. Anthranilate phosphoribosyl transferase (TrpD) generates phosphoribosylamine for thiamine synthesis from enamines and phosphoribosyl pyrophosphate. ACS Chem. Biol. 8, 242–248. https://doi.org/10.1021/cb300364k

Lanéelle, M.-A., Tropis, M., Daffé, M., 2013. Current knowledge on mycolic acids in *Corynebacterium glutamicum* and their relevance for biotechnological processes. Appl. Microbiol. Biotechnol. 97, 9923–9930. https://doi.org/10.1007/s00253-013-5265-3

Lange, J., Müller, F., Takors, R., Blombach, B., 2017. Harnessing novel chromosomal integration loci to utilize an organosolv-derived hemicellulose fraction for isobutanol production with engineered *Corynebacterium glutamicum*. Microb. Biotechnol. 11, 257–263. https://doi.org/10.1111/1751-7915.12879

Lange, J., Münch, E., Müller, J., Busche, T., Kalinowski, J., Takors, R., Blombach, B., 2018. Deciphering the adaptation of *Corynebacterium glutamicum* in transition from aerobiosis via microaerobiosis to anaerobiosis. Genes 9, 297. https://doi.org/10.3390/genes9060297

Lee, S.Y., Kim, H.U., Park, J.H., Park, J.M., Kim, T.Y., 2009. Metabolic engineering of microorganisms: general strategies and drug production. Drug Discov. Today 14, 78–88. https://doi.org/10.1016/j.drudis.2008.08.004

Lee, W.-H., Kim, M.-D., Jin, Y.-S., Seo, J.-H., 2013. Engineering of NADPH regenerators in *Escherichia coli* for enhanced biotransformation. Appl. Microbiol. Biotechnol. 97, 2761–2772. https://doi.org/10.1007/s00253-013-4750-z

Lengeler, J.W., Jahreis, K., Wehmeier, U.F., 1994. Enzymes II of the phosphoenolpyruvate-dependent phosphotransferase systems: Their structure and function in carbohydrate transport. Biochim. Biophys. Acta 1188, 1–28. https://doi.org/10.1016/0005-2728(94)90017-5

Leonardi, R., Roach, P.L., 2004. Thiamine biosynthesis in *Escherichia coli*. J. Biol. Chem. 279, 17054–17062. https://doi.org/10.1074/jbc.M312714200

Leyval, D., Uy, D., Delaunay, S., Goergen, J.L., Engasser, J.M., 2003. Characterisation of the enzyme activities involved in the valine biosynthetic pathway in a valine-producing strain of *Corynebacterium glutamicum*. J. Biotechnol. 104, 241–252. https://doi.org/10.1016/S0168-1656(03)00162-7

Li, Ying, Cong, H., Liu, B., Song, J., Sun, X., Zhang, J., Yang, Q., 2016. Metabolic engineering of *Corynebacterium glutamicum* for methionine production by removing feedback inhibition and increasing NADPH level. Antonie van Leeuwenhoek 109, 1185–1197. https://doi.org/10.1007/s10482-016-0719-0

Li, Yanjun, Sun, L., Feng, J., Wu, R., Xu, Q., Zhang, C., Chen, N., Xie, X., 2016. Efficient production of α-ketoglutarate in the *gdh* deleted *Corynebacterium glutamicum* by novel double-phase pH and biotin control strategy. Bioprocess Biosyst. Eng. 39, 967–976. https://doi.org/10.1007/s00449-016-1576-y

Liao, S.-M., Du, Q.-S., Meng, J.-Z., Pang, Z.-W., Huang, R.-B., 2013. The multiple roles of histidine in protein interactions. Chem. Cent. J. 7, 44. https://doi.org/10.1186/1752-153X-7-44

Liebl, W., Klamer, R., Schleifer, K.-H., 1989. Requirement of chelating compounds for the growth of *Corynebacterium glutamicum* in synthetic media. Appl. Microbiol. Biotechnol. 32, 205–210. https://doi.org/10.1007/BF00165889

Lin, J.-L., Wagner, J.M., Alper, H.S., 2017. Enabling tools for high-throughput detection of metabolites: Metabolic engineering and directed evolution applications. Biotechnol. Adv. https://doi.org/10.1016/j.biotechadv.2017.07.005

Litsanov, B., Brocker, M., Bott, M., 2013. Glycerol as a substrate for aerobic succinate production in minimal medium with *Corynebacterium glutamicum*: Succinate production from glycerol. Microb. Biotechnol. 6, 189–195. https://doi.org/10.1111/j.1751-7915.2012.00347.x

Litsanov, B., Kabus, A., Brocker, M., Bott, M., 2012. Efficient aerobic succinate production from glucose in minimal medium with *Corynebacterium glutamicum*. Microb. Biotechnol. 5, 116–128. https://doi.org/10.1111/j.1751-7915.2011.00310.x

Liu, M., Ding, Y., Xian, M., Zhao, G., 2018. Metabolic engineering of a xylose pathway for biotechnological production of glycolate in *Escherichia coli*. Microb. Cell Fact. 17, 51. https://doi.org/10.1186/s12934-018-0900-4

Liu, Q., Zhang, J., Wei, X.-X., Ouyang, S.-P., Wu, Q., Chen, G.-Q., 2008. Microbial production of L-glutamate and L-glutamine by recombinant *Corynebacterium glutamicum* harboring *Vitreoscilla* hemoglobin gene *vgb*. Appl. Microbiol. Biotechnol. 77, 1297–1304. https://doi.org/10.1007/s00253-007-1254-8

Löffler, M., Simen, J.D., Jäger, G., Schäferhoff, K., Freund, A., Takors, R., 2016. Engineering *E. coli* for large-scale production – strategies considering ATP expenses and transcriptional responses. Metab. Eng. 38, 73–85. https://doi.org/10.1016/j.ymben.2016.06.008

Löliger, J., 2000. Function and importance of glutamate for savory foods. J. Nutr. 130, 915-920. https://doi.org/10.1093/jn/130.4.915S

Losen, M., Frölich, B., Pohl, M., Büchs, J., 2004. Effect of oxygen limitation and medium composition on *Escherichia coli* fermentation in shake-flask cultures. Biotechnol. Prog. 20, 1062–1068. https://doi.org/10.1021/bp034282t

Lu, W., Kwon, Y.K., Rabinowitz, J.D., 2007. Isotope ratio-based profiling of microbial folates. J. Am. Soc. Mass Spectrom. 18, 898–909. https://doi.org/10.1016/j.jasms.2007.01.017

Ma, Q., Zhang, Q., Xu, Q., Zhang, C., Li, Y., Fan, X., Xie, X., Chen, N., 2017. Systems metabolic engineering strategies for the production of amino acids. Synth. Syst. Biotechnol. 2, 87–96. https://doi.org/10.1016/j.synbio.2017.07.003

Mahr, R., Gätgens, C., Gätgens, J., Polen, T., Kalinowski, J., Frunzke, J., 2015. Biosensor-driven adaptive laboratory evolution of L-valine production in *Corynebacterium glutamicum*. Metab. Eng. 32, 184–194. https://doi.org/10.1016/j.ymben.2015.09.017

Malykh, E.A., Butov, I.A., Ravcheeva, A.B., Krylov, A.A., Mashko, S.V., Stoynova, N.V., 2018. Specific features of L-histidine production by *Escherichia coli* concerned with feedback control of AICAR formation and inorganic phosphate/metal transport. Microb. Cell Fact. 17. https://doi.org/10.1186/s12934-018-0890-2

Marienfeld, S., Uhlemann, E.-M., Schmid, R., Krämer, R., Burkovski, A., 1997. Ultrastructure of the *Corynebacterium glutamicum* cell wall. Antonie Van Leeuwenhoek 72, 291–297. https://doi.org/10.1023/A:1000578811089

Marienhagen, J., Sandalova, T., Sahm, H., Eggeling, L., Schneider, G., 2008. Insights into the structural basis of substrate recognition by histidinol-phosphate aminotransferase from *Corynebacterium glutamicum*. Acta Cryst. 64, 675–685. https://doi.org/10.1107/S0907444908009438

Matsui, H., Kawasaki, H., Shimaoka, M., Kurahashi, O., 2001. Investigation of various genotype characteristics for inosine accumulation in *Escherichia coli* W3110. Biosc. Biotechnol. Biochem. 65, 570–578. https://doi.org/10.1271/bbb.65.570

McCullum, E.O., Williams, B.A.R., Zhang, J., Chaput, J.C., 2010. Random mutagenesis by error-prone PCR, in: Braman, J. (Ed) *In vitro* mutagenesis protocols. Methods in molecular biology (Methods and protocols). Humana Press, Totowa, NJ, p. 103–109. https://doi.org/10.1007/978-1-60761-652-8_7

McDaniel, L.E., Bailey, E.G., 1969. Effect of shaking speed and type of closure on shake flask cultures. Appl. Microbiol. 17, 286–290.

McGuire, J.J., Rabinowitz, J.C., 1978. Studies on the mechanism of formyltetrahydrofolate synthetase. The *Peptococcus aerogenes* enzyme. J. Biol. Chem. 253, 1079–1085.

McHardy, A.C., Tauch, A., Rückert, C., Pühler, A., Kalinowski, J., 2003. Genome-based analysis of biosynthetic aminotransferase genes of *Corynebacterium glutamicum*. J. Biotechnol. 104, 229–240. https://doi.org/10.1016/S0168-1656(03)00161-5

Meedel, T.H., Pizer, L.I., 1974. Regulation of one-carbon biosynthesis and utilization in *Escherichia coli*. J Bacteriol 118, 905–910.

Meng, L.M., Kilstrup, M., Nygaard, P., 1990. Autoregulation of PurR repressor synthesis and involvement of *purR* in the regulation of *purB*, *purC*, *purL*, *purMN* and *guaBA* expression in *Escherichia coli*. Eur. J. Biochem. 187, 373–379. https://doi.org/10.1111/j.1432-1033.1990.tb15314.x

Michel, A., Koch-Koerfges, A., Krumbach, K., Brocker, M., Bott, M., 2015. Anaerobic growth of *Corynebacterium glutamicum* via mixed-acid fermentation. Appl. Environ. Microbiol. 81, 7496–7508. https://doi.org/10.1128/AEM.02413-15

Mimitsuka, T., Sawai, H., Hatsu, M., Yamada, K., 2007. Metabolic engineering of *Corynebacterium glutamicum* for cadaverine fermentation. Biosci. Biotechnol. Biochem. 71, 2130–2135. https://doi.org/10.1271/bbb.60699

Minami, M., Ando, T., Hashikawa, S., Torii, K., Hasegawa, T., Israel, D.A., Ina, K., Kusugami, K., Goto, H., Ohta, M., 2004. Effect of glycine on *Helicobacter pylori in vitro*. Antimicrob. Agents Chemother. 48, 3782–3788. https://doi.org/10.1128/AAC.48.10.3782-3788.2004

Mizukami, T., Hamu, A., Ikeda, M., Oka, T., Katsumata, R., 1994. Cloning of the ATP phosphoribosyl transferase gene of *Corynebacterium glutamicum* and application of the gene to L-histidine production. Biosci. Biotechnol. Biochem. 58, 635–638. https://doi.org/10.1271/bbb.58.635

Moon, M.-W., Kim, H.-J., Oh, T.-K., Shin, C.-S., Lee, J.-S., Kim, S.-J., Lee, J.-K., 2005. Analyses of enzyme II gene mutants for sugar transport and heterologous expression of fructokinase gene in *Corynebacterium glutamicum* ATCC 13032. FEMS Microbiol. Lett. 244, 259–266. https://doi.org/10.1016/j.femsle.2005.01.053

Moon, M.-W., Park, S.-Y., Choi, S.-K., Lee, J.-K., 2007. The phosphotransferase system of *Corynebacterium glutamicum* features of sugar transport and carbon regulation. J. Mol. Microbiol. Biotechnol. 12, 43–50. https://doi.org/10.1159/000096458

Morikawa, M., Izui, K., Taguchi, M., Katsuki, H., 1980. Regulation of *Escherichia coli* phosphoenolpyruvate carboxylase by multiple effectors *in vivo*. J. Biochem. 87, 441–449.

Moritz, B., Striegel, K., de Graaf, A.A., Sahm, H., 2000. Kinetic properties of the glucose-6-phosphate and 6 phosphogluconate dehydrogenases from *Corynebacterium glutamicum* and their application for predicting pentose phosphate pathway flux *in vivo*. Eur. J. Biochem. 267, 3442–3452. https://doi.org/10.1046/j.1432-1327.2000.01354.x

Mormann, S., Lömker, A., Rückert, C., Gaigalat, L., Tauch, A., Pühler, A., Kalinowski, J., 2006. Random mutagenesis in *Corynebacterium glutamicum* ATCC 13032 using an IS6100-based transposon vector identified the last unknown gene in the histidine biosynthesis pathway. BMC Genomics 7, 205. https://doi.org/10.1186/1471-2164-7-205

Morton, D.P., Parsons, S.M., 1977. Synergistic inhibition of ATP phosphoribosyltransferase by guanosine tetraphosphate and histidine. Biochem. Biophys. Res. Commun. 74, 172–177. https://doi.org/10.1016/0006-291X(77)91390-0

Motter, A.E., Gulbahce, N., Almaas, E., Barabási, A.-L., 2008. Predicting synthetic rescues in metabolic networks. Mol. Syst. Biol. 4, 168. https://doi.org/10.1038/msb.2008.1

Mueller, E.J., Meyer, E., Rudolph, J., Davisson, V.J., Stubbe, J., 1994. N_5-carboxyaminoimidazole ribonucleotide: Evidence for a new intermediate and two new enzymic activities in the *de novo* purine biosynthetic pathway of *Escherichia coli*. Biochemistry 33, 2269–2278. https://doi.org/10.1021/bi00174a038

Mullis, K.B., Faloona, F.A., 1987. Specific synthesis of DNA *in vitro* via a polymerase-catalyzed chain reaction, in: Methods in Enzymology 155, p. 335–350. https://doi.org/10.1016/0076-6879(87)55023-6

Murakami, H., Hohsaka, T., Sisido, M., 2002. Random insertion and deletion of arbitrary number of bases for codon-based random mutation of DNAs. Nat. Biotechnol. 20, 76–81.

Murray, A.W., 1971. The biological significance of purine salvage. Annu. Rev. Biochem. 40, 811–826. https://doi.org/10.1146/annurev.bi.40.070171.004115

Mussatto, S.I., Ballesteros, L.F., Teixeira, S.M. and J.A., 2012. Use of agro-industrial wastes in solid-state fermentation processes. Industrial Waste. https://doi.org/10.5772/36310

Myers, R.M., Lerman, L.S., Maniatis, T., 1985. A general method for saturation mutagenesis of cloned DNA fragments. Science 229, 242–247. https://doi.org/10.1126/science.2990046

Nagy, P.L., McCorkle, G.M., Zalkin, H., 1993. *purU*, a source of formate for *purT*-dependent phosphoribosyl-N-formylglycinamide synthesis. J. Bacteriol. 175, 7066–7073.

Nelson, D., Cox, M., 2009. Lehninger Biochemie, 4th ed, Springer-Lehrbuch. Springer-Verlag, Berlin Heidelberg.

Ness, J.E., Kim, S., Gottman, A., Pak, R., Krebber, A., Borchert, T.V., Govindarajan, S., Mundorff, E.C., Minshull, J., 2002. Synthetic shuffling expands functional protein diversity by allowing amino acids to recombine independently. Nat. Biotechnol. 20, 1251–1255. https://doi.org/10.1038/nbt754

Nešvera, J., Pátek, M., 2011. Tools for genetic manipulations in *Corynebacterium glutamicum* and their applications. Appl. Microbiol. Biotechnol. 90, 1641. https://doi.org/10.1007/s00253-011-3272-9

Netzer, R., Peters-Wendisch, P., Eggeling, L., Sahm, H., 2004. Cometabolism of a nongrowth substrate: L-Serine utilization by *Corynebacterium glutamicum*. Appl. Environ. Microbiol. 70, 7148–7155. https://doi.org/10.1128/AEM.70.12.7148-7155.2004

Nevo, E., 2011. Evolution under environmental stress at macro- and microscales. Genome Biol. Evol. 3, 1039–1052. https://doi.org/10.1093/gbe/evr052

Nguyen, A.Q.D., Schneider, J., Reddy, G.K., Wendisch, V.F., 2015. Fermentative production of the diamine putrescine: system metabolic engineering of *Corynebacterium glutamicum*. Metabolites 5, 211–231. https://doi.org/10.3390/metabo5020211

Nielsen, J., Keasling, J.D., 2016. Engineering cellular metabolism. Cell 164, 1185–1197. https://doi.org/10.1016/j.cell.2016.02.004

Nishimura, T., Vertès, A.A., Shinoda, Y., Inui, M., Yukawa, H., 2007. Anaerobic growth of *Corynebacterium glutamicum* using nitrate as a terminal electron acceptor. Appl. Microbiol. Biotechnol. 75, 889–897. https://doi.org/10.1007/s00253-007-0879-y

Noh, M.H., Lim, H.G., Park, S., Seo, S.W., Jung, G.Y., 2017. Precise flux redistribution to glyoxylate cycle for 5-aminolevulinic acid production in *Escherichia coli*. Metab. Eng. 43, 1-8. https://doi.org/10.1016/j.ymben.2017.07.006

Nygaard, P., Smith, J.M., 1993. Evidence for a novel glycinamide ribonucleotide transformylase in *Escherichia coli*. J. Bacteriol. 175, 3591–3597.

O'Gara, J.P., Dunican, L.K., 1995. Mutations in the *trpD* gene of *Corynebacterium glutamicum* confer 5-methyltryptophan resistance by encoding a feedback-resistant anthranilate phosphoribosyltransferase. Appl. Environ. Microbiol. 61, 4477–4479.

Ohnishi, J., Katahira, R., Mitsuhashi, S., Kakita, S., Ikeda, M., 2005. A novel *gnd* mutation leading to increased L-lysine production in *Corynebacterium glutamicum*. FEMS Microbiol. Lett. 242, 265–274. https://doi.org/10.1016/j.femsle.2004.11.014

Okamura-Ikeda, K., Ohmura, Y., Fujiwara, K., Motokawa, Y., 1993. Cloning and nucleotide sequence of the *gcv* operon encoding the *Escherichia coli* glycine-cleavage system. Eur. J. Biochem. 216, 539–548. https://doi.org/10.1111/j.1432-1033.1993.tb18172.x

Oldiges, M., Eikmanns, B.J., Blombach, B., 2014. Application of metabolic engineering for the biotechnological production of L-valine. Appl. Microbiol. Biotechnol. 98, 5859–5870. https://doi.org/10.1007/s00253-014-5782-8

O'Mahony, L., Akdis, M., Akdis, C.A., 2011. Regulation of the immune response and inflammation by histamine and histamine receptors. J. Allergy Clin. Immunol. 128, 1153–1162. https://doi.org/10.1016/j.jaci.2011.06.051

Omumasaba, C.A., Okai, N., Inui, M., Yukawa, H., 2005. *Corynebacterium glutamicum* glyceraldehyde-3-phosphate dehydrogenase isoforms with opposite, ATP-dependent regulation. J. Mol. Microbiol. Biotechnol. 8, 91–103. https://doi.org/10.1159/000084564

Orth, J.D., Thiele, I., Palsson, B.Ø., 2010. What is flux balance analysis? Nat. Biotechnol. 28, 245–248. https://doi.org/10.1038/nbt.1614

Ownby, K., Xu, H., White, R.H., 2005. A *Methanocaldococcus jannaschii* archaeal signature gene encodes for a 5-Formaminoimidazole-4-carboxamide-1-β-d-ribofuranosyl 5′-monophosphate synthetase - a new enzyme in purine biosynthesis. J. Biol. Chem. 280, 10881–10887. https://doi.org/10.1074/jbc.M413937200

Pacholarz, K.J., Burnley, R.J., Jowitt, T.A., Ordsmith, V., Pisco, J.P., Porrini, M., Larrouy-Maumus, G., Garlish, R.A., Taylor, R.J., de Carvalho, L.P.S., Barran, P.E., 2017. Hybrid mass spectrometry approaches to determine how L-histidine feedback regulates the enzyzme MtATP-phosphoribosyltransferase. Structure 25, 730-738. https://doi.org/10.1016/j.str.2017.03.005

Papagianni, M., 2012. Recent advances in engineering the central carbon metabolism of industrially important bacteria. Microb. Cell Fact. 11, 50. https://doi.org/10.1186/1475-2859-11-50

Parche, S., Burkovski, A., Sprenger, G.A., Weil, B., Krämer, R., Titgemeyer, F., 2001. *Corynebacterium glutamicum*: a dissection of the PTS. J. Mol. Microbiol. Biotechnol. 3, 423-428.

Park, J.H., Lee, S.Y., 2010. Fermentative production of branched chain amino acids: a focus on metabolic engineering. Appl. Microbiol. Biotechnol. 85, 491–506. https://doi.org/10.1007/s00253-009-2307-y

Park, S.H., Kim, H.U., Kim, T.Y., Park, J.S., Kim, S.-S., Lee, S.Y., 2014. Metabolic engineering of *Corynebacterium glutamicum* for L-arginine production. Nat. Commun. 5. https://doi.org/10.1038/ncomms5618

Park, S.W., Kim, C.H., Namgung, N., Jung, B.Y., Paik, I.K., Kil, D.Y., 2013. Effects of dietary supplementation of histidine, β-alanine, magnesium oxide, and blood meal on carnosine and anserine concentrations of broiler breast meat. J. Poult. Sci. 50, 251–256. https://doi.org/10.2141/jpsa.0120064

Parkhomchuk, D., Amstislavskiy, V., Soldatov, A., Ogryzko, V., 2009. Use of high throughput sequencing to observe genome dynamics at a single cell level. Proc. Natl. Acad. Sci. U.S.A. 106, 20830–20835. https://doi.org/10.1073/pnas.0906681106

Parsons, M.E., Ganellin, C.R., 2006. Histamine and its receptors. Br. J. Pharmacol. 147, 127-135. https://doi.org/10.1038/sj.bjp.0706440

Patrick, W.M., Matsumura, I., 2008. A study in molecular contingency: glutamine phosphoribosylpyrophosphate amidotransferase is a promiscuous and evolvable phosphoribosylanthranilate isomerase. J. Mol. Biol. 377, 323–336. https://doi.org/10.1016/j.jmb.2008.01.043

Pearce, M.J., Mintseris, J., Ferreyra, J., Gygi, S.P., Darwin, K.H., 2008. Ubiquitin-like protein involved in the proteasome pathway of *Mycobacterium tuberculosis*. Science 322, 1104–1107. https://doi.org/10.1126/science.1163885

Pedreño, S., Pisco, J.P., Larrouy-Maumus, G., Kelly, G., de Carvalho, L.P.S., 2012. Mechanism of feedback allosteric inhibition of ATP phosphoribosyltransferase. Biochemistry 51, 8027–8038. https://doi.org/10.1021/bi300808b

Peifer, S., Barduhn, T., Zimmet, S., Volmer, D.A., Heinzle, E., Schneider, K., 2012. Metabolic engineering of the purine biosynthetic pathway in *Corynebacterium glutamicum* results in increased intracellular pool sizes of IMP and hypoxanthine. Microb. Cell Fact. 11, 138. https://doi.org/10.1186/1475-2859-11-138

Petersen, H.U., Danchin, A., Grunberg-Manago, M., 1976a. Toward an understanding of the formylation of initiator tRNA methionine in prokaryotic protein synthesis. II. A two-state model for the 70S ribosome. Biochemistry 15, 1362–1369. https://doi.org/10.1021/bi00652a002

Petersen, H.U., Danchin, A., Grunberg-Manago, M., 1976b. Toward an understanding of the formylation of initiator tRNA methionine in prokaryotic protein synthesis. I. *In vitro* studies of the 30S and 70S ribosomal-tRNA complex. Biochemistry 15, 1357–1362. https://doi.org/10.1021/bi00652a001

Peters-Wendisch, P.G., Eikmanns, B.J., Thierbach, G., Bachmann, B., Sahm, H., 1993. Phosphoenolpyruvate carboxylase in *Corynebacterium glutamicum* is dispensable for growth and lysine production. FEMS Microbiol. Lett. 112, 269–274. https://doi.org/10.1111/j.1574-6968.1993.tb06461.x

Peters-Wendisch, P.G., Kreutzer, C., Kalinowski, J., Pátek, M., Sahm, H., Eikmanns, B.J., 1998. Pyruvate carboxylase from *Corynebacterium glutamicum*: characterization, expression and inactivation of the *pyc* gene. Microbiology 144, 915–927. https://doi.org/10.1099/00221287-144-4-915

Pfeifer, E., Gätgens, C., Polen, T., Frunzke, J., 2017. Adaptive laboratory evolution of *Corynebacterium glutamicum* towards higher growth rates on glucose minimal medium. Sci. Rep. 7, 16780. https://doi.org/10.1038/s41598-017-17014-9

Pfeifer-Sancar, K., Mentz, A., Rückert, C., Kalinowski, J., 2013. Comprehensive analysis of the *Corynebacterium glutamicum* transcriptome using an improved RNAseq technique. BMC Genomics 14, 888.

Pharkya, P., Maranas, C.D., 2006. An optimization framework for identifying reaction activation/inhibition or elimination candidates for overproduction in microbial systems. Metab. Eng. 8, 1–13. https://doi.org/10.1016/j.ymben.2005.08.003

Piper, M.D., Hong, S.-P., Ball, G.E., Dawes, I.W., 2000. Regulation of the balance of one-carbon metabolism in *Saccharomyces cerevisiae*. J. Biol. Chem. 275, 30987–30995. https://doi.org/10.1074/jbc.M004248200

Polgár, L., 2005. The catalytic triad of serine peptidases. Cell. Mol. Life Sci. 62, 2161–2172. https://doi.org/10.1007/s00018-005-5160-x

Post, D.A., Switzer, R.L., 1991. *prsB* is an allele of the *Salmonella typhimurium prsA* gene: characterization of a mutant phosphoribosylpyrophosphate synthetase. J. Bacteriol. 173, 1978-1986.

Pridmore, R.D., 1987. New and versatile cloning vectors with kanamycin-resistance marker. Gene 56, 309–312.

Radmacher, E., Vaitsikova, A., Burger, U., Krumbach, K., Sahm, H., Eggeling, L., 2002. Linking central metabolism with increased pathway flux: L-Valine accumulation by *Corynebacterium glutamicum*. Appl. Environ. Microbiol. 68, 2246–2250. https://doi.org/10.1128/AEM.68.5.2246-2250.2002

Radoš, D., Turner, D.L., Fonseca, L.L., Carvalho, A.L., Blombach, B., Eikmanns, B.J., Neves, A.R., Santos, H., 2014. Carbon flux analysis by ^{13}C nuclear magnetic resonance to determine the effect of CO_2 on anaerobic succinate production by *Corynebacterium glutamicum*. Appl. Environ. Microbiol. 80, 3015–3024. https://doi.org/10.1128/AEM.04189-13

Raman, K., Chandra, N., 2009. Flux balance analysis of biological systems: applications and challenges. Brief. Bioinform. 10, 435–449. https://doi.org/10.1093/bib/bbp011

Ramos, I., Vivas, E.I., Downs, D.M., 2008. Mutations in the tryptophan operon allow PurF-independent thiamine synthesis by altering flux *in vivo*. J. Bacteriol. 190, 815–822. https://doi.org/10.1128/JB.00582-07

Rebek, J., 1990. On the structure of histidine and its role in enzyme active sites. Struct. Chem. 1, 129–131. https://doi.org/10.1007/BF00675792

Reinscheid, D.J., Eikmanns, B.J., Sahm, H., 1994a. Characterization of the isocitrate lyase gene from *Corynebacterium glutamicum* and biochemical analysis of the enzyme. J. Bacteriol. 176, 3474–3483.

Reinscheid, D.J., Eikmanns, B.J., Sahm, H., 1994b. Malate synthase from *Corynebacterium glutamicum*: sequence analysis of the gene and biochemical characterization of the enzyme. Microbiology 140, 3099–3108. https://doi.org/10.1099/13500872-140-11-3099

Reisman, H.B., 1993. Problems in scale-up of biotechnology production processes. Crit. Rev. Biotechnol. 13, 195–253. https://doi.org/10.3109/07388559309041319

Riedel, C., Rittmann, D., Dangel, P., Möckel, B., Petersen, S., Sahm, H., Eikmanns, B.J., 2001. Characterization of the phosphoenolpyruvate carboxykinase gene from *Corynebacterium glutamicum* and significance of the enzyme for growth and amino acid production. J. Mol. Microbiol. Biotechnol. 3, 573–583.

Rittmann, D., Lindner, S.N., Wendisch, V.F., 2008. Engineering of a glycerol utilization pathway for amino acid production by *Corynebacterium glutamicum*. Appl. Environ. Microbiol. 74, 6216–6222. https://doi.org/10.1128/AEM.00963-08

Roetzer, A., Diel, R., Kohl, T.A., Rückert, C., Nübel, U., Blom, J., Wirth, T., Jaenicke, S., Schuback, S., Rüsch-Gerdes, S., Supply, P., Kalinowski, J., Niemann, S., 2013. Whole genome sequencing versus traditional genotyping for investigation of a *Mycobacterium tuberculosis* outbreak: A longitudinal molecular epidemiological study. PLoS Med. 10. https://doi.org/10.1371/journal.pmed.1001387

Rohlman, C.E., Matthews, R.G., 1990. Role of purine biosynthetic intermediates in response to folate stress in *Escherichia coli*. J. Bacteriol. 172, 7200–7210.

Rolfes, R.J., Zalkin, H., 1988. *Escherichia coli* gene *purR* encoding a repressor protein for purine nucleotide synthesis. Cloning, nucleotide sequence, and interaction with the *purF* operator. J. Biol. Chem. 263, 19653–19661.

Sabina, R.L., Holmes, E.W., Becker, M.A., 1984. The enzymatic synthesis of 5-amino-4-imidazolecarboxamide riboside triphosphate (ZTP). Science 223, 1193–1195. https://doi.org/10.1126/science.6199843

Sabina, R.L., Patterson, D., Holmes, E.W., 1985. 5-Amino-4-imidazolecarboxamide riboside (Z-riboside) metabolism in eukaryotic cells. J. Biol. Chem. 260, 6107–6114.

Sah, S., Aluri, S., Rex, K., Varshney, U., 2015. One-carbon metabolic pathway rewiring in *Escherichia coli* reveals an evolutionary advantage of 10-formyltetrahydrofolate synthetase (Fhs) in survival under hypoxia. J. Bacteriol. 197, 717–726. https://doi.org/10.1128/JB.02365-14

Saiki, R.K., Gelfand, D.H., Stoffel, S., Scharf, S.J., Higuchi, R., Horn, G.T., Mullis, K.B., Erlich, H.A., 1988. Primer-directed enzymatic amplification of DNA with a thermostable DNA polymerase. Science 239, 487–491. https://doi.org/10.1126/science.239.4839.487

Sambrook, J., Russel, D., Irwin, N., Janssen, U., 2001. Molecular cloning: a laboratory manual, 3rd ed. Cold Spring Harbor Laboratory Press, Cold Spring Harbor, NY.

Sánchez, A.M., Andrews, J., Hussein, I., Bennett, G.N., San, K.-Y., 2008. Effect of overexpression of a soluble pyridine nucleotide transhydrogenase (UdhA) on the production of poly(3-hydroxybutyrate) in *Escherichia coli*. Biotechnol. Progr. 22, 420–425. https://doi.org/10.1021/bp050375u

Sasaki, M., Teramoto, H., Inui, M., Yukawa, H., 2011. Identification of mannose uptake and catabolism genes in *Corynebacterium glutamicum* and genetic engineering for simultaneous utilization of mannose and glucose. Appl. Microbiol. Biotechnol. 89, 1905–1916. https://doi.org/10.1007/s00253-010-3002-8

Sauer, U., Canonaco, F., Heri, S., Perrenoud, A., Fischer, E., 2004. The soluble and membrane-bound transhydrogenases UdhA and PntAB have divergent functions in NADPH metabolism of *Escherichia coli*. J. Biol. Chem. 279, 6613–6619. https://doi.org/10.1074/jbc.M311657200

Sauer, U., Eikmanns, B.J., 2005. The PEP–pyruvate–oxaloacetate node as the switch point for carbon flux distribution in bacteria. FEMS Microbiol. Rev. 29, 765–794. https://doi.org/10.1016/j.femsre.2004.11.002

Saxild, H.H., Brunstedt, K., Nielsen, K.I., Jarmer, H., Nygaard, P., 2001. Definition of the *Bacillus subtilis* PurR operator using genetic and bioinformatic tools and rxpansion of the PurR regulon with *glyA*, *guaC*, *pbuG*, *xpt-pbuX*, *yqhZ-folD*, and *pbuO*. J. Bacteriol. 183, 6175–6183. https://doi.org/10.1128/JB.183.21.6175-6183.2001

Saxild, H.H., Jacobsen, J.H., Nygaard, P., 1995. Functional analysis of the *Bacillus subtilis purT* gene encoding formate-dependent glycinamide ribonucleotide transformylase. Microbiology 141, 2211–2218. https://doi.org/10.1099/13500872-141-9-2211

Schäfer, A., Tauch, A., Jäger, W., Kalinowski, J., Thierbach, G., Pühler, A., 1994. Small mobilizable multi-purpose cloning vectors derived from the *Escherichia coli* plasmids pK18 and pK19: selection of defined deletions in the chromosome of *Corynebacterium glutamicum*. Gene 145, 69–73.

Schellenberger, J., Que, R., Fleming, R.M.T., Thiele, I., Orth, J.D., Feist, A.M., Zielinski, D.C., Bordbar, A., Lewis, N.E., Rahmanian, S., Kang, J., Hyduke, D.R., Palsson, B.Ø., 2011. Quantitative prediction of cellular metabolism with constraint-based models: the COBRA Toolbox v2.0. Nat. Protoc. 6, 1290–1307. https://doi.org/10.1038/nprot.2011.308

Schendzielorz, G., Dippong, M., Grünberger, A., Kohlheyer, D., Yoshida, A., Binder, S., Nishiyama, C., Nishiyama, M., Bott, M., Eggeling, L., 2014. Taking control over control: Use of product sensing in single cells to remove flux control at key enzymes in biosynthesis pathways. ACS Synth. Biol. 3, 21–29. https://doi.org/10.1021/sb400059y

Schirch, V., Hopkins, S., Villar, E., Angelaccio, S., 1985. Serine hydroxymethyltransferase from *Escherichia coli*: purification and properties. J. Bacteriol. 163, 1–7.

Schneider, J., Eberhardt, D., Wendisch, V.F., 2012. Improving putrescine production by *Corynebacterium glutamicum* by fine-tuning ornithine transcarbamoylase activity using a plasmid addiction system. Appl. Microbiol. Biotechnol. 95, 169–178. https://doi.org/10.1007/s00253-012-3956-9

Schobert, P., Bowien, B., 1984. Unusual C3 and C4 metabolism in the chemoautotroph *Alcaligenes eutrophus*. J. Bacteriol. 159, 167–172

Schweitzer, J.-E., Stolz, M., Diesveld, R., Etterich, H., Eggeling, L., 2009. The serine hydroxymethyltransferase gene *glyA* in *Corynebacterium glutamicum* is controlled by GlyR. J. Biotechnol. 139, 214–221. https://doi.org/10.1016/j.jbiotec.2008.12.008

Schwentner, A., Feith, A., Münch, E., Busche, T., Rückert, C., Kalinowski, J., Takors, R., Blombach, B., 2018. Metabolic engineering to guide evolution – Creating a novel mode for L-valine production with *Corynebacterium glutamicum*. Metab. Eng. 47, 31–41. https://doi.org/10.1016/j.ymben.2018.02.015

Schwentner, A., Feith, A., Münch, E., Stiefelmaier, J., Lauer, I., Favilli, L., Massner, C., Öhrlein, J., Grund, B., Hüser, A., Takors, R., Blombach, B., 2019. Modular systems metabolic engineering enables balancing of relevant pathways for L-histidine production with *Corynebacterium glutamicum*. Biotechnol. Biofuels 12, 65. https://doi.org/10.1186/s13068-019-1410-2

Sega, G.A., 1984. A review of the genetic effects of ethyl methanesulfonate. Mut. Res.-Rev. Gen. Toxicol. 134, 113–142. https://doi.org/10.1016/0165-1110(84)90007-1

Segrè, D., Vitkup, D., Church, G.M., 2002. Analysis of optimality in natural and perturbed metabolic networks. Proc. Natl. Acad. Sci. U.S.A. 99, 15112–15117. https://doi.org/10.1073/pnas.232349399

Seibold, G., Auchter, M., Berens, S., Kalinowski, J., Eikmanns, B.J., 2006. Utilization of soluble starch by a recombinant *Corynebacterium glutamicum* strain: Growth and lysine production. J. Biotechnol. 124, 381–391. https://doi.org/10.1016/j.jbiotec.2005.12.027

Seibold, G.M., Eikmanns, B.J., 2013. Inactivation of the phosphoglucomutase gene *pgm* in *Corynebacterium glutamicum* affects cell shape and glycogen metabolism. Biosci. Rep. 33. https://doi.org/10.1042/BSR20130076

Selbitschka, W., Niemann, S., Pühler, A., 1993. Construction of gene replacement vectors for Gram$^-$ bacteria using a genetically modified *sacRB* gene as a positve selection marker. Appl. Microbiol. Biotechnol. 38, 615–618. https://doi.org/10.1007/BF00182799

Setlow, P., Kornberg, A., 1970. Biochemical studies of bacterial sporulation and germination XXIII. Nucleotide metabolism during spore germination. J. Biol. Chem. 245, 3645–3652.

Shah, A., Blombach, B., Gauttam, R., Eikmanns, B.J., 2018. The RamA regulon: complex regulatory interactions in relation to central metabolism in *Corynebacterium glutamicum*. Appl. Microbiol. Biotechnol. 102, 5901–5910. https://doi.org/10.1007/s00253-018-9085-3

Shahid, M., Tripathi, T., Sobia, F., Moin, S., Siddiqui, M., Khan, R.A., 2009. Histamine, histamine receptors, and their role in immunomodulation: An updated systematic review. Open Immunol. J. 2, 9-41.

Sheppard, D.E., 1964. Mutants of *Salmonella typhimurium* resistant to feedback inhibition by L-histidine. Genetics 50, 611–623.

Shi, T., Wang, Y., Wang, Z., Wang, G., Liu, D., Fu, J., Chen, T., Zhao, X., 2014. Deregulation of purine pathway in *Bacillus subtilis* and its use in riboflavin biosynthesis. Microb. Cell Fact. 13, 101. https://doi.org/10.1186/s12934-014-0101-8

Shibasaki, M., Kanai, M., Mita, T., 2008. The catalytic asymmetric Strecker reaction, in: Organic Reactions. American Cancer Society, p. 1–119. https://doi.org/10.1002/0471264180.or070.01

Shimaoka, M., Takenaka, Y., Kurahashi, O., Kawasaki, H., Matsui, H., 2007. Effect of amplification of desensitized *purF* and *prs* on inosine accumulation in *Escherichia coli*. J. Biosci. Bioeng. 103, 255–261. https://doi.org/10.1263/jbb.103.255

Shimizu, H., Shimizu, N., Shioya, S., 2002. Roles of glucose and acetate as carbon sources in L-histidine production with *Brevibacterium flavum* FERM1564 revealed by metabolic flux analysis. Biotechnol. Bioprocess Eng. 7, 171–177. https://doi.org/10.1007/BF02932915

Shin, B.S., Stein, A., Zalkin, H., 1997. Interaction of *Bacillus subtilis* purine repressor with DNA. J. Bacteriol. 179, 7394–7402. https://doi.org/10.1128/jb.179.23.7394-7402.1997

Shin, J.H., Park, S.H., Oh, Y.H., Choi, J.W., Lee, M.H., Cho, J.S., Jeong, K.J., Joo, J.C., Yu, J., Park, S.J., Lee, S.Y., 2016. Metabolic engineering of *Corynebacterium glutamicum* for enhanced production of 5-aminovaleric acid. Microb. Cell Fact. 15. https://doi.org/10.1186/s12934-016-0566-8

Shirai, T., Fujimura, K., Furusawa, C., Nagahisa, K., Shioya, S., Shimizu, H., 2007. Study on roles of anaplerotic pathways in glutamate overproduction of *Corynebacterium glutamicum* by metabolic flux analysis. Microb. Cell Fact. 6, 19. https://doi.org/10.1186/1475-2859-6-19

Siebert, D., Wendisch, V.F., 2015. Metabolic pathway engineering for production of 1,2-propanediol and 1-propanol by *Corynebacterium glutamicum*. Biotechnol. Biofuels 8. https://doi.org/10.1186/s13068-015-0269-0

Simic, P., Willuhn, J., Sahm, H., Eggeling, L., 2002. Identification of *glyA* (encoding serine hydroxymethyltransferase) and its use together with the exporter ThrE to increase L-threonine accumulation by *Corynebacterium glutamicum*. Appl. Environ. Microbiol. 68, 3321–3327. https://doi.org/10.1128/AEM.68.7.3321-3327.2002

Song, J., Yang, L., Nan, D., He, Q., Wan, Y., Guo, H., 2018. Histidine alleviates impairments induced by chronic cerebral hypoperfusion in mice. Front. Physiol. 9. https://doi.org/10.3389/fphys.2018.00662

Spaans, S.K., Weusthuis, R.A., van der Oost, J., Kengen, S.W.M., 2015. NADPH-generating systems in bacteria and archaea. Front. Microbiol. 6. https://doi.org/10.3389/fmicb.2015.00742

Sprenger, G.A., 2007. From scratch to value: engineering *Escherichia coli* wild type cells to the production of L-phenylalanine and other fine chemicals derived from chorismate. Appl. Microbiol. Biotechnol. 75, 739–749. https://doi.org/10.1007/s00253-007-0931-y

Stäbler, N., Oikawa, T., Bott, M., Eggeling, L., 2011. *Corynebacterium glutamicum* as a host for synthesis and export of D-amino acids. J. Bacteriol. 193, 1702–1709. https://doi.org/10.1128/JB.01295-10

Stauffer, L.T., Plamann, M.D., Staufferer, G.V., 1986. Cloning and characterization of the glycine-cleavage enzyme system of *Escherichia coli*. Gene 44, 219–226. https://doi.org/10.1016/0378-1119(86)90185-X

Stemmer, W.P.C., 1994. Rapid evolution of a protein *in vitro* by DNA shuffling. Nature 370, 389–391. https://doi.org/10.1038/370389a0

Stolz, M., Peters-Wendisch, P., Etterich, H., Gerharz, T., Faurie, R., Sahm, H., Fersterra, H., Eggeling, L., 2007. Reduced folate supply as a key to enhanced L-serine production by *Corynebacterium glutamicum*. Appl. Environ. Microbiol. 73, 750–755. https://doi.org/10.1128/AEM.02208-06

Strange, R.E., Wade, H.E., Dark, F.A., 1963. Effect of starvation on adenosine triphosphate concentration in *Aerobacter aerogenes*. Nature 199, 55–58. https://doi.org/10.1038/199055a0

Strominger, J.L., Birge, C.H., 1965. Nucleotide accumulation induced in *Staphylococcus aureus* by glycine. J. Bacteriol. 89, 1124–1127.

Switzer, R.L., Gibson, K.J., 1978. Phosphoribosylprophosphate synthetase (ribose-5-phosphate pyrophosphokinase) from *Salmonella typhimurium*, in: Methods in enzymology, purine and pyrimidine nucleotide metabolism. Academic Press, p. 3–11. https://doi.org/10.1016/S0076-6879(78)51003-3

Takeno, S., Murata, R., Kobayashi, R., Mitsuhashi, S., Ikeda, M., 2010. Engineering of *Corynebacterium glutamicum* with an NADPH-generating glycolytic pathway for L-lysine production. Appl. Environ. Microbiol. 76, 7154–7160. https://doi.org/10.1128/AEM.01464-10

Takeno, S., Takasaki, M., Urabayashi, A., Mimura, A., Muramatsu, T., Mitsuhashi, S., Ikeda, M., 2013. Development of fatty acid-producing *Corynebacterium glutamicum* strains. Appl. Environ. Microbiol. 79, 6776–6783. https://doi.org/10.1128/AEM.02003-13

Tanaka, Y., Okai, N., Teramoto, H., Inui, M., Yukawa, H., 2008. Regulation of the expression of phosphoenolpyruvate: carbohydrate phosphotransferase system (PTS) genes in *Corynebacterium glutamicum* R. Microbiology 154, 264–274. https://doi.org/10.1099/mic.0.2007/008862-0

Tauch, A., Kaiser, O., Hain, T., Goesmann, A., Weisshaar, B., Albersmeier, A., Bekel, T., Bischoff, N., Brune, I., Chakraborty, T., Kalinowski, J., Meyer, F., Rupp, O., Schneiker, S., Viehoever, P., Pühler, A., 2005. Complete genome sequence and analysis of the multiresistant nosocomial pathogen *Corynebacterium jeikeium* K411, a lipid-requiring bacterium of the human skin flora. J. Bacteriol. 187, 4671–4682. https://doi.org/10.1128/JB.187.13.4671-4682.2005

Tauch, A., Kirchner, O., Löffler, B., Götker, S., Pühler, A., Kalinowski, J., 2002. Efficient electrotransformation of *Corynebacterium diphtheriae* with a mini-replicon derived from the *Corynebacterium glutamicum* plasmid pGA1. Curr. Microbiol. 45, 362–367. https://doi.org/10.1007/s00284-002-3728-3

Tébar, A.R., Ballesteros, A.O., 1976. Kinetic properties of ATP phosphoribosyltransferase of *Escherichia coli*. Mol. Cell. Biochem. 11, 131–136. https://doi.org/10.1007/BF01744993

Teleki, A., Sánchez-Kopper, A., Takors, R., 2015. Alkaline conditions in hydrophilic interaction liquid chromatography for intracellular metabolite quantification using tandem mass spectrometry. Anal. Biochem. 475, 4–13. https://doi.org/10.1016/j.ab.2015.01.002

Teramoto, H., Inui, M., Yukawa, H., 2011. Transcriptional regulators of multiple genes involved in carbon metabolism in *Corynebacterium glutamicum*. J. Biotechnol. 154, 114–125. https://doi.org/10.1016/j.jbiotec.2011.01.016

Teramoto, H., Suda, M., Inui, M., Yukawa, H., 2010. Regulation of the expression of genes involved in NAD *de novo* biosynthesis in *Corynebacterium glutamicum*. Appl. Environ. Microbiol. 76, 5488–5495. https://doi.org/10.1128/AEM.00906-10

Tezuka, T., Ohnishi, Y., 2014. Two glycine riboswitches activate the glycine cleavage system essential for glycine detoxification in *Streptomyces griseus*. J. Bacteriol. 196, 1369–1376. https://doi.org/10.1128/JB.01480-13

Thiry, M., Cingolani, D., 2002. Optimizing scale-up fermentation processes. Trends Biotechnol. 20, 103–105. https://doi.org/10.1016/S0167-7799(02)01913-3

Toyoda, K., Teramoto, H., Gunji, W., Inui, M., Yukawa, H., 2013. Involvement of regulatory interactions among global regulators GlxR, SugR, and RamA in expression of *ramA* in *Corynebacterium glutamicum*. J. Bacteriol. 195, 1718–1726. https://doi.org/10.1128/JB.00016-13

Traxler, M.F., Summers, S.M., Nguyen, H.-T., Zacharia, V.M., Hightower, G.A., Smith, J.T., Conway, T., 2008. The global, ppGpp-mediated stringent response to amino acid starvation in *Escherichia coli*. Mol. Microbiol. 68, 1128–1148. https://doi.org/10.1111/j.1365-2958.2008.06229.x

Turnbough, C.L., Switzer, R.L., 2008. Regulation of pyrimidine biosynthetic gene expression in bacteria: Repression without repressors. Microbiol. Mol. Biol. Rev. 72, 266–300. https://doi.org/10.1128/MMBR.00001-08

Turner, N.J., 2009. Directed evolution drives the next generation of biocatalysts. Nat. Chem. Biol. 5, 567–573. https://doi.org/10.1038/nchembio.203

Tuttle, K.R., Milton, J.E., Packard, D.P., Shuler, L.A., Short, R.A., 2012. Dietary amino acids and blood pressure: A cohort study of patients with cardiovascular disease. Am. J. Kidney Dis. 59, 803–809. https://doi.org/10.1053/j.ajkd.2011.12.026

Unthan, S., Grünberger, A., Ooyen, J. van, Gätgens, J., Heinrich, J., Paczia, N., Wiechert, W., Kohlheyer, D., Noack, S., 2014. Beyond growth rate 0.6: What drives *Corynebacterium glutamicum* to higher growth rates in defined medium. Biotechnol. Bioeng. 111, 359–371. https://doi.org/10.1002/bit.25103

van der Rest, M.E., Lange, C., Molenaar, D., 1999. A heat shock following electroporation induces highly efficient transformation of *Corynebacterium glutamicum* with xenogeneic plasmid DNA. Appl. Microbiol. Biotechnol. 52, 541–545.

van Zeeland, A.A., Mohn, G.R., Aaron, C.S., Glickman, B.W., Brendel, M., de Serres, F.J., Hung, C.Y., Brockman, H.E., 1983. Molecular dosimetry of the chemical mutagen ethyl methanesulfonate: Quantitative comparison of the mutagenic potency in *Neurospora crassa* and *Saccharomyces cerevisiae*. Mut. Res. Lett. 119, 45–54. https://doi.org/10.1016/0165-7992(83)90036-2

Vašicová, P., Pátek, M., Nešvera, J., Sahm, H., Eikmanns, B., 1999. Analysis of the *Corynebacterium glutamicum dapA* Promoter. J. Bacteriol. 181, 6188–6191.

Vickery, H.B., Leavenworth, C.S., 1928. On the separation of histidine and arginine IV. The preparation of histidine. J. Biol. Chem. 78, 627–635.

Vogt, M., Haas, S., Klaffl, S., Polen, T., Eggeling, L., van Ooyen, J., Bott, M., 2014a. Pushing product formation to its limit: Metabolic engineering of *Corynebacterium glutamicum* for L-leucine overproduction. Metab. Eng. 22, 40–52. https://doi.org/10.1016/j.ymben.2013.12.001

Vogt, M., Krumbach, K., Bang, W.-G., Ooyen, J. van, Noack, S., Klein, B., Bott, M., Eggeling, L., 2014b. The contest for precursors: channelling L-isoleucine synthesis in *Corynebacterium glutamicum* without byproduct formation. Appl. Microbiol. Biotechnol. 1–10. https://doi.org/10.1007/s00253-014-6109-5

Waagbø, R., Tröße, C., Koppe, W., Fontanillas, R., Breck, O., 2010. Dietary histidine supplementation prevents cataract development in adult Atlantic salmon, *Salmo salar* L., in seawater. Br. J. Nutr. 104, 1460–1470. https://doi.org/10.1017/S0007114510002485

Wada, M., Hijikata, N., Aoki, R., Takesue, N., Yokota, A., 2008. Enhanced valine production in *Corynebacterium glutamicum* with defective H^+-ATPase and C-terminal truncated acetohydroxyacid synthase. Biosci. Biotechnol. Biochem. 72, 2959–2965. https://doi.org/10.1271/bbb.80434

Wade, A.M., Tucker, H.N., 1998. Antioxidant characteristics of L-histidine. J. Nutr. Biochem. 9, 308–315. https://doi.org/10.1016/S0955-2863(98)00022-9

Wainscott, V.J., Ferretti, J.J., 1978. Biochemical-genetic study of the first enzyme of histidine biosynthesis in *Salmonella typhimurium*: Substrate and feedback binding regions. J. Bacteriol. 133, 114-121.

Walker-Simmons, M., Atkinson, D.E., 1977. Functional capacities and the adenylate energy charge in *Escherichia coli* under conditions of nutritional stress. J. Bacteriol. 130, 676–683.

Wang, H.H., Isaacs, F.J., Carr, P.A., Sun, Z.Z., Xu, G., Forest, C.R., Church, G.M., 2009. Programming cells by multiplex genome engineering and accelerated evolution. Nature 460, 894–898. https://doi.org/10.1038/nature08187

Wang, X., Zhang, H., Quinn, P.J., 2018. Production of L-valine from metabolically engineered *Corynebacterium glutamicum*. Appl. Microbiol. Biotechnol. 102, 4319–4330. https://doi.org/10.1007/s00253-018-8952-2

Wang, Z., Chan, S.H.J., Sudarsan, S., Blank, L.M., Jensen, P.R., Solem, C., 2016. Elucidation of the regulatory role of the fructose operon reveals a novel target for enhancing the NADPH supply in *Corynebacterium glutamicum*. Metab. Eng. 38, 344–357. https://doi.org/10.1016/j.ymben.2016.08.004

Watanabe, M., Suliman, M.E., Qureshi, A.R., Garcia-Lopez, E., Bárány, P., Heimbürger, O., Stenvinkel, P., Lindholm, B., 2008. Consequences of low plasma histidine in chronic kidney disease patients: associations with inflammation, oxidative stress, and mortality. Am. J. Clin. Nutr. 87, 1860–1866. https://doi.org/10.1093/ajcn/87.6.1860

Wei, L., Xu, N., Wang, Y., Zhou, W., Han, G., Ma, Y., Liu, J., 2018. Promoter library-based module combination (PLMC) technology for optimization of threonine biosynthesis in *Corynebacterium glutamicum*. Appl. Microbiol. Biotechnol. 102, 4117–4130. https://doi.org/10.1007/s00253-018-8911-y

Wendisch, V.F., 2003. Genome-wide expression analysis in *Corynebacterium glutamicum* using DNA microarrays. J. Biotechnol. 104, 273–285. https://doi.org/10.1016/S0168-1656(03)00147-0

Wendisch, V.F., de Graaf, A.A., Sahm, H., Eikmanns, B.J., 2000. Quantitative determination of metabolic fluxes during coutilization of two carbon sources: Comparative analyses with *Corynebacterium glutamicum* during growth on acetate and/or glucose. J. Bacteriol. 182, 3088-3096.

Wendisch, V.F., Jorge, J.M.P., Pérez-García, F., Sgobba, E., 2016. Updates on industrial production of amino acids using *Corynebacterium glutamicum*. World J. Microbiol. Biotechnol. 32. https://doi.org/10.1007/s11274-016-2060-1

Wendisch, V.F., Spies, M., Reinscheid, D.J., Schnicke, S., Sahm, H., Eikmanns, B.J., 1997. Regulation of acetate metabolism in *Corynebacterium glutamicum*: transcriptional control of the isocitrate lyase and malate synthase genes. Arch. Microbiol. 168, 262–269.

Wieschalka, S., Blombach, B., Eikmanns, B.J., 2012. Engineering *Corynebacterium glutamicum* for the production of pyruvate. Appl. Microbiol. Biotechnol. 94, 449–459. https://doi.org/10.1007/s00253-011-3843-9

Wilson, D.S., Keefe, A.D., 2001. Random mutagenesis by PCR. Curr. Protoc. Mol. Biol. 51. https://doi.org/10.1002/0471142727.mb0803s51

Winkler, M.E., Ramos-Montañez, S., 2009. Biosynthesis of histidine. Ecosal Plus 2009. https://doi.org/10.1128/ecosalplus.3.6.1.9

Witthoff, S., Eggeling, L., Bott, M., Polen, T., 2012. *Corynebacterium glutamicum* harbours a molybdenum cofactor-dependent formate dehydrogenase which alleviates growth inhibition in the presence of formate. Microbiology 158, 2428–2439. https://doi.org/10.1099/mic.0.059196-0

Wong, T.S., Tee, K.L., Hauer, B., Schwaneberg, U., 2004. Sequence saturation mutagenesis (SeSaM): a novel method for directed evolution. Nucleic Acids Res. 32, e26. https://doi.org/10.1093/nar/gnh028

Wyngaarden, J.B., 1976. Regulation of purine biosynthesis and turnover. Adv. Enzyme Regul. 14, 25–42. https://doi.org/10.1016/0065-2571(76)90006-6

Yadav, V.G., De Mey, M., Lim, C.G., Ajikumar, P.K., Stephanopoulos, G., 2012. The future of metabolic engineering and synthetic biology: Towards a systematic practice. Metab. Eng. 14, 233–241. https://doi.org/10.1016/j.ymben.2012.02.001

Yamaguchi, S., 1991. Basic properties of umami and effects on humans. Physiology & Behavior 49, 833–841. https://doi.org/10.1016/0031-9384(91)90192-Q

Yang, J., Yang, S., 2017. Comparative analysis of *Corynebacterium glutamicum* genomes: a new perspective for the industrial production of amino acids. BMC Genomics 18. https://doi.org/10.1186/s12864-016-3255-4

Yokobayashi, Y., Weiss, R., Arnold, F.H., 2002. Directed evolution of a genetic circuit. Proc. Natl. Acad. Sci. U.S.A. 99, 16587–16591. https://doi.org/10.1073/pnas.252535999

Yokota, A., Lindley, N.D., 2005. Central metabolism: sugar uptake and conversion, in: Eggeling, L. and Bott, M. (Eds). Handbook of Corynebacterium Glutamicum. CRC Press, Boca Raton, FL, USA, p. 215–240.

Yokota, A., Sawada, K., Wada, M., 2017. Boosting anaplerotic reactions by pyruvate kinase gene deletion and phosphoenolpyruvate carboxylase desensitization for glutamic acid and lysine production in *Corynebacterium glutamicum*. Adv. Biochem. Eng. Biotechnol. 159, 181-198. https://doi.org/10.1007/10_2016_31

Yukawa, H., Omumasaba, C.A., Nonaka, H., Kós, P., Okai, N., Suzuki, N., Suda, M., Tsuge, Y., Watanabe, J., Ikeda, Y., Vertès, A.A., Inui, M., 2007. Comparative analysis of the *Corynebacterium glutamicum* group and complete genome sequence of strain R. Microbiology 153, 1042–1058. https://doi.org/10.1099/mic.0.2006/003657-0

Zalkin, H., 1983. Structure, function, and regulation of amidophosphoribosyltransferase from prokaryotes. Adv. Enzyme Regul. 21, 225–237. https://doi.org/10.1016/0065-2571(83)90016-X

Zelle, R.M., Trueheart, J., Harrison, J.C., Pronk, J.T., van Maris, A.J.A., 2010. Phosphoenolpyruvate carboxykinase as the sole anaplerotic enzyme in *Saccharomyces cerevisiae*. Appl. Environ. Microbiol. 76, 5383–5389. https://doi.org/10.1128/AEM.01077-10

Zha, W., Rubin-Pitel, S.B., Zhao, H., 2008. Exploiting genetic diversity by directed evolution: molecular breeding of type III polyketide synthases improves productivity. Mol. BioSyst. 4, 246–248. https://doi.org/10.1039/B717705D

Zhang, C., Zhang, J., Kang, Z., Du, G., Chen, J., 2015. Rational engineering of multiple module pathways for the production of L-phenylalanine in *Corynebacterium glutamicum*. J. Ind. Microbiol. Biotechnol. 42, 787–797. https://doi.org/10.1007/s10295-015-1593-x

Zhang, J., Reddy, J., Buckland, B., Greasham, R., 2003. Toward consistent and productive complex media for industrial fermentations: Studies on yeast extract for a recombinant yeast fermentation process. Biotechnol. Bioeng. 82, 640–652. https://doi.org/10.1002/bit.10608

Zhang, Y., Morar, M., Ealick, S.E., 2008. Structural biology of the purine biosynthetic pathway. Cell. Mol. Life Sci. 65, 3699–3724. https://doi.org/10.1007/s00018-008-8295-8

Zhang, Y., Shang, X., Deng, A., Chai, X., Lai, S., Zhang, G., Wen, T., 2012. Genetic and biochemical characterization of *Corynebacterium glutamicum* ATP phosphoribosyltransferase and its three mutants resistant to feedback inhibition by histidine. Biochimie 94, 829–838. https://doi.org/10.1016/j.biochi.2011.11.015

Zhang, Yu, Cai, J., Shang, X., Wang, B., Liu, S., Chai, X., Tan, T., Zhang, Yun, Wen, T., 2017. A new genome-scale metabolic model of *Corynebacterium glutamicum* and its application. Biotechnol. Biofuels 10, 169. https://doi.org/10.1186/s13068-017-0856-3

Zhang, Yun, Shang, X., Lai, S., Zhang, Yu, Hu, Q., Chai, X., Wang, B., Liu, S., Wen, T., 2018. Reprogramming ene-carbon metabolic pathways to decouple L-serine catabolism from cell growth in *Corynebacterium glutamicum*. ACS Synth. Biol. 7, 635–646. https://doi.org/10.1021/acssynbio.7b00373

Zhao, H., Arnold, F.H., 1997. Optimization of DNA shuffling for high fidelity recombination. Nucleic Acids Res. 25, 1307–1308. https://doi.org/10.1093/nar/25.6.1307

Zheng, X., Hu, G.Q., She, Z.S., Zhu, H., 2011. Leaderless genes in bacteria: clue to the evolution of translation initiation mechanisms in prokaryotes. BMC Genomics 12, 361–361. https://doi.org/10.1186/1471-2164-12-361

Zhou, G., Charbonneau, H., Colman, R.F., Zalkin, H., 1993. Identification of sites for feedback regulation of glutamine 5-phosphoribosylpyrophosphate amidotransferase by nucleotides and relationship to residues important for catalysis. J. Biol. Chem. 268, 10471–10481.

Zhou, G., Smith, J.L., Zalkin, H., 1994. Binding of purine nucleotides to two regulatory sites results in synergistic feedback inhibition of glutamine 5-phosphoribosylpyrophosphate amidotransferase. J. Biol. Chem. 269, 6784–6789.

Zhou, J., Liu, L., Shi, Z., Du, G., Chen, J., 2009. ATP in current biotechnology: Regulation, applications and perspectives. Biotechnol. Adv. 27, 94–101. https://doi.org/10.1016/j.biotechadv.2008.10.005

Zhou, S., Alper, H.S., 2018. Strategies for directed and adapted evolution as part of microbial strain engineering. J. Chem. Technol. Biotechnol. https://doi.org/10.1002/jctb.5746

Zhu, N., Xia, H., Yang, J., Zhao, X., Chen, T., 2014. Improved succinate production in *Corynebacterium glutamicum* by engineering glyoxylate pathway and succinate export system. Biotechnol. Lett. 36, 553–560. https://doi.org/10.1007/s10529-013-1376-2

Zhu, Q., Zhang, X., Luo, Y., Guo, W., Xu, G., Shi, J., Xu, Z., 2014. L-Serine overproduction with minimization of by-product synthesis by engineered *Corynebacterium glutamicum*. Appl. Microbiol. Biotechnol. 99, 1665–1673. https://doi.org/10.1007/s00253-014-6243-0

Zhu, Z., Zhang, J., Ji, X., Fang, Z., Wu, Z., Chen, J., Du, G., 2018. Evolutionary engineering of industrial microorganisms-strategies and applications. Appl. Microbiol. Biotechnol. 102, 4615–4627. https://doi.org/10.1007/s00253-018-8937-1

CHAPTER 6: APPENDIX

6.1. Supplementary results

6.1.1. *Differential $Y_{P/S}^{his}$ during fed-batch fermentation*

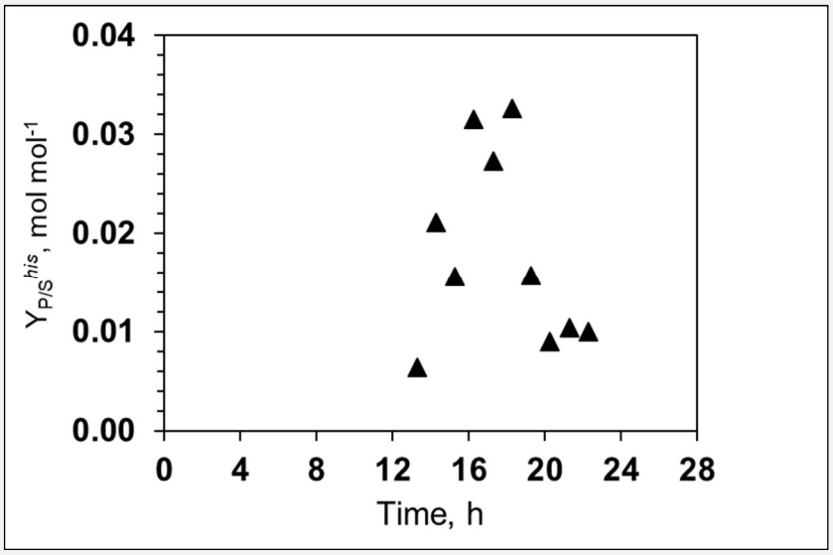

Fig. 32. Differential product substrate yields for L-histidine ($Y_{P/S}^{his}$) over the process time during the fed-batch phase of a STR fed-batch fermentation of *C. glutamicum* CM2.

6.1.2. *C. glutamicum CM2 shaking flask vs. reactor cultivation*

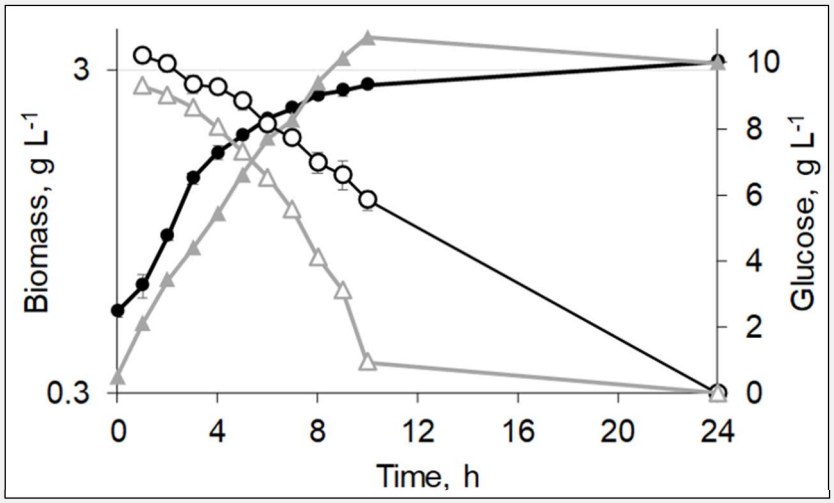

Fig. 33. Comparison of growth profiles of *C. glutamicum* CM2 in shaking flasks (circles) and small scale reactor cultivations (triangles). Filled symbols represent biomass, open symbols represent glucose concentration. Depicted shaking flask cultivations were performed in triplicates and bars show standard error, for reactor cultivation one representative experiment is shown.

6.1.3. *pH profiles in shaking flasks and reactor cultivations*

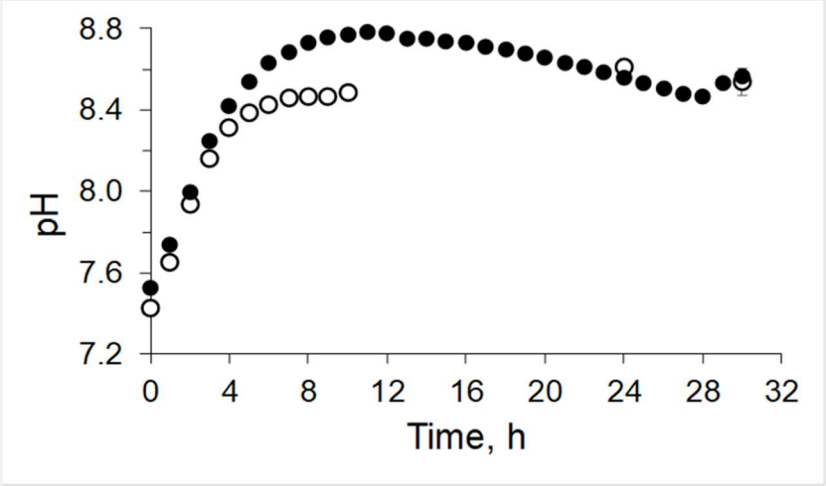

Fig. 34. pH profiles in shaking flask cultivations (white circles) and in a small scale fermentation (black circles) with *C. glutamicum* CM2 w/o pH regulation. Starting values of both cultivations were in the range of 7.4-7.5. Shaking flask cultivations were performed in triplicate and error bars give standard deviations. For the small scale fermentation a representative pH profile of one cultivation is shown.

Erklärung

Die hier vorgelegte Dissertation wurde von mir eigenständig und ohne unerlaubte Hilfe angefertigt.

Ich versichere, dass ich keine anderen als die angegebenen Quellen und Hilfsmittel verwendet, sowie Zitate kenntlich gemacht, habe.

Die Dissertation wurde in der hier vorgelegten oder in ähnlicher Form noch bei keiner anderen Institution eingereicht.

Ich habe bisher keine erfolglosen Promotionsversuche unternommen.

Ort, Datum Unterschrift